Applying isotope geochemistry to identify mechanisms regulating the aquatic-terrestrial carbon and nitrogen dynamics across scales in a moraine landscape

DISSERTATION
zur Erlangung des akademischen Grades

Doctor of Philosophy
(Ph.D.)

eingereicht an der
Lebenswissenschaftlichen Fakultät der Humboldt-Universität zu Berlin

von
M.Sc. Kai Nitzsche

Präsidentin der Humboldt-Universität zu Berlin
Prof. Dr.-Ing. Dr. Sabine Kunst

Dekan der Lebenswissenschaftlichen Fakultät
der Humboldt-Universität zu Berlin
Prof. Dr. Bernhard Grimm

Gutachter/innen: 1. Prof. Dr. Jutta Zeitz
2. PD Dr. Arthur Gessler
3. PD Dr. Michael Zech

Tag der mündlichen Prüfung: 10.5.2017

Table of contents

List of abbreviations

a	C isotope fractionation during stomata CO_2 diffusion
A	carbon assimilation
AIC	Akaike information criterion
ANOVA	analysis of variance
b	discrimination during carboxylation of RuBisCO
c_a	ambient atmospheric concentration of CO_2
caRG	Calcaric Regosol
c_i	intracellular CO_2 content in the stomata
Cl^-	chloride
coRG	Colluvic Regosol
coST	Colluvic Stagnosols
CH_4	methane
CO_2	carbon dioxide
$\delta^{13}C$	carbon isotopic composition relative to international standard VPDB
$\Delta^{13}C$	net ^{13}C discrimination during photosynthesis
δ^2H, δD	hydrogen isotopic composition relative to international standard VSMOW
$\delta^{15}N$	nitrogen isotopic composition relative to international standard AIR
$\Delta^{15}N$	plant ^{15}N normalized by soil ^{15}N
$\delta^{18}O$	oxygen isotopic composition relative to international standard VSMOW
DEM	digital elevation model
f	evaporative loss
E	leaf transpiration
eLV	Eroded Luvisol
GDR	German Democratic Republic
GMWL	Global Meteoric Water Line
GL	Gleysols
g_s	stomatal conductance
HS	Histosol
isoscape	*iso*topic land*scape*
Kr	the village Kraatz
LAI	leaf area index
LEL	isotopic evaporation line
LME	linear mixed effects model
LMWL	local Meteoric Water Line
LV	non-eroded Luvisols
MRT	mean residence time

n	number of samples
n.a.	not analyzed
N_2O	nitrous oxide
NH_4^+	ammonium
NO_3^-	nitrate
n.s.	not significant
OC	organic carbon
OM	organic matter
OM_{bulk}	organic matter in the bulk soil
OM_{ER}	organic matter in the extraction residue
OM_{PYP}	Na-pyrophosphate extractable and HCl-insoluble organic matter
OM_{PYS}	Na-pyrophosphate extractable and HCl-soluble organic matter
OP_A	aggregate occluded organic particles
OP_{free}	loosely bound organic particles
p	probability value
r	correlation coefficient
r^2	coefficient of determination
Ri	the village Rittgarten
RubisCO	ribulose 1,5-bisphosphate carboxylase oxygenase
SE	standard error
SO_4^{2-}	sulfate
SOC	soil organic carbon
SOM	soil organic matter
sp-type	semi-permanently water-filled
T	temperature
t-type	temporarily water-filled
TPI	topographic position index
TWI	topographical wetness index
$WEOM_A$	aggregate-bound water-extractable organic matter
$WEOM_{free}$	loosely attached water-extractable organic matter
WUE_i	intrinsic water use efficiency

List of tables

List of figures

Summary

In moraine landscapes, carbon (C) and nitrogen (N) dynamics can vary greatly across landscape structures and soil types. An integral feature of these landscapes are small inland water bodies, so-called kettle holes, the roles of which on the C and N dynamics of a landscape are often neglected. Given the strong spatial heterogeneity of moraine landscapes, the sole focus on larger (landscape) scale processes may result in the ignorance of small-scale variability in C and N dynamics. To improve predictions of the impacts of global change on landscapes and to ensure their sustainable use, it is essential to identify the driving mechanisms underlying the aquatic-terrestrial C and N dynamics. This study uses stable isotopes to identify these regulating mechanisms across different scales (from regional landscape over kettle hole to aggregate scale) in the moraine landscape of NE Germany – a landscape that is intensively used for agriculture and interspersed with countless kettle holes.

At the regional landscape scale, $\delta^{13}C$ isoscapes (*iso*topic land*scapes*) of topsoil bulk soil organic matter (SOM) and plant leaves collected from 38.2 km^2 landscape unit revealed long-term inputs of organic matter (OM) from C_3 crops, which imprinted their water use efficiency status onto the soil, as well as short-term inputs from corn (C_4 crop). The $\delta^{15}N$ SOM isoscape identified fertilization-induced impacts of land-management on the N dynamics of agricultural fields and grasslands, while showing that the forest N cycle was rather closed.

At the regional kettle hole scale, surface sediments were analyzed for 51 kettle holes located in the same landscape unit but differing with respect to the surrounding land-use type and the hydroperiod. Results for $\delta^{13}C$ and $\delta^{15}N$ reflected recent OM inputs and processes and pointed at the effect of anoxic sediment conditions and fertilization in the catchment. Deeper sediments recorded the degree to which OM had been processed within the kettle hole depending on the hydroperiod and indicated the burial of OM originating from terrestrial plants.

At the transect scale, erosion and plant productivity were the dominant drivers affecting mineral-associated OM fractions in topsoil sampled along transects spanning erosional to depositional areas in the catchment of one arable kettle hole. In contrast, freely available and aggregated OM fractions were influenced by microbial decomposition and slurry fertilization. At the aggregate scale, the pathway and magnitude of OM-mineral associations changed along the transect while binding OM of different status of decomposition. OM in mineral-associated fractions from sediments was derived from clay- and silt-sized particles from the agricultural field together with emergent macrophyte contributions to freely available and aggregated OM fractions.

By means of stable isotopes techniques, different mechanisms were successfully identified at the individual scales. Consideration of the spatial heterogeneity of all scales from aggregate scale to the entire landscape is essential to understand landscape C and N dynamics. Small inland water bodies like kettle holes are key constituents with respect to C and N dynamics

in moraine agricultural landscapes, because they function as important sinks for OM and alter the environmental conditions in their catchments. However, their net role as C and N sinks or sources in landscapes needs to be determined by future studies comprising longer time scales and more detailed studies on N and C fluxes.

Zusammenfassung

Die Kohlenstoff- und Stickstoffdynamiken in Moränenlandschaften können über Landschaftsstrukturen und Bodentypen hinweg stark variieren. Ein besonderes Merkmal dieser Landschaften sind kleine Inlandwasserkörper, die sogenannten Sölle oder Toteislöcher, deren Rolle auf die C- und N-Dynamik der Landschaft oft vernachlässigt wird. Aufgrund der starken räumlichen Heterogenität von Moränenlandschaften kann der alleinige Fokus auf Prozesse auf größeren Skalenebenen (Landschaftsskala) zur Vernachlässigung kleinskaliger Variabilität in der C- und N-Dynamik führen. Um die Voraussagen der Einflüsse des globalen Klimawandels auf Landschaften und deren nachhaltiger Nutzung sicher zu stellen, ist es daher essenziell, die Steuerungsmechanismen der zugrundeliegenden aquatisch-terrestrischen C- und N-Dynamik zu identifizieren. In dieser Studie werden stabile Isotope und deren Verhältnisse genutzt, um diese Mechanismen über verschiedene Skalenebenen (von der regionalen Landschaftsskala bis zur Aggregatskala) hinweg in der Moränenlandschaft von Nordostdeutschland zu identifizieren; einer Landschaft, die stark landwirtschaftlich genutzt wird und in der es eine Vielzahl von Söllen gibt.

Auf der regionalen Landschaftsskala spiegeln $\delta^{13}C$-Isotopenkarten des organischen Materials in Oberböden und von Pflanzenblättern eines 38.2 km^2 großen Landschaftsausschnittes zum einen den langfristigen Eintrag von organischem Material von C_3-Pflanzen, deren Wassernutzungseffizienz im organischen Material des Bodens eingeprägt wurde, sowie den kurzfristigen Eintrag von Mais (C_4-Pflanze) wider. Die $\delta^{15}N$-Isotopenkarte des organischen Materials in Böden weist auf bewirtschaftungsbedingte Einflüsse (v.a. Düngungseffekte) auf die N-Dynamik von Feldern und Wiesen hin, während der N-Kreislauf in Wäldern eher geschlossen ist.

Auf der im Hinblick auf die Sölle regionalen Skalenebene wurden Oberflächensedimente von 51 Söllen mit verschiedener Landnutzung im Einzugsgebiet und unterschiedlicher Wasserführung im o.g. Untersuchungsgebiet analysiert. Die $\delta^{13}C$- und $\delta^{15}N$-Isotopenwerte deuten auf kürzliche Einträge organischen Materials und auf Prozesse wie saisonale Anoxia im Sediment sowie Düngung im Einzugsgebiet hin. Tiefere Sedimente sind hingegen durch die Ablagerung organischen Materials von terrestrischen Pflanzen sowie dessen Umsetzungsgrad geprägt, welcher abhängig von der Wasserführung ist.

Auf der Transekt-Skala, d.h. entlang von Transekten von Erosions- zu Depositionsgebieten im Einzugsgebiet eines Solls in einem Feld, sind Erosion und Pflanzenproduktion die dominanten Steuerungsmechanismen des mineral-assoziierten organischen Materials. Im Gegensatz dazu sind das frei verfügbare und das aggregatgebundene organische Material v.a. durch mikrobielle Umsetzungsprozesse und Gülledüngung beeinflusst. Auf der Aggregat-Skalenebene sind die Art und der Anteil spezifischer organo-mineral Assoziationen entlang des Transekts variabel, wobei organisches

Material verschiedenen Umsetzungsgrades und Ursprungs gebunden ist. In Sedimenten sind Ton- und Siltpartikel vom angrenzenden Feld die dominante Quelle des mineral-assoziierten organischen Materials, während das dort frei verfügbare und aggregatgebundene organische Material terrestrischen Ursprungs ist.

Diese Studie hat erfolgreich stabile Isotopenverhältnisse zur Identifikation von Mechanismen der C- und N-Dynamik auf individuellen Skalenebenen angewendet. Die Berücksichtigung räumlicher Heterogenität auf allen Skalenebenen von der Aggregat- bis zur Landschaftsskala erwies sich als essenziell für das Verständnis der C- und N-Dynamik in der Landschaft. Aufgrund ihrer Funktion als Senken für organisches Material sowie durch die Alteration der Umweltbedingungen im Einzugsgebiet sind kleine Inlandwasserkörper Schlüsselelemente für die C- und N-Dynamik in landwirtschaftlich genutzten Moränenlandschaften. Ihre Rolle als potentielle Netto C- und N-Senken oder -quellen in der Landschaft muss jedoch durch weitere Studien mit längeren Untersuchungszeiträumen und detaillierten Messungen von C- und N-Flüssen gezeigt werden.

1. Introduction

1.1 Motivation

Understanding the processes that regulate carbon (C) and nitrogen (N) dynamics in landscapes is crucial in order to make solid predictions on global climate change impacts on the environment and human society (Houghton, 2007; Ussiri and Lal, 2013). Landscapes can be regarded as spatial heterogeneous areas consisting of different landscape structures that encompass both terrestrial and aquatic ecosystems (Premke et al., 2016). Yet, studies attempting to estimate landscape C dynamics often account for terrestrial ecosystems solely, therefore neglecting the role of aquatic inland ecosystems that may considerably increase the C budget of a landscape (Cole et al., 2007). Furthermore, though wetlands and their riparian zones play profound roles in N dynamics of a landscape (Merbach et al., 2002; Verhoeven et al., 2006; Ussiri and Lal, 2013), but are often ignored when trying to assess the N dynamics of a landscape.

Recent estimates suggest that the soil organic carbon (SOC) stock is around ~4000 Pg C and thus higher than the global vegetation and atmosphere C reservoirs combined (IPCC, 2013). As such, even small transformations of SOC into greenhouse gases (GHG) may considerably increase GHG concentrations in the atmosphere (IPCC, 2013). Past estimates suggest that agriculture accounts for ~50 % of global methane (CH_4) and for ~60 % of nitrous oxide (N_2O) emissions in 2005 (Smith et al., 2007). Agricultural landscapes are therefore under pressure to keep SOC belowground and prevent SOC from transformations into CH_4 and CO_2, which is in a conflict of interest with their function as ecosystem services. While many studies focus on SOC dynamics in agricultural landscapes solely (e.g. van Oost et al., 2007; Doetterl et al., 2015; Nadeu et al., 2015), microbial transformations of N into N_2O and NH_3 especially after fertilization practices highlights the importance of N dynamics in agricultural landscapes (Webb et al., 2010; Wolf et al., 2014). Today, agricultural lands occupy 30% to 40% of the earth‘ s ice-free surface (Foley et al., 2005; Smith et al., 2008). Agricultural landscapes show strong interactions between land-use, topography, soil types, microbial activity and climate. To date, large uncertainties especially remain on how land-use and management and climate affect biogeochemical cycles potentially altering the C and N dynamics of the landscape (Doetterl et al., 2016; Premke et al., 2016).

Terrestrial and aquatic C and N dynamics are closely linked to each other because of C, nutrient and mass transfer between both systems. New data show that standing freshwater bodies ≤ 10 ha make up to 10 % (Verpoorter et al., 2014) and ponds < 0.1 ha constitute 8.6 % (Holgerson and Raymond, 2016) of the global inland water surface area. These water bodies are characterized by high perimeter-to-area ratios emphasizing the influences of the littoral zone and allowing for strong aquatic-terrestrial interactions (Palik et al., 2001). Today, there is still a debate about C fluxes in these small ponds and impoundments: on the one hand, they are

regarded as C sinks through high OC burial in sediments (Stallard, 1998; Downing et al., 2008) and on the other hand and more recently, they have been identified as hotspots for C cycling in landscapes (Cole et al., 2007; Tranvik et al., 2009; Aufdenkampe et al., 2011; Buffam et al., 2011; Premke et al., 2016).

To successfully estimate terrestrial ecosystem C and N dynamics it is therefore essential to understand the underlying mechanisms of the interactions between the aquatic and terrestrial domains (Premke et al., 2016). In agricultural landscapes in general, beside biological activity (microbial decomposition, plant productivity), and intrinsic soil properties (e.g. texture, moisture, and aggregation), spatio-temporal patterns of SOC largely depend on extrinsic factors like climate, management activities and erosion (Kirkels et al., 2014; Doetterl et al., 2016), with the latter regarded as redistributing large amounts of SOC in moraine agricultural landscapes (Doetterl et al., 2012; Aldana Jague et al., 2016; Sommer et al., 2016).

Moraine landscapes cover around 1.6×10^{12} m^2 of cool-humid climate regions in the northern hemisphere and are often of agricultural use (Sommer et al., 2004). The moraine landscape of NE Germany represents an ideal investigation area since it is widely populated by small (< 1 ha) water bodies, the so-called kettle holes, that are interspersed in the landscape (Kalettka and Rudat, 2006). Hence, they pose the challenge at different spatial scales of organization, which help to characterize the major processes regulating the C and N dynamics across scales: from aggregate to the landscape level. According to Sun et al. (2012) and Zhao and Liu (2014), the sampling density largely determines SOC estimates in agricultural landscapes in general and in the moraine agricultural landscape of NE Germany in particular (Miller et al., 2016). Therefore, investigating C and N dynamics even at small scales and including small water bodies is crucial because the sole focus on the landscape scale may not consider small scale heterogeneities of C and N dynamics and the underlying processes (Kirkels et al., 2014; Hanson et al., 2015; Premke et al., 2016). Moreover, understanding the underlying driving C and N mechanisms at individual scales will allow for better policies to protect and enhance existing SOC stocks and ensure sustainable use of soils (O'Rourke et al., 2015).

1.2 Biogeochemical plant-atmosphere-soil interaction in complex agricultural landscapes

Crop productivity is the key element in agricultural landscapes to fulfill their function as food supplier. Climate variability may significantly drive crop production even in fields with high crop yield (Kang et al., 2009). We can expect significant impacts on crop productivity as result of the ongoing global climate, which leads to a rise of carbon dioxide (CO_2) in the atmosphere, a temperature increase and more extreme climatic events such as drought (Olesen and Bindi, 2002; Kang et al., 2009). Climatic impacts on plant growth, i.e. via precipitation, may already be investigated at the landscape scale when microclimate variability exists.

In addition to nutrient availability and CO_2 for photosynthesis, plant productivity heavily relies on water availability. Precipitation is the ultimate source of water in the soil (Vepraskas and Craft, 2016). The vegetation also strongly interfered with the landscape water cycle since plants take up water through their roots during photosynthesis, which is either incorporated (to a very small part) into their biomass or emitted back to the atmosphere through transpiration and thus this water cannot function as groundwater recharge. Provided that sufficient water is available, plants open their stomata and assimilate C while transpiring water (Saurer et al., 1995). However, when the plant is water-stressed, then the photosynthetic activity and therefore plant productivity will be reduced. Changes in the water availability directly leads to changes in the assimilation rate of C, therefore altering the C cycle of the landscape. Assuming now microclimate variability in a given landscape, we can expect differences in the C assimilation rate over the landscape for particular plant species. After plant death, plant biomass enters the soil, where it undergoes and decomposition processes and contributes to the soil organic matter (SOM) pool. Consequently, the C input into soils will be reduced in more dry areas. This directly illustrates the feedbacks between climate, plant productivity and C dynamics in the landscape. Since agricultural crops have been have developed for specific traits, climate variability may have profound impacts on resisting water deficit of individual plant species (Varshney et al., 2011).

Water availability to plants does not necessarily directly depend on precipitation, but also on the topographic shape of a landscape. The infiltrated water percolates through the pore space following hydraulic gradients. Depending on hydraulic gradients and the soil matrix, the water can remain in the soil where it is either taken up by plants, or directly lost through evaporation, or it can act as groundwater recharge (Vepraskas and Craft, 2016). With respect to the latter, water can collect in wet depressions changing the soil moisture of the adjacent area and providing a water source to plants depending on the topography. Thus, we may expect increasing plant productivity around small wet depressions within an agricultural field.

Next to plant productivity, soil moisture is a key player for the retention of SOM (Sierra et al., 2015). Soil fauna including earthworms, fungi and microbes decompose SOM. While on more elevated landscape positions aerobic microbial decomposition overwhelms, aerobic microbial activity is inhibited in more wet areas due to less oxygen (O_2) availability because the pore space is blocked by water (Trumbore, 2009). The combined effects of plant productivity and microbial decomposition taking place at small scales as a result of topography can therefore directly drive the C and N dynamics of the landscape. Another topographic consequence on C dynamics is the transport of soils by erosion, which is a widespread phenomenon in arable landscapes that can alter the distribution and fate of SOM (Lal, 2003; Doetterl et al., 2016). As such, the mechanical stress during the transport of soil particles during water and wind erosion leads to a breakdown of aggregates and makes SOC susceptible to microbes (Lal, 2003). This

process may considerably impact the C dynamics of agricultural landscapes. However, there is still a debate ongoing whether soil erosion acts as C sink for atmospheric CO_2 (Stallard, 1998; Berhe et al., 2007; van Oost et al., 2007) or source (Lal, 2008). The criterion whether a watershed acts as CO_2 sink is met when the combined effects of dynamic replacement of eroded C by the assimilation of new photosynthate (Harden et al., 1999) and reduced microbial decomposition in the depositional area compensate for C losses through decomposition and leaching at erosional positions (Berhe et al., 2007; Ito, 2007).

Soil erosion in agricultural landscapes is strongly enhanced via land-management practices. Conventional tillage management is common in non-organic farming and enhances the translocation of soil particles, which ultimately reshapes the landscape (Beniston et al., 2015). On smaller scales, tillage favors the breakdown of macro-aggregates and makes the OM more susceptible to microbial decomposition (Paustian et al., 2000; Six et al., 2000). As a second consequence, long-term and strong erosion may remove sorptive minerals and destroy soil matrixes, which may cause water and nutrient losses and in the end reduces plant productivity (Doetterl et al., 2016). With respect to moraine landscapes, tillage erosion can expose the glacial tills with their low clay contents reducing plant growth.

An important practice to improve soil fertility and increase crop yields is the addition nutrients via the application of fertilizers. These may include chemical fertilizers such as urea or ammonium phosphate, or organic manure and compost derived from livestock. The resulting nitrate (NO_3^-), ammonium (NH_4^+) and organic N (e.g. amino acids) are taken up by plants and increase plant productivity and plant N level (Choi et al., 2006). After plant death, the N liberated during decomposition contributes to the soil N pool. Since compost may lead to higher soil N levels than the application of chemical fertilizers solely (e.g. Choi et al., 2003), the fertilization pathway may lead to legacy effects on the N levels of a field. Fertilization therefore strongly changes the N cycle, which can be characterized as open N in arable fields. Important N losses are through leaching and gaseous N losses especially after fertilization (Goulding et al., 2000; Zech et al., 2011). Soil fertility is further improved via catch crops to increase the humus and thus SOC content (Poeplau et al., 2015) as well as to increase soil N content since catch crops retain N from leaching (Constantin et al., 2011). In addition, soil fertility is improved via crop rotations including species differing in their C and N contents. For instance, primary crop species and catch crops can vary in their C:N ratios provided that they are not limited by N (Heal et al., 1997). As such, plant litter with high C:N ratios may cause microorganisms to immobilize N leading to lower decomposition rates, while plant litter with low C:N ratios can be preferentially decomposed since N is no longer the limiting element (Wang et al., 2008; Zhou et al., 2008; Berhe, 2012). C and N dynamics are additionally altered depending on whether the straw leftovers are removed or remain on the fields (Blanco-Canqui and Lal, 2007; Saffih-Hdadi and

Mary, 2008). Consequently, the complex plant cultivation together with fertilization history will considerably alter the C and N dynamics on a field.

Next to arable fields, agricultural landscapes consist of various landscape structures such as forests, grasslands, fallows, hedgerows, villages and water bodies that are present over a range of soil types and topography (Roschewitz et al., 2005). There are not only different landscape structures, but their intrinsic biogeochemical cycles may vary themselves. As such, grasslands can be used for different purpose like pasture, hay and silage production or can be of no use. Furthermore, some grasslands may experience chemical fertilizer or slurry input as an additional N source altering the N cycle of these ecosystems. With respect to forests, deciduous, coniferous or mixed type forests may be different in their C and N dynamics also depending on age and underlying soil types (Bauhus et al., 1998; Côté et al., 2000). Without anthropogenic inputs the N cycle may be regarding closed (Zech et al., 2011). However, forest N dynamics may further be altered by land-management activities performed on adjacent fields. Land-use changes like the transformation of forests, grassland and wetlands into arable fields to gain more land for food and biofuel production are common all over the world. Several studies showed that starting land-management, the removal of old and the introduction of new plant species considerably change the C and N dynamics of a landscape while often decreasing SOC stocks (Houghton and Goodale, 2004; Poeplau et al., 2011).

Given both the various impacts on the biogeochemical cycles due to land-use changes and management practices as well as the complexity described by different landscape structures, makes it challenging to precisely assess C and N dynamics in agricultural landscapes. We are therefore challenged to develop tools, which may visualize these complex dynamics variable over space and time based on the primary drivers land-use and management and climate.

1.3 The Quillow catchment – a hummocky agricultural landscape in NE Germany

The investigation area from this study is located in the Quillow catchment (~168 km^2) as part of the young and hummocky moraine plain of NE Germany that is intensively used for agriculture. The Quillow catchment is part of the Uckermark region, located west of the town Prenzlau and covers parts of the federal states Brandenburg and Mecklenburg-Vorpommern. The name ‘Quillow catchment’ goes back to the Quillow, which is a stream that drains the Quillow catchment from west to east until it flows into the river Ucker close to Prenzlau.

The settlement and the modulation of land in the Uckermark region started in the 12^{th} century that caused deforestation and led to enhanced agricultural use (Kalettka et al., 2001; Bayerl, 2006). As such, the proportion of agricultural and pasture use was around 47 % in 1864 (Müller, 1998). In the 18^{th}/19^{th} centuries, agrarian reforms were carried out, which not only led to the separation of fields, but also improved the value of the agricultural soils via dewatering of

wetlands (Bayerl, 2006; Kleeberg et al., 2016a). Agricultural intensification due to the 'Reichsnährstandssgesetz' during the World War II resulted again in widespread land clearance and the first introduction of fertilizers to improve soil fertility (Neyen, 2014; Kleeberg et al., 2016a). Further agrarian reforms such as the 'Bodenreform' and the 'Flurneuordnung' carried out the German Democratic Republic (GDR), led in turn to the consolidation and collectivization of agricultural fields with more than 200 ha, industrialization and the absence of erosion-inhibiting structures (Bayerl, 2006; Neyen, 2014; Kleeberg et al., 2016a. Finally, the reunion of the GDR with the Federal Republic of Germany (FRG) introduced new European Union (EU) and German laws that again impacted agricultural use (Kleeberg et al., 2016a).

The hummocky topography of the Uckermark has been shaped during repeated advances and retreats of glaciers during the Weichselian glaciation (Lischeid et al., 2016). The altitude ranges from −1 to 140 a.m.s.l. (Kleeberg et al., 2016a). Owing to the young at of the landscape, the widespread land clearance and agricultural intensification, soils are prone to water and wind erosion (Deumlich et al., 2010). Together with soil redistribution via tillage, the soil landscape is today characterized by a spatial 3D continuum typical for glacial landscapes consisting of mainly sandy to loamy soils (Sommer et al., 2008). However, due to the numerous erosion processes, soils are in a continuous change (Rieckh et al., 2014). In hummocky moraine landscapes, the topsoil is the uppermost due to tillage well-mixed layer referred to as Ap horizon, while the subsoil comprises of the clay-rich Bt horizon underlain by the carbonate-rich glacial till, the C horizon (Fig. 1.1) (Gerke et al., 2010; Deumlich et al., 2010; Gerke and Hierold, 2012). Non-eroded Luvisols (LV) with undisturbed Ap-Al-Bt-C sequences prevail on plateaus, while the relatively sandy Al horizon is a result of the vertical downward transport of clay. Calcaric Regosols (caRG) prevail on steep slopes, in which the C horizon is already underlying the Ap horizon (FAO classification, IUSS Working Group WRB, 2014). As such, these soils are discernible by the lighter colors in the landscape. Mid slopes are characterized by Eroded, sometimes also Calcic Luvisols (eLV) with the typical Ap-Bt-C sequence. Colluvic Stagnosols (coST) occur on footslopes with Sw and Sd horizons resulted from stagnating water. However, Gleysols (GL) can be found when groundwater affects the soil. Brownish and darker Colluvic Regosols (coRG) with M horizons indicating deposited material are found in depressions. These topographical depressions may have been or are still filled with water during longer periods, in which case Histosols (HS) are the result of the formation of peat bodies. Often, these depressions are referred to as kettle holes.

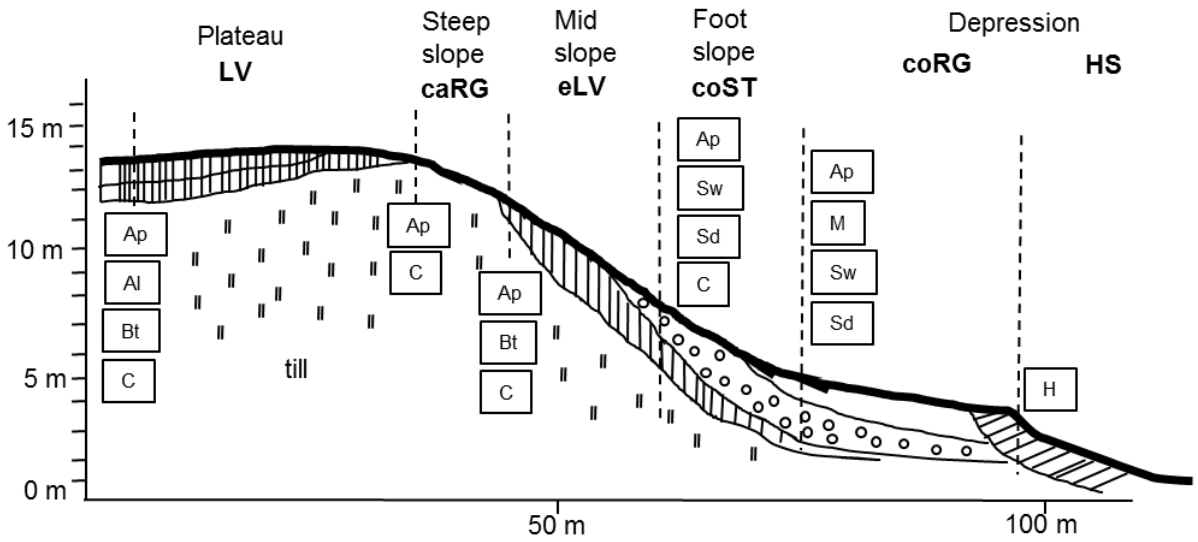

Fig. 1.1. Schematic cross-section through the hummocky moraine landscape of NE Germany with locations of characteristic soil profiles (dashed vertical lines) and accompanied soil horizons (in boxes) as well as the typical geomorphic structures and their soil types (adapted after Gerke and Hierold, 2012). The soil classification is based on the classification the FAO, IUSS Working Group WRB (2014): LV = Luvisol; caRG = Calcaric Regosol; eLV = Eroded Luvisol; coST = Colluvic Stagnosol; coRG = Colluvic Regosol; HS = Histosol.

1.4. Kettle holes in the Quillow catchment and their linkage to the terrestrial environment

Kettle holes (German: Sölle or Toteislöcher) are widespread features in the Quillow catchment. They can be best described as small pond-like depressional wetlands of glaciofluvial origin. Similar water bodies can be found around the world: in northern America where they are commonly termed 'pot holes' (Euliss et al., 2004; van der Kamp and Hayashi, 2009), in other regions of central Europe like Poland (Gołdyn et al., 2015), northern Europe and Asia. Kalettka and Rudat (2006) estimated that 150,000 to 300,000 kettle holes with depressions ranging from 0.01 to 3 ha are present in terminal and ground moraines of NE German that covers approximately 38,000 km^2. Since in Germany standing water bodies >1 ha are defined as lakes by nature, the water body of a kettle hole may not exceed 1 ha (Kalettka and Rudat, 2006). Kettle holes can be primarily found in arable fields with up to 40 per km^2 (Fig. 1.2), where they cover approximately 5 % of arable land (Kalettka et al., 2001; Kalettka and Rudat, 2006). They are primarily located in agricultural fields, but also occur in grasslands and forests.

Fig. 1.2. Aerial photograph of the moraine landscape of NE Germany with several kettle holes distributed in a rapeseed field (from Premke et al., 2016; picture: G Verch).

Kettle holes were formed due to the delayed melting of buried dead ice blocks after the discontinuous retreat of the Weichselian glaciers approximately 12,000 to 10,000 years ago (Kalettka et al., 2001). 'True' kettle holes developed on top of post-glacigenic muds as sealing layers that allowed water to trap in (Kalettka et al., 2001). These kettle holes bear up to 8 m thick fen mires due to organogenic silting up of depressions in natural woodland (Kalettka et al., 2001; Merbach et al., 2002). However, some depressions remained dry due to water deficiency and because they were just relief-caused depressions resulted from the undulated glacial ice (Kalettka et al., 2001; Merbach et al., 2002). The deforestation starting in the 12th century resulted in low water retention in the uplands and increased erosion leading to flooding and continuous silting up of the 'true' kettle holes again, which caused a decrease in size of the kettle holes (Kalettka et al., 2001; Merbach et al., 2002). Furthermore, the former dry depressions were flooded and referred to as 'pseudo' kettle holes, which lack of post-glacigenic muds, but may comprise of several dm thick peat layers (Kalettka et al., 2001; Merbach et al., 2002). With intensification of agriculture after 1950, kettle holes became obstacles in the agricultural fields and attempts were made to seal or drain them (Kalettka et al., 2001). Today, kettle holes are protected by law because they are biodiversity havens (Pätzig et al., 2012), but protection strategies are not specific enough and are often ignored by farmers (Kalettka and Rudat, 2006). Based on geomorphological and hydrological variables of 268 kettle holes (hydroperiod, shore overflow tendency, depth, area, form, shore width and slope) as well as those of their catchments (area, wetland to catchment area ratio, relief), Kalettka and Rudat (2006) defined 10 hydrogeomorphic types that are regarded to support kettle hole conversation strategies.

Due to the young age of the moraine landscape, stream networks could not fully develop yet and therefore most kettle holes are not connected to any streams via groundwater flow (Lischeid and Kalettka, 2012). Kettle holes receive water input primarily in winter and early spring via snowmelt and runoff over partially frozen soils, direct precipitation, and seasonal lateral flow (van der Kamp and Hayashi, 2009; Gerke et al., 2010; Shaw et al., 2012). Water losses are through evapotranspiration, spillover, and lateral shallow groundwater recharge (Berthold et al., 2004; van der Kamp and Hayashi, 2009). Kettle holes can be temporarily in contact with shallow groundwater potentially resulting in discharge or recharge from the groundwater (van der Kamp and Hayashi, 2009; Heagle and others, 2013). Given their location in depressions, kettle holes are especially prone to evaporation as any other stagnant water bodies. To date, no studies exist that describe the connectivity to ground water aquifers nor studies exist that quantify the water losses of kettle holes of NE Germany, though attempts were made to assess water losses of prairie pot holes in northern America (e.g. Ferone and Devito, 2004; Hayashi et al., 1998). Further uncertainties remain on the timing and magnitude of water losses depending on land-use (arable fields, forests, grasslands). Due to climate variability, geomorphic site conditions including site conditions, many kettle hole experience pronounced wet-dry cycles.

The duration of the wet period of a kettle hole over the year is defined as hydroperiod (Kalettka and Rudat, 2006). The resulting pronounced wet-dry cycles can lead to the complete drying and rewetting of some sediments (Johnson et al., 2004; van der Kamp and Hayashi, 2009) while others may stay submerged or partially submerged over the year. Strong water level fluctuations result in changes in OM dynamics and O_2 exposure during desiccation (Boon, 2006). The shift in redox conditions, from anoxic to oxic, affect organic matter availability for microbial degradation (Foulquier et al., 2013) and can change microorganism communities or their carbon metabolism, resulting in accelerated OM turnover (Fromin et al., 2010; Reverey et al., 2016; Weise et al., 2016). While in submerged conditions, anoxia is a common phenomenon and causes OM to be less efficiently used for decomposition by heterotrophic microorganisms and could therefore lead to a more intensive burial of OM in the sediment (Sobek et al., 2009). During long-term wet conditions, internal primary production via phytoplankton and periphytic algae and OM from submerged and floating macrophytes within the kettle hole can be an important autochthonous OM source (lignin-poor OM). On the other hand, desiccation can lead to the encroachment of emergent macrophytes into kettle holes as external OM sources (= allochthonous OM rich in lignin), which may subsequently result in the formation of peat bodies (Gaudig et al., 2006). Thus, the wet-dry cycles impact the environmental site conditions and leave an imprint in the sediment record as distinct layers that may yield information about the sources of OM and the degree of OM microbial decomposition.

Kettle holes lie on the boundary between the aquatic and terrestrial domain and are closely linked to their catchments. Due to their location in depression they receive substantial matter input. These include soils via erosion triggered by tillage (Frielinghaus and Vahrson, 1998), plant biomass, nutrients (nitrogen and phosphorous) due to fertilization (Lischeid and Kalettka, 2012) and heavy cation contaminants originating from artificial fertilizers (Gołdyn et al., 2015). Especially the input of nutrients is problematic because it can lead to eutrophication. Given large shifts in hydroperiod, high eutrophication and resulting high autochthonous OM production and its strong effects on sediment OM transformations, kettle holes might be a potential sources of CO_2 and other trace gases (Merbach et al., 2002; Premke et al., 2016). Furthermore, the general form of land-use, land-management practices have a large influence on terrestrial biogeochemistry. However, broad investigations of kettle hole biogeochemistry in the landscape context are few and we do not know the extent to which external (i.e. terrestrial) factors such as fertilization affect kettle hole internal OM turnover or how this is represented in the sediment column. This is information is crucial do understand kettle holes' potential as sinks for OM in agricultural landscapes. Due to the water logging of kettle holes, their surroundings can be characterized by steep environmental gradients in moisture and texture (Merbach et al., 2002). Therefore, the moisture gradient may also influence plant productivity and SOM dynamics in the kettle hole catchment.

1.5 Soil organic matter dynamics – small scale processes and their importance on the landscape scale

Dead plant material enters the soil where it undergoes biological, physical and chemical transformations processes that decompose dead plant compounds on different rates depending on their chemical composition. Next to plant-derived molecules, molecules of microbially origin are the second important class in SOM (Schmidt et al., 2011). While microbial decomposition mineralizes a part of OM into inorganic CO_2 – therefore termed mineralization – other molecules undergo further transformation and condensation processes into macro-molecules (humification) that where long time regarded as stable against further decomposition (chemical 'recalcitrant') and allowed for long-time stabilization of OM in soil (Stevenson, 1994; Lehmann and Kleber, 2015). Nowadays, this traditional view has changed into an emergent view in which SOM can be conceptualized as a continuum of progressively decomposing organic compounds encompassing intact plant material and low molecular, highly oxidized OM such as carboxylic acids (Schmidt et al., 2011; Lehmann and Kleber, 2015). The heterogeneous bulk SOM can be experimentally subdivided into more homogenous fractions of varying mean residence time (MRT) resulting from differences in their stabilization against microbial decomposition. Because of their different turnover dynamics, such fractions have contrasting ecological functions.

For example, organic particles with a recognizable morphological structure made up of residues from plants and animals serve as a readily decomposable substrate for soil organisms (Gregorich et al., 2006). Organic particle fractions from surface soils are most sensitive to climatic, land-use or management changes because of their relatively fast turnover and close connection to litter input (Bird et al., 2008). Furthermore, a small part of the soil OM can be present in soil as dissolved OM (DOM) in pore water. OM that is found in the dissolved phase is highly mobile and important when considering vertical (percolation) and lateral (water erosion) transport processes (e.g. Kaiser and Kalbitz, 2012). The DOM is considered in part easily biodegradable (Gregorich et al., 2003; von Lützow et al., 2007) because aqueous mobilization of SOM is postulated to be a critical first step towards its decomposition. However, organic particles as well as DOM in soils are not labile in total but consist of sub-fractions with various degrees of lability (Kalbitz et al., 2003). An explanation might be that organic particles as well as DOM act as binding agents during the formation of aggregates in soils (Golchin et al., 1994; Six et al., 2000).

The long-term stabilization of OM (MRT > 100 years) in aerated, temperate topsoils against microbial decomposition is highly important for the function of soils to act as a long-term C-sink and to mitigate climate change. Here, microbial access to OM is hindered due to (i) aggregation (Six et al., 2004; Bachmann et al., 2008) (ii) interactions of the OM with polyvalent cations (chelate, crosslinking) (e.g. Masiello et al., 2004; Mouvenchery et al., 2012), (iii) associations of the OM with mineral surfaces via polyvalent cations (cation bridges) (von Lützow et al., 2006), or (iv) direct bond formation between OM and mainly Fe or Al oxides (ligand exchange reactions) (Mikutta et al., 2007; Kleber et al., 2015).

An understanding of the key factors and processes that regulate the OM stabilization in soils requires the separation of stabilized OM fractions according to specific mechanisms (Mikutta et al., 2006). During the last decades, the scientific community has developed numerous physio-chemical. These techniques are physically based only including particle-size separations (Balesdent, 1996), density-separations (Sollins et al., 2009) or combinations of both (Moni et al., 2012). On the other hand, different extraction mediums are used to extract OM such as simply water (Kaiser et al., 2010) or chemical agents (Wagai et al., 2013).

The amount and percentage of OM bound via organo-mineral associations varies greatly between soil types and depth (Kögel-Knabner et al., 2008). Soil erosion leads to the downslope transport of DOM but also of OM that is associated to clay- and silt-sized particles. In addition, organic particles either free or released from disintegrated aggregates (due to tillage or raindrop impact) are preferentially targeted by erosive transport. Especially clay- and silt-sized mineral particles < 53 µm are usually enriched in OC relative to the bulk soil (Hu et al., 2016) as they comprise of comprise of complexed, poorly crystalline and well-crystallized mineral phases as well as clay minerals (e.g. oxides, layer-silicates), which can interact with OM (Kaiser et al.,

2007; Doetterl et al., 2015). For instance, erosion may remove reactive minerals phases from erosive areas and accumulate them in depositional areas (Berhe et al., 2012; Ellerbrock et al., 2016). Their preferential transport during erosion events consequently leads to higher SOC concentrations in depositional profiles (Doetterl et al., 2016). As such, understanding OM associated via mineral phases at small scales is crucial to make solid estimates on the SOC distribution in the landscape (O'Rourke et al., 2015).

Where the transport capacity is high enough, the mobilized organic and clay-sized particles might not be deposited but instead may end up in the sediments of water bodies (Stallard, 1998). Yet, large uncertainties remain on the fate of OM in the aquatic ecosystems especially related to changes in climate and land-use (Marín-Spiotta et al., 2014). Stabilization mechanisms of OM in sediments substantiality differ from soils due to the water saturation (Hedges and Oades, 1997). As such, macro-aggregate formation is inhibited, partly because of bioturbation. The amount of OM and stabilization mechanism greatly varies with the oxygen exposure time (Arnarson and Keil, 2007). Organic particles can dominate the OC in sediments with very short oxygen exposure times of < 1 year (anaerobic stabilization), while highly stable mineral-aggregated OM can prevail over oxygen exposure times of several years and even decades (Arnarson and Keil, 2007). During longer exposure times of centuries to millennia, the adsorption of OM to mineral surfaces is the major stabilization mechanism in marine sediments (Mayer, 1994; Hedges and Keil, 1995; Arnarson and Keil, 2007). Recently, Lalonde et al. (2012) found a preferential stabilization of OM via reactive iron surfaces. However, the pathway and as such the amount of OM bound via these iron phases was shown to change from complexation (anaerobic conditions) to poorly and well-crystallized iron phases (Rue and Bruland, 1995; Lalonde et al., 2012). In general, stabilization mechanisms of sedimentary OM are still largely unknown. Given the water fluctuations of kettle holes with longer wet periods or pronounced wet-dry cycles, the amount and pathway of OM associated in sediments can show large variations over the landscape.

1.6 Stable isotopes and their use in environmental sciences

All those described processes may manifest in the stable isotopic composition of OM, which therefore represents an ecological archive. Isotopes are forms of the same element that differ in the number of neutrons in their nucleus (Fry, 2006). The five elements that cycle with OM and that are of particular interest are C, N, O, H and S. Stable isotope ratios are described by the ratio *R* of the heavy isotope to the light isotope in a sample and referenced to an international standard following EQ. 1.1:

$$\delta = \left(\frac{R_{sample}}{R_{standard}} - 1\right) \cdot 1000 \qquad 1.1.$$

Given the usually low differences between the ratio of the sample and the standard, stable isotope ratios are reported in δ notation by multiplying with 1000. In this study, I only focus on C, N, O, and H and as such the ratios are: $^{13}C/^{12}C$ for $\delta^{13}C$, $^{15}N/^{14}N$ for $\delta^{15}N$, $^{18}O/^{16}O$ for $\delta^{18}O$ and $^{2}H/^{1}H$ for δD.

Stable isotopes fractionate during biotic and abiotic processes, i.e. one isotope is preferred against another (Fry, 2006). As such, the difference between the natural isotopic abundance of the educt and the product can be used to gain insights into complex environmental processes (Brüggemann et al., 2011). Two principles of isotopic fractionation occur, which can be related to their system. In a closed system, equilibrium fractionation tries to minimize the energy in a system, i.e. isotopes will be distributed to minimize the vibrational, rotational, and translational energy (White, 2015). This fractionation is primarily temperature-dependent and reversible. Fast, incomplete or unidirectional processes or reactions occur in open systems leading to irreversible kinetic isotopic fractionation (White, 2015). Biologically mediated reactions are typical for causing kinetic isotopic fractionation. As such, plants fractionate against the heavier $^{13}CO_2$ and take up the lighter $^{12}CO_2$ during photosynthesis, which is then assimilated into their biomass. This preference of the light isotope will leave the plant leaf depleted in the heavy ^{13}C. The depletion is plant dependent. C_3 (3-carbon) plants like trees usually have $\delta^{13}C$ values around -28 ‰, while C_4 (4-carbon) plants like corn or sugar cane have higher $\delta^{13}C$ values around -13 ‰ (Farquhar et al., 1989). This difference in $\delta^{13}C$ between C_3 and C_4 plants is due to differences in primary CO_2 fixation (Farquhar et al., 1982). With respect to C_3 plants, the C isotopic discrimination during photosynthesis $\Delta^{13}C$ can be described by the simplified Farquhar model, which only accounts for the isotopic fractionation during the stomata diffusion *a* with 4.4 ‰ and the discrimination during carboxylation of RuBisCO *b* with 27 ‰ following EQ. 1.2 (Farquhar et al., 1982; Farquhar et al., 1989):

$$\Delta^{13}C = a + (b - a) \cdot \frac{c_i}{c_a} \qquad 1.2.$$

Here, c_i is the intracellular CO_2 content in the stomata and c_a represents the ambient atmospheric CO_2 concentrations of ~380 ppm. The $\Delta^{13}C$ can also be calculated when the $\delta^{13}C$ of the atmosphere with -8 ‰ ($\delta^{13}C_a$) and of the plant leaf ($\delta^{13}C_p$) are known (Farquhar and Richards, 1984) following EQ. 1.3:

$$\Delta^{13}C = \frac{\delta^{13}C_a - \delta^{13}C_p}{1 + \delta^{13}C_p/1000} \quad 1.3.$$

The WUE_i in µmol C^{-1} describes the ratio of carbon assimilated *A* to water transpired *E* (Farquhar and Richards, 1984). WUE_i is generally not directly linked to *E*, but shows a negative correlation with the ratio of c_i/c_a. The ratio of c_i/c_a reflects in turn the balance between *A* and the stomatal conductance g_s after EQ 1.4 (Seibt et al., 2008):

$$A = g_s \cdot (c_a - c_i) \quad 1.4.$$

Given that g_s and the stomatal conductance of the water vapor g_{sw} are related by the constant factor 1.6 (g_{sw} = 1.6 g_s), the WUE_i calculates according to EQ. 1.5 as follows (Saurer and Siegwolf, 2007; Seibt et al., 2008):

$$WUE_i = \frac{c_a}{1.6} \cdot \frac{b - \delta^{13}C_a + \delta^{13}C_p}{b - a} \quad 1.5.$$

Consequently, there the WUE_i can be directly calculated based on the $\delta^{13}C$ of the plant leaf. Provided that sufficient water is available, plants open their stomata to take up $^{12}CO_2$ resulting in a high c_i, while assimilating less carbon in their biomass (low *A*) and transpiring water (high g_s). This will result in lower $\delta^{13}C$ values. However, during drier conditions, plants close their stomata to avoid water loss (low g_s), whereas no new $^{12}CO_2$ can be taken up (low c_i), but carbon will be assimilated (high *A*), leading in the end to higher $\delta^{13}C$ values. As such, the $\delta^{13}C$ of plant can be used as a proxy of the water availibility to a plant over time in the landscape.

In contrast to C, N sources to plants a more complex. N sources encompass NH_4^+, NO_3^-, dissolved organic nitrogen (DON; e.g. amino acids) and atmospheric N_2 in N limited systems (Houlton et al., 2007). The enzymatic formation of these N sources in the soil system is often accompanied by the discrimination against the heavy isotope ^{15}N (Robinson, 2001). As such, nitrification causes an enrichment in ^{15}N in the remaining NH_4^+ in aerobic soils, while denitrification leads to higher contents of ^{15}N in the remaining NO_3^- in more anaerobic soils (Mariotti et al., 1981; Robinson, 2001; Choi et al., 2003). However, the isotopic discrimination is much larger for nitrification causing higher $\delta^{15}N$ values of the remaining NH_4^+ (Mariotti et al., 1981; Casciotti et al., 2003). It is generally accepted plants can discriminate against ^{15}N directly or indirectly via mycorrhizal fungi leading to lower $\delta^{15}N$ values in plant leaves compared to the N source (Robinson, 2001; Houlton et al., 2007; Hobbie and Högberg, 2012). However, changes in NH_4^+:NO_3^- uptake ratios, the use of atmospheric N_2 with a $\delta^{15}N$ of ~ 0 ‰, or the use of high

DON high in $\delta^{15}N$ can further change the foliar $\delta^{15}N$ (Evans, 2001; Houlton et al., 2007; Kahmen et al., 2008; Takebayashi et al., 2010). When the plants leaves remain in the system are returned to the N-soil pool by plant litter degradation, and no additional losses N inputs/occur, then the N cycle can be characterized as closed (Zech et al., 2011). In this case, with an ultimate only atmospheric N_2 source, the soil $\delta^{15}N$ could be expected to be close to 0 ‰.

However, the N cycle in agricultural landscapes can usually not characterized as closed given N losses via the harvest of plants and land-management practices as N sources. Organic manure is known to be enriched in ^{15}N due to the preferential loss of ^{14}N during ammonia (NH_3) volatilization (Kreitler, 1979; Kerley and Jarvis, 1996) and was found to range from +5 - 20 ‰ (Heaton, 1986; Yoneyama et al., 1990; Choi et al., 2003; Bateman et al., 2005). Volatilization continues after application on the field leading to high N emissions (Webb et al., 2010). Nutrients (NH_4^+, NO_3^-) originating from the manure will be enriched in ^{15}N (Choi et al., 2003). The uptake of these enriched nutrients can lead to higher $\delta^{15}N$ values in plants (Bateman et al., 2005; Choi et al., 2006; Senbayram et al., 2008). On the other hand, it is known that chemical fertilizers such as urea or ammonium phosphate are less enriched in ^{15}N as they originate from atmospheric N_2 (Choi et al., 2003; Michalski et al., 2015). Consequently, $\delta^{15}N$ of plants were found to be lower when only chemical fertilizers were applied (e.g. Choi et al., 2006). After plant death, the plant OM with its high $\delta^{15}N$ contributes to the bulk SOM leaving the soil enriched in ^{15}N (Yoneyama et al., 1990; Choi et al., 2003). As such, high $\delta^{15}N$ values of soils are indicative for an open N cycle. One way to get stronger insights into the N cycle is the calculation of the $\Delta\delta^{15}N$ as the difference between $\delta^{15}N_{plant}$ and $\delta^{15}N_{soil}$ (Amundson et al., 2003; Kahmen et al., 2008). While on global scales temperature and precipitation are of importance on the $\Delta\delta^{15}N$ (Amundson et al., 2003), differences in the NH_4^+/NO_3^- uptake ratios dominate at local scales (Kahmen et al., 2008; Takebayashi et al., 2010). Therefore, the $\delta^{15}N$ of SOM can be a complex archive of multiple processes and sources in the landscape.

An important C and N loss in soils is given by microbial decomposition, which can be also described as kinetic isotopic fraction. During aerobic decomposition, microbes preferentially take of the light isotopes ^{12}C and ^{14}C leaving the residual OM enriched in the heavy isotopes ^{13}C and ^{15}N (Torn et al., 2002; Dijkstra et al., 2008; Craine et al., 2015). This process leads to a downward increase in $\delta^{13}C$ and $\delta^{15}N$ in soil profiles (Meusburger et al., 2013). The enrichment is especially assumed in mineral-associated OM fractions and increases with density (Sollins et al., 2009; Schrumpf et al., 2013), decreases with particle size (Asano and Wagai, 2014) and is also found in chemically extracted fractions (Kayler et al., 2011). Since other studies found lower $\delta^{13}C$ with decreasing particle size (Hu et al., 2016), microbial decomposition can be variable. Furthermore, microbial decomposition is accompanied by a decrease in the C:N ratio of the residual OM because of the catabolic loss of C (Paul and Clark, 1996). However, anaerobic microbial decomposition may either lead to no enrichment or even

a decrease of the heavy isotopes in the residual OM (Lehmann et al., 2002; Menzel et al., 2013). Furthermore, reactive Fe phases are hypothesized to preferentially stabilize more labile OM enriched in ^{13}C such as carbohydrates or proteins (Lalonde et al., 2012). Consequently, the $\delta^{13}C$ and $\delta^{15}N$ of SOM and specific OM fractions can be used as tracer for microbial processing (Kayler et al., 2011), N transformation processes via aerobic or anaerobic processes (Pennock et al., 1992), land-use changes (e.g. change from C_3 to C_4 plants) (Häring et al., 2013), the encroachment of invasive plant species (Bai et al., 2013), land-management effects through fertilization (Choi et al., 2003), and the water availibility to plants.

In the hydrological cycle, water from the tropical and temperate ocean evaporates at the equator and forms clouds. As clouds move towards the poles, condensation of liquid water droplets from clouds removes the heavier isotopes ^{18}O and ^{2}H leaving the vapor in the cloud enriched in the light isotopes ^{16}O and ^{1}H (Kendall and Caldwell, 1998; White, 2015). The fractionation between the vapor and liquid phase is temperature-dependent, i.e. colder temperatures at mountain ranges will lead to lower $\delta^{18}O$ and δD values of rain (White, 2015). Secondly, the fractionation depends on the amount of water condensed from a cloud, i.e. when more water condenses, vapor and liquid be become both more depleted (Gat, 1996). This process is also termed as Rayleigh fractionation as a kinetic isotopic fractionation (White, 2015). As a consequence, precipitation will become more and more depleted in ^{18}O and ^{2}H over the continents. As such, snow as the final product will have the lowest $\delta^{18}O$ and δD values (Maclean et al., 1995). The meltwater progressively increases by a few per mil during snowmelt due to isotopic exchange between liquid meltwater and snowpack (Clark and Fritz, 1997; Taylor et al., 2001). All natural water bodies that are not prone to further kinetic isotopic fractionation, for instance via the evaporation as kinetic fractional (Gat, 1996), fall along the Global Meteoric Water Line (GMWL) expressed by the equation $\delta^{2}H = 8 \cdot \delta^{18}O + 10$ (Craig, 1961; Dansgaard, 1964).

Evaporation leads to an enrichment of the heavy isotopes ^{18}O and ^{2}H in the water body due to smaller diffusivities in air (Gonfiantini, 1986; Gibson et al., 2005). This kinetic isotopic fractionation during evaporation leads to a deviation from the GMLW indicated by lower slopes and can be best explained by the linear-resistance Craig-Gordon-model (Craig and Gordon, 1965). Evaporated water bodies have lower slopes than the GMWL ranging from 4.0 to 5.5 and cluster on the local evaporation line (LEL) (Gibson et al., 2008). The intersection point of the LEL with the GMWL describes the source water, i.e. the weighted mean isotopic composition of the local precipitation (Gibson and Edwards, 2002). Evaporation is typical for standing water bodies such as lakes, wetlands or basins (Gibson and Edwards, 2002; Wolfe et al., 2007; Yuan et al., 2011). However, soil water can also be subjected to evaporation with slopes for the LEL of < 3 due to vapor transport through the diffusion-dominated soil matrix (Barnes and Allison,

1988; Gibson et al., 2008). Therefore, the $\delta^{18}O$ and δD of a water bodies gives evidence on the source water and post fractionation processes such as evaporation.

Spatio-temporal variation in stable isotope ratios provide useful information on ecological processes given the dynamics of biological and chemical processes (West et al., 2010). A novel way of visualization the isotopic pattern of single points is the creating of isoscapes (i.e. *iso*topic land*scapes*), which can be linked to background information such as climatic parameters (Bowen, 2010). Here, an interpolation is performed between the isotopic composition of single sampling points (isotopic mapping) using a geographic mapping program such as ArcGIS (geographic information system software, Environmental Systems Research Institute 2012, Redlands, CA). The application of isoscapes ranges from small scales (isotopic variation over several meters) (Rascher et al., 2012; Bai et al., 2013; Hellmann et al., 2016), to catchment scales (Brooks et al., 2012), to continental scales (Kendall and Coplen, 2001; Still and Powell, 2010) and finally to global scales (Amundson et al., 2003; West et al., 2008).

1.7 About this study

To summarize, the C and N dynamics may vary greatly across scales as indicated by the isotopic fingerprint that can be used as a proxy for land-use changes and land-management practices, land-use changes plant response to climate, plant-soil interactions, sources of OM in soils and sediments, microbial turnover, stabilization of OM via mineral associations. The variation might be related to i) the isotopic composition of OM fractions at a single point, ii) isotope values from bulk SOM and fractions in a single field or kettle hole catchment and iii) isotope values from bulk SOM from samples covering a large number of fields and different land-use. Furthermore, the isotopic composition of sediments from kettle holes distributed in the landscape may tell us how kettle holes are interacting with the surrounding landscape and how they contribute to the C and N dynamics in the landscape. It is thus important to link the biogeochemical information imprinted on the isotope signatures across scales to capture the factors driving landscape C and N dynamics. As such, the following overall objective arises for this study:

Main objective: Identify the mechanisms that regulate the aquatic-terrestrial C and N dynamics in the moraine landscape of NE Germany at different spatial scales of organization.

To achieve this objective (*O*), this study is separated into three different chapters that represent the scales of organization: C and N dynamics in an 38.2 km^2 wide area heavily used for agriculture at the regional landscape scale (chapter 2), C and N dynamics in sediments across 51 kettle holes interspersed within the area at the regional kettle hole scale (chapter 3) and C and N dynamics in soils in the catchment of one kettle hole at the transect and aggregate scale (chapter 4) (Fig. 1.3). The aggregate scale is defined as encompassing specific OM fractions as part of the bulk SOM. To fulfill this goal, this study heavily relies on the application of stable isotope geochemistry. This study was conducted as part of the SAW project LandScales - 'Connecting processes and structures driving landscape carbon dynamics over scales' funded through the Pact for Innovation and Research of the Gottfried Wilhelm Leibniz Association.

1.7.1 Regional landscape scale

The climatic conditions, past and present land-use and management considerably drive the biogeochemical cycles in agricultural landscapes. Agricultural landscapes are complex mosaics of landscape structures, which puts a challenge on precisely assessing C and N dynamics in such systems. As such, little is known about the heterogeneities of biogeochemical cycles across fields and land-use structures, and tools are required for the visualization of these dynamics. I took advantage of isoscapes in order to understand the C and N dynamics in a

38.2 km^2 wide area of the Quillow catchment that is heavily used for agriculture (74.4 %) and encompasses with arable fields, forests and grasslands different land-use structures. I chose for a relatively dense sampling grid (250 m) in contrast to other studies that also created isoscapes, which provided us with soil and plant samples from around 600 sampling points. In this study, I created both $\delta^{13}C$ and $\delta^{15}N$ soil and plant isoscapes that helped to understand plant-soil interactions and land-management impacts. I use information on the historical land-management obtained from AgroScapeLab Quillow, Dedelow, a field station from the Leibniz-Centre for Agricultural Landscape Research (ZALF) adjacent to my study site and from the Agricultural Data Centre (DZA) located at ZALF in order to explain the isoscapes. The DZA provided further high-resolution gridded maps on the elevation, water body distribution and a precipitation map that show a slight precipitation gradient ranging from NW to SE of the study site. By using isoscapes, I expected to get strong insights into the C and N dynamics of the complex, moraine agricultural landscape of NE Germany.

Objectives:

O2.1 I expected to observe patterns in soil and plant $\delta^{13}C$ and $\delta^{15}N$ across different landscape structures (arable fields, forests, grasslands) in response to climatic conditions.

O2.2 Furthermore, I expected to detect different land-management and land-use impacts on C and N biogeochemical cycles within each land-use.

O2.3 Finally, I attempted to explore whether the isotopic signals from plants and soils in the surrounding of kettle holes are sources to OM of surface sediments in order to reveal aquatic-terrestrial linkages.

1.7.2 Regional kettle hole scale

Kettle holes are widespread in our study site (~ 290), where they make up approximately 1.4 % of the area. Given their numerous occurrence and the close linkage to their terrestrial catchments, we can assume that kettle holes considerably affect the C and N dynamics and therefore the C sequestration potential of moraine, agricultural landscapes. However, kettle holes not only occur in arable fields, where I can assume strong land-management impacts, but also in grasslands and less anthropogenically disturbed forests. Furthermore, kettle holes show strong fluctuations in water table. Both factors (land-use and hydroperiod) may affect the source and fate of OM stored in sediments from kettle holes across the landscape. I used the $\delta^{13}C$ and $\delta^{15}N$ of sediments of different depths in order to study the land-use and hydroperiod impacts on sedimentary C and N dynamics of 51 kettle holes that represented the spatial and hydrodynamic variability of the 290 kettle holes in my study site. Furthermore, I used $\delta^{18}O$ and δD isotope values of surface water to get stronger insights into the hydrology of the kettle holes.

Objectives:

O3.1 Firstly, I assumed to find differences in $\delta^{13}C$, $\delta^{15}N$ and C:N ratios from sediments of kettle holes of different land-use (arable, forest, grassland). Different environmental conditions with respect to land-use, land-management activities during the last 60 years and fluctuating water regimes were expected to have profound impacts on the OM sources (autochthonous vs. allochthonous) into kettle holes.

O3.2 Secondly, based on the fluctuating water regime that may affect the status of OM in sediments, I expected to find significant differences in $\delta^{13}C$, $\delta^{15}N$ and C:N ratios of OM between sediments from kettle holes that store water throughout the year and others that fall dry during certain periods.

O3.3 Since water losses and the connectivity to groundwater bodies are poorly understand for kettle holes of NE Germany, I aimed to characterize the magnitude of evaporation and kettle hole-groundwater connectivity based on the $\delta^{18}O$ and δD isotope values of kettle hole water over several years and from different seasons.

1.7.3 Transect and aggregate scale

The spatio-temporal distribution of OM varies greatly across topography and soil types in agricultural landscapes especially when small water bodies are interspersed in the landscape, which alter the environmental gradients such as soil moisture driving plant growth and microbial decomposition in the catchment. Erosion is a dominant mechanism in distributing OM and can be accelerated by tillage. Furthermore, fertilization can impact OM distribution by increasing plant growth. Yet, large uncertainties remain on the impact of the mechanisms on the C and N dynamics of individual OM fractions of different stability. I quantified isotopic patterns of specific OM fractions representative for freely available, aggregated and mineral-associated fractions that are indicative of OM stabilization mechanisms and sources along transects spanning topographic positions from erosional to depositional areas including aquatic sediments within a single kettle hole. I analyzed the $\delta^{13}C$, $\delta^{15}N$, OC and N contents of all obtained fractions to understand OM dynamics over the toposequence. I further related stable isotope ratios of mineral-associated OM fractions to mineralogical properties to examine possible mechanisms of OM stabilization via mineral interaction and use our isotope ratios to infer input of OM from the agricultural field into the kettle hole. Topographic indices inferred from the digital elevation model (DEM) were used to relate catchment properties to the isotope ratios.

Objectives:

O4.1 On the transect scale, I expected that the combined effects of plant growth, erosion, fertilization and microbial decomposition would explain the variability in the OC and N contents, and $\delta^{13}C$ and $\delta^{15}N$ of the bulk SOM and of specific OM fractions.

O4.2 On the aggregate scale (i.e. soil fractions), I expected OM in mineral-associated fractions to be stabilized via different binding mechanisms because I assumed a strong gradient in polyvalent cations, poorly crystalline and well-crystallized oxides, and clay- and silt-sized soil particles and different environmental conditions along the transect.

O4.3 Finally, given the assumed close connection between the aquatic kettle hole and terrestrial catchments, I expected that $\delta^{13}C$ and $\delta^{15}N$ from OM fractions of subsurface sediments to indicate a terrestrial origin.

In chapter 5, I firstly summarize the outcomes of the three individual studies 2 to 4, i.e. the identified driving mechanisms on the C and N dynamics. I provide further boxes with the major outcomes of each individual chapter. Finally, in the synthesis chapter 6, I will link the scales while discussing the implications of the mechanisms identified on each particular scale for the C and N dynamics of the complex, moraine agricultural landscape of NE Germany.

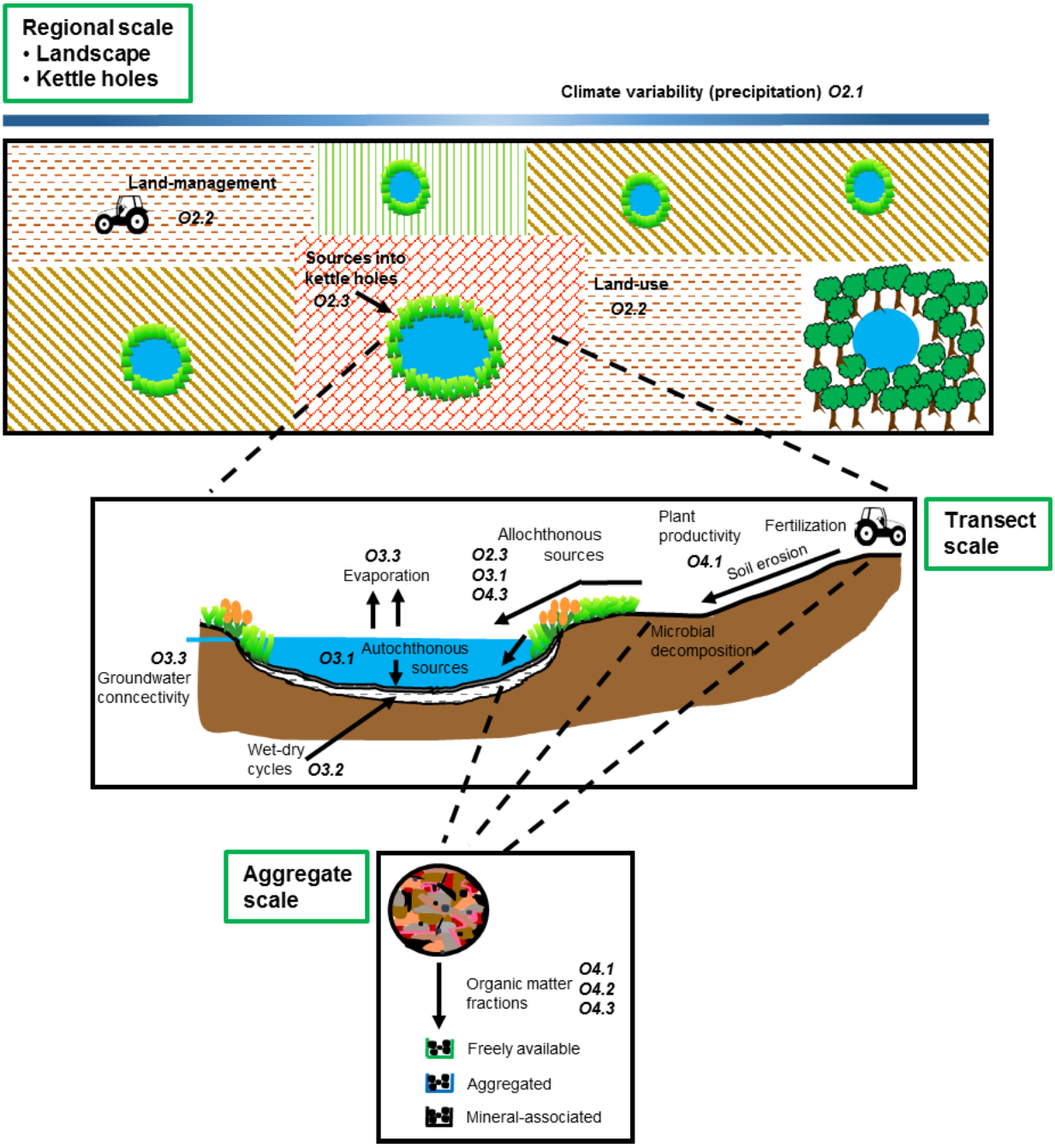

Fig. 1.3. Schematic sketch showing the scales that are target of this study, the mechanisms that may drive C and N dynamics on each scale and the objectives O (in italics), which shall be answered on each scale. On the regional scale (top), different structures indicate different agricultural fields, with a grassland and a forest highlighting the land-use complexity of the landscape. Kettle holes (blue circles with green vegetation belts) are interspersed in the landscape. On the transect scale (center), a cross-section through one kettle hole in an arable field is exemplarily shown with the major mechanisms affecting the carbon and nitrogen dynamics within the kettle hole sediment and on the surrounding agricultural field. On the aggregate scale, organic matter fractions of different stability can be different in their carbon and nitrogen dynamics as they are related to the mechanisms taking place at different topographic positions. The aggregate scale is defined as encompassing specific organic matter fractions as part of the bulk soil organic matter.

2. Regional landscape scale

Visualizing land-use and management complexity within biogeochemical cycles of an agricultural landscape

This manuscript was published in the international peer-reviewed journal *Ecosphere.* The original article was published by John Wiley & Sons Inc.:

Nitzsche K.N., Verch G., Premke K., Gessler A. and Kayler Z.E. *(2016)* Visualizing land-use and management complexity within biogeochemical cycles of an agricultural landscape**.** *Ecosphere*, 7(5):e01282. 10.1002/ecs2.1282.

A collective list of the participating co-authors and their affiliations of the manuscripts presented in this thesis can be found at the end of the thesis (List of co-authors) All references cited in the manuscripts were joint to one list (References). All figures and tables from the appendices of first two manuscripts are shown at the end of this thesis (Appendix).

2.1 Abstract

Crop fields are cultivated across continuities of soil, topography, and local climate that drive biological processes and nutrient cycling at the landscape scale; yet land management and agricultural research are often performed at the field scale, potentially neglecting the context of the surrounding landscape. Adding to this complexity is the overlap of ecosystems and their biogeochemical legacies, as a patchwork of crops fields, natural grasslands and forests develops across the landscape. Furthermore, as new technologies and policies are introduced management practices change, including fertilization strategies, which further alters biological productivity and nutrient cycling. All of these environmental, biological, and historical legacies are potentially recorded in the isotopic signal of plant, soil, and sediment organic matter across the landscape. We mapped over 1500 plant, soil, and sediment isotopic values and generated an isotopic landscape (isoscape) over a 40 km^2 agricultural site in NE Germany. We observed distinct patterns in the isotopic composition of organic matter sampled from the landscape that clearly reflect the landscape complexity. C_3 crop intrinsic water use efficiency reflected a precipitation gradient, while native forest and grassland plant species did not, suggesting that native plants are more adapted to predominant climatic conditions. $\delta^{13}C_{soil}$ patterns reflected both the long-term input of plant organic matter, which was affected by the local climate conditions, and the repeated cultivation of corn. Soil organic matter ^{15}N isotopic values also

revealed spatial differences in fertilization regimes. Forest fragments, in which the nitrogen cycle was relatively open, were more water use efficient. Sediments from small water bodies received substantial inputs from surrounding field vegetation but were also affected by seasonal drying. These isotopic maps can be used to visualize large spatial heterogeneity and complexity, and they are a powerful means to interpret past and current trends in agricultural landscapes.

2.2 Introduction

Societal demands for food, energy, shelter, and commerce have resulted in the modification of landscapes globally (Tilman et al., 2002). The ecosystem services these landscapes yield has become a point of focus as climate change and land-use disrupt essential landscape functions (DeFries et al., 2004; Foley et al., 2005). Land-use is the modality in which the land cover is changed for human purposes including management practices (Foley et al., 2005; Verburg et al., 2011). Land-use changes not only the physical appearance of the land cover but also intrinsic properties, such as plant communities, soil development, and water and nutrient cycles. Furthermore, the landscape is often broken into management units creating abrupt transitions between land-use types and landscape elements. Thus, the intensity and duration of land-use and management across a landscape is not homogenous despite the underlying connectivity in terms of topography, ground water, and soil type.

Agricultural landscapes are complex mosaics of overlapping types of land-use, ecosystems, and soils, and can be characterized by high levels of heterogeneity (Roschewitz et al., 2005). Past estimates of agricultural and pastureland range from 30-40% of the earth's ice free land (Olesen and Bindi, 2002; Foley et al., 2005), and agricultural land is under pressure to increase production and mitigate effects from climate change (West et al., 2010). Strategies to fulfill this goal include the introduction of improved crop varietals optimized for productivity, fertilizer application, irrigation, crop rotation, and land conversion, all of which impact or leave a legacy on local biogeochemical cycles (Olesen and Bindi, 2002; Tilman et al., 2002).Thus, to assess current land management and policies we need tools for observing and quantifying the potential biogeochemical impacts within and across different landscape elements, such as forests, grasslands, and water bodies, challenging researchers to develop measurements and proxies that reflect both biological and environmental patterns at broad spatial scales.

Generating isoscapes (i.e. *iso*topic land*scapes*) from natural abundance stable isotopes is one approach to understanding biogeochemical responses both spatially and quantitatively (Bowen, 2010). Physical and biochemical transformations that are influenced by the environment and organism metabolism are imprinted on the isotopic value (ratio of heavy to light isotope referenced to a) of organic matter (Lichtfouse et al., 1995; Brüggemann et al., 2011; Werner et al., 2012). Plants within the agricultural landscape, including crop and plant species native to forests and grasslands, are therefore *in situ* biological recorders of changes in

precipitation regime, temperature, light, and CO_2 concentrations (Tubiello et al., 2007; Hatfield et al., 2011) as well as land management practices (Bateman et al., 2005; Choi et al., 2006). Soil organic matter is an amalgam of recent plant litter, microbial products, and management inputs that are stored and released over time providing information about current and past conditions.

When the isotopic composition of these different sources are used in combination with well-constrained isotope fractionation models (e.g., discrimination associated with photosynthesis) then the isotopic signal of a relatively few representative samples can be extrapolated over space allowing for the interpretation of different physical and biological processes. Isoscapes have been created at local scales to track the spatial-temporal impact of exotic N_2-fixing invaders (Rascher et al., 2012; Bai et al., 2013); at regional and continental scales to identify source water dynamics of rivers (Kendall and Coplen, 2001; Brooks et al., 2012); and at global scales to reveal plant responses to climate (Amundson et al., 2003; West et al., 2008).

While the isotope values (^{13}C and ^{15}N) of organic matter alone can yield information about changes across the landscape, they can also be used to derive proxies of plant stress and nutrient cycles. Intrinsic water use efficiency (WUE_i) is one such proxy that describes the ratio of carbon assimilated to water transpired, which directly links water stress during photosynthesis to the $\delta^{13}C$ signals of plant leaves (Saurer and Siegwolf, 2007; Seibt et al., 2008). Plant ^{15}N normalized by soil ^{15}N ($\Delta\delta^{15}N$) is another integrative index that has been positively correlated with increased N availability through mineralization (Kahmen et al., 2008), N transformations through nitrification (Takebayashi et al., 2010) and N losses through denitrification (Houlton and Bai, 2009), and leaching (Fang et al., 2010; Cheng et al., 2010). Thus, isotopic values and proxies that capture these biological and physical processes are proven tools to interpret land management activities, such as the application of chemical and organic fertilizers (Yoneyama et al., 1990; Choi et al., 2003) and tillage leading to erosion (Dungait et al., 2013; Beniston et al., 2015).

Isoscapes have the potential to help understand complex land-use and management patterns of agricultural landscapes, but little is known about the heterogeneity of organic matter across fields and landscape structures. Based on a high-spatial resolution isotopic ($\delta^{13}C$ and $\delta^{15}N$) data set, we created plant and soil isoscapes of a moraine landscape of NE Germany. The landscape is primarily used for agriculture (Fig. 2.1) and consists of numerous landscape structures (e.g. arable fields, grasslands, forests, and villages), including kettle holes. Kettle holes are small water bodies (< 1 ha in size) present across different land-use types that function as internal drainage systems (Kalettka et al., 2001). Kettle holes are hypothesized to be important hot-spots of biogeochemistry (Lischeid and Kalettka, 2012), thus providing an opportunity to test for terrestrial-aquatic linkages at the landscape scale. Using isoscapes we

expect to: 1) observe plant and soil patterns across different landscape structures in response to climate or past land-use thereby revealing landscape connectivity; 2) detect different land management practices and land-use effects on carbon and nitrogen biogeochemical cycles; and 3) explore whether kettle hole sediments and surrounding plants and soil exhibit tight aquatic-terrestrial linkages.

2.3 Material and methods

2.3.1 Study site

The study site is located within the Quillow catchment (168 km^2) and is part of the complex hummocky young ground and terminal moraine landscape typical for NE Germany. The catchment contains typical elements of postglacial landscapes including eroded hilltops, slopes, plains, and depressions (Sommer et al., 2008). Arable land use began in the area after massive deforestation in the 12th century. The study site is one of the most fertile areas in NE Brandenburg (D. Barkusky, *personal communication*). The climate is sub humid with a mean annual temperature of 8.6°C and mean annual precipitation varies between 350 and 750 mm yr^{-1}.

The proportions of land-use types across the study site were 74.4 % arable, grasslands 10.4 %, and forest 5.9 %. Towns and industrial areas (4.5 %), and larger stagnant water bodies of > 1 ha (moors, lakes, reed dominated; 3.4 %) were also dispersed over the area (Fig. 2.1). Kettle holes made up approximately 1.4 % of the area and were present in all land-use types. In general, the NW and center contained more water bodies, including lakes and moors. Arable soils consisted of albeluvisols with minor arenosols, luvisols and planosols. Grasslands consisted of stagnant planosols and albeluvisols as well as histosols of peat origin. Forests consisted of planosols and albeluvisols including luvisols and arenosols in minor proportions. Forest areas within the site varied by size. The largest forest (approx. 261 ha) located within our site was in the SE, followed by a 158 ha forest in the NW. We refer to these two forests as “intact” due to their large size. These two larger forests only partly extended into our site while two others (71 and 34 ha) were located entirely within the sampling area. Based on local weather station data spanning from 1981 to 2010 a 45 mm gradient in precipitation exists from 590 mm in the NW to 545 mm in the SE (see Appendix: Fig. A1). The landscape is moderately rolling with elevations ranging from 40 to 112 m a.s.l. and a general downward slope of 0.15° to the SE.

2.3.2 Sampling design

We divided the isoscape study area (3.25 x 11.75 km; 38.2 km^2) into 611 subplots each 0.25 x 0.25 km^2. This yielded an average of ~4.7 sampling points within each polygon (i.e., borders of fields and different land-use types depicted in Fig. 21). Because few isoscapes have

the same spatial scale as our study, we compiled sample densities from previous studies that range in spatial extent from < 1 km^2 to the globe for comparison (Fig. A2). Our sampling density was above average given the area of our investigation, thus assuring at least a similar representation to previous isoscape research.

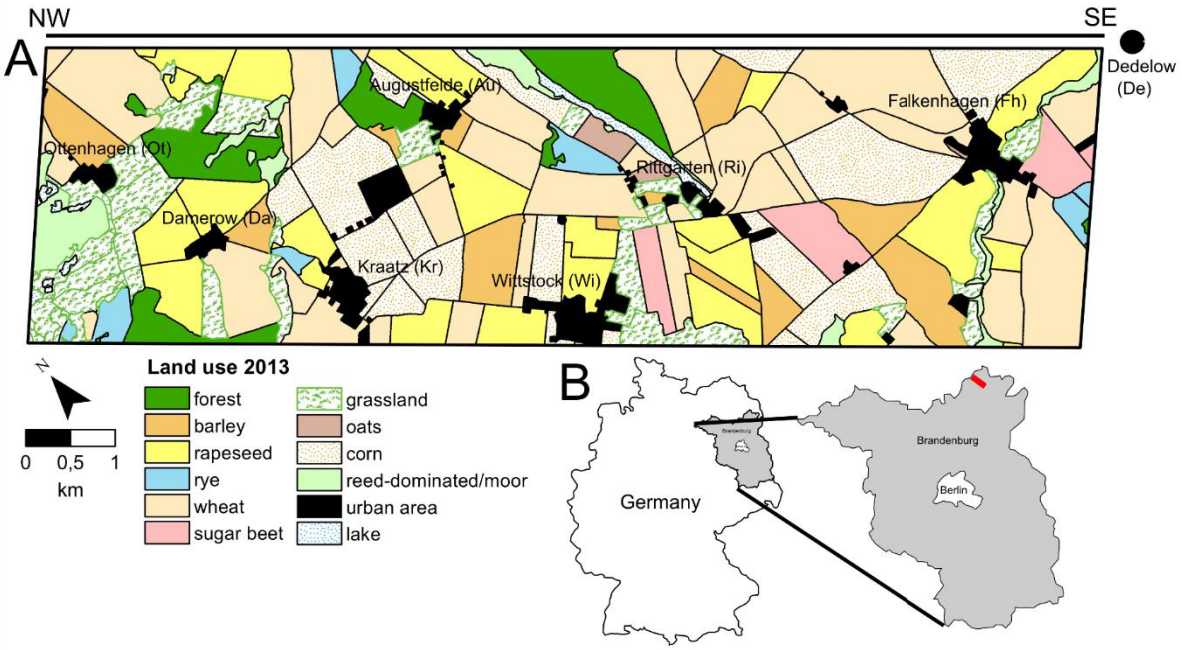

Fig. 2.1. Land-use map from 2013 (A) showing the three dominant land-use types: grasslands, forests and arable fields including the crops cultivated in 2013 and villages (ZALF Research Station, Dedelow, and Department of Landscape Information Systems, ZALF, Muencheberg). Location of the study site (red rectangle) in the federal state of Brandenburg within Germany (B). Note that the study site map has been rotated 40° for horizontal display and a NW to SE transect has been added above the map to further orient the reader.

Samples were taken from the center of each accessible subplot (Fig. A3). Not all grid points were sampled. Towns, industrial grounds and streets were omitted, as were protected grasslands and wetlands > 1 ha. When sampling points were positioned along a boundary of two different land-use types then one sample of each land-use type was taken approximately 20 m from the boundary. If the center of a polygon could not be reached, the sample was taken as close as possible (c. 50 m) to the original sampling coordinate. Arable fields were relatively large and the range of samples taken from one field varied from 1 to 22 depending on size and shape.

During the 2013 growing period (May/June), we collected 595 soil samples and 589 plant samples (499 crop, 57 grassland and 34 forest). In agricultural fields we sampled crops, dandelion (*Taraxacum* sect. *Ruderalia)* on grassland sites, and beech (*Fagus sylvatica*) in forests. Beech trees were usually young and less than 2 m in height. Crop species included winter wheat (*Triticum L.*), winter barley (*Hordeum vulgare*), winter rye (*Secale cereale*), oats (*Avena sativa*), rapeseed (*Brassica napus*), sugar beet (*Beta vulgaris*) and corn (*Zea mays*).

Our plant samples were composites of leaves from three different plants near the sampling point. For soils, we assumed that the plow layer (30 cm) is well mixed in arable fields and provide a representative sample of land-use and management effects on the soil. We took 200 – 300 g soil sample from 2 to 15 cm depth for all land-use types after removing the top 2 cm, which was rich in fresh plant residues from the previous growing period.

From mid-July to the end of August, we sampled sediment (51) and plants (34) from 51 kettle holes out of the approximately 290 present. We sampled *Phalaris arundinacea* to represent a kettle hole plant sample because it was present at almost all sites. We based our kettle hole selection on: 1) size class, ensuring that we covered the distribution of different size classes, 2) land-use type, and 3) spatial distribution (we ensured to cover the study area, Fig. A3). We mixed the top 2 cm from three sediment cores for each kettle hole sediment sample.

2.3.3 Sample preparation

All samples were stored at 4°C in dark conditions prior to preparation. Plant, soil and sediment samples were oven-dried at 65°C for 48 h. We ground plant and sediment samples to a powder. Soil samples were passed through a 2 mm sieve and visible plant residues were removed. To identify samples for acid fumigation, we determined carbonate concentrations (in % CO_3-C) in soil and sediment samples using a RC612 multiphase carbon and nitrogen analyzer (LECO Corporation, Michigan, USA).

2.3.4 Stable isotope analysis

Prior to $\delta^{13}C$ stable isotope analysis of soil samples, inorganic carbon was removed from samples containing > 0.05 % CO_3-C by acid fumigation after Harris et al. (2001). Soil, plant, and sediment samples were weighed into tin capsules. All isotope measurements were analyzed on a Thermo-Scientific, Delta V advantage isotope ratio mass spectrometer. The isotopic values are expressed in delta notation (in ‰ units), relative to VPDB (Vienna Pee Dee Belemnite) for carbon and N_2 in air for nitrogen. Analysis of internal laboratory standards (apple leaves, ulva, high organic carbon content sediment, low organic carbon content soil) ensured that the estimates of the isotopic values were accurate to within < 0.1 ‰ for $\delta^{13}C$ and < 0.5 ‰ for $\delta^{15}N$.

2.3.5 Plant physiological related calculations

We calculated the photosynthetic carbon isotope discrimination $\Delta^{13}C$ between the ambient atmospheric $\delta^{13}C_a$ (-8 ‰) and the measured $\delta^{13}C_{plant}$ of C_3 plants (Farquhar and Richards, 1984):

$$\Delta^{13}C = \frac{\delta^{13}C_a - \delta^{13}C_{plant}}{1+\delta^{13}C_plant/1000} \quad 2.1.$$

The intrinsic water use efficiency (WUE_i) in µmol C mol^{-1} is calculated on the basis of the measured plant $\delta^{13}C$ following the equation of Saurer and Siegwolf (2007):

$$WUE_i = \frac{c_a}{1.6} \cdot \frac{b - \delta^{13}C_a + \delta^{13}C_{plant}}{b - a} \quad 2.2.$$

Here, c_a is the ambient atmospheric concentration of CO_2 of 380 µmol mol^{-1}, *a* is the C isotope fractionation during stomata CO_2 diffusion (4.4 ‰), *b* represents the C isotope fractionation during the CO_2 fixation during RuBisCO (27 ‰), and the value of 1.6 is the ratio of the diffusivities of CO_2 and water in air.

In terms of connecting soil and plant $\delta^{15}N$, we calculated the difference between both compartments ($\Delta\delta^{15}N$, Amundson et al. 2003):

$$\Delta\delta^{15}N = \delta^{15}N_{plant} - \delta^{15}N_{soil} \quad 2.3.$$

The resulting value is also a proxy for the status of nitrogen cycling. Due to fractionation involved during the formation of nitrogen sources belowground, especially those associated with denitrification (Kahmen et al., 2008), leaves tend to be depleted in ^{15}N compared to bulk soil values (Robinson, 2001). Thus, when $\Delta\delta^{15}N$ values are near 0 ‰, resulting from an enriched plant isotopic value, then the N cycle is considered to be open, indicating the possible occurrence of nitrogen sources depleted in ^{15}N leaching or that different N sources are available (Zech et al., 2011).

2.3.6 Statistical analysis

To test statistical significances between plant and soil $\delta^{13}C$ and $\delta^{15}N$ across our three land-use types and for kettle hole sediments, we performed ANOVA, post-hoc significance test (Tukey's HSD), and linear regression using R (version 3.1.1, R Foundation for Statistical Computing, Vienna, Austria, http://www.R-project.org/). Interpolations were made using ordinary kriging within the Geostatistical Analyst function of ArcGIS geographic information system software (version 10.1, Environmental Systems Research Institute 2012, Redlands, CA). We omitted wetlands of > 1 ha (lakes, reed-dominated areas, moors) and urban areas from interpolation. We created our WUE_i plant isoscapes by interpolating across C_3 crops in arable land-use types, beech in forests, and dandelion in grasslands. Land-use boundaries were based on a land-use map from 2013. Subsequently, we compiled all land-use interpolations into an overall WUE_i isoscape. We used a single scale to achieve a better visualization of patterns across the three land-use types, which still allows for discerning patterns within each single land-use type. We followed the same procedure for the creation of our $\Delta\delta^{15}N$, $\delta^{15}N$ plant, and soil isoscapes. However, for the $\delta^{13}C_{soil}$ isoscape we did not divide the landscape by land-use since the difference between mean $\delta^{13}C_{soil}$ for each land-use type was not greater than 1 ‰ (Table 2.1).

Table 2.1. Soil and sediment $\delta^{13}C$, $\delta^{15}N$ (‰), and $\Delta\delta^{15}N$ (‰) mean ± SE.

Land-use	$\delta^{13}C$ (‰)	$\delta^{15}N$ (‰)	$\Delta\delta^{15}N$ (‰)
soils			
arable (n = 497)	-26.5 ± 0.0	6.1 ± 0.1	-2.7 ± 0.1
forest (n = 38)	-27.0 ± 0.1	0.8 ± 0.3	-5.4 ± 0.4
grassland (n = 60)	-27.5 ± 0.1	4.7 ± 0.1	-2.7 ± 0.3
sediments			
arable (n = 36)	-28.7 ± 0.2	3.7 ± 0.2	
forest (n = 6)	-28.5 ± 0.3	-0.3 ± 0.3	
grassland (n = 9)	-28.4 ± 0.3	2.8 ± 0.3	

2.3.7 Mixing model

We assumed three primary $\delta^{13}C$ and $\delta^{15}N$ organic matter sources to the kettle hole sediments: surrounding soil, kettle hole plants, and surrounding vegetation in the fields (e.g., crops, grasses). We used the SIAR mixing model package that is implemented in R (Parnell et al., 2008). The model allows for the estimation of a fractionation factor associated with the transformation of plant or soil organic matter before it reaches the sediment. We chose conservative fractionation values of 0.7 ‰ for $\delta^{13}C$ (Brüggemann et al., 2011) as well as $\delta^{15}N$ (Yoneyama, 1996). The software reports credibility intervals (95, 75, and 25 %) for the partitioning results.

2.4 Results

2.4.1 Plant $\delta^{13}C$ isoscape patterns

We grouped plants by land-use type for interpolation of isotopic values and associated proxies across the site. For the arable land-use type, we grouped our C_3 crops based on estimates of photosynthetic discrimination ($\Delta^{13}C$). Photosynthetic discrimination was on average -21.0 ± 0.1 ‰ and the total range did not exceed ± 1.5 ‰. Plant isotopic values (Table 2.2) exhibited patterns across the research site that reflected climate and differences in vegetation. Interpolated $\delta^{13}C_{plant}$ of arable fields (C_3) spanned from -31.6 to -26.7 ‰ (Fig. A5). For C_3crop leaf organic matter in general, we found a pattern in $\delta^{13}C$ depletion from the SE to NW of our site, except for a small area in the NW (Fig. A4 panel A) where the plants were slightly enriched in ^{13}C (~1 ‰) compared to the surrounding fields. A clear trend was not visible for cornfields across the site, and small local variations occurred within each field ranging from -13.7 to -12.7 ‰ (Fig. A4 panel C). In the forest land-use type, we found beech trees in the NW were more enriched relative to forests near the center of the site (Fig. A4 panel B). Interpolated $\delta^{13}C_{beech}$ had a range from -34.7 to -28.3 ‰. In the grassland land-use type, we found very little variation in the interpolated $\delta^{13}C$ (Fig. A4 panel B) among the sampled dandelion (-31.3 to -29.3 ‰) (Fig. A4 panel B).

Table 2.2. Plant leaf $\delta^{13}C$, $\delta^{15}N$ (‰) and $\Delta\delta^{15}N$ (‰) mean ± SE of different species.

Plant	Leaf $\delta^{13}C$ (‰) (‰)	Leaf $\delta^{15}N$ (‰) (‰)	$\Delta\delta^{15}N$ (‰)
C_3 crops (n = 386)	-29.0 ± 0.1	3.4 ± 0.1	-2.6 ± 0.1
barley (n = 56)	-29.1 ± 0.1	2.1 ± 0.4	-3.8 ± 0.3
oats (n = 7)	-29.9 ± 0.2	4.8 ± 0.7	-1.1 ± 0.9
rapeseed (n = 110)	-29.9 ± 0.1	4.7 ± 0.2	-1.4 ± 0.3
rye (n = 12)	-29.2 ± 0.2	2.2 ± 0.3	-3.1 ± 0.3
sugar beet (n = 22)	-28.9 ± 0.2	3.7 ± 0.6	-2.9 ± 0.6
wheat (n = 179)	-28.4 ± 0.1	2.9 ± 0.1	-3.1 ± 0.2
C_4 crops			
corn (n = 110)	-13.2 ± 0.0	3.5 ± 0.3	-2.7 ± 0.3
Forest plants			
beech (n = 34)	-32.4 ± 0.2	-4.5 ± 0.4	-5.4 ± 0.4
Grassland plants			
dandelion (n = 57)	-30.3 ± 0.1	2.0 ± 0.3	-2.7 ± 0.3
Kettle hole plants			
Phalaris arundinacea (n = 34)	-27.3 ± 0.1	5.0 ± 0.4	

2.4.2 Intrinsic water use efficiency

The patterns in WUE_i across the arable land-use type show an overall decrease from SE to NW. In addition, interpolated WUE_i values exhibited a wide range in values of 28 to 80 µmol mol^{-1} compared to plants from the other land-use types (Fig. 2.2). Within the forest land-use type, beech was more water-use efficient in the NW compared to the center of the site. Beech exhibited the smallest WUE_i of all sampled plants with a range of 1 to 61 µmol mol^{-1}. Within the grassland land-use type, dandelion was more water-use efficient in the NW compared to the SE and had a range of 31 to 53 µmol mol^{-1}.

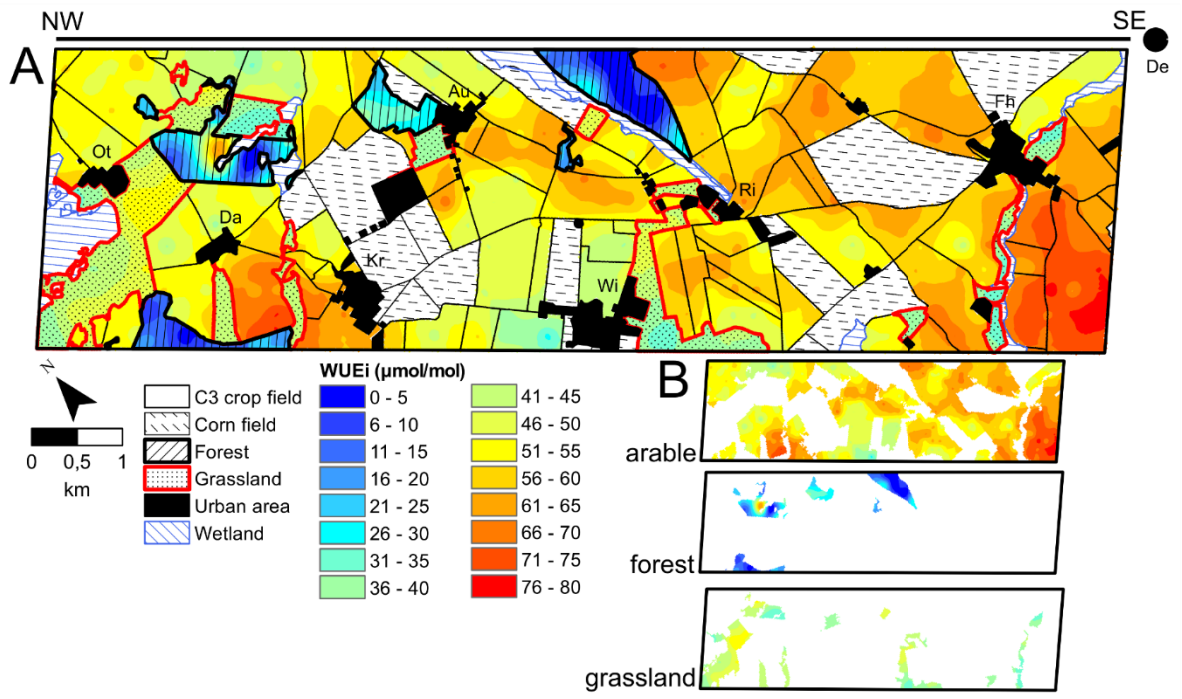

Fig. 2.2. Isoscapes (A) of intrinsic water use efficiency (WUE_i) for plants sampled from the three land-use types using ordinary kriging. Interpolation was performed first for each land-use type independent of other types. The three isoscapes were then compiled into one overall isoscape using a common scale. Grasslands are highlighted with red borders and forests with black borders. The area interpolated to generate each land-use type isoscape is shown in (B) and includes the same scale. Areas not interpolated include fields with corn, wetlands > 1 ha, and urban areas.

2.4.3 Soil $\delta^{13}C$

The overall variation in $\delta^{13}C_{soil}$ ranged from -28.3 to -24.7 ‰ with the most enriched values found in the SE of our site. With such a small range in values (Table 2.1) we interpolated $\delta^{13}C$ over the whole sampling area without separating areas into different land-use types. Similar to patterns of WUE_i, there was a small decrease in $\delta^{13}C_{soil}$ from SE to NW (Fig. 2.3).

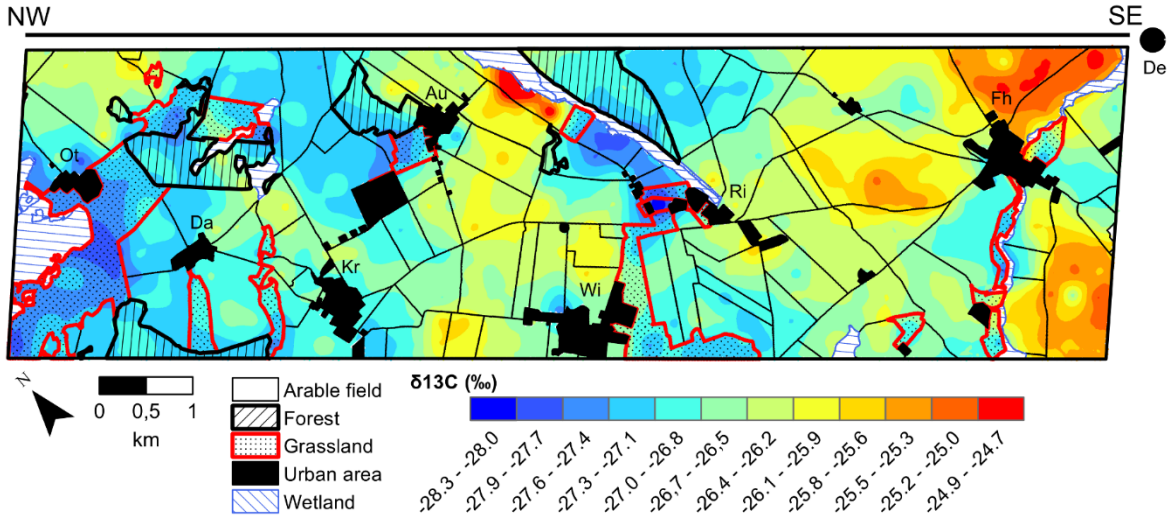

Fig. 2.3. $\delta^{13}C$ (‰) soil isoscape. Interpolation was performed over the whole sampling area without separating land-use types. Grasslands are highlighted with red borders and forests with bold-black borders.

2.4.4 $\Delta\delta^{15}N$ pattern

We found strong variations in plant and soil $\delta^{15}N$ among the three land-use types (Table A1), consequently we interpolated ^{15}N within each type. In general, $\Delta\delta^{15}N$ patterns (Fig. 2.4) were similar to the foliar $\delta^{15}N$ pattern (Fig. A5) indicating the disequilibrium between plant and soil. There was a wide range of $\Delta\delta^{15}N$ (-5.8 to +0.6 ‰) within arable fields that was clearly related to crop species. In particular, we found oat and rapeseed to have the least negative values, i.e. these were the plant species most enriched in ^{15}N. Forest $\Delta\delta^{15}N$ values were the most negative (-7.8 to -3.3 ‰) and were strongly positively correlated with WUE_i of beech (Fig. A6). The two fragmented forests stands were the most water efficient and exhibited the most open nitrogen cycle between plant and soil (i.e., the $\Delta\delta^{15}N$ was closest to zero). In the grassland land-use type the range of dandelion $\Delta\delta^{15}N$ was -4.5 to -1.1 ‰, but values were also variable across the site, especially in the NW (Fig. 2.4).

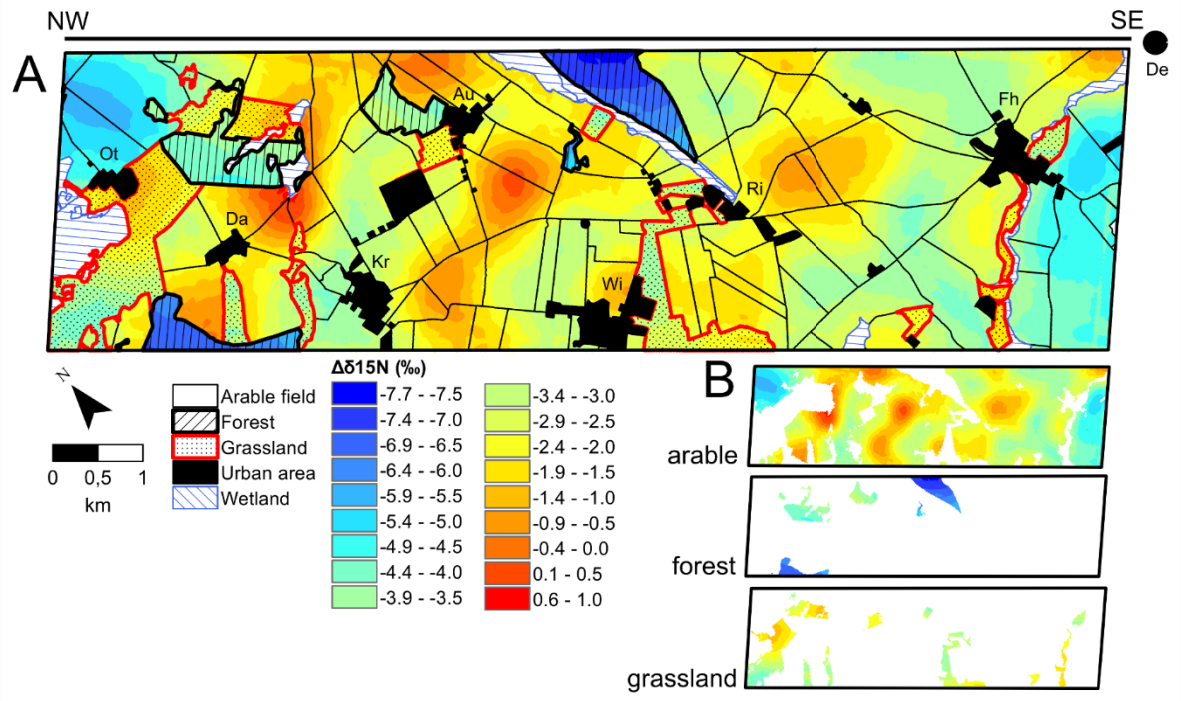

Fig. 2.4. Isoscapes (A) of $\Delta\delta^{15}N$ (‰) for plants and soils sampled from the three land-use types using ordinary kriging. Interpolation was performed first for each land-use type independent of other types. The three isoscapes were then compiled into one overall isoscape using a common scale. Grasslands are highlighted with red borders and forests with bold-black borders. The area interpolated to generate each land-use type isoscape is shown in (B) and includes the same scale. Areas not interpolated include wetlands >1 ha, and urban areas.

2.4.5 Soil $\delta^{15}N$

The isoscape of $\delta^{15}N_{soil}$ was interpolated for each land-use type. Interpolated arable field $\delta^{15}N_{soil}$ values had a range of 3.0 to 8.5 ‰ and fields near villages were typically enriched. In the SE, around a wide area of the village Falkenhagen (Fh), we found soils with the most enriched $\delta^{15}N$ isotopic values (Fig. 2.5). The area close to the village Kraatz (Kr) in the NW was also enriched in ^{15}N as well as a small area south of the village Rittgarten (Ri). Soils near the center of the study area and the NW were less enriched in ^{15}N. Forest soil was the least enriched in ^{15}N (0 to +3.0 ‰) of all land-use types. The northern most intact forest was most enriched of the four stands. Grassland land-use type soils varied only slightly in their $\delta^{15}N$ values (4.1 to 5.2 ‰), although we observed small differences among the different locations. Grasslands in the west were enriched in ^{15}N relative to those in the east.

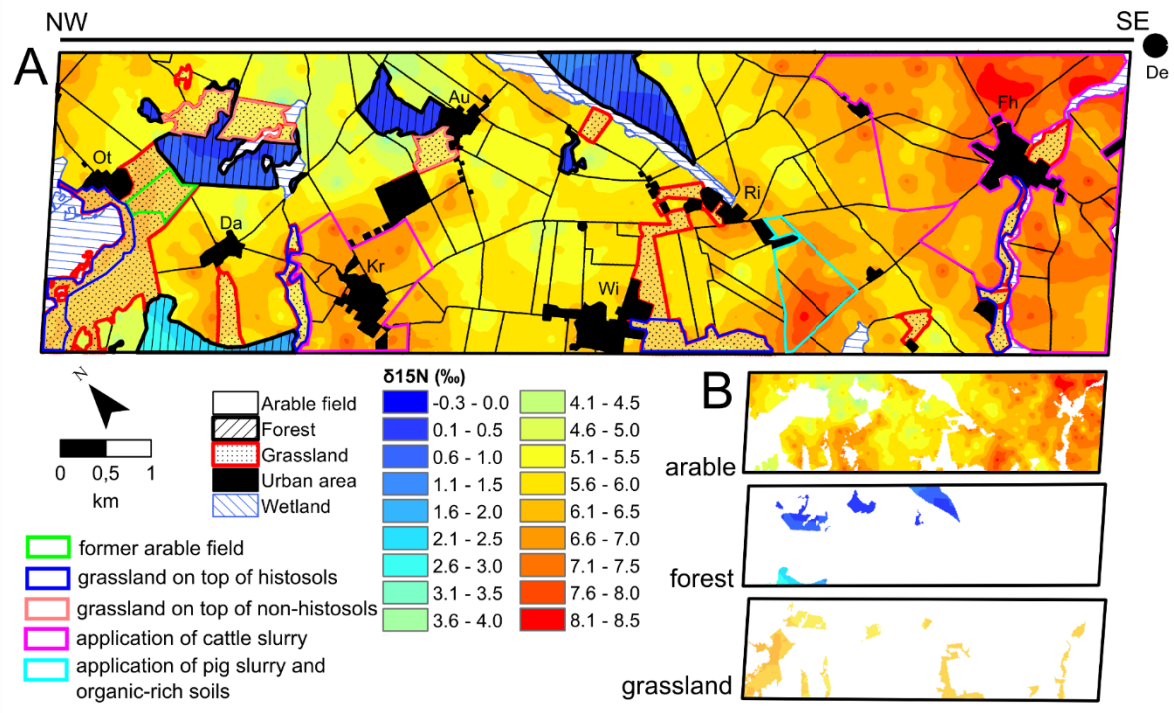

Fig. 2.5. Isoscapes (A) of $\delta^{15}N$ (‰) for soils sampled from the three land-use types using ordinary kriging. Interpolation was performed first for each land-use type independent of other types. The three isoscapes were then compiled into one overall isoscape using a common scale. Grasslands are highlighted with red borders and forests with bold-black borders. The area interpolated to generate each land-use type isoscape is shown in (B) and includes the same scale. Areas not interpolated include wetlands > 1 ha and urban areas. Highlighted areas show land-management effects: grasslands growing on Histosols (blue borders) or non-Histosols (light red borders), conversion of arable fields (green borders), application of cattle slurry (violet borders), application of pig slurry plus organic-rich soils (cyan borders).

2.4.6 Terrestrial-aquatic linkages

We could not detect a difference in sediment $\delta^{13}C$ among the three land-use types, however, we did find differences based on $\delta^{15}N_{sediment}$ values (Table A1). Forest kettle hole sediment $\delta^{15}N$ isotopic values were significantly different than grassland ($p < 0.05$) and arable ($p < 0.01$) kettle hole sediments. We could not detect a significant difference between sediments of kettle holes from grassland and arable land-use types. Given the land-use type differences between sediments and the surrounding vegetation isotopic composition, we found it reasonable to analyze the sediment–plant–soil relationship within the three land-use types.

We tested for linkages between terrestrial plant and soil organic matter sources to the kettle hole sediments. We assumed at steady-state the kettle hole sediments would reflect these dominant sources. The soil and plant sources near the kettle hole were isotopically similar and often the sediments were relatively depleted in the heavy isotope, while plant organic matter from the fields, grasslands and forests were the most depleted (Fig. 2.6). The sediment $\delta^{13}C$ and $\delta^{15}N$ mixing-model results (Fig. A7a-c) largely reflected these different plant sources, although the mixing patterns are primarily driven by variation in $\delta^{15}N$. Within the arable land-use type organic matter from the surrounding C_3 crops contributed between 90 to 95 % to the sediment organic matter isotopic value. In contrast, the sediment isotopic composition from the grassland land-use type received a large contribution from the surrounding vegetation (50 to 90 %; 95 % credibility interval) and only a smaller contribution from vegetation growing directly in the kettle hole vicinity. Sediment $\delta^{15}N$ from one kettle hole was significantly (> 2σ) enriched compared to the others and was removed from the source partitioning analysis. For the forest land-use type, there were only two sources, beech leaves and soil, that could contribute to the sediment isotopic value. The soil was estimated to contribute less (5 to 60 %, 95 % credibility interval) than the contribution from beech leaves (40 to 95 %; 95 % credibility interval). In general among all the kettle holes, we found the most enriched $\delta^{15}N$ sediments to originate from kettle holes that tend to dry-out over the year.

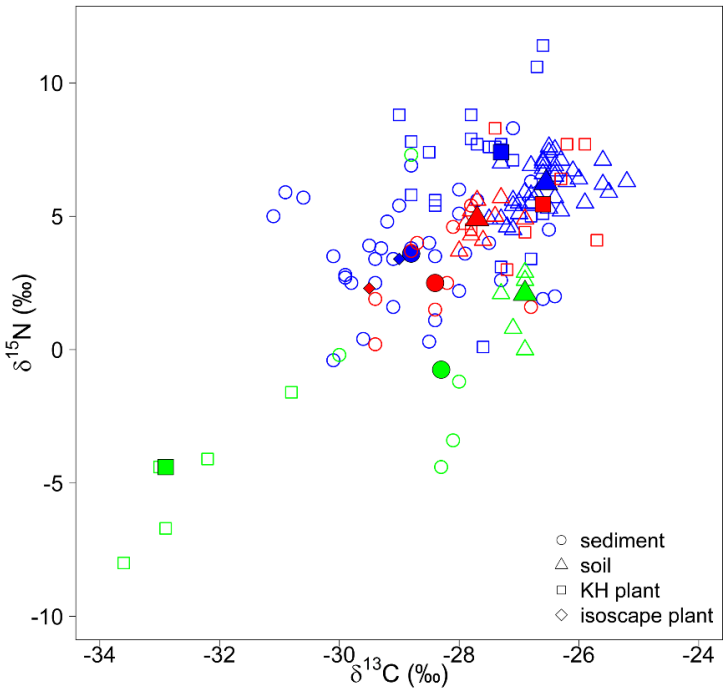

Fig. 2.6. Bi-plot of plant, soil, and sediment isotopic composition used in kettle hole mixing-model analysis. Different land-use types are identified by colour: blue (arable), red (grassland), and green (forest). Enlarged symbols are the median for each group. Kettle hole (KH) plants are represented by *Phalaris arundinacea* in arable fields and grasslands. Isoscape plants are represented by sampled C_3 crops in arable fields, dandelion in grasslands, and beech in forests. Soils represent mean values of four soil isoscape samples nearest to a kettle holes. For arable fields, we constrained soil values to isoscape sampling points within the same field as the kettle hole.

2.5 Discussion

We observed distinct patterns in the isotopic composition of organic matter sampled from the landscape that clearly reflect the complexity of land-use, land management, and local environmental conditions. Water use efficiency and nutrient dynamics between crop and native plants were different, leaving a lasting imprint on the soil organic matter. From the subsequent soil organic matter patterns we were able to observe land management effects that extended beyond a single field or a single growing season. We found the kettle hole sediment isotopic values exhibited a high range of variability across the site that largely reflected the surrounding land-use. In the following, we discuss these two primary drivers of the heterogeneity across the isoscapes: the abiotic environmental conditions and land management, and their overall impact on plant, soil, and sediment of different land-uses.

2.5.1 Plant and soil response to the environment

Crop C_3 plants from the eastern area of our site were more affected by lower water availability than native plants. The range of WUE_i for native plants (beech, dandelion) was smaller than the C_3 crops indicating that these plants were perhaps under less water stress than their cultivated counterparts (Grossiord et al., 2014). Plants in the arable fields may face water stress from management practices resulting in less organic matter in the upper soil horizons thereby reducing soil moisture holding capacity (Hudson, 1994; Emerson, 1995) or the roots from the crop plants may not reach deeper soil water sources available to native species. The C_3 crop plants WUE_i patterns also followed a small 45 mm precipitation gradient across our site, while native species, including those surrounding kettle holes, did not. Besides water sources, genetic selection of crop traits to endure water stress may also explain the different response between native and crop plants. Indeed, native plants have been recognized to exhibit fitness homeostasis to fluctuating environmental conditions with respect to invasive species (Davidson et al., 2012) and while crop species are not invasive species *per se* they have been developed for specific traits and performance (Varshney et al., 2011; Garnier and Navas, 2011) that may differ from native species. Thus, we hypothesize that native plants are more adapted to predominant climatic conditions than crops at the landscape scale.

The soil organic matter isoscapes integrate plant and management inputs over time and are therefore a conservative proxy of their impact, which could lead to a diffuse signal within a landscape. However, the soil organic matter isotopic patterns provided a clear indication of the environmental gradient and land management at our site. For example, the $\delta^{13}C_{soil}$ values of arable land reflected the precipitation gradient, most likely resulting from organic matter deposited from plants that have responded physiologically to the local environmental conditions. There was a slight correlation of $\delta^{13}C_{soil}$ with precipitation ($r^2 = 0.27$), which we infer as the long-term influence of plant organic matter on the $\delta^{13}C_{soil}$ signal. Land management, in terms of corn cultivation is also evident. Based on land-use maps between 1999 and 2012, we found a strong correlation between $\delta^{13}C_{soil}$ vs. corn rotation ($r^2 = 0.97$, $p < 0.01$, Fig. A8). The effect of corn on $\delta^{13}C_{soil}$ values is relatively small after only a few rotations (~1 ‰, Fig. 2.3), but after four rotations the impact on $\delta^{13}C_{soil}$ was larger than 1 ‰. However, we are cautious with our interpretation since only five fields were planted more than four times with corn. Soil type and the topographic position, generally known to influence $\delta^{13}C$ and $\delta^{15}N$ of soils (Fox and Papanicolaou, 2007; Alewell et al., 2009), were not highly correlated with $\delta^{13}C_{soil}$ and $\delta^{15}N_{soil}$, another indication of the strong role of land-use and management. The approximate 0.15° slope across the whole site may not induce erosion dynamics that are strong enough to alter the isotopic composition of soil organic matter at our spatial resolution. Overall, we hypothesize that $\delta^{13}C_{soil}$ patterns reflect both, the long-term accumulation of $\delta^{13}C_{plant}$ affected by the climatic conditions as well as the imprint of the distinct C_4 isotope value of corn.

2.5.2 Land-use and land management effects

There was a strong interaction between land-use and land management. We categorized land-use by the predominant vegetation cover type (forest, arable, and grasslands), and within each there was a different land-use legacy that formed the backdrop for recent management effects. We observed strong spatial variations in $\Delta\delta^{15}N$ at the field scale that could not be explained by plant-specific differences in the discrimination against ^{15}N during N uptake, thus, we found the ^{15}N of organic matter to respond most strongly to management effects.

In the 1970s within arable fields in Brandenburg, farmers began to intensively apply organic manure, which generally results in enriched $\delta^{15}N_{soil}$ (Yoneyama et al., 1990; Choi et al., 2003; Bateman et al., 2005), thus the level of fertilization intensity and type of fertilization was visible in our isoscapes. While we were not able to measure the different varieties of slurry used in the area, we find it reasonable to assume a relatively enriched $\delta^{15}N$ isotopic signal given the many biological, chemical, and physical processes involved to generate slurry. For example, within the village Dedelow (De) located near the SE boundary of the study area is a large dairy farm (> 2000 livestock). Slurry originating from the dairy is transported underground via pipes to fields near the village Falkenhagen (Fh), and distributed on the fields with tractors. We also found soils near the village Kraatz (Kr) enriched in ^{15}N (Fig. 2.5) that are known to receive cattle slurry, again providing evidence of slurry application prior to German reunification. Soils from the field south of the village Rittgarten (Ri) are also enriched in ^{15}N, in this instance the soil is reflecting the practice of pig slurry application occurring after the German Democratic Republic (GDR) period.

In addition to slurry, other fertilization practices at the site were captured by the isoscapes. For example, a field south of Rittgarten (Ri) is fertilized with a peat soil originating from a mushroom farm in addition to pig slurry application (Fig. 2.5). Fields that were not known to be fertilized by slurry tended to be less enriched in ^{15}N ($p < 0.01$). We infer that these fields were treated with chemical fertilizers that are usually less enriched in $\delta^{15}N$ than organic fertilizers (Choi et al., 2003; Michalski et al., 2015) and are quickly mobilized by plants and microbes. This observation is consistent with land-use maps (ZALF, 2014), which show fields between the villages Kraatz (Kr) and Augustfelde (Au) that were recently cultivated as strips by small farmers, who often applied only small amounts of chemical fertilizers. These fields have recently been merged and are now cultivated by larger farms.

Forested areas were not influenced by fertilization management and exhibited the lowest $\Delta\delta^{15}N$ and $\delta^{15}N_{soil}$ values. In this case environmental and structural effects were more apparent across the landscape. We found that forests in which the nitrogen cycle was relatively open ($\Delta\delta^{15}N \sim 0$) were more water use efficient. Intrinsic water-use efficiency is a proxy for the relative amount of carbon assimilated to the amount of water transpired. Plants can manage this trade-off by assimilating more carbon when stomata are open (i.e., increase the photosynthetic

capacity) and by reducing the amount of water loss by closing their stomata (i.e., lowering stomatal conductance). In the forests we observed an increase in WUE_i along with an increase in leaf ^{15}N, which suggests an increase in leaf N content that can be attributed to an increase in Rubisco content and therefore photosynthetic capacity (Lopes and Araus 2006, Milcu et al. 2014). Furthermore, the isotopic patterns of two smaller forests fragments exhibit greater WUE_i and $\Delta\delta^{15}N$ levels with respect to the larger intact forests that are at least twice the size of the fragments. Fragmentation increases the perimeter to area ratio, which can change biodiversity levels and increase the exposure to surrounding land management (Weathers et al., 2001; Billings and Gaydess, 2008; Ziter et al., 2014). Our replication of the different forest fragments is relatively low for conclusive statements, but our finding of plant leaves enriched in ^{15}N relative to the soil ^{15}N values (leading to a $\Delta\delta^{15}N \sim 0$) is initial evidence of a change in intrinsic N cycling within the fragments that the trees are able to take advantage of by increasing WUE_i. The relative open N cycle within the forest fragments manifests either directly from possible fertilization practices that we were not able to detect, or indirectly through changes in the local biotic dynamics (e.g., understory plant and microbial community N dynamics).

Grassland patterns were predominantly a function of soil type and land management (i.e., fertilization, grazing livestock, and grass harvested for hay or silage). Grassland plants adjust to the different water regimes, as indicated by the WUE_i patterns, but the normalized leaf isotopic values ($\Delta\delta^{15}N$) indicate that land management had a larger effect on plant nitrogen balance. Grasslands across the sampling area were primarily located on histosols (i.e., peat soils; Fig. 2.5) containing high levels of N and were relatively enriched in $\delta^{15}N$ at our site. However, we also detected enriched $\delta^{15}N_{soil}$ in grasslands not associated with histosols, especially those close to the village Ottenhagen (Ot). This pattern can be partly attributed to the conversion of grasslands to croplands and vice-versa. For example, the most enriched $\delta^{15}N_{soil}$ for a grassland not growing on histosols had been converted from agriculture just the previous year. Other management prescriptions, such as grazing or fertilization may also contribute to the enriched $^{15}N_{soil}$ over time (Frank and Evans, 1997; Choi et al., 2003)

2.5.3 Terrestrial-aquatic linkages

Land-use and kettle hole hydrology played a large role in the $\delta^{15}N_{sediment}$ isotopic patterns across our site. Sediments of kettle holes from the forest land-use type reflected the dominant beech vegetation type, resulting in significant differences from arable and grassland types. Both arable and grassland kettle hole sediments exhibited a large range in values and we could not determine the immediate land management impact on them. Farmers till and fertilize in a close proximity to the kettle holes (often the managed land is < 1 m away from the water body) that may result in possible direct transfers of N to the kettle hole through erosion or subsurface flow (Lischeid and Kalettka, 2012). However, the influence of land-use was readily apparent within

sediments of one forest kettle hole lying directly between arable and forested land, which was substantially enriched in ^{15}N. Interestingly, sediments from kettle holes in the arable and grassland land-use type that were the most enriched in ^{15}N were also those that are known to dry out during the year. Kettle holes experience dynamic hydrologic conditions including wet-dry cycles (Ireland et al., 2012), these cycles are known to accelerate organic matter turnover (Fierer and Schimel, 2002; Miller et al., 2005; Xiang et al., 2008), which may drive the ^{15}N enrichment of sediment organic matter in these kettle holes.

In partitioning the potential carbon and nitrogen sources to sediments, we found plant organic matter from surrounding fields (i.e., crops and grasses) was the dominant input to arable and grassland land-use type kettle holes. Kettle holes within the forest land-use type received a relative equitable contribution from both soil and plant (beech litter). Our partitioning results of the isotopic value of sediments highlight the importance of terrestrial contributions, and while the surrounding terrestrial ecosystems supply a large portion of productivity to water bodies (Cole et al., 2006; Jansson et al., 2008; Berggren et al., 2010), inputs from floating plants, plankton, and encroaching kettle hole semi-aquatic vegetation such as typha and reed plants also occur, which will significantly contribute to the sediment isotopic value.

2.5.4 Insights from isoscapes in complex landscapes

We have analyzed over 1500 organic matter samples originating from different plant species, soils, and sediments across a relatively small agricultural landscape divided into at least 80 different management units. This unusually high sample density in a uniform grid was necessary because of the unknown degree of isotopic heterogeneity within a field and across a landscape varying in land-use history and management. Previous isoscapes at all scales have interpolated over at most five-hundred samples to yield insights into ecological and hydrological spatial patterns (Fig. A2).

Generating isoscapes across complex landscapes does pose significant challenges regarding scaling and temporal dynamics. Small landscape features (< 250 x 250 m, in our case), represented as polygons in Geographical Information Science, are not always accurately accounted for when interpolating across a landscape, yielding a more simplified perspective. In the case of agricultural fields, we may lose resolution because the interpolation across the isoscapes is not constrained by field boundaries. Sample density and grid design are also dependent on the temporal dynamics of the system of interest. For our study, we were careful to observe the different plant sowing times and phenologies, for example, corn and sugar beet were planted in the end of April in contrast to other crops that were planted in the previous winter.

We found land-use and management effects were dominant over the environmental drivers of the landscape and that the heterogeneity in biogeochemistry reflected the local

management activity. Land use practices change with different societal demands and policies necessitating specific field and management information. Our study clearly benefitted from a local research station that serves as a center for outreach and communication to local landowners and managers, providing a wealth of information on changes in land-use and practices for decades. With such a repository, changes in agricultural management, such as applying organic slurries in lieu of chemical fertilizers, to cultural shifts, in our case the reunification of Germany, become tractable. We have shown that isoscapes can be used in complex agricultural landscapes to help visualize multiple sources of biogeochemical, agricultural, and historical information. Future studies may be able to expand upon the initial information we presented to help provide a global view of the different biogeochemical patterns across agricultural landscapes.

2.6 Acknowledgments

We thank the Research Station of ZALF at Dedelow for the logistical support and Frau Remus and Thomas Wagner for their help with the sample preparation. We kindly thank the LandScales team for their support and discussions including Thomas Kalettka for assistance with kettle hole selection. This research was funded through the Pact for Innovation and Research of the Gottfried Wilhelm Leibniz association (project LandScales, http://landscales.de).

3. Regional kettle hole scale

Land-use and hydroperiod affect kettle hole sediment carbon and nitrogen biogeochemistry

This manuscript was published in the international peer-reviewed journal *Science of the Total Environment.* The original article was published by ELSEVIER:

Nitzsche K.N., Kalettka T., Premke K., Lischeid G., Gessler A. and Kayler Z.E. (2017) Land-use and hydroperiod affect kettle hole sediment carbon and nitrogen biogeochemistry. *Science of the Total Environment*, 574:46-56.

3.1 Abstract

Kettle holes are glaciofluvially created depressional wetlands that collect organic matter (OM) and nutrients from their surrounding catchment. Kettle holes mostly undergo pronounced wet-dry cycles. Fluctuations in water table, land-use, and management can affect sediment biogeochemical transformations and perhaps threaten the carbon stocks of these unique ecosystems. We investigated sediment and water of 51 kettle holes in NE Germany that differ in hydroperiod (i.e. the duration of the wet period of a kettle hole) and land-use. Our objectives were 1) to test if hydroperiod and land management were imprinted on the isotopic values ($\delta^{13}C$, $\delta^{15}N$) and C:N ratios of the sediment OM, and 2) to characterize water loss dynamics and kettle hole-groundwater connectivity by measuring the stable $\delta^{18}O$ and δD isotope values of kettle hole water over several years. We found the uppermost sediment layer reflected recent OM inputs and short-term processes in the catchment, including land-use and management effects. Deeper sediments recorded the degree to which OM is processed within the kettle hole related to the hydroperiod. We see clear indications for the effects of wet-dry cycles for all kettle holes, which can lead to the encroachment of terrestrial plants. We found that the magnitude of evaporation depended on the year, season, and land-use type, that kettle holes are temporarily coupled to shallow ground water, and, as such, kettle holes are described best as partially-closed to open systems.

3.2 Introduction

The landscapes of northern America, central and northern Europe and northern Asia are populated by kettle holes (Tiner, 2003; Kalettka and Rudat, 2006), small (< 1 ha) depressional wetlands of glaciofluvial origin. Land-use and management directly affect individual kettle holes, while site level geomorphology and climate conditions determine kettle hole hydroperiod,

defined as the duration of the wet period of a kettle hole (Kalettka and Rudat, 2006; van der Kamp and Hayashi, 2009). The interactions between the hydrology, organic matter (OM) contributions, and land-use are inherently complex (Song et al., 2014); and how these interactions manifest in kettle hole biogeochemistry across a landscape is less understood (Premke et al., 2016).

The kettle hole water budget consists of winter and early spring inputs primarily driven by snowmelt and runoff over partially frozen soils, direct precipitation, and seasonal lateral flow (van der Kamp and Hayashi, 2009; Gerke et al., 2010; Shaw et al., 2012). Water losses are through evapotranspiration, spillover, and lateral shallow groundwater recharge (Berthold et al., 2004; van der Kamp and Hayashi, 2009). Kettle holes can be temporarily in contact with shallow groundwater potentially resulting in discharge or recharge from the groundwater (van der Kamp and Hayashi, 2009; Heagle and others, 2013). Kettle hole water levels are dynamic, often experiencing seasonal wet-dry cycles. However, for the NE region of Germany the timing of kettle hole water losses and their corresponding magnitudes are not well constrained.

These pronounced wet-dry cycles can lead to the complete drying and rewetting of sediments (Johnson et al., 2004) while others may stay submerged or partially submerged over the year. Strong water level fluctuations result in changes in OM dynamics and oxygen exposure during desiccation (Boon, 2006) that can alter microorganism communities or their carbon metabolism (Fromin et al., 2010; Reverey et al., 2016; Weise et al., 2016). During long-term wet conditions autochthonous primary production within the kettle hole can be an important OM source, while desiccation can lead to terrestrial plant encroachment into kettle holes, which may result in the formation of peat bodies (Gaudig et al., 2006). Thus, the dry-wet cycles impact the environmental conditions and affect OM sources that contribute to the sediment record.

Land management such as the general form of land-use, selection of crop species, fertilization and tillage have a large influence on terrestrial biogeochemistry and consequently for kettle hole surface sediments as well (Nitzsche et al., 2016). Furthermore, substantial material transfer from the surrounding terrestrial ecosystems is known to occur into kettle holes including inputs from plant biomass, soil particles via event based erosion, and nutrients (Frielinghaus and Vahrson, 1998; Gerke et al., 2010; Kleeberg et al., 2016a). However, broad investigations of kettle hole biogeochemistry in the landscape context are few and we do not know the extent to which external (i.e. terrestrial) factors such as fertilization affect kettle hole internal OM turnover or how this is represented in the sediment column.

Kettle hole OM biogeochemistry is thus a function of these primary players: land-use, hydroperiod, and OM sources. We investigated 51 kettle holes with different hydroperiod and land-use by sampling sediment at several depths during one summer. The objectives of our study were, 1) to test if hydroperiod and land management were imprinted on the isotopic values ($\delta^{13}C$, $\delta^{15}N$) and C:N ratios of the sediment OM, and 2) to characterize water loss dynamics and

kettle hole-groundwater connectivity by measuring the stable $\delta^{18}O$ and δD isotope values of kettle hole water over several years.

3.3 Material and methods

3.3.1 Study site

The study site is a 3.25 × 11.75 km (38.2 km^2) wide area and is located within the Quillow catchment (168 km^2; Nitzsche et al., 2016) of NE Germany. The study site comprises of approximately 290 kettle holes in topographic depressions, which were formed due to the delayed melting of buried dead ice blocks after the discontinuous retreat of the Weichselian glaciers approximately 12,000 to 10,000 years ago.

The proportions of land-use types across the study site are 74.4 % arable, grasslands 10.4 %, and forest 5.9 %. Villages and single houses (4.5 %) and larger stagnant water bodies of > 1ha (fens, lakes, reed dominated; 3.4 %) are also dispersed over the area. Kettle holes make up around 1.4 % of the area and are present in all land-use types (Fig. 3.1), and the proportion of stagnant water bodies (kettle holes, moors, reed-dominated, lakes) and streams largely decreases from NW to SE (Fig. A9). The application of chemical fertilizers is common in the area since the second half of the 19th century and slurry application is common since 1970 (Neyen, 2014; Nitzsche et al., 2016). The landscape relief is moderately rolling ranging in elevation from 40 to 112 m a.s.l. The climate is sub humid with a mean annual temperature of 8.6°C and mean annual precipitation of 495 mm as determined per year between 1992 and 2015 (AgroScapeLab Quillow, Dedelow, E 013°48´12´´, N 53°21´59´´). The mean annual temperature was 8.0°C in 2013, 9.4°C in 2014 and 9.1°C in 2015. The mean annual precipitation was 446 mm in 2013, 561 mm in 2014 and 414 mm in 2015.

3.3.2 Sampling design

We sampled 51 kettle holes for sediments from the middle July to the end of August 2013. We based our kettle hole selection on: 1) size class, ensuring that we covered the range of different size classes following the classification of Kalettka and Rudat (2006), 2) land-use type (arable fields, grassland, forest), 3) distribution (we ensured to cover the entire study area), and 4) targeting at sampling kettle holes of different hydroperiod. We classified the kettle hole hydroperiod after several years of observation (2013 - 2015). We defined kettle holes as semi-permanently water-filled (sp-type) when they were water-filled during all water sampling campaigns from 2013, 2014 and 2015, and those that dried out at least one time over all sampling campaigns were classified as temporarily water-filled (t-type). Consequently, we sampled 13 sp-type and 24 t-type kettle holes in arable fields, 3 sp-type and 3 t-type kettle holes in forests, and 2 sp-type and 6 t-type kettle holes in grasslands (Table A2). Sampled kettle holes were predominantly of edge type (42) with *Phalaris arundinacea,* minor full-reed (7) dominated

by *Phragmites australis* and wood type (2) (see the classification of Pätzig et al., 2012) (Table A2).

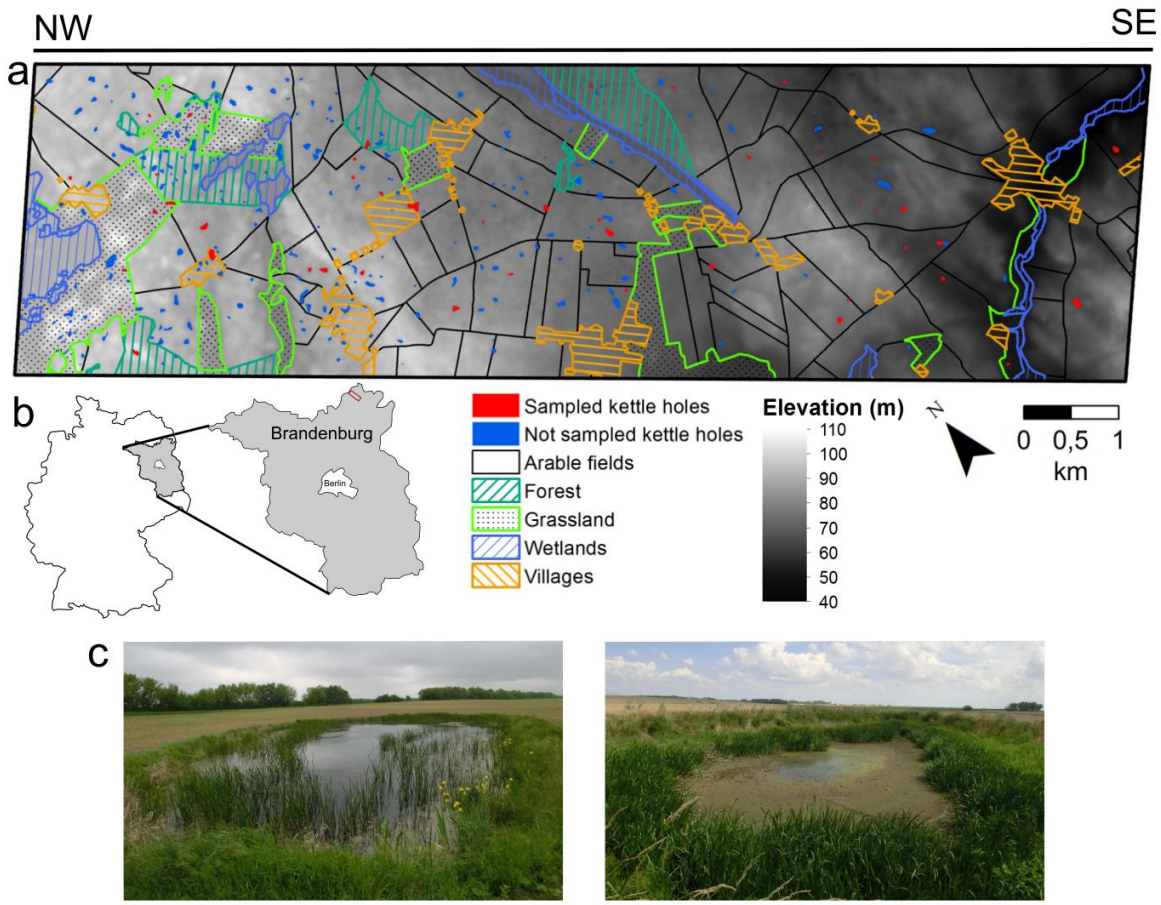

Fig. 3.1. Study site (a), the location of the study site (red rectangle) in NE Germany (b) and photographs of a temporarily water-filled (t-type) kettle hole in July 2013 (left) and the same kettle hole in July 2014 (right) (c). Sampled kettle holes (n =5 1) (red) out of approximately 290 being present in the sampling area underlain by a shaded relief map (in m a.s.l.) and with covers, showing the land-use in which a kettle holes is present (a). Note that in the figure, the study site (a) has been rotated by 40°.

To capture the sediment spatial variability within kettle holes, three undisturbed sediment cores were taken by a gravity corer (UWITEC, Austria, i.d. 60 mm) in a transect from a shallow location (ca. 40 cm) to the deepest site (ca. 80 cm). If a kettle hole was dry (no water present in the sediment), we used a soil auger (Eijkelkamp, Netherlands, 2 cm ø). We took surface sediments (0 - 2 cm; presented earlier in Nitzsche et al., 2016), and deeper sediments (2 - 75 cm) from each kettle hole. The deeper sediment layer, according to Kleeberg et al. (2016a) spans the last ca.120 years.

From deeper layers, we sampled a mineral-dominated sediment and an organic-rich counterpart (e.g. a peat horizon) provided sufficient material was present. The one or two samples were usually taken over a 5 cm depth range (Table A3). We combined the same sediment horizons from the three sampling points along a transect. Thus, it was possible for a

single kettle hole to have two different deeper sediment samples, but this was not consistent across all kettle holes. In total, we collected 83 deeper sediment samples from which 32 kettle holes contained both a mineral and peat horizon, and 19 kettle holes that had only one sample. These samples can be further classified by hydroperiod: 27 samples were taken from sp-type and 56 samples from t-type kettle holes.

We took surface water samples from the center of the kettle holes, which were stored in 12ml gas-tight exetainers (Labco Ltd High Wycombe, UK) sealed with parafilm. We sampled during the growing season (July to August) in 2013-2015 ($n_{July/August\ 2013}$ = 45; $n_{July\ 2014}$ = 23; $n_{July\ 2015}$ = 20) and additionally two times in the dormant season ($n_{December\ 2014}$ = 19; $n_{April\ 2015}$ = 42) (Table A4). At the end of July 2014, we also sampled water (n = 20) for water chemistry related to evaporation (Cl^-, SO_4^{2-}, Ca, K, Na, Mg, P, Si). We also measured pH, electric conductivity and O_2 concentration in-situ with electronic probes (SenTix, TetraCon, and CellOx) directly in the surface water at the edge of the kettle hole.

3.3.3 Sample preparation

All samples were stored in gas-tight containers at 4°C in dark conditions prior to preparation. Sediment samples were oven-dried at 65°C for 48 h and subsequently ground to a powder. Water samples were filtered (0.45 µm cellulose acetate filter) before analysis.

3.3.4 Stable isotope analysis

We relied primarily on the isotopic signature ($\delta^{13}C$, $\delta^{15}N$) and C:N ratios of sediment OM to determine the source (e.g. terrestrial vs. aquatic) as well as the degree of microbial processing and identify potential land-management impacts (Andrews et al., 1998; Herczeg et al., 2001; Thevenon et al., 2012). Prior to carbon stable isotope analysis of sediment samples, inorganic carbon was removed from all sediment samples by acid fumigation according to Harris et al. (2001). Sediment samples were weighed into tin capsules and combusted in an elemental analyzer (Flash HT, Thermo Scientific, Bremen, Germany). Stable isotope ratios of sediments were measured with a Thermo-Scientific, Delta V Advantage isotope ratio mass spectrometer (Bremen, Germany). Stable oxygen and hydrogen isotope ratios of kettle hole water were measured via cavity ring down spectrometry (CRDS). Water samples were vaporized at 110°C (Isotopic H_2O A0211) and the vapor was analyzed with a L2130-I Isotopic H_2O analyzer from Picarro (San Jose, CA, USA).

Stable isotope ratios are reported in delta notation (in ‰ units) after EQ. 3.1, where the ratio *R* of the heavy isotope to lighter isotope in a sample is referenced to an international standard (Brüggemann et al., 2011):

$$\delta = \left(\frac{R_{sample}}{R_{standard}} - 1\right) \cdot 1000. \qquad 3.1$$

We used the ratios $^{13}C/^{12}C$ for $\delta^{13}C$, $^{15}N/^{14}N$ for $\delta^{15}N$, $^{18}O/^{16}O$ for $\delta^{18}O$ and $^{2}H/^{1}H$ for δD. Isotope values are reported relative to Vienna Pee Dee Belemnite (VPDB) for carbon, to N_2 in air for nitrogen and to Vienna Standard Mean Ocean Water (SMOW) for oxygen and hydrogen. Isotopic calibration for EA-IRMS measurements was to IAEA-CH-6 (sucrose), USGS40 (L-glutamic acid) and IAEA-N-1 (ammonium sulfate). Analysis of internal laboratory standards ensured that the estimates of the isotopic values were precise to within < 0.1 ‰ for $\delta^{13}C$ and < 0.5 ‰ for $\delta^{15}N$. Total organic carbon and total nitrogen concentrations (in wt%) of sediment samples were also obtained by EA-IRMS measurements. Repetitive measurements of laboratory standards with the Picarro yielded a precision of < 0.1 ‰ for $\delta^{18}O$ and < 1.5 ‰ for δD.

3.3.5 Chemical analysis of water

Elemental concentrations (Ca, K, Na, Mg, P, Si) were analyzed via inductively coupled plasma atomic emission spectroscopy (ICP-OES) with an ICP-iCAP 6300 DUO (Thermo Scientific, Bremen). Sulfate (SO_4^{2-}) and Chloride (Cl^-) concentrations were measured via ion chromatography (Thermo Scientific Dionex, Bremen).

3.3.6 Evaporation in water bodies

There is a global relationship of $\delta^{18}O$ and δD of precipitation expressed by the equation $\delta^2H = 8 \cdot \delta^{18}O + 10$ – the Global Meteoric Water Line (GMWL) (Craig, 1961; Dansgaard, 1964). Evaporation leads to an enrichment of the heavy isotopes ^{18}O and ^{2}H in the water body due to smaller diffusivities in air (Gonfiantini, 1986; Gibson et al., 2005). This kinetic isotopic fractionation during evaporation leads to a deviation from the GMLW indicated by a decrease in the slope of this relationship and is best explained by the Craig-Gordon-model (Craig and Gordon, 1965). Evaporated water bodies plot to the right of the GMWL and cluster on a local evaporation line (LEL), which is indicated by a slope commonly ranging between 4.0 and 5.5 for water bodies (Gibson et al., 2008). The intersection point between the LEL and GMWL describes the source water, i.e. the weighted mean isotopic composition of the local precipitation (Gibson and Edwards, 2002).

Based on the $\delta^{18}O$ and δD isotope values of kettle hole water we calculated the evaporative water volume loss *f* from kettle holes sampled in the growing season (July/August 2013, 2014 and 2015) with the *Hydrocalculator* software developed by (Skrzypek et al., 2015). *Hydrocalculator* allows for estimations of *f* based on the revised Craig-Gordon model (Horita et al., 2008) and includes modification of the Craig-Gordon model based on field studies, including sites from North America (Skrzypek et al., 2015), thus justifying its use in humid regions such as NE Germany. We assumed a non-steady-state hydrological regime of the kettle holes with no out- and inflows after filling was complete. For each year, we calculated *f* between beginning

of April and the time of sampling in July. Though we did not take water samples in the beginning of April for each year (only in April of 2015), we chose this time as the time when the filling was expected to be complete and for the onset of evaporation based on daily potential evapotranspiration data for 2013 and 2014. We constructed the LEL based on the isotopic composition δ_L (‰) of kettle hole water at the time of sampling. To estimate the initial isotopic composition δ_P (‰) of kettle hole water we used the intersection between the LEL and local meteoric water line (LMWL; see below) for each year (Table A5). In addition, we calculated *f* from April to July 2015 using the measured $\delta^{18}O$ and δD isotope values from our April 2015 sampling campaign as δ_P which allows for considering the deviation of April 2015 isotope values from the LWML (see below).

Mean temperature T (in °C) and relative humidity were obtained from a weather station in the center of the study area located 2 m above the water surface from one sp-type kettle hole. The weather station failed in the end of 2014, thereafter we used mean daily temperature and relative humidity from the ZALF AgroScapeLab Quillow station. We sampled monthly local rain using a ball-type collector (Kazahaya and Yasuhara,1994). We used the rain isotopic composition (δ_{rain}) to construct the LMWL and calculate the mean $\delta^{18}O$ and δD of local precipitation between April and July. The stable isotopic composition of the ambient air moisture ($\delta_{A)}$ was determined based on stable isotopic composition of local precipitation and the slope of the LEL. An implicit assumption is that there is an equilibrium isotopic fractionation between δ_{rain} and δ_A, which is a function only of temperature. δ_A can also affected by relative humidity, wind speed, and direct sunlight over short time periods, but because our estimates are for two seasons, we assume daily fluctuations in these parameters have a small effect.

3.3.7 Statistical analysis

To test for statistical differences in $\delta^{13}C$, $\delta^{15}N$ and C:N ratios of surface sediments with respect to land-use, hydroperiod and their interactions, we used a two-way ANOVA followed by a post hoc significance test (Tukey's HSD) after testing for normally distributed data with the Shapiro-Wilk test. We tested for differences in $\delta^{13}C$, $\delta^{15}N$ and C:N ratios of deeper sediments with respect to hydroperiod, land-use, and TOC content by performing a nested ANOVA including the kettle hole in the error term of the model to account for the unbalanced sample size. We performed a three-way ANOVA followed by Tukey's HSD to test for significant differences in evaporative loss with respect to land-use, hydroperiod, and year sampled after testing for normally distributed data with the Shapiro-Wilk test. We used a generalized linear model (GLM) to test for significant differences in water chemistry data across land-use and hydroperiod types. We refrained from reporting p values of statistical tests for the evaporative loss *f* and water chemistry between grassland kettle holes and kettle holes of other land-use given the low *n* of two for grassland kettle holes. We used Moran's I to test for spatial

autocorrelation of sediment $\delta^{13}C$ and $\delta^{15}N$, water chemistry data, and evaporative loss *f* in kettle holes from the different sampling periods. We used non-linear regression for curve fitting of deeper sediment $\delta^{15}N$ vs. C:N ratio. We calculated the Akaike's Information Criterion (AIC) to test whether a linear fit or a curve fit was better. We used a second order polynomial to fit the $\delta^{15}N$ and C:N ratio vs. depth for deeper sediments of sp-type kettle holes, and a local polynomial regression (loess) for the patterns of t-type deeper sediments. We applied linear regressions between the evaporative loss *f* of 2014 and water chemistry data, $\delta^{18}O$ vs. δD of kettle hole water, and $\delta^{13}C$ and $\delta^{15}N$ vs. the geographical distance (i.e. longitude × latitude). We used the student's t test to test for significant differences in mean slope of the growing season (July/August 2013, July 2014, July 2015) over the mean slope of the dormant season (December 2014, April 2015).

We used agglomerative clustering, a form of hierarchical clustering, to determine whether kettle holes reflect the hydroperiod and surrounding land-use based on their OM biogeochemistry. We performed an agglomerative (Euclidean distances using average linkage and standardized values) clustering using $\delta^{13}C$, $\delta^{15}N$ isotope data and molar C:N ratios of the surface sediments.

Agglomerative clustering is a common method to group similar samples and represent them in a dendrogram. This is achieved by creating and merging clusters that are made up of similar samples, while moving up in the hierarchy ('bottom-up' approach). To decide which clusters are merged, a distance metric is created as a measure for the dissimilarity between the samples and a linkage criterion is defined. The resulting dendrogram has the interlinkage distance (or height) on the y-axis that corresponds to the distance between clusters and allows for identifying similar clusters. All statistical analysis including the agglomerative clustering approaches were performed with R (version 3.1.1, R Foundation for Statistical Computing, Vienna, Austria, http://www.R-project.org/).

3.4 Results

3.4.1 Sediment $\delta^{13}C$, $\delta^{15}N$ and C:N data

We did not find any significant differences in surface sediment $\delta^{13}C$ with respect to land-use ($p = 0.57$) and hydroperiod ($p = 0.44$). In contrast, across all kettle holes, we found large differences in $\delta^{15}N$ with respect to land-use and hydroperiod (Fig. 3.2a; $p < 0.01$). Within arable fields, we found t-type kettle holes were significantly more enriched in ^{15}N compared to sp-type kettle holes by 2.1 ‰ ($p < 0.01$; Table A6). Within grasslands, t-type kettle holes were enriched in ^{15}N by 2.8 ‰, and within forests by 3.3 ‰ compared to sp-type kettle holes, although the difference was not significant. Surface sediments from kettle holes in forests were significantly ($p < 0.01$) more depleted in ^{15}N compared to surface sediments in kettle holes from arable fields and grasslands. Overall, we found surface sediments to slightly decrease in $\delta^{15}N$ from SE to

NW (Moran's I = 0.09, $p < 0.01$, n = 51). More precisely, surface sediments from kettle holes located in arable fields were weakly spatially autocorrelated (Moran's I = 0.18, $p < 0.01$, n = 37) in which the $\delta^{15}N$ decreased slightly from the SE to NW or by ca 0.6 ‰ ($r^2 = 0.26$, $p < 0.01$) for each unit of geographical distance (longitude × latitude).

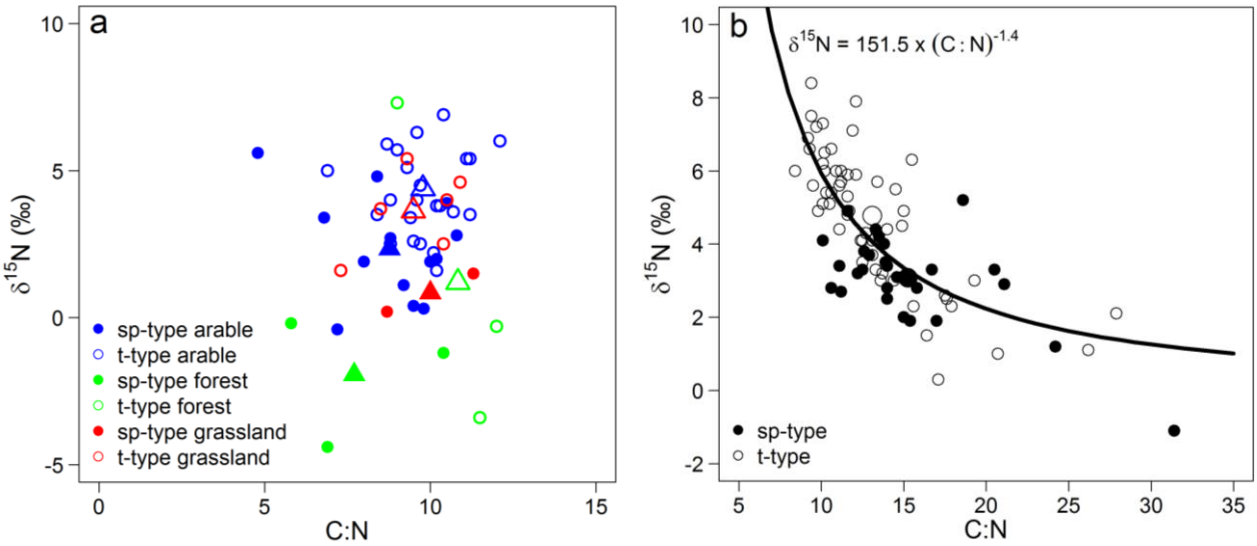

Fig. 3.2. Bi-plot of $\delta^{15}N$ (‰) vs. the C:N ratio for (a) surface sediments and (b) deeper sediments. Enlarged triangles (a) and enlarged circles and triangles (b) are the mean for each group. The black solid line in (b) represents a non-linear least square curve fit through all 83 deeper sediment samples.

Land-use was not significant in explaining the variation of $\delta^{13}C$, $\delta^{15}N$ and C:N ratios of deeper sediments. Sediment $\delta^{13}C$ values from t-type and sp-type kettle holes were similar (range of $\delta^{13}C$ from -27.7 to -28.9 ‰). $\delta^{15}N$ of sediments from t-type kettle holes (mean of 4.8 ± 0.3 ‰, n = 56) were consistently more enriched ($p < 0.01$) than sediments from sp-type kettle holes (mean of 3.1 ± 0.2 ‰, n = 27; Table A7). Sediments from sp-type kettle holes had significantly ($p < 0.05$) higher C:N ratios (mean of 15.2 ± 0.9) than sediments from t-type kettle holes (mean of 13.1 ± 0.5).

In contrast to surface sediments, deeper sediments showed a clear tendency of an increase in $\delta^{15}N$ alongside a decrease in C:N (Fig. 3.2b). This trend is best explained by a non-linear function ($r^2 = 0.59$, $p_{coefficient} = 0.01$, $p_{exponent} < 0.01$), compared to a liner regression model ($AIC_{NLS} = 271$ vs. $ACI_{LM} = 281$). Both sediments from the t-type and sp-type kettle holes showed a decrease in $\delta^{15}N$ with depth ($r^2_{sp\text{-}type} = 0.02$; $r^2_{t\text{-}type} = 0.31$) (Fig. 3.3a). Similarly, C:N ratios from the t-type and sp-type kettle hole sediments increased with depth ($r^2_{sp\text{-}type} = 0.17$; $r^2_{t\text{-}type} = 0.30$) (Fig. 3.3b).

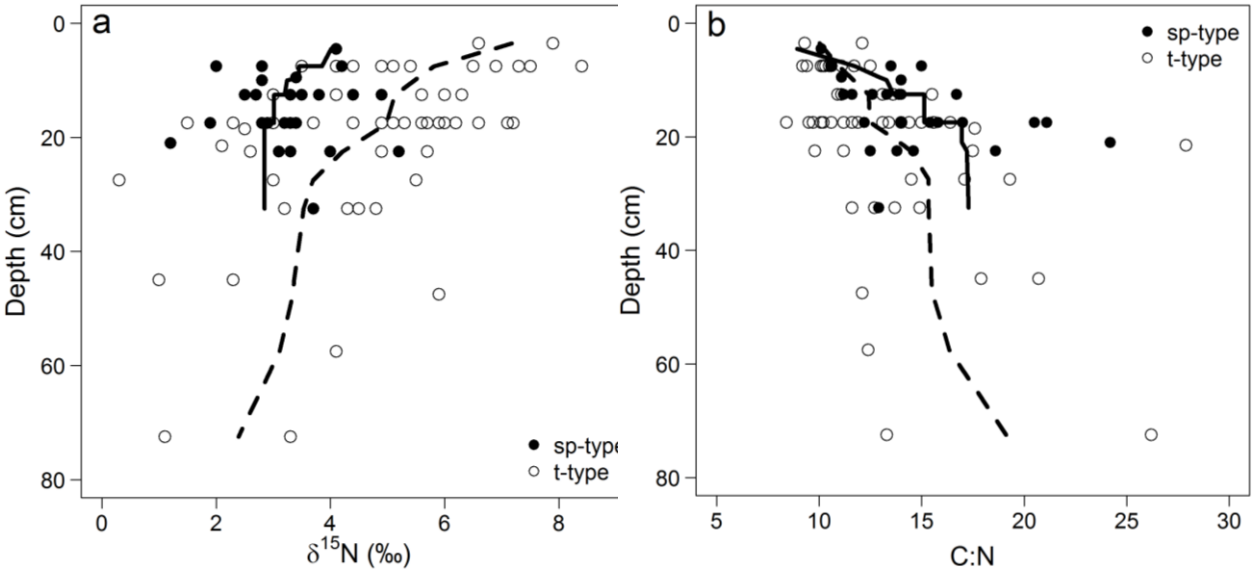

Fig. 3.3. Bi-plot of the δ^{15}N (in ‰) (a) the C:N ratio (b). vs. mean depth dimension for each deeper sediment sample (in cm). The black solid lines represent second order polynomial fit for deeper sediments of sp-type kettle holes (n = 27), and the black dashed lines local polynomial regressions (loess) for the patterns of t-type deeper sediments (n = 56). A total of 83 samples are shown because sometimes two samples per kettle hole were taken.

3.4.2 Kettle hole surface water δ^{18}O and δD data and evaporative loss f

We observed evaporative enrichment in kettle hole surface waters over all sampling periods (Fig. 3.4). The mean slope for the local evaporation line (LEL) for the late growing season (July/August 2013, 2014 and 2015) was 3.76, significantly lower ($p < 0.01$) than the mean slope (4.68) of the dormant season (December 2014 and July 2015 sampling campaigns). To estimate the water loss at the site scale, we first calculated the difference between the slopes of LELs (growing and dormant season) from the LMWL. We then subtract the difference between the normalized seasonal slopes and express this relative to the dormant season LEL, which results in an estimate of a site level evaporative loss (28 %) during our measurement period. Using a similar method but with reference to the growing season (instead of the dormant season), we can estimate how much water from the previous growing season contributes to the beginning of the next water year. On average about 20 % of the kettle hole water volume has been refilled by shallow groundwater or interflow, and suggests a mean kettle hole water residence time of about 5 years.

The calculated evaporative loss (*f*) values varied by the year sampled and kettle hole hydroperiod and land use. The t-type arable kettle holes had the greatest δ^{18}O and δD values (Table A8) and the corresponding evaporative loss *f* averaged 56 % in July 2014 (Table 3.1), which was higher compared to sp-type kettle holes (mean of 38 %), although the difference was not significant. However, there were values of *f* that greatly exceeded the mean, for example, for two t-type and two sp-type kettle holes *f* was 60 %, and for one t-type kettle hole in 2014 *f*

was 75 %, furthermore, some kettle holes were dry at the time of sampling indicating that rates for some kettle holes might have been higher. For example, in the 2015 growing season, only sp-type kettle holes could be sampled except for two t-type forests kettle hole. The sp-type kettle hole *f* estimates (mean of 23 %) in arable land sampled in 2013 was significantly lower ($p < 0.01$) than the 2014-2015 growing season campaigns. Forest kettle holes were least affected by evaporation with $f < 20$ %, which was significantly lower compared to that of arable kettle holes ($p < 0.01$). The number of grassland kettle holes was too low for reporting representative values.

Table 3.1. Calculated average evaporative losses (*f*) ± SE (in %) for kettle holes.

Land-use	Hydroperiod	July/August 2013 (%)	July 2014 (%)	July 2015 (%)	April-July 2015 (%)
Arable	all	20 ± 2[a] (n = 35)	43 ± 4 (n = 17)	39 ± 2 (n = 13)	33 ± 2 (n = 13)
	t-type	17 ± 2 (n = 22)	56 ± 8 (n = 5)	n.a.	n.a.
	sp-type	23 ± 3 (n = 13)	38 ± 4 (n = 12)	39 ± 2 (n = 13)	33 ± 2 (n = 13)
Grassland	all	14 ± 4 (n = 4)	29 ± 8 (n = 2)	28 ± 5 (n = 2)	23 ± 3 (n = 2)
	t-type	10 ± 1 (n = 2)	n.a.	n.a.	n.a.
	sp-type	19 ± 7 (n = 2)	29 ± 8 (n = 2)	28 ± 5 (n = 2)	23 ± 3 (n = 2)
Forest	all	7 ± 2 (n = 6)	12 ± 2 (n = 4)	16 ± 5 (n = 5)	16 ± 1 (n = 5)
	t-type	10 ± 2 (n = 3)	15 (n = 1)	18 ± 2 (n = 2)	16 ± 2 (n = 2)
	sp-type	5 ± 1 (n = 3)	11 ± 0 (n = 3)	15 ± 2 (n = 3)	16 ± 1 (n = 3)

[a]Calculated *f* values represent mean values between *f* obtained each by $\delta^{18}O$ and δD.

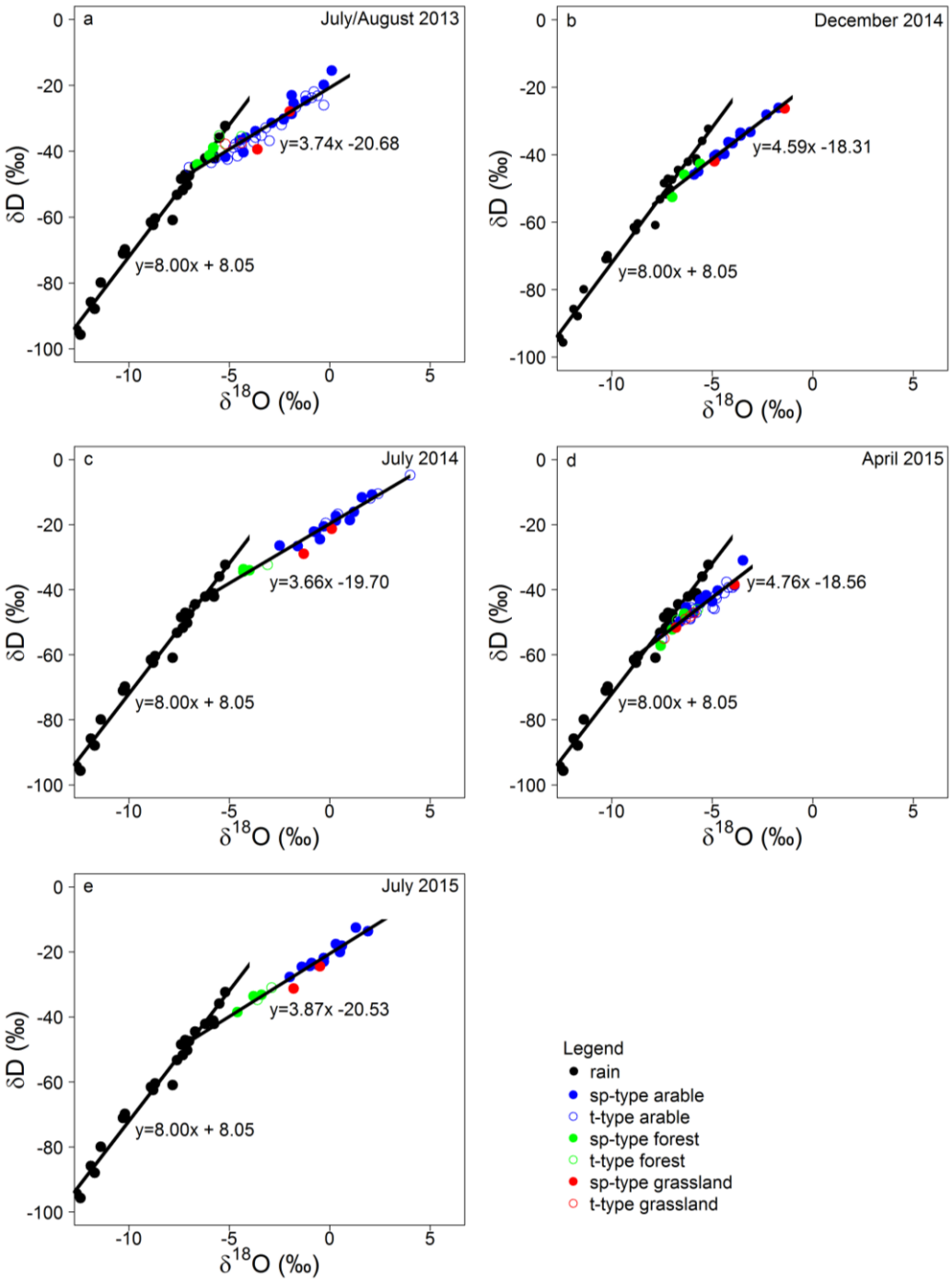

Fig. 3.4. Bi-plots of δD vs. $\delta^{18}O$ (in ‰) of kettle hole water from July/August 2013 (n = 45) (a), December 2014 (n = 19) (b), July 2014 (n = 23) (c), April 2015 (n = 42) (d) and July 2015 (n = 20) (e). Black solid circles depict rain water sampled monthly from August 2013 to July 2015. Two snow samples from winters 2014 and 2015 were also included in the regression line of the local meteoric water line (black solid line through rain water samples), but not shown because they were very depleted in the heavy isotopes.

3.4.3 Surface water chemistry data

In-situ surface water parameters (pH, O_2, electrical conductivity) measured in the 2014 growing season were consistently lower for forest sp-type kettle holes compared to arable sp-type kettle holes (Table 3.2). Forest kettle holes also had lower concentrations (mg l^{-1}) of Cl^-, SO_4^{2-}, Ca, K, Mg, Na, but dissolved total phosphorous (DTP) and Si concentrations were both greater in forest kettle holes compared to arable kettle holes, but the difference was not significant. Furthermore, we found O_2 to be significantly lower in forest kettle holes ($p < 0.06$). The concentrations of Cl^-, SO_4^{2-}, Ca, K, Mg, Na and Si in surface water from t-type kettle holes were consistently greater, but not significantly. Temporarily water-filled kettle holes had on average an electric conductivity that was significantly greater by 224 µs cm^{-1} than that of sp-type kettle holes ($p < 0.05$) and higher O_2 levels ($p < 0.06$). However, neither the electric conductivity, nor O_2 showed a correlation between with *f* for 2014. Instead, using all 23 sampled kettle holes in 2014, we found slight positive correlations between *f* and concentrations of Cl^- ($r^2 = 0.18$, $p < 0.05$), K ($r^2 = 0.2$, $p < 0.05$), Mg ($r^2 = 0.14$, $p < 0.05$) and a slight negative correlation with P ($r^2 = 0.18$, $p < 0.05$).

Table 3.2. Elemental concentrations (mg l^{-1}) and pH, O_2 and elec. conductivity of kettle hole water sampled in July 2014.

Land-use	Hydroperiod	pH	O_2 (mg l^{-1})	elec. Cond. (µs cm^{-1})	Cl^- (mg l^{-1})	SO_4^{2-} (mg l^{-1})
Arable	all (n = 17)	7.8 ± 0.2	5.9 ± 1.1	400 ± 41	23.6 ± 3.9	5.6 ± 1.7
	t-type (n = 5)	7.6 ± 0.3	6.1 ± 2.9	513 ± 77	31.2 ± 8.0	5.4 ± 2.2
	sp-type (n = 12)	7.9 ± 0.2	5.8 ± 1.1	353 ± 44	20.4 ± 4.3	5.7 ± 2.2
Grassland	sp-type (n = 2)	8.2 ± 1.1	5.5 ± 5.2	249 ± 31	6.9 ± 2.4	1.6 ± 1.3
Forest	all (n = 4)	6.9 ± 0.2	1.3 ± 0.6	404 ± 124	10.2 ± 4.8	5.1 ± 2.2
	t-type (n = 1)	7.5	3.0	755	24.4	10.7
	sp-type (n = 3)	6.8 ± 0.2	0.7 ± 0.2	287 ± 60	5.5 ± 1.4	3.2 ± 1.7

Land-use	Hydroperiod	Ca (mg l^{-1})	K (mg l^{-1})	Mg (mg l^{-1})	Na (mg l^{-1})	P (mg l^{-1})	Si (mg l^{-1})
Arable	all (n = 17)	52.3 ± 5.6	20.4 ± 2.7	10.4 ± 1.3	12.5 ± 2.1	0.4 ± 0.1	4.3 ± 0.9
	t-type (n = 5)	60.0 ± 7.4	26.5 ± 4.2	12.4 ± 2.9	15.3 ± 4.3	0.5 ± 0.2	7.4 ± 1.1
	sp-type (n = 12)	49.1 ± 7.2	17.8 ± 3.3	9.6 ± 1.4	11.3 ± 2.4	0.4 ± 0.1	3.0 ± 1.0
Grassland	sp-type (n = 2)	38.4 ± 14.5	11.0 ± 3.8	5.9 ± 0.2	7.2 ± 1.4	0.2 ± 0.1	0.6 ± 0.1
Forest	all (n = 4)	57.2 ± 33.1	11.2 ± 1.2	6.1 ± 2.7	5.7 ± 2.3	1.1 ± 0.5	5.8 ± 1.8
	t-type (n = 1)	153.3	12.1	13.4	12.3	0.4	10.3
	sp-type (n = 3)	25.1 ± 11.8	10.9 ± 1.6	3.7 ± 1.5	3.5 ± 0.6	1.3 ± 0.6	4.2 ± 1.4

3.4.4 Agglomerative clustering

We performed an agglomerative clustering of surface sediment data ($\delta^{13}C$, $\delta^{15}N$, C:N ratio) to test whether kettle holes are distinguishable by their OM biogeochemistry. The agglomerative clustering yielded five different clusters with an agglomerative coefficient of 0.81 (Fig. 3.5). The clusters clearly separated kettle holes by hydroperiod (sp-type and t-type) and land-use (arable vs. forest). $\delta^{15}N$ was the core driver among the dataset, followed by C:N ratios. Clusters (C) C5 through C3, and a branch of C2 represent primarily t-type kettle holes. Cluster 5 (C5) is dominated by kettle hole sediments depleted in the heavy isotope ^{15}N, and consists primarily of forest kettle holes and one sp-type arable kettle hole. C4 represents one sp-type kettle hole that was classified by itself because the sediments had a high $\delta^{15}N$ value of 5.6 ‰, but low C:N ratio of 4:8. C3 consists of t-type kettle holes (4 arable, 1 forest) that have a greater $\delta^{15}N$ values than C4. C2 represents primarily t-type kettle holes (24), although one branch within C2 clusters near a branch of C1. C1 comprises of 14 kettle holes with a relatively low mean $\delta^{15}N$ of 1.5 ‰ and was dominated by sp-type kettle holes (n = 9). Grassland kettle holes clustered together with arable kettle holes from C1 and C2.

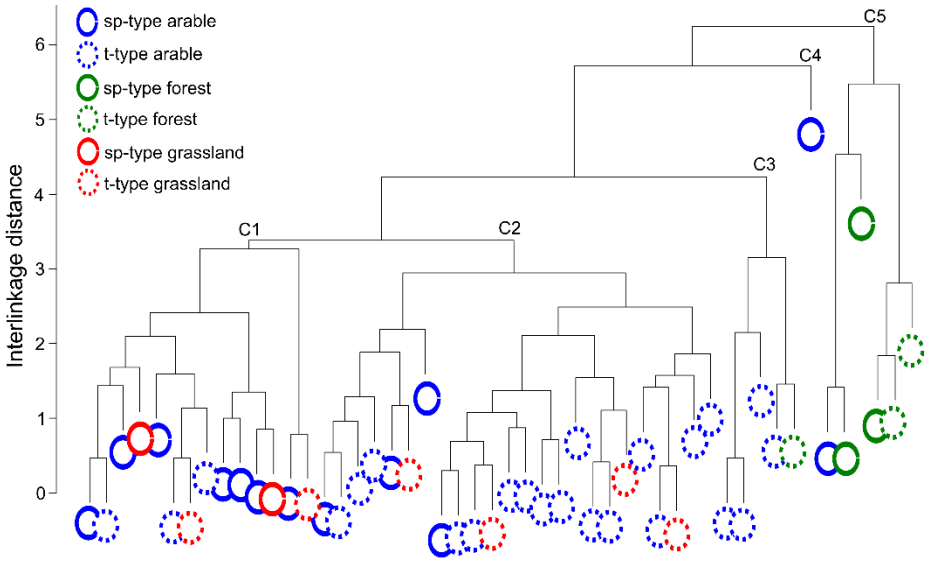

Fig. 3.5. Agglomerative clustering results of kettle hole surface sediment data ($\delta^{13}C$, $\delta^{15}N$, C:N).

3.5 Discussion

We observed isotopic patterns in kettle hole sediment OM that are clearly related to the surrounding land-use and hydroperiod. Surface sediments were impacted the most by land management, while deeper sediment isotopic values and C:N ratios were closely related to the hydroperiod. The shallow ground water dynamics and evaporation were dominant hydrological processes that have potential feedbacks on OM contributions and environmental conditions. In the following, we discuss how the two primary drivers, hydroperiod and land-use, contribute

to kettle hole sediment biogeochemistry and how we can use water isotope data to elucidate the development of the kettle hole water balance.

3.5.1 Surface sediments

For surface sediments, we found significant differences in isotopic composition between two core groups: forests and agriculture including grasslands. Differences due to land-use for all kettle holes were largely driven by $\delta^{15}N$ values. This pattern was especially strong in kettle holes in arable fields between hydroperiod types (Fig. 3.2a). Thus, we infer that activities in arable sites interact with the biotic and abiotic processes associated with hydroperiod to drive sediment C and N biogeochemistry. Previously, we found land use and management to have a profound effect on terrestrial biogeochemistry at our site (Nitzsche et al., 2016), most of which is related to management of crop fields.

Land management directly affects sediment biogeochemistry through OM source input. Slurry (organic fertilizer derived from animal manure) application is used widely in the study region, especially in the SE (Nitzsche et al., 2016) as confirmed by the spatial autocorrelation of $\delta^{15}N$ of surface sediments from arable kettle holes that we observe. This leads to the input of isotopically enriched OM and nutrients ultimately derived from slurry into kettle holes. Indirectly, nutrient run-off can cause eutrophication leading to seasonal anoxia in kettle holes, a phenomenon especially evident in sp-type kettle holes that can result in potential shifts in the isotopic signature of sediments. A seasonally anoxic water column reduces microbial degradation rate in general and favors anaerobic degradation, which can lead to no changes in $\delta^{15}N$ or a relative depletion of ^{15}N in the remaining OM (Lehmann et al., 2002; Menzel et al., 2013), possibly explaining why we observe lower $\delta^{15}N$ in surface sediments of sp-type kettle holes. On the other hand, seasonal anoxia can lead to greater denitrification, which is associated with enrichment of ^{15}N in the remaining dissolved nitrate (Teranes and Bernasconi, 2000), a process possible in sp-type kettle holes. Though we did not measure the $\delta^{15}N$ of nitrate, the low $\delta^{15}N$ in surface sediments of sp-type kettle holes suggests that isotope fractionation due to denitrification is negligible.

Kettle holes within arable fields exhibit considerable variability among the hydroperiod types and for those that often fall dry or nearly dry, terrestrial plants are found mixed with communities that thrive under submerged or semi-submerged conditions (Nitzsche personal observation). The change in plant species associated with the hydroperiod (Euliss et al., 2004), is therefore an additional OM source that varies in isotopic composition (Badrian, 2015; Nitzsche et al., 2016) and can result in shifts in sediment isotopic composition. For example, *Phalaris arundinacea*, which was the most common plant at many kettle holes, has a $\delta^{15}N$ of 6.3 ‰ and a C:N ratio often > 25 (Nitzsche et al., 2016). However, internal kettle hole OM sources, such as phytoplankton or other periphytic algae, may also contribute to the overall

variability we observe in both hydroperiod kettle hole types. To obtain a deeper understanding of the biogeochemistry of surface sediments, more process-oriented research is needed that captures short-term inputs and losses.

Kettle holes present in forests and forest remnants had relatively low surface sediment $\delta^{15}N$ values (< 0 ‰) and classified separately from the other kettle hole types, signifying C and N cycling processes that are different from the arable and grassland kettle holes. We infer that 1) anoxic conditions were particularly important in this land-use resulting in sediments more depleted in ^{15}N, and 2) the influx of beech litter (found in all forests at our site) was an allochthonous source of low $\delta^{15}N$ to the kettle holes. The reduction in O_2 may be caused by microbial decomposition of beech litter exhausting available O_2 as well as tree canopy cover preventing wind induced mixing of the water body. A decrease in O_2 concentration hampers microbial decomposition, and at suboxic conditions or in the absence of O_2, preferentially iron-bound P can be released from the sediment (Søndergaard et al., 2003; Spears et al., 2007); conditions that we observed in our forest kettle holes in July 2014. Beech leaf litter, a major OM contributor to forest kettle holes, has a $\delta^{15}N$ of -4.5 ± 0.4 ‰ at our site (Nitzsche et al., 2016) and, in addition to anoxic conditions, can help to explain the shift in sediment OM isotopic signal.

3.5.2 Deeper sediments

Based on the isotopic and C:N results, land management effects were not detectable within sediment OM from deeper depths. This concurs with previous research on kettle hole sediment stratigraphy within the same region which found low levels of heavy element concentrations derived from chemical fertilizers and pesticides in sediment cores (Kleeberg et al., 2016a). Historically, intensified land management practices began near the end of the first half of the 20th century (Neyen, 2014), and given that our samples are constrained to the last 120 years (Kleeberg et al., 2016a), management effects may be imprinted in the deeper sediment record from our study but at nominal levels.

The $\delta^{15}N$ and C:N of the t-type sediment OM from the deeper strata were significantly different from sp-type kettle holes pointing to potentially distinct environmental conditions that may affect decomposition. In the absence of large contributions of OM resulting from land management, we infer that internal cycling from microbes drives these patterns (Paul and Clark, 1996; Kramer et al., 2003). Microbes preferentially utilize the lighter isotopes ^{12}C and ^{14}N during decomposition increasing the stable isotope values of the remaining OM (Dijkstra et al., 2008). Microbial decomposition may be enhanced during longer dry periods, expected for the t-type kettle holes, as oxygen availability is high, especially in the surface near parts of the sediment (Boon, 2006; Reverey et al., 2016; Weise et al., 2016). The pattern in $\delta^{15}N$ vs. C:N suggests that the environmental conditions in the t-type kettle holes such as variations of

aeration and temperature (Johnson et al., 2004) during dry-wet cycles contribute to stronger OM turnover (Hulthe et al., 1998; Mikha et al., 2005). The analyses we present in this study is, however, limited by our sampling design in that we did not perform a complete stratigraphic analysis such as Kleeberg et al. (2016a), and further research that includes dating will add certainty to the inferences we draw here.

Interestingly, the $\delta^{15}N$ values of the sediments in t-type kettle holes drive the curve of the relationship between $\delta^{15}N$ and C:N (Fig. 3.2b). Lake sediment studies have found a similar trend but with depth (e.g. Esmeijer-Liu et al., 2012), and the relation between soil $\delta^{15}N$ and C:N is depicted as linear (Craine et al., 2015). Our data are novel in that and we find this pattern across a landscape (i.e., not a single kettle hole) and across different hydroperiod types. We hypothesize that OM samples in which the C:N values remained approximately constant (C:N < 7) experienced the recycling of OM within microbial communities (i.e., maintaining metabolic stoichiometry) while the isotopic signature increased with the degree of recycling. This pattern can also be observed in the data of Craine et al. (2015). The curvature in the relationship may, therefore, indicate a threshold at which new inputs are restricted to microbial communities; for example, the stabilization of OM via organo-mineral associations has been shown to potentially preserve OM from microbial decomposition (Lalonde et al., 2012; Vogel et al., 2014).

Deeper layer sediment OM C:N ratios were often > 15 and the layers contained peat. These buried organic horizons are clearly protected from complete decomposition and much of the material collected in these layers still appeared plant-like. This is supported by lower $\delta^{15}N$ values and higher C:N ratios in the deeper sediment horizons of the t-type kettle holes (Fig. 3.2b), indicating less microbial processing downward, possibly because the terrestrial OM was quickly buried by eroded soil particles (Frielinghaus and Vahrson, 1998; Kleeberg et al., 2016a). The $\delta^{15}N$ might also be low because of atmospheric deposition. Atmospheric N isotopic composition has been becoming depleted in the heavy isotope over time due to anthropogenic emissions (Hastings et al., 2009; Holtgrieve et al., 2011). Wet deposition with low $\delta^{15}N$ in nitrate and ammonium was suggested as a potential impact on peat layers in Northern Finland leading to more ^{15}N depleted isotope values toward the surface (Esmeijer-Liu et al., 2012). However, in the deeper sediments present in our study the opposite trend occurs in which $\delta^{15}N$ values are lower in the deepest sediments (where we would expect higher values if deposition was important) suggesting that wet deposition has little to no effect on the deeper sediment OM.

3.5.3 Kettle hole hydrology

Overall, we found that the kettle holes of different land-use types and hydroperiod fell along an isotopic evaporation line (LEL). Thus, the kettle holes are reflecting a similar source

water and climate response (e.g. relative humidity, potential evaporation), confirming the findings of Thomas and others (2012) regarding minor climate variability in the region. We also captured strong intra-annual patterns during our study. For example, winter 2012/2013 was characterized by substantial snowfall and temperatures below freezing resulting in snow accumulation on adjacent fields until the beginning of April. A substantial volume of meltwater relatively depleted in ^{18}O contributed to the isotopic source of 2013 sampled kettle holes via infiltration from the surrounding soil. This affects not only the isotopic signal of the source water but also the evaporation patterns by increasing the water volume and subsequently increase heat storage capacity (Abtew and Melesse, 2012) reducing the effect of evaporative fractionation. Thus, the initial conditions (isotopic composition and water volume) of the kettle hole, as predicated by snow levels and snowmelt contributions, constrain evaporative loss.

We used the isotopic enrichment of water in each kettle hole as a proxy for the fraction of water evaporated for two periods (winter-summer) over three years. We captured the onset of evaporation in the kettle holes between our April and June sampling, thus constraining the time point at which evaporation impacts the isotopic signature of water, and presumably, the water budget. We found that evaporative loss could be as little as 7 % to as much as 75 % based on the year, season, and land-use type. From a landscape perspective (i.e., estimates based on slopes of evaporative enrichment lines), we estimate that kettle holes experience an evaporative loss of 28 %. We also found electric conductivity, Cl^-, Ca, Na, K, Mg and Si concentrations to be higher in t-type kettle holes, thus confirming evaporation is more dominant in t-type than in sp-type kettle holes. Evaporative loss *f*, explained 14 to 20 % of the variation in Cl^-, K, Mg and P concentrations in 2014. However, these correlations indicate that internal biogeochemical processes, such as carbonate precipitation, leaching and re-dissolution of salts during wet-dry cycles and transpiration, may have greater importance in the cycling of these elements at our site (Berthold et al., 2004; Dogramaci et al., 2015).

While we found evaporation rates can be relatively high, evaporation alone cannot explain the complete dry-out of some of the kettle holes. Lateral groundwater flow to the wet margins of the water body is a dominant water loss for wetlands (Hayashi et al., 1998; Ferone and Devito, 2004; Gerke et al., 2010). For instance, Hayashi and others (1998) found that shallow groundwater lateral flow could explain 75 % of the total water loss. The magnitude of this flow can even be enhanced when the water is taken up by plants from the vegetation belt and the crop fields, for transpiration (Woo and Rowsell, 1993; Hayashi et al., 1998; van der Kamp and Hayashi, 2009). Since both lateral groundwater flow and evaporation contribute to kettle hole water loss, we can state that most of these kettle holes are partially-closed to open systems. Similar shallow water bodies have been found to be in contact with the shallow groundwater over the year and either discharge or recharge groundwater depending on the season (Euliss et al., 2004; van der Kamp and Hayashi, 2009; Heagle et al., 2013).

At our site, water transfer between the kettle hole and surrounding soil is strong particularly during the dormant season in which 20 % kettle hole water volume is refilled. However, contact to the shallow groundwater can weaken during the growing season, in which case evaporation from the kettle hole water body and transpiration of plants in the surrounding vegetation belt most likely dominate kettle hole water loss. T-type kettle holes, in particular, might have a stronger linkage to the groundwater system. In this case, when the groundwater level decreases, the t-type kettle hole water table decreases concomitantly, and when the groundwater level rises again, so does the water table in these kettle hole types. Future research of kettle hole hydrology will need to address groundwater connectivity as well as vegetation transpiration losses in the late summer season to fully understand the kettle hole water budget.

3.5.4 Links between kettle hole biogeochemistry, hydroperiod, and land-use

Kettle holes lie at the nexus between land-use, hydrology, and aquatic-terrestrial ecology. Understanding the role of each over time is requisite to characterizing their biogeochemical function across this landscape. Our data show 1) how land-use can influence kettle hole biogeochemistry through actions such as slurry application and erosion, 2) how hydrology and plant communities interact resulting in peat layers; and 3) how the hydroperiod regulates important environmental conditions such as oxygen availability triggering aerobic decomposition.

Essential to characterizing kettle hole biogeochemistry is the observation that t-type kettle holes are fundamentally different than sp-type. However, assigning a kettle hole to one hydroperiod class or another is very subjective given the length of time kettle hole sediments integrate. In order to test for long-term differences in kettle hole biogeochemistry, we performed a data driven classification on surface sediments that was not constrained by our original observational classification. The clustering analysis revealed that kettle hole biogeochemistry is different for those which are more likely to be water filled or not over time. Furthermore, we are not surprised by the range in hydroperiod implicated by the clustering results given that the sediments are integrating shifts in hydroperiod over a relatively long time span. To the contrary, the fact that we do see a separation in the sediments that correspond to our hydroperiod classification provides strong evidence of the important role hydroperiod plays as a driver of kettle hole biogeochemistry. Future studies may build on such a classification to include deeper sediments as well.

3.6 Conclusion

We have provided evidence that kettle hole hydroperiod is a predominant driver of (OM) turnover and biogeochemistry. By analyzing shallow and deep sediment we captured both current and past conditions. We recognize that our research strategy to capture many different types of kettle holes across a large spatial extent does not provide the temporal resolution to capture past conditions with high accuracy; however, the findings and patterns from our study are robust and highly relevant to kettle hole biogeochemistry. The surface sediments reflect recent OM inputs and short-term processes, including management and land-use effects, while deeper sediments record different longer-term patterns of hydroperiod and the degree to which OM is processed. We found that kettle holes currently deemed sp-type, in the past also experienced prolonged drying and possible terrestrial plant encroachment that developed into peat layers over time pointing to the feedbacks between hydroperiod and plant communities. Interestingly, the deeper layer sediments from the t-type kettle holes did not show an increase in decomposition relative to the sp-type kettle holes. The change in environmental conditions (i.e., aeration/redox potential changes) during past dry periods may not have shifted enough to induce significant decomposition of the peat layers in the t-type kettle holes. Thus, the potential for kettle holes to sequester carbon remains high even under changing environmental conditions. We found kettle holes within the t-type or sp-type hydroperiod to exhibit similar hydrological patterns over the year. Evaporation was greatest in the t-type kettle holes on average, which, along with lateral flow, contributes to changes in redox and potential plant encroachment. The initial hydrological conditions are determined by larger climate controls (e.g., flood or drought) and winter precipitation, which modulate the role of lateral groundwater flow and evaporation.

3.7 Acknowledgments

We thank the staff of the AgroScapeLab Quillow, Dedelow, for the logistical support and Frau Remus and Thomas Wagner for their help with the sample preparation. We kindly thank the LandScales team, especially Dr. Andreas Kleeberg, for their support and discussions. This research was funded through the Pact for Innovation and Research of the Gottfried Wilhelm Leibniz association (project LandScales - 'Connecting processes and structures driving landscape carbon dynamics over scales')).

4. Transect and aggregate scale

Organic matter distribution and retention along transects from hilltop to kettle hole within an agricultural landscape

This manuscript was submitted to the international peer-reviewed journal *Geochimica et Cosmochimica Acta:*

Nitzsche K.N., Kaiser M., Premke K., Gessler A., Ellerbrock R., Hoffmann C., Kleeberg A. and Kayler Z.E. Organic matter distribution and retention along transects from hilltops to kettle hole within an agricultural landscape. *Geochimica et Cosmochimica Acta*, submitted.

4.1 Abstract

In agricultural landscapes, the spatio-temporal distribution of organic matter (OM) varies greatly across landscape structures and soil types. This is especially relevant at the intersection of aquatic and terrestrial domains, as large environmental gradients develop across the catchment. Land-management practices, such as tillage or fertilization, can further impact OM distribution by accelerating erosion or increasing plant growth, but how these environmental conditions, management, and transport effects manifest at different spatial scales is relatively unknown. We investigated patterns of organic carbon (OC) content, polyvalent cations, isotopic values, for specific OM fractions that are indicative of different OM stabilization mechanisms and sources along transects spanning topographic positions from erosional to depositional areas, including aquatic sediments within a single kettle hole. We expected different drivers of the OM isotopic signal and OC content exist at different spatial scales. At the transect scale, we hypothesized 1) landscape form (e.g. curvature and slope) and land management to explain observed patterns of OC contents and $\delta^{13}C$ and $\delta^{15}N$ of the OM fractions. At the aggregate scale, 2) we hypothesized different OM-mineral associations to explain stabilized OM. We also hypothesized, 3) that shallow sediment $\delta^{13}C$ and $\delta^{15}N$ of kettle holes reflected inputs from surrounding terrestrial sources. We found that erosion along with patterns in plant productivity are large scale drivers of mineral-associated fractions over the transect, while microbial decomposition and the application of slurry influence freely available and aggregated OM fractions. Stabilization of poorly decomposed OM via organically complexed and poorly crystalline Fe and Al phases was dominant in depositional areas, while associations of microbially decomposed OM with well-crystallized Fe phases and via clay-Ca^{2+} interaction seemed to be prevalent in erosional areas. OM in mineral-associated fractions from sediments derived from clay- and silt-sized particles from the field with macrophyte

contributions to freely available and aggregated OM fractions. We conclude that kettle holes constitute important sinks for terrestrial born OM in the landscape.

4.2 Introduction

Agricultural landscapes encompass multiple land-use histories, landscape structures, soil types and water paths leading to a region characterized by high levels of environmental and biogeochemical heterogeneity (Nitzsche et al., 2016). This is especially apparent where aquatic and terrestrial domains converge, where transition zones in environmental variables emerge, including soil moisture, redox potential, and microclimate (Stallard, 1998; Cole et al., 2007; Premke et al., 2016). The distribution of organic matter (OM) also varies in catchments as erosion transfers material from the terrestrial to the aquatic domain (Doetterl et al., 2016; Hu et al., 2016; Nitzsche et al., 2017) or plant derived OM contributions increase in soil that is associated with greater soil moisture availability near the water body. Accelerated erosion through tillage might also alter the distribution of clay- and silt-sized soil particles and polyvalent cations involved in organo-mineral association, and fertilization might affect spatial patterns of productivity and as such OM inputs into the soil (Berhe et al., 2012; Kirkels et al., 2014). Consequently, patterns in soil OM materialize from the relative influence of environmental gradients, sources of OM, and management practices across different spatial scales.

Landscape topography plays an important role in OM distribution (Doetterl et al., 2016), and terrain attributes, inferred from digital elevation models, for example, have been widely used to predict soil organic matter (SOM) distribution. For instance, concave slopes as indicated by negative curvature are considered areas of SOM accumulation, while convex slopes are represented by positive curvature, which are prone to erosion (Liu et al., 2013). Other indices (e.g., topographic position index (TPI) and topographic wetness index (TWI)) can convey information about the large-scale landscape characteristics as they relate to the variability in OM distribution, erosion, and plant productivity.

Soil erosion leads to the downslope transport of OM and soil particles from hilltops, exposing lower soil horizons in some cases, to areas of deposition, thus creating gradients in nutrients, soil moisture, and soil chemistry (Doetterl et al., 2016). Accordingly, eroded soils may exhibit reduced nutrient content and water holding capacity due to leaching, the destruction of the physical soil matrix, and the accompanied washout of nutrient-adsorbing clays, potentially reducing soil fertility and plant productivity on eroding slopes. In contrast, soil fertility may be higher in depositional areas from eroding hillslopes due to the additional SOM. Especially clay- and silt-sized mineral particles and highly stable micro-aggregates < 53 µm are usually enriched in organic carbon (OC) relative to the bulk soil (Hu et al., 2016). These particles and micro-aggregates are generally comprised of complexed, poorly crystalline and

well-crystallized mineral phases as well as clay minerals (e.g. oxides, layer-silicates) that can interact with OM (Kaiser et al., 2007; Doetterl et al., 2015).Their preferential transport during erosion events consequently leads to higher soil OC (SOC) concentration in depositional areas (Doetterl et al., 2016). Thus, OM bound in micro-aggregates < 53 µm and attached to mineral surfaces could be transported into small water bodies via erosion (Stallard, 1998) and contribute to the C storage potential of the landscape (Premke et al., 2016). Recent studies have shown that erosion distributes poorly crystalline mineral phases over the landscape (Berhe et al., 2012; Ellerbrock et al., 2016), but the source of OM (e.g. poorly vs. strongly microbially processed) associated with these mineral phases remains largely unknown.

Heterogeneous bulk soil OM can be experimentally subdivided into more homogenous fractions. For example, organic particles made up of residues from plants and animals serve as a readily decomposable substrate for soil organisms (Gregorich et al., 2006). An understanding of the key factors and processes that regulate the OM stabilization in soils requires the separation of OM fractions stabilized according to specific mechanisms (Mikutta et al., 2006). Such OM stabilization in aerated mineral soils results from (i) interactions of the OM with polyvalent cations (chelate, crosslinking) (e.g. Masiello et al., 2004; Mouvenchery et al., 2012), (ii) associations of the OM with mineral surfaces via polyvalent cations (cation bridges) (von Lützow et al., 2006) , or (iii) direct bond formation between OM and mainly Fe- or Al-oxides (ligand exchange reactions) (Mikutta et al., 2007; Kleber et al., 2015). Stabilization mechanisms of OM in aquatic sediments may substantiality differ from soils given the fact that there are permanently water saturated (Hedges and Oades, 1997). Macro-aggregate formation is inhibited partly in sediments because of bioturbation. Studies showed correlations between the OC content with density fractions, particle sizes and surface areas of the mineral matrix suggesting the adsorption of OM to mineral surfaces as the major stabilization mechanism in sediments (Mayer, 1994; Hedges and Keil, 1995). Recently, Lalonde et al. (2012) found a preferential stabilization of OM via reactive iron surfaces. But in general, stabilization mechanisms of sedimentary OM are still largely unknown.

Across a toposequence in a kettle hole catchment in the moraine landscape of NE Germany (Kalettka and Rudat, 2006), in which erosion is ubiquitous, we investigated patterns of OM stabilization and assessed OM sources along transects spanning topographic positions from erosional hilltops and hillslopes to depositional footslopes and edges, extending to sediments within a single kettle hole (Fig. 4.1). We used OM fractions (i.e., organic particles, water extractable OM, and mineral associated OM) from these topographic positions separated by a sequential fractionation (Kaiser et al., 2010; Kaiser et al., 2012). The availability of OM in these fractions to erosion or mineralization differ and we therefore measured the OM fraction stable isotope values to infer the OM fate and origin. Stable isotopes are used to track the transport of OM across landscapes, determine source contributions, and assess the

degree of OM transformation (e.g. Alewell et al., 2009; Brüggemann et al., 2011; McCorkle et al., 2016). They have also been used in tandem with OM fractions for inferring mechanisms of OM stabilization (Sollins et al., 2009; Kayler et al., 2011; Schrumpf and Kaiser, 2015).

We related our isotopic data to landscape proxies (TPI, TWI) and leaf area index (LAI) to estimate the effects of landscape topography and plant productivity on OM dynamics. We hypothesized: 1) at the transect scale, topography would explain the variability in the OC contents and $\delta^{13}C$ and $\delta^{15}N$ of the bulk soil and sediment as well as the OM fractions. We also used an isotopic distillation model that accounts for the changes in isotopic composition of OM and the corresponding OC concentration, to infer the impact of mass transport, OM source contributions, and possible impacts of management. And, 2) at the aggregate scale (i.e., soil fractions), we expected OM to be stabilized via different binding mechanisms that reflect potentially strong gradient in cations, crystalline and non-crystalline oxides, and clay- and silt-sized soil particles induced by erosion. Given the close proximity of the kettle hole and hillslope we hypothesized, 3) surface sediment $\delta^{13}C$ and $\delta^{15}N$ will reflect input from terrestrial sources.

4.3 Material and methods

4.3.1 Study site

The study site is located in the Quillow catchment (~ 168 km^2) as part of the young and hummocky moraine plain of NE Germany that is intensively used for agriculture. Within the glacial landscape, around 150,000 to 300,000 kettle holes exist (Kalettka and Rudat, 2006). We selected a single kettle hole surrounded by an agricultural field (E 013°39′57″, N 53°23′51″) and located in the center of a runoff catchment area (3.4 ha) near the village Kraatz. Elevation ranged from 88.2 m to 101.1 m a.s.l and slopes were short and steep and as high as 7.9° (Fig. 4.2). The climate is sub humid with an average annual temperature of 8.6°C and average annual precipitation of 499 mm as determined between 1992 and 2013 (AgroScapeLab Quillow, Dedelow, E 013°48′12″, N 53°21′59″).

In hummocky, agricultural landscapes, the topsoil is the uppermost due to tillage well-mixed layer referred to as Ap horizon, while the subsoil comprises of the clay-rich Bt horizon underlain by the carbonate-rich glacial till, the C horizon. Characteristic soil types at hilltops and upper slope positions are Calcaric Regosols and Calcic Luvisol, which are strongly eroded into the subsoil. In depressions, nearby the kettle hole, Colluvic Regosols with M-horizon thicker than 50 cm and soils developed under groundwater and stagnant water (Gleysols, Stagnosols) dominate. For two hilltop and two hillslope locations, the C-horizon was near the surface (23 cm to 37 cm) and already strongly mixed into the Ap horizon. In the depositional area around the kettle hole, the C-horizon was more than 150 cm below the surface.

The field has been under agricultural use for several centuries, and since the 1950s, the field has been cultivated with a rotation of winter wheat (*Triticum L.*)– winter barley

(*Hordeum vulgare*)– rapeseed (*Brassica napus*). Rapeseed was cultivated in 2013. Annual plowing was common until 2005, thereafter plowing occurred every third year. Chemical fertilizers have been applied since the second half of the 19th century and slurry from a near pig farm has been applied approximately since 1980. The last slurry application prior to sampling was in August 2012.

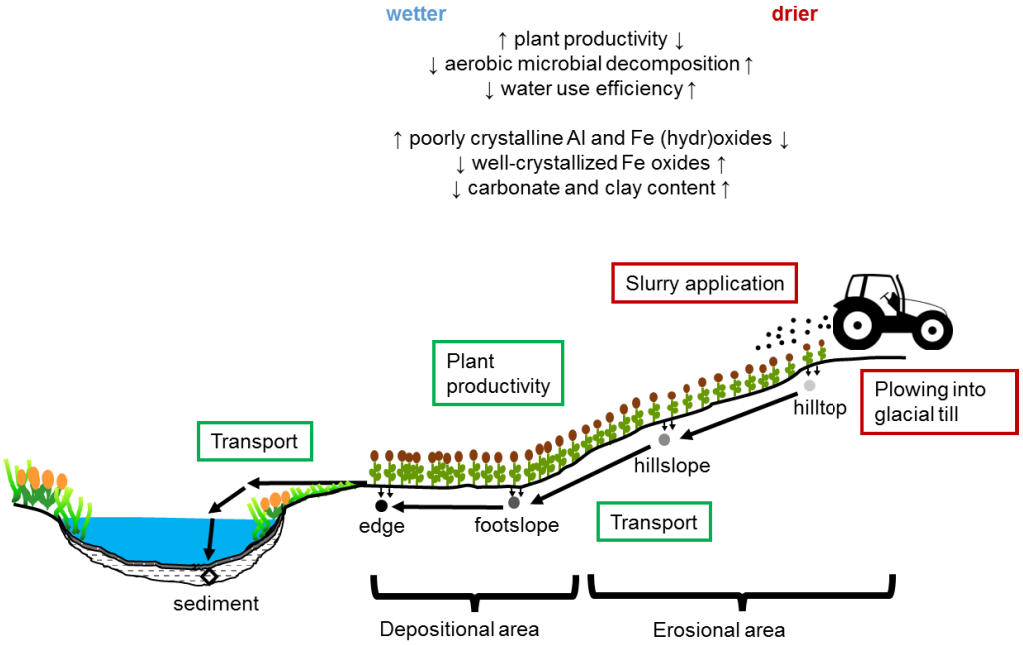

Fig. 4.1. Schematic cross-section through the catchment of the kettle hole. Assumed differences in biological activity and soil mineral and environmental characteristics between depositional (wetter) and erosional (drier) areas are highlighted with upward arrows (increase) and downward arrows (decrease). Black arrows highlight primary organic matter inputs (transport and plant productivity in green boxes) that contribute to the OM $\delta^{13}C$ and $\delta^{15}N$ at each topographic position. Land-management activities are indicated by red boxes. Sampling positions are shown by filled circles (soils) and the open diamond (sediment).

4.3.2 Sampling design

In 2013, we took topsoil samples (0 to 15 cm) from the kettle hole catchment. We sampled four transects consisting of four slope positions (hilltop, hillslope, footslope, depression edge) terminating with one position in the kettle hole (Fig. 4.1 and 4.2) amounting to a total of 20 plots (n = 20); thus, we have sixteen individual plots along the hillside resulting in four plots at each terrestrial position and four plots within the kettle hole. At each slope position, we took three subsamples of 100 g soil each in a 1 m^2 area and mixed the samples afterward. We sampled sediment cores from the kettle hole at positions with a water levels of approximately 1 m with a sediment corer (UWITEC, Austria, i.d. 60 mm). Sampling positions in the kettle holes were considered an extension of the four transects, thus functioning as depositional areas for each transect. Sediment sample depth encompassed 2 to 7 cm, we removed the top two cm due to it containing primarily fresh, recently, deposited OM. All

samples were stored in gas-tight containers at 4 °C in dark conditions prior to preparation. Soil and sediment samples were air-dried and passed through a 2 mm sieve.

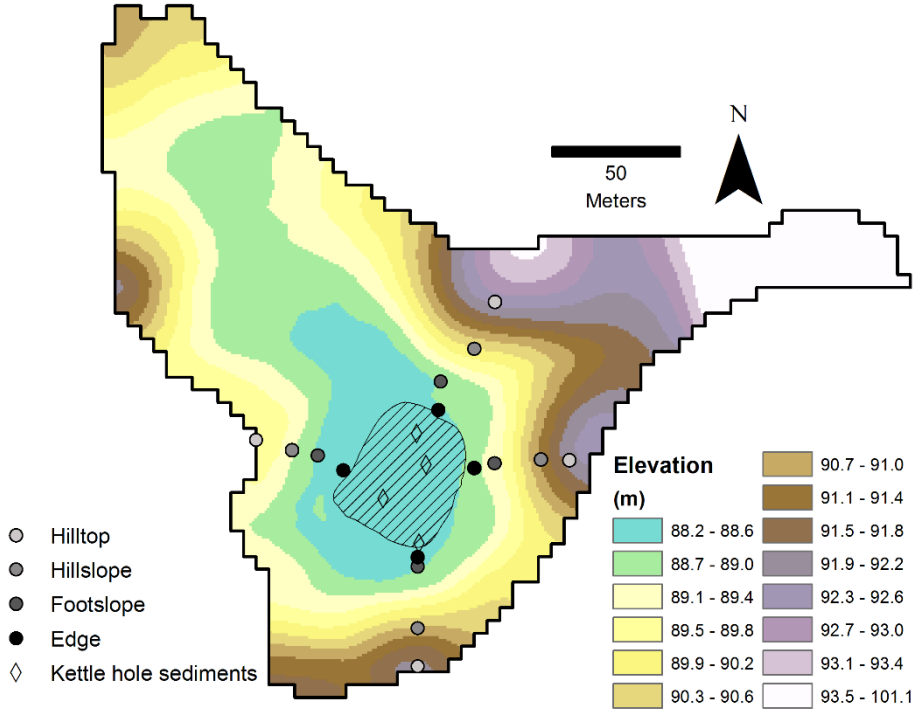

Fig. 4.2. Elevation map of the catchment (m) with sampling locations (filled circles for soils and open diamonds for sediments).

4.3.3 Leaf area index

We quantified leaf area index (LAI) using a SunScan, (Delta-T Devices Ltd.) biweekly during April and July 2014 for wheat and 2015 for barley along eight sampling points near our southern and eastern transects (max. ± 2 m). From these measurements we used the maximum LAI values (occurring in June) at each position then averaged the values for two years. We used LAI estimates based on the topographic positions from the two transects for further analyses.

4.3.4 Bulk soil and sediment properties

As a first step, we removed the physically uncomplexed coarse organic particles (> 0.315 mm; defined as OP_{el}) by electrostatic attraction according to Kaiser et al. (2009). The clay, silt and sand contents (fine, medium, coarse) were determined by wet-sieving and sedimentation after the destruction of OM via H_2O_2 and of carbonates via HCl following the German guideline DIN ISO 11277 (2002). The pH of "coarse-OP_{el}-free" soil and sediment samples was measured in a 0.01 M $CaCl_2$ solution with a pH electrode following DIN ISO 10390 (1997). The cation exchange capacity (CEC) and the exchangeable cations Ca (Ca_{ex}) and Mg (Mg_{ex}) were analyzed via inductively coupled plasma optical emission spectroscopy (ICP-OES) with an ICP-iCAP 6300 DUO (Thermo Scientific, Bremen) after samples were

treated according to DIN ISO 11260 (1994). The amount of oxalate-extractable Fe (Fe_{ox}) and Al (Al_{ox}) were determined according to (DIN 19684-6, 1997) by ICP-OES, while dithionite-citrate-bicarbonate extractable Fe (Fe_{DCB}) and Al (Al_{DCB}) were measured by ICP-OES after treatment according to Schlichting et al. (1995). Total inorganic carbon (TIC) content was analyzed in ground samples using a RC612 multiphase C/N analyzer (LECO Corporation, Michigan, USA) according to DIN ISO 10694 (1995).

4.3.5 Sequential organic matter extraction

Physically uncomplexed and aggregate occluded organic particles (OP) as well as water-extractable OM (WEOM, i.e., surrogate for dissolved OM) and mineral associated OM (i.e., mediated by cations) fractions can be sequentially separated from agricultural soil by combining electrostatic attraction, wet-sieving, water-extraction, ultrasonication, and $Na_4P_2O_7$-extraction (Kaiser et al., 2009 2010, 2012, 2016). Considering interactions between soil OM and minerals in agricultural soils with a circum neutral pH agricultural soils (Kaiser et al., 2012), the alkaline Na-pyrophosphate extraction procedure is supposed to separate OM interacting with polyvalent cations (Bremner et al., 1946; Masiello et al., 2004) and via polyvalent cations with soil mineral surfaces (Bremner and Lees, 1949; Wattel-Koekkoek et al., 2003).

Our sequential extraction method is based on those described in: Kaiser et al., 2009, 2010, 2012, 2016. Briefly, step (1) 5 g of "coarse-OP_{el}-free" soil and sediment samples were mixed with 50ml of deionized water for 12h at room temperature on a rock and roll shaker. The samples were centrifuged for 35 min at 1400 g and the supernatant was poured through two sieves (250 and 63 µm) into a beaker to obtain physically uncomplexed organic particles not separated during electrostatic attraction. Organic particles in the sieves were freeze-dried and called $OP_{W1\text{-}250}$ and $OP_{W1\text{-}63\text{-}250}$. The decanted supernatants were vacuum-filtrated using polyamide membrane filters with a mesh size 0.45 µm (Whatman; VWR, Darmstadt, Germany), denoted as water-extractable OM ($WEOM_{free}$) and an aliquot was taken for dissolved organic carbon (DOC) and dissolved total nitrogen (DTN) analysis. Vacuum filtration prior to separation of aliquots was carried out for all the following extractions. Step (2), the solid pellet was mixed with 25 ml deionized water and sonicated with 60 J ml^{-1} to disperse macroaggregates (MaA) (Amelung and Zech, 1999). The suspension was shaken and allowed to settle for 5 min to allow organic particles to float. The supernatant was passed through two sieves (250 and 63 µm) and collected in a beaker. The solid residuum was mixed with 20 ml deionized water, shaken, allowed to settle for 5min and again passed through the sieves. This procedure was repeated two more times. Organic particles in the sieves were freeze-dried and denoted $OP_{MaA\text{-}250}$ and $OP_{MaA\text{-}63\text{-}250}$. The combined supernatants were centrifuged and decanted. The remaining solid particles in the centrifuge tube were mixed with the residuum of the first centrifugation. The decanted, vacuum-filtrated supernatants were denoted as

$WEOM_{MaA}$. Step (3), the remaining solid residuum was sonicated with 440 J ml^{-1} to disperse microaggregates (Amelung and Zech, 1999). Organic particles were obtained according to step (2), using a 63µm sieve and denoted as OP_{MiA-63}. Vacuum-filtrated combined supernatants were denoted as $WEOM_{MiA}$. Step (4), the remaining pellet was washed with deionized water to extract potential remaining water-extractable OM. This OM was discarded afterward.

For step (5), the solid residuum was extracted with 50 ml of 0.1 M Na-pyrophosphate solution ($Na_4P_2O_7$; pH = 9 - 10). The decanted supernatant was centrifuged, vacuum-filtered and denoted as NaPy-I. The solid residuum from this step was extracted a second time following step (5) to extract Na-pyrophosphate-extractable OM as far as possible. The obtained vacuum-filtered supernatant was denoted as NaPy-II. Subsequently, NaPy-I and NaPy-II were combined and denoted as OM_{PYt}. In addition to an aliquot for DOC and DTN analysis, a further aliquot was taken for the determination of polyvalent cations Fe, Al, Mg, Mn, Ca. Subsequently, the pH of the filtrate OM_{PYt} was adjusted with 1 M HCl to pH = 2 and cooled in a refrigerator overnight to precipitate OM. The mixture was centrifuged to separate HCl insoluble that precipitated under low pH conditions (denoted as OM_{PYP}) from HCl soluble OM (denoted as OM_{PYS}). An aliquote was taken from the latter. Both fractions were dialyzed against deionized water using cellulose hydrate membranes of 25 to 30 nm pore size (NADIR; Carlroth, Karlsruhe, Germany) until an electric conductivity of < 4 µS cm^{-1} was observed. The solid extraction residuum after $Na_4P_2O_7$ extraction was four times washed with deionized water, centrifuged, dialyzed and denoted as OM_{ER}. All obtained fractions were freeze dried. All extraction steps were done in three replicates per sample.

4.3.6 Stable isotope analysis

Prior to $\delta^{13}C$ stable isotope analysis of the "coarse-OP_{el}-free" samples (OM_{bulk}) and OM_{ER}, inorganic C was removed by acid fumigation according to Harris et al. (2001). Inorganic C in the freeze-dried WEOM fractions was also removed according to Harris et al. (2001); however, without the addition of water because water would re-dissolve freeze-dried OM. $\delta^{13}C$ of the two OP fractions and $\delta^{15}N$ for all fractions were analyzed on samples that were not acidified. Samples were weighed into tin capsules and combusted in an elemental analyzer (Flash HT, Thermo Scientific, Bremen, Germany). Isotope ratios were measured with a Thermo-Scientific, Delta V advantage isotope ratio mass spectrometer (Bremen, Germany) coupled to the elemental analyzer. Isotopic calibration was to IAEA-CH-6 (sucrose), USGS40 (L-glutamic acid) and IAEA-N-1 (ammonium sulfate). The isotopic values are expressed in delta notation (in ‰ units), relative to VPDB (Vienna Pee Dee Belemnite) for carbon and N_2 in air for nitrogen. Analysis of internal laboratory standards ensured that the estimates of the isotopic values were precise to within < 0.1 ‰ for $\delta^{13}C$ and < 0.5 ‰ for $\delta^{15}N$.

4.3.7 Organic C and N contents of Na-pyrophosphate extractable cations

Total organic carbon (TOC) and total nitrogen (TN) concentrations (in wt.%) of OM_{bulk}, OM_{ER} and OP fractions were measured by EA-IRMS measurements. DOC and DTN of WEOM and OM_{PYt} fractions were measured using a Shimadzu TOC-Vpch after acidifying the samples with 1 M HCl to pH < 3. Concentrations of Fe and Al in the Na-pyrophosphate extract OM_{PYt} were analyzed via ICP-OES with a ICP-iCAP 6300 DUO (Thermo Scientific, Bremen).

4.3.8. Combination of fractions

To reduce the number of fractions to be discussed in this study, we combined the results of the single OM fractions that constituted less than 1.5 % of SOC. $\delta^{13}C$ and $\delta^{15}N$ of the combined fractions were calculated based on their mass. We combined the results of OP_{el}, $OP_{W1\text{-}250}$ and $OP_{W1\text{-}63\text{-}250}$ and denoted the combined fractions as OP_{free} that represented loosely bound OM susceptible to management (Table 4.1). Furthermore, the results of $OP_{MaA\text{-}250}$, $OP_{MaA\text{-}63\text{-}250}$ and $OP_{MiA\text{-}63}$ were combined and named OP_A thus representing aggregate occluded OP released after ultra-sonication. Similarly, the results from $WEOM_{MaA}$ and $WEOM_{MiA}$ were combined, denoted as $WEOM_A$ and representing aggregate protected WEOM released after ultra-sonication.

4.3.9 Topographic indices

Different terrain attributes and indices, such as curvature, slope and TWI were calculated from a high resolution digital elevation model (DEM) (grid-cell size 1 m x 1 m, derived by airborne laser scanning) using the geographic information system SAGA GIS (Conrad et al., 2015). To characterize the relative topographical position of points in the field compared to the neighborhood (25 m, circle) the Topographic Position Index (TPI25) was calculated using an algorithm described in Deumlich et al. (2010).

4.3.10 Rayleigh distillation

The Rayleigh distillation model is a way to describe isotopic dynamics of substrates over space or time. In a closed system, there is a lack of new inputs leading to a progressive conversion of the initial substrate (Fry, 2006). During the reaction and with decreasing mass of the initial substrate an isotopic change in the remaining substrate occurs. In this case, the relationship between δ in the remaining substrate and the reacted fraction of the substrate is described with an exponential model. However, in an open system new substrate with a potentially different isotopic composition is added continually as the initial substrate changes simultaneously (Fry, 2006). In our case, we assumed an open system in which new OM inputs are introduced by plant production or slurry and by the transport of organic particles or OM attached to mineral surfaces from higher topographic positions (Fig. 4.1). Losses of OM at

each topographic position occur through transport and microbial decomposition of OM, As such, we do not interpret the results of a Rayleigh model strictly in terms of isotopic fractionation, but we use it as a conceptual model (*sensu* Cohen, 2003) to infer different OM sources and transport gains or losses at the spatial scale of the transect.

4.3.11 Statistical analysis

We used the Shapiro-Wilk test to test for normally distributed data. We used analysis of variance (ANOVA) to test for differences in soil chemical and mineral characteristics, $\delta^{13}C$ and $\delta^{15}N$ isotope signatures, OC contents and molar C:N ratios between topographic positions and OM fractions using R (version 3.1.1, R Foundation for Statistical Computing, Vienna, Austria, http://www.R-project.org/). We performed Tukey's HSD post-hoc test to identify these differences. To explore relationships of $\delta^{13}C$, $\delta^{15}N$ and OC content with soil chemical and mineral characteristics we used Pearson product-moment correlation analyses when the data were normally distributed and Spearman rank order correlation analyses for non-normally distributed data. Correlation coefficients were considered to be significant at the $p \leq 0.05$ level. In order to test for relationships of $\delta^{13}C$, $\delta^{15}N$ and OC contents with catchment characteristics and plant productivity, we performed a linear mixed effects model (LME; R package nlme Kuznetsova et al., 2016). Here, we used TWI, TPI25, elevation, curvature, slope, LAI and interactions among them as continuous fixed effect variables, whereas the transects and fractions were considered as random effect variables while nesting fractions in transects: lme(y ~ curvature + slope + elevation + TWI + TPI25 + LAI, random~1|transect/fraction). To identify the most parsimonious model including only significant predictor variables for each explanatory variable, we used a step-wise ANOVA approach based on the Akaike information criterion (AIC) to achieve an optimal model that explains the most variation with the fewest variables.

Table 4.1. Overview of the fractionation scheme, fractions discussed in this study and their ecological relevance.

Step	Task	Fraction	Ecological relevance
Soil sample < 2 mm		OM_{bulk}	Combination of all fractions
Electrostatic attraction	Separation of OP > 315 µm		
Water extraction 12 h	Separation of OP floating on water (> 250 µm, 63-250 µm; $\rho < 1$ g cm^{-3})	OP_{free}	Freely available/loosely bound OP, originating from plant production, susceptible to management, poorly decomposed
	Separation of water-extractable OM	$WEOM_{free}$	Freely available water-extractable OM, susceptible to management and erosion
Ultra-sonication 60 J ml^{-1}	Separation of OP subsequent to macro-aggregate dispergation (> 250 µm, 63 - 250 µm; $\rho > 1$ g cm^{-3})	OP_A	Aggregate bound OP, susceptible to management, stronger decomposed
	Separation of water-extractable OM subsequent to macro-aggregate dispergation	$WEOM_A$	Aggregate bound water-extractable OM, stronger decomposed and stabilized, susceptible to management and erosion
Ultra-sonication 440 J ml^{-1}	Separation of water-extractable OM subsequent to micro-aggregate dispergation		
Na-pyrophosphate extraction followed by acidification to pH < 2	Separation of Na-pyrophosphate extractable and HCl-soluble OM	OM_{PYS}	OM bound via cation mediated interactions
	Separation of Na-pyrophosphate extractable and HCl-insoluble OM	OM_{PYP}	OM bound via cation mediated interactions, larger molecules compared to OM_{PYS}
Extraction residue		OM_{ER}	OM occluded in highly stable micro-aggregates

4.4 Results

4.4.1 Pattern of topographic indices and leaf area index

We found the largest mean curvature at hilltops with 0.6 ± 0.1° (n = 4) and the smallest curvature at footslopes with -0.1 ± 0.1° (Table 4.2). The steepest slope was found at hillslopes with a mean of 5.7 ± 0.4°. While the TWI was similar between hilltops (4.8 ± 0.5) and hillslopes (5.0 ± 0.3), it was significantly higher for footslopes (8.9 ± 0.8) and edges (8.7 ± 0.4) ($p < 0.01$). The significantly highest TPI25 was found for hilltops (0.6 ± 0.1) and the lowest TPI25 for footslopes (-0.3 ± 0.0). LAI increased toward the kettle hole from only 2.8 ± 0.3 at hilltops to 4.9 ± 0.3 at edges ($p < 0.01$).

Table 4.2. Topographic indices of soil sampling locations (mean ± standard error) TPI25 = topographic position index; TWI = topographic wetness index; LAI = leaf area index.

Landscape position	Distance[#]	Elevation	Curvature	Slope	TWI	TPI25	LAI[§]
	(m)	(m a.s.l.)	(°)	(°)			
Hilltop	42.0 ± 3.0	91.5 ± 0.6	0.6 ± 0.1*	2.9 ± 1.0	4.8 ± 0.5*	0.6 ± 0.1*	2.8 ± 0.3*
Hillslope	27.1 ± 1.6	90.3 ± 0.4	0.2 ± 0.1	5.7 ± 0.4	5.0 ± 0.3	0.2 ± 0.1	3.9 ± 0.4
Footslope	10.1 ± 2.0	88.8 ± 0.1	-0.1 ± 0.1*	2.3 ± 0.4	8.9 ± 0.8*	-0.3 ± 0.0*	4.9 ± 0.5*
Edge	2.0 ± 0.3	88.6 ± 0.1	0.1 ± 0.2	2.4 ± 0.6	8.7 ± 0.4*	-0.1 ± 0.1	4.9 ± 0.3*

[#]Horizontal distance
[§]n = 8
*indicates whether a topographic index at a given landscape position is significantly lower or higher compared the other positions on a $p \leq 0.05$ level.

4.4.2 Soil and sediment chemical and mineral characteristics

Clay content in the catchment was greatest at hillslopes (145 ± 12 g kg^{-1}) and smallest at edges (73 ± 15 g kg^{-1}) (Table 4.3). Kettle hole sediments had much greater clay contents than the soil (328 ± 49 g kg^{-1}, n = 2), but contained almost no sand (52 ± 39 g kg^{-1}). The pH decreased toward the kettle hole with 7.6 ± 0.0 at hilltops being significantly higher compared to the other topographic positions ($p = 0.03$) to 6.4 ± 0.4 at edges as does TIC with 7.20 ± 1.97 g kg^{-1} ($p < 0.01$) at hilltops to 1.35 ± 0.25 g kg^{-1} at edges. Similarly, the CEC decreased from 9.32 ± 1.17 $cmol_c$ kg^{-1} at hilltops to 7.00 ± 1.61 $cmol_c$ kg^{-1} at edges and Ca_{ex} patterns were similar, while Mg_{ex} increased toward the kettle hole with the content of Mg_{ex} being significantly lower at hilltops ($p = 0.04$). The CEC was significantly higher in kettle hole sediments compared to soils with 23.57 ± 1.19 $cmol_c$ kg^{-1}, similar patterns were also found for Ca_{ex} and Mg_{ex} ($p < 0.01$). The content of Fe_{DCB} was larger in the erosional areas compared to depositional areas and the largest content was found in sediments (8.42 ± 1.15 g kg^{-1}) (Fig. 4.3). The concentration of Fe_{ox} was smaller than Fe_{DCB}, but increased from 0.96 ± 0.12 g kg^{-1} at hilltops to 1.26 ± 0.6 g kg^{-1} at edges and were almost four times higher in sediments (5.58 ± 0.52 g kg^{-1}) ($p < 0.01$). As such, the ratio of Fe_{ox}:Fe_{DCB} significantly decreased with topographic position and distance from the kettle hole shoreline ($p < 0.01$). Fe_{PYt} contents were again significantly lower than those of Fe_{ox} ($p < 0.01$), but followed the same pattern.

Correspondingly, the ratio of Fe_{PYt}:Fe_{DCB} was even lower than of Fe_{ox}:Fe_{DCB}, but decreased significantly with topographic position ($p < 0.01$). Similar to the contents of extractable Fe, the Al contents decreased from $Al_{DCB} > Al_{ox} > Al_{PYt}$, whereas Al_{PYt} increased with topographic position.

Table 4.3. Clay, silt, total inorganic carbon (TIC) contents, cation exchange capacity (CEC), amounts of exchangeable Ca (Ca_{ex}) and Mg (Mg_{ex}), and pH of each soil (n = 4) sampling location (mean ± standard error).

Landscape position	Clay	Silt	pH	TIC	CEC	Ca_{ex}	Mg_{ex}
	(g kg^{-1})	(g kg^{-1})		(g kg^{-1})	($cmol_c$ kg^{-1})	($cmol_c$ kg^{-1})	($cmol_c$ kg^{-1})
Hilltop	135 ± 15	238 ± 19	7.6 ± 0.0*	7.20 ± 1.97*	9.32 ± 1.17	10.60 ± 0.99	0.45 ± 0.05*
Hillslope	145 ± 12	248 ± 3	7.2 ± 0.0	4.06 ± 2.82	9.00 ± 0.71	9.35 ± 0 .63	1.03 ± 0.24
Footslope	90 ± 16	243 ± 6	6.9 ± 0.2	2.19 ± 1.05	7.47 ± 1.01	7.00 ± 1.37	1.26 ± 0.29
Edge	73 ± 15	260 ± 11	6.4 ± 0.4*	1.35 ± 0.25	7.00 ± 1.61	6.28 ± 1.47	0.96 ± 0.15
Kettle hole	328 ± 49§	620 ± 9§	7.1 ± 0.1§	2.72 ± 0.24	23.57 ± 1.19*	23.96 ± 1.72*	1.61 ± 0.39*

§n = 2

*indicates whether a soil mineral parameter at a given landscape position is significantly lower or higher compared the other positions on a $p \leq 0.05$ level.

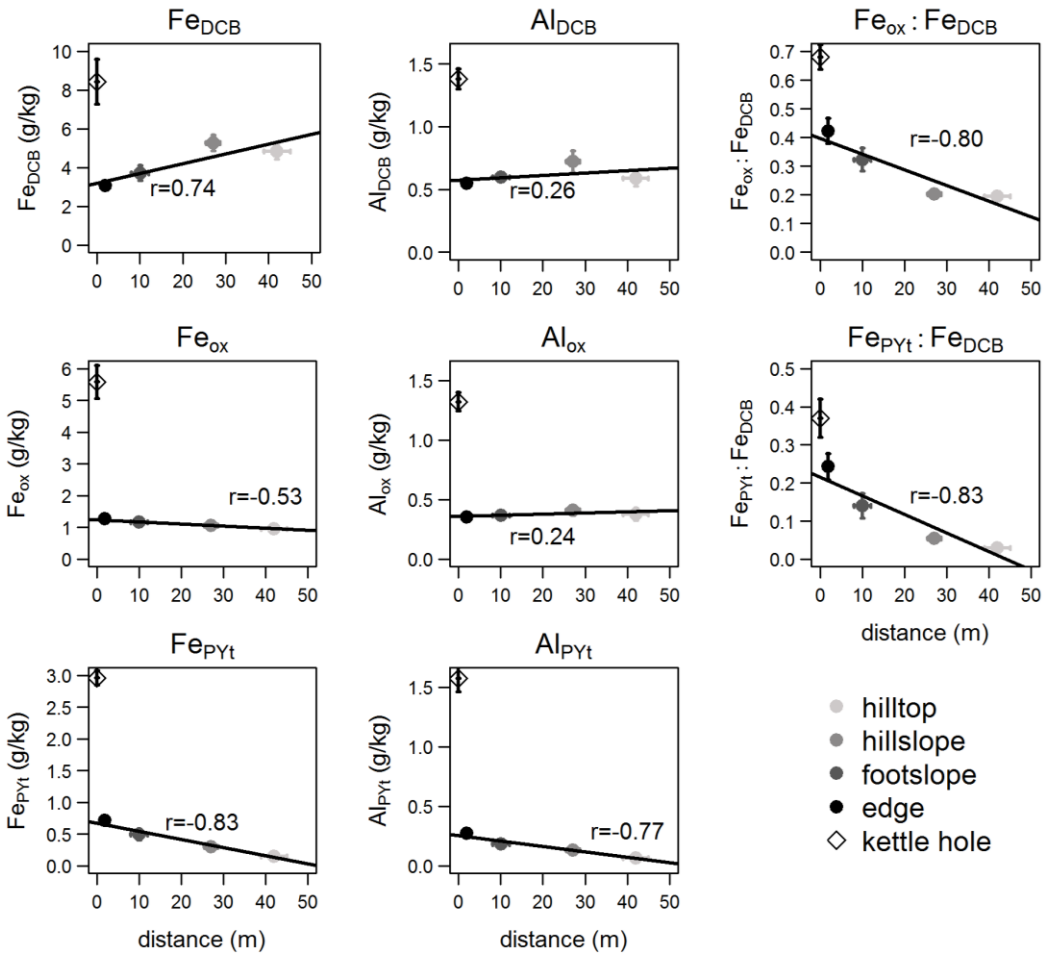

Fig. 4.3. Contents of the dithionite-citrate-bicarbonate extractable Fe (Fe_{PYt}) and Al (Al_{DCB}), oxalate extractable Fe (Fe_{ox}) and Al (Al_{ox}), Na-pyrophosphate extractable Fe (Fe_{PYt}) and Al (Al_{PYt}), and the ratios of Fe_{ox}:Fe_{DCB} and Fe_{PYt}:Fe_{DCB} versus the distance of the sampling position to the kettle hole shoreline (m). The black solid lines are regressions lines through all soil sampling points along the four transects (n = 4 per position). Pearson correlation coefficients (r) are reported for each regression. Kettle hole values are presented as reference and are not included in the regression, thus the distance from the shoreline is not reported.

4.4.3 Organic carbon

The OM_{bulk} average OC contents increased toward the kettle hole (Table 4.4). Similarly, mean OC contents across all fractions were found to increase from hilltops to the kettle hole edge and were highest in the kettle hole sediments (Table 4.4), however their percentage of SOC varied depending on the fraction (Fig. 4.4). Overall, we found OC contents of all fractions from the kettle hole sediment significantly larger compared to the OC contents from the soils ($p < 0.01$). While the OC made up by the sum of OP_{free} and OP_A made up on average 5.9 ± 0.5 % of SOC at hilltops, their proportion was with 12.5 ± 1.1 % and 11.0 ± 0.5 % significantly greater at footslopes and edges, respectively ($p < 0.01$). OC contents in OP_{free} and OP_A from sediments was again significantly larger and made up 22.8 ± 8.0 % of SOC ($p < 0.01$), though having a large range from 4.7 to 44.4 % among the four samples with > 90 %

OC from OP found in OP_A. Accordingly, all other sediment fractions varied greatly in percentage of SOC across the four replicate samples. The proportion of $WEOM_{free}$ was small ranging on average from 1.2 ± 0.0 to 1.5 ± 0.1 % depending on topographic position, while $WEOM_A$ made up 2.6 ± 0.1 to 3.9 ± 0.3 % of total SOC, except for sediments where it was only 1.7 ± 0.3 %. The proportion of OM_{PYt} ranged from 12.9 ± 2.2% in sediments to 17.8 ± 1.4 % at the edges. The largest proportion of OC was left in OM_{ER}, where it averaged to 45.8 ± 6.3 % in sediments and reaching up to 70.8 ± 2.0 % at hilltops. Therefore, stable isotope values of OM_{bulk} are dominated by the mineral-associated fractions (OM_{PYS}, OM_{PYP}, OM_{ER}). The sum of our fractions was less than 100 % of total SOC, we assume this was a result from measurement uncertainties and OM attached to mineral particles larger than 0.45 µm, which were lost during vacuum filtration.

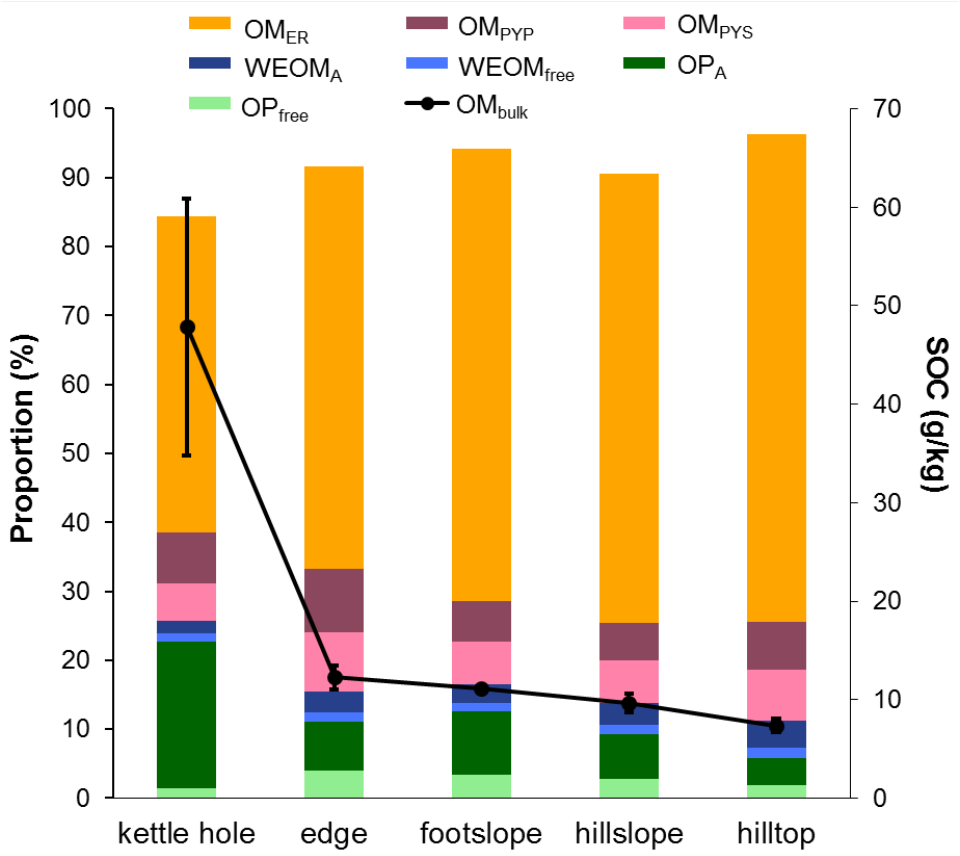

Fig. 4.4. Proportion of organic carbon contents of organic matter (OM) fractions (in wt. %) with respect to the total soil organic carbon (SOC) for the topographic positions (n = 4 per position). Black points connected by solid black lines represent SOC contents (in g kg^{-1} soil). OM_{bulk} = organic matter in the bulk soil; OP_{free} = loosely bound organic particles; OP_A = aggregate occluded organic particles; $WEOM_{free}$ = loosely attached water-extractable organic matter; $WEOM_A$ = aggregate-bound water-extractable organic matter; OM_{PYS} = Na-pyrophosphate extractable and HCl-soluble organic matter; OM_{PYP} = Na-pyrophosphate extractable and HCl-insoluble organic matter; OM_{ER} = organic matter in the extraction residue.

4.4.4 $\delta^{13}C$, $\delta^{15}N$ and C:N ratio patterns

$\delta^{13}C$ values of OM_{bulk} from soils gradually decreased from hilltops toward the kettle hole with -26.5 ± 0.1 ‰ to edges with -27.8 ± 0.2 ‰ (Fig. 4.5). $\delta^{13}C$ values of OM_{bulk} from the kettle hole sediments were lower with -28.5 ± 0.3 ‰. $\delta^{13}C$ of both OP fractions, both OM_{PY} fractions, and OM_{ER} and fell along the Rayleigh distillation line. The same fractions from the kettle holes sediments were often more depleted in ^{13}C than the edge sample, following the Rayleigh trend, but the OC contents were substantially higher. Generally, the significantly highest $\delta^{13}C$ values were observed for OM_{PYS} from hilltops with -26.0 ± 0.1 ‰ ($p = 0.01$) and the significantly lowest values were measured in OP_A from the kettle hole with -29.1 ± 0.2 ‰ ($p < 0.01$) (Table 4.4). OM_{PYS} was always found to be more enriched in ^{13}C than OM_{PYP}. Interestingly, $WEOM_{free}$ and $WEOM_A$ showed different pattern; in fact, $\delta^{13}C$ in $WEOM_A$ from edges was even significantly higher compared to the other topographic positions ($p < 0.01$).

In contrast to soils, the $\delta^{13}C$ of OP_{free} in sediments was significantly higher than $\delta^{13}C$ of OP_A ($p < 0.01$). The $\delta^{13}C$ of $WEOM_A$ from footslopes and edges was significantly higher compared to $WEOM_{free}$ ($p < 0.01$) from the same positions. The $\delta^{13}C$ of both fractions was in the same range at hilltops and hillslopes. In contrast, kettle hole sediment $\delta^{13}C$ of $WEOM_A$ was significantly lower than $\delta^{13}C$ from $WEOM_{free}$ ($p < 0.01$). While OM_{PYS}, OM_{PYP} and OM_{ER} from hilltops, hillslopes and footslopes were always more enriched in ^{13}C than $WEOM_{free}$ and $WEOM_A$ ($p < 0.01$; except for OM_{PYP} from footslopes), the same fractions were in similar range to kettle hole sediments.

$\delta^{15}N$ values of OM_{bulk} did not show any clear trend and were found to be significantly highest at footslopes with $\delta^{15}N = 6.2 \pm 0.3$ ‰ and lowest in the kettle hole sediments with $\delta^{15}N = 3.4 \pm 0.4$ ‰ ($p < 0.01$) (Fig. 4.6, Table 4.4). In general, $\delta^{15}N$ was always lower for sediment fractions expect for $WEOM_{free}$. In agreement with $\delta^{15}N$ in OM_{bulk}, $\delta^{15}N$ from OP_{free}, OP_A and OM_{ER} were always significantly highest at footslopes ($p < 0.01$). Ignoring footslopes, $\delta^{15}N$ of OP_A and OM_{ER} decreased towards the kettle hole. In fact, only $\delta^{15}N$ of OM_{PYS} and OM_{PYP} decreased towards the kettle hole. Similarly to $\delta^{13}C$, $WEOM_{free}$ and $WEOM_A$ were increasingly enriched in ^{15}N toward the kettle hole ($p < 0.01$). Similar to $\delta^{13}C$, sediment $\delta^{15}N$ from $WEOM_{free}$ was significantly higher compared to $\delta^{15}N$ from $WEOM_{free}$ ($p < 0.01$), whereas the opposite was observed for the other topographic positions. Furthermore, $\delta^{15}N$ from OM_{PYP} was significantly lower by 1.8 ‰ compared to $\delta^{15}N$ from OM_{PYS} ($p < 0.01$), which was also the case for edges footslopes but with a lower difference between both fractions.

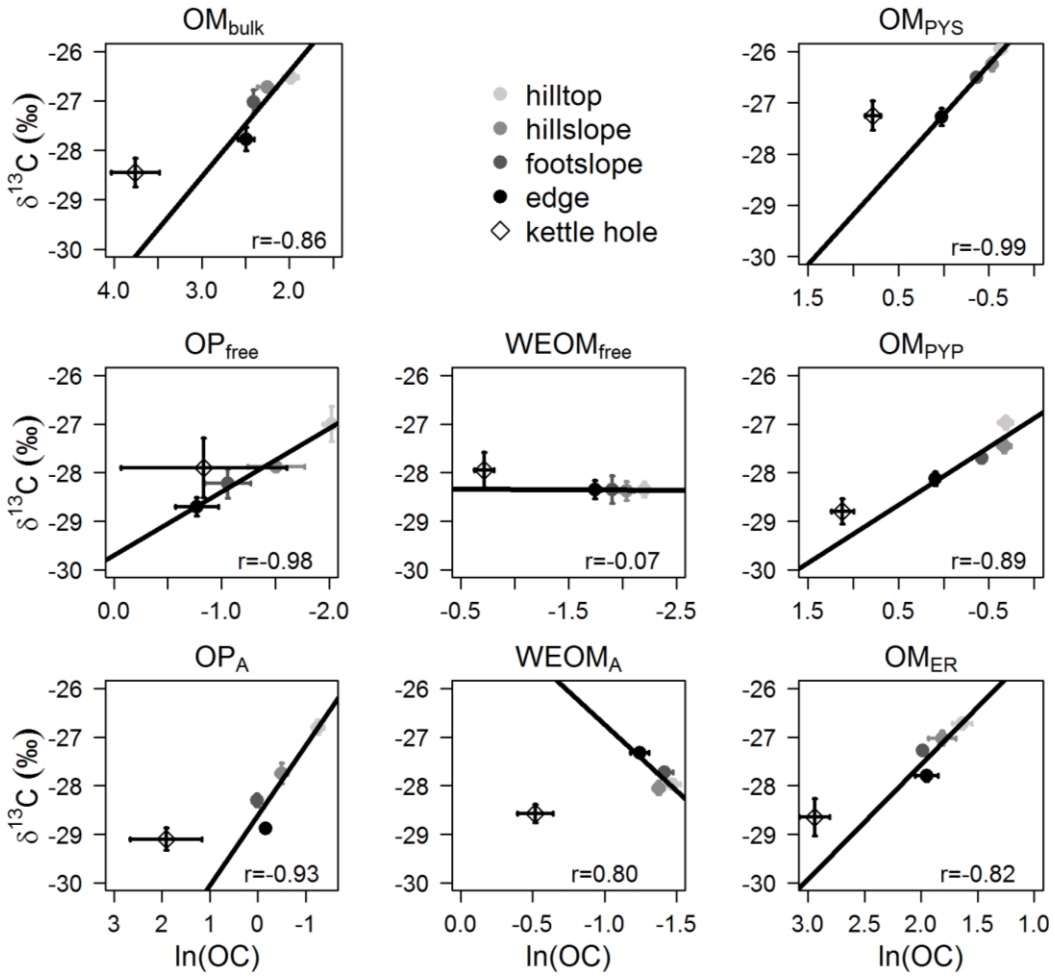

Fig. 4.5. Plot of $\delta^{13}C$ vs. the natural logarithm of the organic carbon (OC) concentration in the form of a Rayleigh distillation model for each fraction for each topographic position (n = 4 per position). The black solid lines represent linear regressions through the four topographic positions in the catchment. The p values represent the goodness of the fit. OM_{bulk} = organic matter in the bulk soil; OP_{free} = loosely bound organic particles; OP_A = aggregate occluded organic particles; $WEOM_{free}$ = loosely attached water-extractable organic matter; $WEOM_A$ = aggregate-bound water-extractable organic matter; OM_{PYS} = Na-pyrophosphate extractable and HCl-soluble organic matter; OM_{PYP} = Na-pyrophosphate extractable and HCl-insoluble organic matter; OM_{ER} = organic matter in the extraction residue.

There was no particular pattern in molar C:N ratio of OM_{bulk} or any OM fractions visible with landscape position (Table 4.4). Molar C:N ratios of OM_{bulk} ranged from in mean 9.9 ± 0.2 at hillslopes to 11.7 ± 0.8 in kettle hole sediments. The highest molar C:N ratios were found in OP_{free} and OP_A ranging from on average 15.0 ± 1.8 to 20.1 ± 1.2 at hilltops. The lowest C:N ratios were detected in $WEOM_{free}$ and $WEOM_A$ ranging between 3.2 ± 0.4 and 7.7 ± 0.3. Molar C:N ratios from OM_{PYS} and OM_{PYP} were higher and ranged from 11.3 ± 0.4 to 15.7 ± 0.7. Molar C:N ratios from OM_{ER} were always significantly lower than OM_{bulk} ($p < 0.01$) and ranged from 6.9 ± 0.5 to 8.5 ± 1.0.

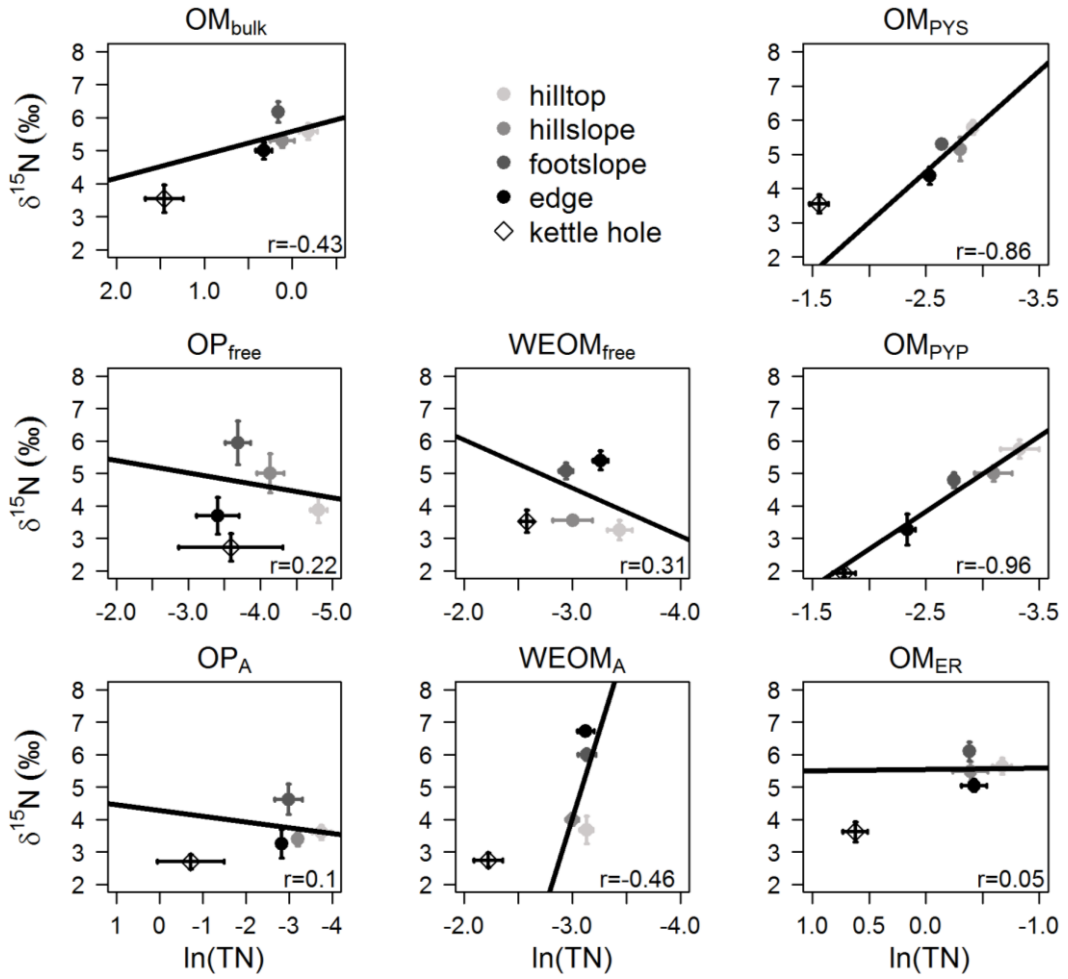

Fig. 4.6. Plot of $\delta^{15}N$ vs. the natural logarithm of the total nitrogen (TN) concentration based in the form of a Rayleigh distillation model for each fraction for each topographic position (n = 4 per position). The solid black lines represents linear regression through the four topographic positions in the catchment. The p values represent the goodness of the fit. OM_{bulk} = organic matter in the bulk soil; OP_{free} = loosely bound organic particles; OP_A = aggregate occluded organic particles; $WEOM_{free}$ = loosely attached water-extractable organic matter; $WEOM_A$ = aggregate-bound water-extractable organic matter; OM_{PYS} = Na-pyrophosphate extractable and HCl-soluble organic matter; OM_{PYP} = Na-pyrophosphate extractable and HCl-insoluble organic matter; OM_{ER} = organic matter in the extraction residue.

Table 4.4. Mean organic carbon (OC) contents and below in brackets their percentage of soil organic carbon, $\delta^{13}C$ and $\delta^{15}N$ and molar C:N ratio ± standard errors of the different fractions for four each landscape positions. OM_{bulk} = organic matter in the bulk soil; OP_{free} = loosely bound organic particles; OP_A = aggregate occluded organic particles; $WEOM_{free}$ = loosely attached water-extractable organic matter; $WEOM_A$ = aggregate-bound water-extractable organic matter; OM_{PYS} = Na-pyrophosphate extractable and HCl-soluble organic matter; OM_{PYP} = Na-pyrophosphate extractable and HCl-insoluble organic matter; OM_{ER} = organic matter in the extraction residue.

Variable	Landscape position	OM_{bulk}	OP_{free}	OP_A	$WEOM_{free}$	$WEOM_A$	OM_{PYS}	OM_{PYP}	OM_{ER}
OC ($g\ kg^{-1}$)	Hilltop	7.36 ± 0.66	0.14 ± 0.01 (1.9 ± 0.2)	0.29 ± 0.04 (3.9 ± 0.4)	0.11 ± 0.01 (1.5 ± 0.1)	0.23 ± 0.01 (5.4 ±0 .3)	0.54 ± 0.03 (7.3 ± 0.3)	0.51 ± 0.04 (7.4 ± 0.3)	5.19 ± 0.45 (70.8 ± 2.0)
	Hillslope	9.63 ± 0.97	0.25 ± 0.06 (2.8 ± 0.9)	0.61 ± 0.08 (6.5 ± 0.7)	0.13 ± 0.01 (1.4 ± 0.1)	0.25 ± 0.01 (4.6 ± 0.3)	0.59 ± 0.03 (6.2 ± 0.4)	0.52 ± 0.04 (5.0 ± 0.3)	6.28 ± 0.69 (65.1 ± 1.9)
	Footslope	11.13 ± 0.19	0.37 ± 0.08 (3.4 ± 0.7)	1.02 ± 0.08 (9.1 ± 0.6)	0.15 ± 0.00 (1.3 ± 0.0	0.24 ±0.02 (4.0 ± 0.1)	0.70 ± 0.02 (6.3 ± 0.3)	0.66 ± 0.02 (5.4 ± 0.2)	7.30 ±0 .30 (65.5 ± 2.1)
	Edge	12.24 ± 1.22	0.49 ± 0.01 (4.0 ± 0.5)	0.86 ± 0.05 (7.1 ± 0.2)	0.18 ± 0.01 (1.5 ± 0.1)	0.29 ± 0.02 (4.5 ± 0.2)	1.03 ± 0.05 (8.6 ± 0.5)	1.10 ± 0.05 (9.2 ± 0.9)	7.15 ±0 .75 (58.3 ± 1.0)
	Kettle hole	47.48 ± 13.05*	0.96 ± 0.65* (1.5 ± 0.7)	13.27 ± 7.30* (21.8 ± 8.0)	0.50 ± 0.04* (1.2 ± 0.2)	0.61 ± 0.08* (1.7 ± 0.3)	2.21 ± 0.19* (5.4 ± 1.0)	3.14 ± 0.39* (7.5 ± 1.3)	19.47 ± 2.57* (45.8 ± 6.3)
$\delta^{13}C$ (‰)	Hilltop	-26.5 ± 0.1*	-27.0 ± 0.4*	-26.8 ± 0.1*	-28.4 ± 0.2	-28.0 ± 0.0	-26.0 ± 0.1*	-27.0 ± 0.1*	-26.7 ± 0.1*
	Hillslope	-26.7 ± 0.1	-27.9 ± 0.1	-27.8 ± 0.2	-28.4 ± 0.2	-28.1 ± 0.1	-26.3 ± 0.1	-27.5 ± 0.2	-27.0 ± 0.1
	Footslope	-27.0 ± 0.2	-28.2 ± 0.3	-28.3 ± 0.1	-28.4 ± 0.3	-27.7 ± 0.1	-26.5 ± 0.0	-27.7 ± 0.1	-27.3 ± 0.1
	Edge	-27.8 ± 0.2	-28.7 ± 0.2*	-28.9 ± 0.1	-28.4 ± 0.2	-27.3 ± 0.1*	-27.3 ± 0.2*	-28.1 ± 0.1	-27.8 ± 0.1
	Kettle hole	-28.5 ± 0.3	-27.9 ± 0.6	-29.1 ± 0.2	-28.0 ± 0.3	-28.6 ± 0.2*	-27.3 ± 0.3*	-28.8 ± 0.3*	-28.7 ± 0.4*
$\delta^{15}N$ (‰)	Hilltop	5.6 ± 0.2	3.9 ± 0.4	3.6 ± 0.2	3.3 ± 0.3*	3.7 ± 0.4	5.8 ± 0.2*	5.8 ± 0.3*	5.7 ± 0.2
	Hillslope	5.3 ± 0.2	5.0 ± 0.6	3.4 ± 0.2	3.6 ± 0.1	4.0 ± 0.2	5.2 ± 0.3	5.0 ± 0.2	5.5 ± 0.3
	Footslope	6.2 ± 0.3*	6.0 ± 0.7*	4.6 ± 0.5*	5.1 ± 0.2*	6.0 ± 0.2*	5.3 ± 0.1	4.8 ± 0.2	6.1 ± 0.3*
	Edge	5.0 ± 0.3	3.7 ± 0.6	3.3 ± 0.4	5.4 ± 0.3*	6.7 ± 0.1*	4.4 ± 0.3	3.3 ± 0.5	5.4 ± 0.2
	Kettle hole	3.5 ± 0.4*	2.7 ± 0.4*	2.7 ± 0.2*	3.5 ± 0.3	2.8 ± 0.2*	3.6 ± 0.3*	1.9 ± 0.1*	3.6 ± 0.3*
C:N	Hilltop	10.2 ± 0.3	20.1 ± 1.2	15.0 ± 1.8	4.0 ± 0.3	6.2 ± 0.1	11.5 ± 0.4	15.7 ± 0.7*	7.9 ± 0.6
	Hillslope	9.9 ± 0.2	16.5 ± 2.0	16.2 ± 0.9	3.2 ± 0.4*	6.0 ± 0.1*	11.3 ± 0.4	12.6 ± 0.5	7.7 ± 0.4
	Footslope	11.1 ± 0.3	17.0 ± 1.0	17.8 ± 0.6	3.2 ± 0.3*	6.6 ± 0.1	11.4 ± 0.4	11.8 ± 0.3*	8.2 ± 0.2
	Edge	10.2 ± 0.1	17.1 ± 1.5	16.7 ± 0.7	5.3 ± 0.2	7.7 ± 0.3*	15.5 ± 0.2*	12.7 ± 0.5	8.5 ± 1.0
	Kettle hole	11.7 ± 0.8*	17.0 ± 2.0	16.5 ± 0.6	6.8 ± 0.5*	6.5 ± 0.1	12.1 ± 0.2	13.7 ± 0.1	6.9 ± 0.5*

*indicates whether the OC content, $\delta^{13}C$, $\delta^{15}N$ or the molar C:N ratio from a specific OM fraction at a given landscape position is significantly lower or higher compared the other positions on a $p \leq 0.05$ level.

4.4.5 Linear mixed effects model

The LME results revealed that TPI25 and curvature had the most significant effect on the OC content (Table 4.5). With respect to $\delta^{13}C$, strong significant effects could also be observed for LAI, TPI and the interaction term between LAI, TPI25, and curvature. Elevation and curvature were found to have the largest effects on $\delta^{15}N$.

Table 4.5. Results of the statistical linear mixed effects (LME) model on organic carbon (OC) content and stable isotope ratios as explanatory variables and the significant effects. TPI25 = topographic position index; LAI = leaf area index.

Explanatory variable	Predictor variable	Estimate	SE	t value	p value
OC	Curvature	-2368.70	499.69	-4.74	< 0.01
	TPI25	996.42	385.46	2.69	0.01
$\delta^{13}C$	LAI	-0.59	0.13	-4.58	< 0.01
	TPI25	-0.82	0.38	-2.17	0.03
	LAI:TPI25: Curvature	0.24	0.10	2.45	0.02
$\delta^{15}N$	Elevation	0.20	0.10	2.06	0.04
	Curvature	-1.16	0.28	-4.10	< 0.01

4.4.6 Correlation analyses of organic carbon content, $\delta^{13}C$ and $\delta^{15}N$ with soil characteristics

There were positive correlations ($r > 0.8$, $n = 16$) between OC contents of OM_{PYS} and OM_{PYP} with Fe_{PYt} and Al_{PYt} (Table 4.6). Positive correlations were also found between OC in OM_{PYS} and OM_{PYP} with Fe_{ox} but the correlation coefficients were not as strong. Negative correlations could be observed for OC in OM_{PYS} and OM_{PYP} with the content of clay-sized particles and Ca_{ex}.

Table 4.6. Correlation coefficients (Pearson for normally distributed and Spearman rank for non-normally distributed data) between the organic carbon (OC) content, $\delta^{13}C$ and $\delta^{15}N$ and soil characteristic including all topographic positions and transects (n = 16) soil samples. OM_{bulk} = organic matter in the bulk soil; OP_{free} = loosely bound organic particles; OP_A = aggregate occluded organic particles; $WEOM_{free}$ = loosely attached water-extractable organic matter; $WEOM_A$ = aggregate-bound water-extractable organic matter; OM_{PYS} = Na-pyrophosphate extractable and HCl-soluble organic matter; OM_{PYP} = Na-pyrophosphate extractable and HCl-insoluble organic matter; OM_{ER} = organic matter in the extraction residue.

Soil characteristic	OM_{PYS}	OM_{PYP}	OM_{ER}	OM_{PYS}	OM_{PYP}	OM_{ER}	OM_{PYS}	OM_{PYP}	OM_{ER}
		OC			$\delta^{13}C$			$\delta^{15}N$	
clay	-0.69*	-0.66	n.s.‡	0.58	0.62	0.7	0.42	0.43	n.s.
Fe_{DCB}	-0.60*	-0.62*	n.s.	0.61	0.55	0.62	n.s.	0.43	n.s.
Fe_{ox}	0.60*	0.56	n.s.	-0.56	-0.63	-0.68	-0.52	-0.6	-0.42
Fe_{PYt}	0.90*	0.85	0.49	-0.79	-0.89	-0.93	-0.74	-0.78	-0.49
Al_{DCB}	n.s.	n.s.	n.s.	n.s.	n.s.	n.s.	n.s.	n.s.	n.s.
Al_{ox}	n.s.	n.s.	n.s.	n.s.	n.s.	n.s.	n.s.	n.s.	-0.47
Al_{PYt}	0.87*	0.81	0.47	-0.69	-0.85	-0.89	-0.78	-0.72	-0.55
Ca_{ex}	-0.54*	-0.53	n.s.	0.49	0.66	0.74	0.44	n.s.	n.s.

*Spearman rank
‡n.s.: not significiant

4.5 Discussion

From the hilltop to kettle hole, we observed distinct patterns in the physical and chemical properties of the soil and sediment. The relatively high clay content at the hilltop position indicates that tillage has exposed the clay rich Bt horizon, and is clear evidence of the history of erosion across the site. Clay and silt contents were greatest in the kettle hole sediments highlighting the importance of the transport of terrestrial material into the kettle hole over time. The transport of soil along the transect resulted in an increase of oxalate and Na pyrophosphate extractable cations toward the kettle hole similar to the patterns found previously by Berhe et al. (2012) and Ellerbrock et al. (2016). For the cations extracted by dithionite-citrate-bicarbonate solution a reverse trend is observed conforming the findings of Berhe et al. (2012). As a result, the OC content also increased along the transect from hilltop to edge, which corresponded to the landscape curvature and TPI25. The OC content was especially large in the kettle hole, emphasizing the depositional nature of these water bodies. Thus, the drivers of OM distribution across the hillslope and into the kettle hole span the scales of the transect to the aggregate and we found that the combination of plant production, transport of material, and soil chemical properties can lead to different mechanisms of OM stabilization as well as the source of the OM that is stabilized.

4.5.1 Transect scale

We hypothesized that the $\delta^{13}C$, $\delta^{15}N$, and OC content pattern of OM fractions across the transects to be a result of land management or isotopic effects that occur with erosion, OM production, and turnover. We used the Rayleigh distillation model as a general test to infer if land management versus isotopic fractionation that occurs along the transect explained patterns in fraction OM content and isotopic values. Interestingly, we found similar Rayleigh results for both $\delta^{13}C$ and $\delta^{15}N$ among the OM bound by mineral associations, fractions which contribute to the majority of OM_{bulk} with > 65 %: OM_{PYS}, OM_{PYP}, and the OM_{ER} fractions. We propose that there are at least two non-mutually exclusive explanations for the patterns we observed that can be generalized to biological and transport related isotope effects.

The linear statistical model (LME) identified LAI, a proxy of plant productivity, as a significant variable that explains the variation of $\delta^{13}C$ along the transect (Table 4.5). LAI was greater in positions closer to the kettle hole and corresponds to more negative values of OM $\delta^{13}C$, presumably sites near the kettle hole are more favorable to plant growth which can lead to greater isotopic discrimination during photosynthesis and consequently OM depleted in the ^{13}C (Brüggemann et al., 2011). We acknowledge that LAI is only a proxy for plant growth and subsequent C reaching sites of stabilization within soil, and we need to assume that productivity has been maintained over SOM development time scales (Gerke et al., 2016), but a plant response to the transect gradient would explain the trend toward more negative isotopic

values from hilltop to edge. In this case, the system is open and OM is repeatedly introduced for stabilization, a process often referred to as dynamic replacement (Berhe et al., 2007; Harden et al., 1999; Berhe et al., 2008).

The second explanation of the Rayleigh results of the mineral associated fractions is the transport of OM and soil particles and aggregates during erosion. Based on their settling velocities, the smallest particles and aggregates are selectively transported furthest along the hillslope (Hu et al., 2016). This leads to an enrichment of clay and silt at depositional sites, in our case, in the kettle hole sediments. Fine particles and aggregates especially < 53 µm are generally comprised of complexed, poorly crystalline and well-crystallized mineral phases as well as clay minerals (e.g. oxides, layer-silicates), which can interact with OM (Kaiser et al., 2007; Wagai et al., 2013; Doetterl et al., 2015). We therefore hypothesize that fine particles and aggregates are associated with OM that is relatively depleted in ^{13}C and ^{15}N explaining the patterns of the mineral associated fractions OM_{PYS}, OM_{PYP} and OM_{ER} across the topographic positions. In one of the most in-depth studies to date on particle size and corresponding isotopic values, Hu et al. (2016) found lower $\delta^{13}C$ and a higher OC content with decreasing particle size independent from topographic position. In our study, we discuss the possible mechanisms behind the association of OM with poorly crystalline and well-crystallized mineral phases in the aggregate scale discussion below (chapter 4.5.2).

The non-mineral associated OP and WEOM fractions exhibit origins from plant inputs, effects from land management, and transformations from microbial decomposition. For example, the OP_{free} can be regarded as fresh, poorly decomposed OM, and therefore reflects plant C isotopic composition. However, the overall ^{15}N of OP_{free} does not conform to the Rayleigh distillation patterns (Fig. 4.6). Such nonconformity may result from inputs or slurry fertilization, which is known to lead to high $\delta^{15}N$ values of plants (Bateman et al., 2005; Senbayram et al., 2008). The downslope transport of slurry and its nutrients (Lloyd et al., 2016) may subsequently have led to higher ^{15}N values at the footslopes and edges (Choi et al., 2003) as evidenced by the significant effects of elevation and curvature. The contrast in Rayleigh patterns between the loosely and aggregate bound with mineral associated OM suggests that the loosely bound material is more sensitive to recent plant inputs and land management including tillage and fertilization. Furthermore, the pattern of $\delta^{13}C$ of OP_{free} parallels that of OM_{PYS}, OM_{PYP} and OM_{ER} (Fig. 4.5) suggesting that recent plant inputs is also important in the mineral associated fractions.

In addition to the pattern of OM isotopic depletion, we also observed a pattern of enrichment in the water extractable fractions. Patterns of enrichment in ^{13}C and ^{15}N of soil OM is often attributed to the processing of soil OM by microbes (Dijkstra et al., 2008; Kayler et al., 2011; Brüggemann et al., 2011). Microbial processing of OM has also been suggested in previous studies, for example, Schaub and Alewell (2009) inferred faster decomposition rates

based on higher $\delta^{13}C$ values in oxic upland compared to anoxic wetland soils in mountain grasslands. Comparable gradients in microbial processing might occur in our study at the transect scale: the $\delta^{15}N$ of WEOM fractions increased from the hilltop to kettle hole edge (Fig. 4.6) indicating stronger impact of microbial degradation at erosional positions. However, we also need to consider that slurry application might have contributed to the increase in $\delta^{15}N$ of $WEOM_{free}$ and $WEOM_A$ via inorganic N in these fractions (Table 4.4). Gregorich et al. (2003) suggested inorganic N derived from manure to have led to low C:N ratios in water extractable fractions, which is in agreement with our C:N ratios of the $WEOM_{free}$ and $WEOM_A$ fractions. Alternatively, denitrification potentially occurring during periods of anoxia along the kettle hole edge may have produced nitrate enriched in ^{15}N that was later incorporated in OM (Pennock et al., 1992; Sutherland et al., 1993; Dungait et al., 2013). Based on the decreasing trend of isotopic values with OC content, we can confirm our first hypothesis, that at the transect scale OM patterns are largely driven by material transport and inputs from plant productivity and, to a lesser extent, land management. Microbial processing was not an important factor in the OM isotopic patterns along the transect; however, the role of microbes may still be relevant at the aggregate scale.

4.5.2 Aggregate scale

The transect provided a strong gradient in clay, silt, and cation concentrations as well as different forms of Fe and Al that allowed us to infer OM stabilization dynamics in the soil. Our OC recovery rate of 84 to 96 % (Fig. 4.4) was similar to other studies (Balesdent et al., 1998; Moni et al., 2012) and indicated that we lost a minor part of OC that we attribute to the vacuum filtration especially after the ultrasonication. As such, we might have slightly underestimated the OC contents of the OM_{PYS}, OM_{PYP} and OM_{ER} fractions. We observed >65% of OC in the presumably stabilized fractions OM_{PYS}, OM_{PYP} and OM_{ER} highlighting the importance of organo-mineral interactions. The strong positive correlations between Fe_{PYt} and Al_{PYt} with OC in the OM_{PYS} and OM_{PYP} fractions (Table 4,6) indicate the occurrence of Fe-OM and Al-OM associations (Fig. 4.7). Furthermore, correlations between the Fe_{ox} content with OM_{PYS} and OM_{PYP} suggests that poorly crystalline Fe oxides may also be involved in binding OM.

At the footslopes and edges we found the largest Fe_{PYt}, Fe_{ox}, Al_{PYt}, and OC contents, similar to Berhe et al. (2012) and Ellerbrock et al. (2016), that corresponds with the lowest $\delta^{13}C$ and $\delta^{15}N$ values of OM_{PYS} and OM_{PYP} (Fig. 4.3 and Table 4.4). In contrast, we found greater concentrations of well-crystallized Fe phases (Fe_{DCB}) at hilltops and hillslopes due to more oxic conditions. This is indicated by the increase in the Fe_{ox}:Fe_{DCB} and Fe_{PYt}:Fe_{DCB} ratios toward the kettle hole (Fig. 4.3). Berhe et al. (2012), found similar patterns at their site and suggested that

soil from eroding positions may have maximized the capacity to stabilize OM via organo-mineral complexes.

We found negative correlations between Fe_{PYt}, Fe_{ox} and Al_{PYt} with $\delta^{13}C$ and $\delta^{15}N$ (Table 4.6) suggesting that OM that is only poorly microbially processed is stabilized via Fe-OM and Al-OM associations. We contend that the there is a preferential sorption of recent plant assimilates (e.g., root exudates) that are low in $\delta^{13}C$ and $\delta^{15}N$. However, the permanence of mineral associated OM is uncertain, as hypotheses exist that suggest root-derived OM is protected from microbial decomposition (Farrar et al., 2003; Rasse et al., 2005) while other research shows oxalic acid derived from roots liberates mineral associated OM (Keiluweit et al., 2015). Both concepts can explain the patterns we observed in our data. Isotopically light material associates with mineral surfaces which may become protected from decomposition or may be lost, freeing up binding sites, that are then reoccupied later. Despite lacking a clear mechanism at this time, our data contribute to the understanding that mineral associated OM can potentially be a mixture of carbon of different ages (Swanston et al., 2005; Kaiser et al., 2016).

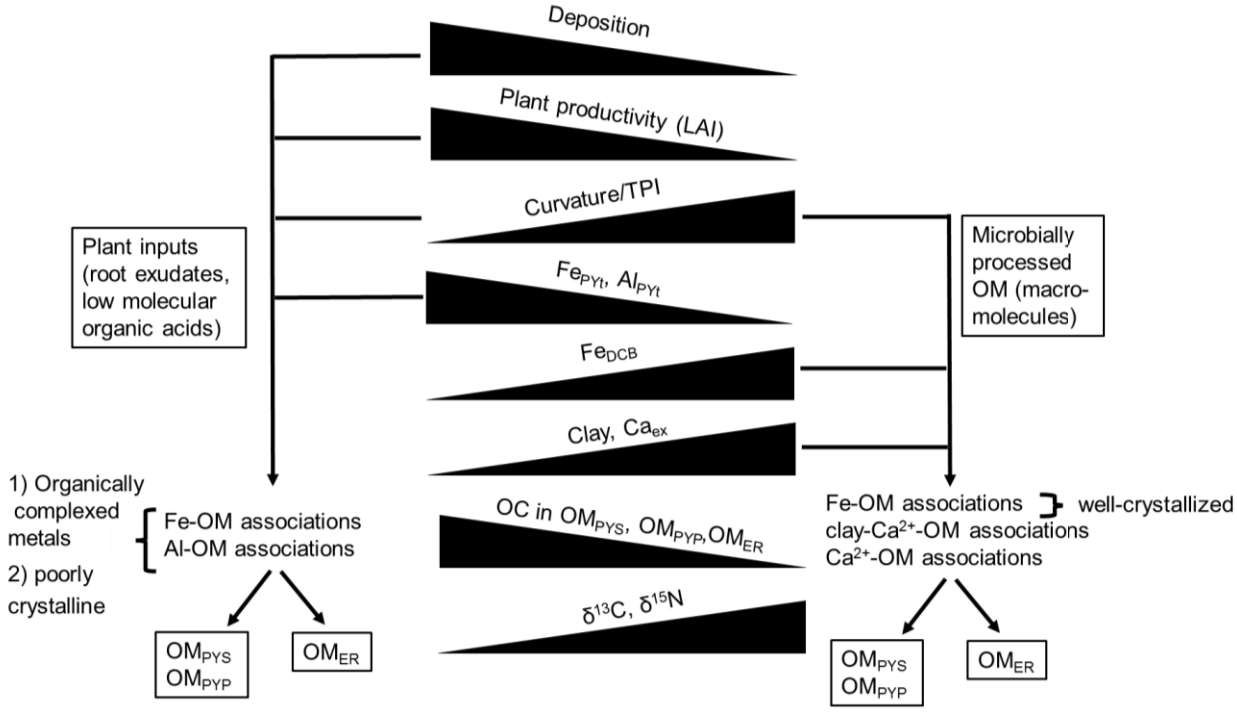

Fig. 4.7. Conceptual model illustrating the origin and parameters as well as pathways and processes that affect the fate of Na-pyrophosphate extractable and HCl-soluble organic matter (OM_{PYS}), Na-pyrophosphate extractable and HCl-insoluble organic matter (OM_{PYP}) and organic matter in the extraction residue (OM_{ER}) across a transect from erosional (right) to depositional (left) areas. The elongated triangles illustrate an increase or decrease of a given process or parameter across the transect. OM was regarded as associated with minerals based on correlations of $\delta^{13}C$, $\delta^{15}N$ and OC contents with soil mineral characteristics (Table 4.6) and on the significant effects obtained from the linear mixed effects model (Table 4.5).

On the other hand, the observed increase in $\delta^{13}C$ of OM_{PYS}, OM_{PYP} and OM_{ER} with increased Fe_{DCB} contents suggests more microbially processed OM is stabilized with well-crystallized Fe phases (Fig. 4.7). Furthermore, the positive correlations between $\delta^{13}C$ of OM_{PYS}, OM_{PYP} and OM_{ER} with the contents of Ca_{ex} and clay (Table 4.6) indicates interactions of OM either directly with Ca^{2+} or via Ca^{2+} with clay-sized Al-silicates (Kayler et al., 2011). Since Fe_{DCB}, Ca_{ex} and clay contents are higher at hilltops and hillslopes, organo-mineral associations are particularly important at these erosional areas corroborating the findings of Berhe et al. (2012). Interestingly, OC contents of OM_{PYS} and OM_{PYP} were negatively correlated with Fe_{DCB}, Ca_{ex} and clay contents, which contradicts the findings of Kaiser et al. (2012) for Ca_{ex}. We attribute our findings to the transport of OM downslope and lower plant productivity at eroding positions. Overall, we confirm hypothesis 2), OM at our site was stabilized by different mineral associations that are slope position dependent; moreover, we found that the OM bound in the different organo-mineral associations range from recent plant inputs to microbially processed material.

4.5.3 Sedimentary organic matter

The kettle hole is clearly collecting and accumulating OM, the sediments had the highest OC content for every fraction. We hypothesized that the source of this OM in the sediment fractions was of terrestrial origin. The lower $\delta^{13}C$ and $\delta^{15}N$ of most sediment fractions largely conform to the Rayleigh model, but not in terms of the very high OC and TN concentrations (Fig. 4.5 and 4.6). The isotopic results are consistent with the framework of a large input of OM depleted in the heavy isotopes transported with small particles such as clay, and silt into the kettle hole, as discussed for the transect results (section 4.1 above). And, the higher OC contents across all sedimentary OM fractions compared to SOM fractions is most likely due the accumulation of transported material over time (Stallard, 1998). Furthermore, molar C:N ratios of aquatic sedimentary OM fractions are in a similar range compared to C:N ratios from SOM fractions. This finding suggests the presence of pond-internal aquatic sources, such as phytoplankton or other periphytic algae, with molar C:N ratios typically ranging from 4 to 10 (Meyers, 1994), unlikely. Therefore, our molar C:N ratios > 12 from OP_{free}, OP_A, OM_{PYS} and OM_{PYP} (Table 4.4) are consistent with a terrestrial OM source.

Based on these findings, we partly confirm hypothesis 3) that OM in sediment fractions is of terrestrial origin; however, emergent macrophytes and inputs from land management are other potential OM sources that contribute to kettle hole sediments. Submerged, emergent, and floating macrophytes rooted in the sediment are present in the kettle hole. These macrophytes represent a direct source of OM into the water column either directly as particulate organic matte (POM) or as dissolved organic matter (DOM) after decay (Nitzsche et al., 2017). Visible plant residues in OP_{free} and OP_A support this assumption, but we lack

estimates of macrophyte isotopic signatures additional research is needed. Knowledge on the isotopic signature of macrophytes is needed to check for the significance of this OM as a source to kettle hole sediments. In addition to macrophyte contributions, slurry application on the agricultural field may contribute to the $\delta^{15}N$ of OM fractions as suggested by Nitzsche et al. (2017) for a larger number of kettle holes located in agricultural fields.

Kleeberg et al. (2016a) found that the sediment accretion rate increased after 1983 for the same kettle hole, due to the intensification of agriculture in the area (Bayerl, 2006) leading to enhanced erosive inputs. Erosion causes translocation of clay, silt, Ca_{ex}, and extractable Fe and Al, which may also serve as a basis for the formation of organo-mineral associations. OM was found to be associated with clay in marine sediments (Keil et al., 1994; Hedges and Oades, 1997), and Lalonde et al. (2012), suggested a preferential stabilization of ^{13}C proteins and carbohydrates via reactive iron surfaces, which is a possibility for our sediments given the high $\delta^{13}C$ values of OM_{PYS}. Though our kettle hole replicate size (n = 4) is too small for robust correlation analyses between $\delta^{13}C$, $\delta^{15}N$ and OC contents with sediment mineral and chemical characteristics, the large OC content of OM_{PYS}, OM_{PYP} and OM_{ER} fractions provide strong evidence for organo-mineral associations (Table 4.4). Furthermore, the higher $\delta^{13}C$ and $\delta^{15}N$ of sediment OP_{free} and $WEOM_{free}$ relative to the other fractions, suggests anaerobic microbial decomposition which can lead to no changes in $\delta^{13}C$ and $\delta^{15}N$ or a relative depletion of ^{13}C and ^{15}N in the remaining OM (Lehmann et al., 2002; Menzel et al., 2013). Anaerobic stabilization may also contribute to the larger OC in OM_{ER} compared to soils hampering OC mineralization and enhancing higher accumulation of OM (Isidorova et al., 2016), while the attachment of NH_4^+ at clay mineral surface may have led to the low C:N ratios of $WEOM_{free}$ and $WEOM_A$ (Table 4.4). According to Kleeberg et al. (2016b), anoxic conditions occur seasonally in the water column and surface sediments of the kettle hole and therefore it is reasonable to assume that our aquatic sediment horizon from 2 to 7 cm is under anoxic conditions almost throughout the year.

4.6 Conclusions

We have shown that OM stabilization and accumulation along agricultural hillslopes is contingent upon relatively large-scale drivers, in our case, erosion and land management that enhances plant productivity including fertilization. Organo-mineral associations with poorly crystalline mineral phases and organically complexed cations were clearly important where fine soil particles accumulated and we were able to demonstrate that the OM associated to these phases tended to be depleted in the heavy isotopes ^{13}C and ^{15}N. The low isotopic signatures emphasize the role of recent plant to stabilized OM and the mechanism behind these patterns deserves further investigation. Similarly, the transport of fine soil particles and associated OM into kettle holes contributes to the large C storage potential of kettle holes in

this hummocky arable landscape and additional research is needed to identify the role of internal OM cycling. Overall, the combination of OM fractions and stable isotopes provided useful information on the source of OM and how OM is distributed within the kettle hole catchment. Accounting for the full range of particle sizes transported along the hillslope as well as quantifying the annual contributions of transported material to the kettle holes, will help improve the understanding of OM dynamics in eroding agricultural landscapes.

4.7 Acknowledgments

We thank Frau Remus, Dr. Sara Herrero Martín, and Ruben Yague for their help with the sample preparation and isotope analysis. We thank Kristina Holz and her team from the Central Laboratory at ZALF for measurements of the soil chemical characteristics as well as Michael Facklam from the Technische Universität Berlin for soil textural analysis. We kindly thank the LandScales team for their support and discussions. This research was funded through the Pact for Innovation and Research of the Gottfried Wilhelm Leibniz association (project LandScales - 'Connecting processes and structures driving landscape carbon dynamics over scales').

5. Summary

In this chapter, I firstly summarize the main outcomes for each manuscript (chapter 2 – 4) as they serve as the basis for the synthesis chapter 6. To get a condensed and concise overview of chapters 2 to 4, I provide small boxes, which highlight the most important results and their implications on the C and N dynamics at each particular scale.

5.1 Regional landscape scale

The overall goal of this chapter was to identify the mechanisms driving the C and N relations in a ~ 38.2 km^2 wide area encompassing a small precipitation gradient of ~ 45 mm over ~ 11 km, different land-use structures (arable fields, forests, grasslands, and kettle holes), and different land-management histories of the agricultural fields. To fulfill this goal, I created $\delta^{13}C$ and $\delta^{15}N$ isoscapes (Bowen, 2010), of plant leaves and top soils sampling a 250 m grid.

I found that C_3 crops were affected by the precipitation gradient with plants potentially experiencing more water stress (c.f. Grossiord et al., 2014) at the lower end of the precipitation gradient. The $\delta^{13}C$ of SOM reflected this long-term microclimate impact on the plant water use efficiency and drought exposure level, but also the short-term imprint of corn after approximately four rotations. The $\delta^{15}N$ of SOM revealed spatial differences in the fertilization regime (only chemical fertilizers vs. slurry application) and differences in the N cycle between forest (open N cycle) and arable fields and grasslands (closed N cycle). An isotopic mixing model (Parnell et al., 2008) using different sources, i.e. the $\delta^{13}C$ and $\delta^{15}N$ of kettle hole plants from the surrounding catchment (*Phalaris arundinacea* from arable and grassland kettle holes; beeches from forest kettle holes), of crop species and of soils, revealed contributions of terrestrial plants to OM in surface sediments.

Based on this chapter, I could show that C and N dynamics differ across land-use structures, land-management has profound impacts on the C and N dynamics of SOM at the regional landscape scale, and the aquatic kettle holes are closely linked to their terrestrial catchments. However, further factors (e.g. hydroperiod), possible other OM sources need to be accounted for and deeper sediments may provide further information (summary chapter 5.2).

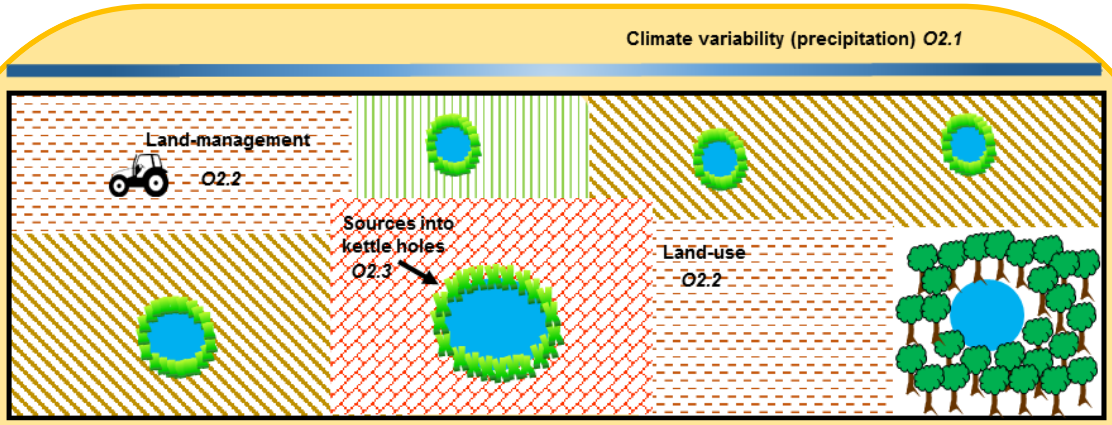

***O2.1*: Climate variability**

- C_3 crops reflected a small local precipitation gradient of ~ 45 mm from NW to SE as indicated by the intrinsic water use efficiency.
- Native plants from forests (beech) and grassland (dandelion) did not
  - ➢ They are assumed to be more adapted to climatic conditions.
- $\delta^{13}C$ of soil organic matter (SOM) seemed to reflect the water-status of the plants.
  - ➢ **Climatic impact** on C dynamics visible on the landscape scale.

***O2.2*: Land-use and management**

- Legacies of corn cultivation are visible in $\delta^{13}C$ of SOM.
  - ➢ **Type of cultivated crops** drives C dynamics.
- Open N cycle in grasslands and arable fields.
- Fertilization regime imprinted in $\delta^{15}N$ of SOM: chemical vs. organic fertilizers
  - ➢ **Land-management** activities visible on the landscape scale that drive N dynamics.
- Smaller forests tended to have a more open N cycle and to be more water-use efficient
  - ➢ Possibly stronger effects through management from the surrounding arable fields.
  - ➢ N dynamics vary with **land-use** over the landscape

***O2.3*: Sources into kettle holes**

- Plants (crops and grasses) were the dominant source to surface sediments from arable and grassland kettle holes, while beech litter and soils were dominant to the surface sediments from forest kettle holes.
  - ➢ **Terrestrial contributions** may alter C and N dynamics in kettle hole sediments.
- Other mainly internal processes within kettle holes might affect the N and C dynamics and thus the OM isotopic composition and need to be accounted for.

Fig. 5.1. Summary of the outcomes of the three objectives (*O*) on the carbon and nitrogen dynamics of different land-use structures (arable fields, grasslands, forests) and surface sediments from kettle holes inferred from chapter 2 – the regional landscape scale.

5.2 Regional kettle hole scale

This chapter aimed at identifying the land-use, management and hydroperiod (i.e. the duration of the wet period of a kettle hole) impacts on the C and N biogeochemistry in sediments of 51 kettle holes within different land-use structures interspersed in the same study site as described in chapter 2. More precisely, I aimed to assess OM sources (allochthonous vs. autochthonous) and turnover based on surface and deeper sediments from theses kettle holes, not only differing in the land-use of the catchment, but also in the hydroperiod thus being characterized as semi-permanently water filled (sp-type) and temporarily water filled (t-type) kettle holes.

I found that surface sediments were affected by more recent processes including slurry application on fields of the surrounding catchment and that anoxic conditions prevailed in sp-type and forest kettle holes favoring anaerobic microbial decomposition. The molar C:N ratios of surface sediments indicated autochthonous OM sources (e.g. phytoplankton and periphytic algae). Deeper sediments reflected allochthonous OM sources from emergent macrophytes and the degree to which OM was microbially processed within the sediment. The microbial processing was related to the hydroperiod, i.e. longer dry periods in t-type kettle holes seemed to have favored aerobic microbial decomposition. Furthermore, arable and grassland kettle holes were prone to loosing water via evaporation with an average of 30 % loss in the growing season from April to July. Additional water loss via shallow lateral groundwater flow was hypothesized.

Based on this chapter, I could show that land-use and management have strong impacts on the C and N dynamics in kettle holes and that the changing climatic conditions from year to year may dynamically alter water level and as a consequence the C and N dynamics in the sediments. Since in this study I only used the isotopic composition of bulk soil and sedimentary OM, specific OM fractions might reveal further mechanisms of the C and N dynamics, i.e. they may reveal a more precise information on the OM sources, OM stabilization mechanisms, possible land-management activities, which was exemplarily assessed for one representative arable kettle hole (summary chapter 5.3).

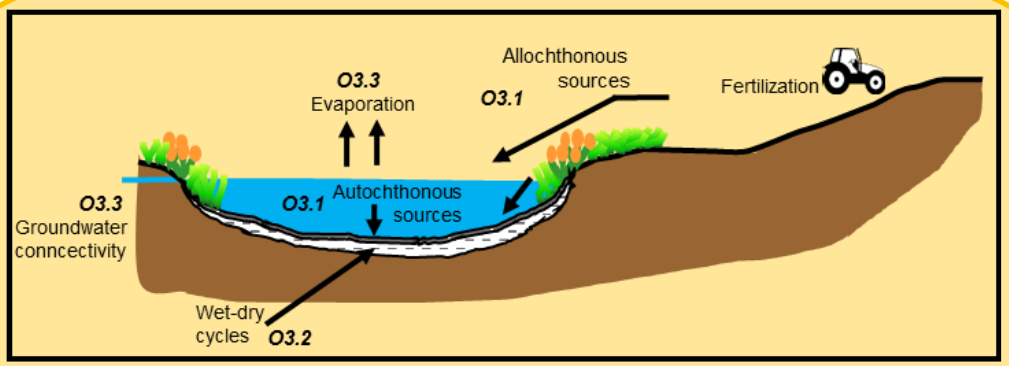

***O3.1*: Land-use and management impacts**

- $\delta^{15}N$ and molar C:N ratios from surface sediments reflected allochthonous OM sources:
  1) beech litter input into kettles holes within forests
  2) macrophyte contributions
- and autochthonous sources (e.g. phytoplankton and periphytic algae)
- Slurry application on surrounded fields increased the $\delta^{15}N$ of individual kettle holes.
- Anoxic conditions were suggested to occur regularly in sp-type and in forest kettle holes.
  - ➢ **Land-use and management** impacts on C and N dynamics are visible for a large number of kettle holes across the landscape

***O3.2*: Hydroperiod impacts**

- $\delta^{15}N$ and molar C:N ratios from deeper sediments reflected the wet-dry cycle impacts on
  1) the source of OM via the encroachment of terrestrial plants forming peat with high C:N
  2) and microbial decomposition that led to an accelerated OM turnover and shifted the $\delta^{15}N$ towards higher values while lowering C:N ratios as particular evident in t-type kettle holes.
  - ➢ **Hydroperiod** considerably affects C and N dynamics of deeper kettle hole sediments that may function as sinks for terrestrial C on a landscape level.

***O3.3*: Hydrology**

- Kettle hole water was prone to evaporation with in average ~ 30 %, but the magnitude depended on the year of observation and thus actual weather conditions and on land-use.
- Winter precipitation was a dominant water input in dormant season.
- Further losses were through shallow groundwater lateral flow followed by transpiration.
  - ➢ Kettle holes are ranging from **partially-closed to open systems** and annually varying climatic conditions may dynamically alter water level and thus C and N dynamics.

Fig. 5.2. Summary of the outcomes of the three objectives (*O*) on the carbon and nitrogen dynamics in kettle hole sediments of different depth and on the hydrology inferred from chapter 3 – the regional kettle hole scale. OM = organic matter. sp-type = semi-permanently water filled. t-type = temporarily water filled.

5.3 Transect and aggregate scale

The main objective of this this chapter was to identify the impact on the C and N dynamics of specific organic matter (OM) fractions of topographic position spanning from erosional to depositional areas, including aquatic sediments within a single semi-permanently water filled arable kettle hole. Environmental conditions driving plant productivity and microbial decomposition as well as soil erosion and fertilization are likely to be effective across the transect. Furthermore, this chapter targeted at the identification of pathways and sources of OM association via mineral interaction across topographic positions and the contribution of OM from the field to subsurface sediments (2 to 7 cm).

On the transect scale, I found that mineral-associated OM fractions still reflected the $\delta^{13}C$ of plants thus showing a link to crop productivity and water relations across the transect, and that erosion led to the transport of organic particles and clay- and silt-sized particles to depositional areas, while slurry application and microbial decomposition rather influenced freely available and aggregated OM fractions. On the aggregate scale, the dominant pathway of OM association changed from erosional areas to depositional areas. In erosional areas, interactions of OM either directly with Ca^{2+} or via Ca^{2+} with clay-sized Al-silicates and via well-crystallized Fe phases rather binding microbially processed OM dominated. In depositional areas, more labile OM was preferentially bound via organically complexed Fe and Al phases and poorly crystalline Fe oxides. With respect to the aquatic-terrestrial linkage, OM in mineral-associated fractions from sediments was derived from clay- and silt-sized particles from the agricultural field together with emergent macrophyte contributions to freely available and aggregated OM fractions.

On the basis of the chapter, I conclude that the combined effects of environmental conditions, erosion and land-management strongly affect the C and N dynamics of specific OM fractions in kettle hole catchments and that kettle holes constitute important sinks for terrestrial born OM.

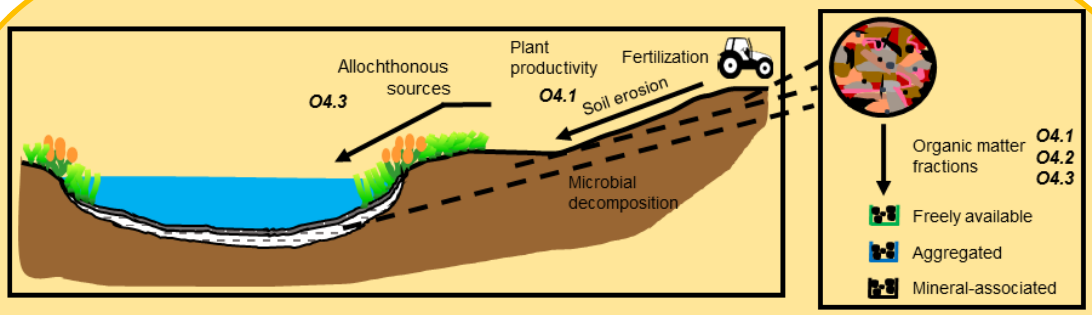

***O4.1*: Transect scale pattern**

- $\delta^{13}C$ and $\delta^{15}N$ of specific organic matter (OM) fractions revealed different mechanisms on the source and fate of OM across topographic positions in the kettle hole catchment:
  1) $\delta^{13}C$ from plant production persisted in mineral-associated fractions over the transect and reflected the water availability of plants.
  2) Erosion led to the transport of small clay- and silt-sized particles low in $\delta^{13}C$ and $\delta^{15}N$.
  3) Enhanced aerobic microbial degradation led to higher $\delta^{13}C$ & $\delta^{15}N$ in erosional areas.
  4) Slurry impacted the $\delta^{15}N$ in freely available and aggregated OM fractions.
  - ➢ The combined effects of **plant growth, transport**, **decomposition** and **land-management** impact specific OM fractions and thus C and N dynamics in catchment.

***O4.2*: Aggregate scale pattern**

- More than 65 % of organic carbon was found in mineral-associated fractions:
  1) More labile OM was associated via organically complexed Fe and Al phases, and poorly crystalline Fe oxides in depositional areas.
  2) More decomposed OM was associated via Ca^{2+}-OM and clay- Ca^{2+}-OM interaction and via well-crystallized Fe phases in erosional areas.
  - ➢ The pathway and source of OM associated via **OM-mineral interaction** changes with topographic position.

***O4.3*: Sources into kettle holes**

- OM from emergent macrophytes contributed to freely available and aggregated fractions.
- OM in mineral-associated fractions derived from clay- and silt-sized particles from the field, which were the basis the formation of OM-mineral associations.
  - ➢ Kettle holes constitutes important sinks for **OM associated with fine soil particles** and for **OM derived from emergent macrophytes** characterizing them as potential C and N sinks in the landscape.

Fig. 5.3. Summary of the outcomes of the three objectives (*O*) on the carbon and nitrogen of specific organic matter (OM) fractions in the catchment and in subsurface sediments of one semi-permanently water filled kettle hole inferred from chapter 4 – the transect and aggregate scale.

6. Synthesis - Linking the scales and implications on carbon and nitrogen dynamics in the landscape

The three individual studies have demonstrated that the mechanisms that drive the aquatic-terrestrial C and N dynamics vary greatly across the investigated scale. In the following, I discuss the identified mechanisms from the particular scales on the C and N dynamics in the complex, moraine agricultural landscape of NE Germany. Thereby, I will firstly discuss C and N dynamics for the terrestrial side, followed by the aquatic the kettle holes.

6.1 The role of the terrestrial biological activity

In the following, I use the identified mechanisms from the aggregate and transect scale (chapter 4) to deduce C and N dynamics for the moraine agricultural landscape. I treat the kettle hole catchment assessed there exemplarily for the hummocky soil landscape covering most of the typical sequence of geomorphic structures and accompanied soil types as shown in Fig. 1.1. As such, hilltops from the transect study correspond to steep slopes with caRG in Fig. 1.1, hillslopes refer to mid slopes with eLV, footslopes correspond to the same position, and edges from the transect study represent depressions with coRG. In contrast to the typical catena, plateaus were not sampled in the transect study, but instead the kettle hole near the village Kraatz (Kr) as a wet depression followed the schematic cross-section.

From a geomorphic perspective, the slope position inferred from the DEM can be used to estimate erosional and depositional areas (Deumlich et al., 2010). As such, the area of depositional flat slopes < 2°, lower slopes (footslopes, toe slopes) and depressions/valleys was around ~ 66 % in the kettle whole catchment of the transect study, whereas depressions/valleys mostly referred to the area of the kettle hole (C. Hoffmann, unpublished). On the other hand, the area of erosional mid and upper/steep slopes summits/ridges/tops > 2° was ~ 34 %. Given that the depositional and erosional areas of the whole study from the regional landscape scale only slightly differed with 73 and 27 %, respectively, the catchment of the Kr kettle hole is representative for the whole study site. Furthermore, I can state that most of the study site in is in theory prone to deposition.

Precipitation was identified as driving the WUE_i and thus plant growth of C_3 crops across the whole study site (chapter 2). High precipitation can lead to an increased depression-centered collection of water such as in the kettle holes. Therefore, climate variability on the landscape scale could alter the environmental conditions like soil moisture favoring plant growth in the catchment of individual kettles holes. A topographical measure for the soil moisture is the TWI derived from the DEM. Though the TWI neither had a significant effect on the $\delta^{13}C$ nor on the OC content of specific OM fractions, I found the LAI (indicative for plant growth) and TWI to be positively correlated with each other ($r = 0.81$, $p < 0.01$). The positive correlation corroborate results from Schaub and Alewell (2009) who suggested higher plant

productivity in the near distance to wetlands compared to erosional uplands leading to a lower WUE_i in lowlands and thus lower $\delta^{13}C$ values of plants. I did not directly measure the $\delta^{13}C$ values and determine the WUE_i of crops. However, I used the $\delta^{13}C$ of OP_{free}, which represented fresh root and stem fragments, as indicator for the water stress level of plants at steep and mid slopes assuming the stomata conductance signal conveyed by $\delta^{13}C$ in plant OM to be a direct indicator of the reaction of pants towards water availability vs. demand (Farquhar et al., 1982; Grossiord et al., 2014). The lower $\delta^{13}C$ in OP_{free} close to the kettle hole therefore indicated sufficient water supply for the plants, while more positive $\delta^{13}C$ in OP_{free} indicated potential water deficiency (Fig. 4.5). In order to generalize this finding for the whole landscape, the kettle whole hydroperiod might need to be accounted for as the effect of kettle holes on the soil moisture in their surroundings might be higher for the sp-type kettle holes given the longer time of waterlogging.

Next to soil moisture, nutrient availibility is the second most important driver on plant growth. I could show that slurry and the nutrients derived from slurry may have accumulated in depositional areas around the kettle hole (Lloyd et al., 2016), which may promote plant growth. The fertilization impacts across the whole study site (Fig. 2.5) further suggest that almost all kettle hole catchments were prone to increased nutrient supply. Moreover, nutrients could also have originated from decomposing organic particles, which were transported along the slope. Next to organic particles, OC-rich clay-sized particles are also deposited close to the kettle hole. This may lead to an increase in the water holding capacity (Manns and Berg, 2014) and the potential for binding nutrients (Tahir and Marschner, 2016), thus favoring soil fertility and ultimately plant growth. Given that the $\delta^{13}C$ of plants persisted in mineral-associated OM fractions over the transect (Fig. 4.5), plant growth was clearly important on SOM and consequently on the C and N dynamics in kettle hole catchments. This finding further indicates that erosion is not necessarily the only dominant mechanism driving C dynamics across the landscape as assumed by many studies (e.g. Bellanger et al., 2004; Fox and Papanicolaou, 2007; Alewell et al., 2009; Hilton et al., 2012; Ellerbrock et al., 2016; Hu et al., 2016; McCorkle et al., 2016), instead the role of dynamic replacement via new photosynthate may not be underestimated.

The importance of water collecting in depressions was recently also highlighted for the CarboZALF experimental site (Sommer et al., 2016), which covered a full gradient of landscape structures typical in hummocky moraine landscapes similar to the transect study (chapter 4). The CarboZALF site is located approximately 5 km northwest of the Kr kettle hole, but the CarboZALF site bears of no kettle hole in the depression. Supporting my assumptions for the Kr kettle hole, Rieckh et al. (2012) suggested fewer plant root growth in haplic Regosols (in this study referred to as Calcaric Regosols – caRG) on erosional steep slopes because the mixing of the high-density glacial till into the topsoil reduced the pore space for roots and the

hydraulic conductivity. Furthermore, Gerke et al. (2016) found highest plant growth based on LAI measurements in the coRG in depositional hollows (in this study referred to as footslopes) due to higher soil moisture. These findings may indicate that a water body (a kettle hole) is not necessary to impact plant growth, instead higher soil moisture in topographic depressions can be sufficient.

Hydroperiod and soil water dynamics during the growing season (and between years) were also pointed out by Gerke et al. (2016) who found reduced plant growth during the growing period of the following year. The authors attributed this finding to the rise of the soil water table in the depression inducing O_2 deficiency in the rooting zone. Therefore, when the soil water content exceeds particular thresholds leading to waterlogging, this may have negative impacts on plant growth and thus potential C inputs into the soil. This hypothesis is in agreement with my own observations during the field campaign in May 2013. Plant height and density was lower or even not apparent in topographic depressions bearing puddles. With respect to kettle holes, given the assumed contact of the kettle hole water with the groundwater table for most of the year (chapter 3), a rise of the kettle hole water table could in turn be at least indicative for a rise of the groundwater table in the subsoil of fields ultimately hampering plant growth on the field. In addition, kettle holes have the tendency of shore overflow when the infiltrated water volume in winter and spring exceeds the volume of the depression (Kalettka and Rudat, 2006), a phenomenon I could also observe during my sampling campaigns in the early growing seasons. It might need to be addressed in future how absence or presence of kettle holes as well as their hydroperiod positively or negatively affect plant growth and subsequently OM into the soil.

Another consequence of higher soil moisture in the surrounding of kettle holes is the impact on the magnitude and pathways of microbial decomposition. A higher soil moisture in wetlands can reduce aerobic microbial activity due to the reduced O_2 availability as the pore space is occupied by water (Schaub and Alewell, 2009; Trumbore, 2009). Based on the higher $\delta^{13}C$ and $\delta^{15}N$ of mineral-associated fractions in erosional areas (Table 4.4), enhanced aerobic microbial decomposition was suggested at erosional hilltops and hillslopes. However, this does not necessarily mean that microbial activity was automatically lower in areas close to the kettle hole. In fact, Hu et al. (2016) and Berhe (2012) found higher decomposition rates in depositional areas, which was suggested due to higher nutrient availibility and the addition of new labile OM from higher topographic positions. This is in agreement with the study from Wirth (1999), who found higher soil basal respiration rates in the surrounding of another kettle hole (catena Bölkendorf) approximately 50 km SE of the Kr kettle hole. Again, variations in the hydroperiod of the kettle hole and the degree of waterlogging in the surrounding terrestrial areas will have strong impact on microbial activities. High soil water content below a waterlogging threshold might allow higher decomposition and OM turnover rates than in

erosional topographic positions. Waterlogging however, might not only restrict plant input to the soil but also aerobic microbial activity and inducing anaerobic microbial pathways to be established.

Higher aerobic microbial activity around kettle holes may lead to enhanced CO_2 emissions compared to higher topographic positions. As such, Lisbôa (unpublished) found an up to three times higher soil respiration rate (autotrophic and heterotrophic) at two sampling points close to the Kr kettle hole (corresponds to the edge position in chapter 4) compared to the mid slope positions using closed chamber measurements biweekly from March to October 2014 when there was wheat cultivated on the field. Given the potentially higher soil moisture close to kettle holes, anaerobic microbial activity was suggested to have led to the higher $\delta^{15}N$ values in depositional areas which were suggested as potentially resulted from denitrification during seasonal anoxia (Pennock et al., 1992; Sutherland et al., 1993). A byproduct of denitrification is the emitted N_2O. Equivalent to that, the surroundings of kettle holes could be sources of CH_4 as suggested for colluvic soils in depressional footslopes in the hummocky ground moraines of the Allgäu, Germany (Sommer et al., 2004). Since the Kr kettle hole has a rather steep catchment and no shore overflow tendency (T. Kalettka, personal communication), N_2O and CH_4 emissions are most likely not typical for the direct surrounding at this site. High emission potentials are thus related to the geomorphology and could rather be expected for other kettle holes prone to shore overflow (Kalettka and Rudat, 2006), which were part of the regional kettle hole study (chapter 3). Therefore, the surrounding of kettle holes may be characterized as potential GHG sources in the landscape. It should be noted that the littoral zone, which comprises the typical kettle hole vegetation (Pätzig et al., 2012) and undergoes water level fluctuations, was not sampled but can be an important GHG source with increasing water level in kettle holes (Richter, 2014; C. Lisbôa, personal communication).

6.2 The role of organo-mineral associations and erosion

OM-mineral associations were of particular importance for the SOM content in the catchment of the Kr kettle hole (Fig. 4.7). Ongoing erosion on steep slopes triggered by tillage will continuously expose the glacial till from the subsoil (caRG) and provide Ca^{2+} cations as the basis for the formation of Ca^{2+}-OM and clay-Ca^{2+}-OM associations. Furthermore, erosion will also expose the Bt horizons of the eLV at mid slopes providing clay-sized Al-silicates and reactive Fe phases. Therefore, we may expect an increasing importance of OM interaction via reactive Fe phases, directly via Ca^{2+} or via Ca^{2+} with clay sized Al-silicates on agricultural fields in the future. From a landscape perspective, the carbonate content bearing of Ca^{2+} can vary greatly across the landscape (Fig. 6.1) and could be attributed to heterogeneities in erosion rates related to the steepness of the slope. Therefore, the magnitude of OM bound directly via Ca^{2+} or via Ca^{2+} with clay-sized Al-silicates interaction might vary across the landscape. In

addition to the release of Ca^{2+} from caRG, continuous tillage allows inorganic C to enter the topsoils at the steep slopes. This further alters the C dynamics of the landscape because the dissolution of carbonates via carbonic acids or oxalic acids from roots leads to the release of CO_2 into the atmosphere.

OM associated via organically complexed Fe and Al and poorly crystalline Fe phases was particular important close to the Kr kettle hole. While here the higher ratio of poorly crystalline to well-crystallized Fe was suggested as a result of erosive transport, the crystallinity of Fe also depends on redox conditions and on the pH value. Fe in soils can be brought into solution at acidic pH values and during reducing conditions (Colombo et al., 2014), conditions likely to occur at least periodically in depositional areas leading to the breakdown of well-crystallized Fe phases and accelerated via oxalic acids from roots (Keiluweit et al., 2015). The subsequent formation of poorly-crystalline Fe phases during more oxic conditions can then lead to new OM-Fe associations as it was suggested for root-derived OM (Farrar et al., 2003; Rasse et al., 2005). Furthermore, other cations such as manganese (Mn) could be important in interacting with OM as shown by Doetterl et al. (2015). These authors showed that cations could be involved in the formation of aggregates in depositional areas, as also hypothesized by Berhe et al. (2012). Therefore, the direct surroundings of kettle holes are considerably important for the OM-mineral associations. Ellerbrock et al. (2016) also suggested the erosive transport of reactive Fe and Al phases for the CarboZALF site indicating that the importance of depressions for OM-mineral associations is common and might be considered as a process that can be generalized for the whole landscape.

Whether these OM-cation associations are relevant on larger time scales remains of great interest given the changing redox conditions in depressions and the suggested preferential stabilization of rather fresh, poorly decomposed root exudates. When we consider the continuous deposition of polyvalent cation rich clay- and silt-sized soil particles in depressional areas, then OM-cation associations could be of high importance for the long-term stabilization of OM in the subsoil. As such, Ellerbrock et al. (2016) also found high contents of organically complexed and poorly crystalline Fe phases in the Go-M horizon from the coRG at their hollow position (here: footslope). However, with respect to kettle holes, the long-term stabilization of OM via cation interaction in the subsoil might be less distinctive given the outwash of small particles into the kettle holes (Frielinghaus and Vahrson, 1998; Kleeberg et al., 2016a).

Finally, land-management effects could also alter the magnitude and pathway of OM-mineral associations. Chemical fertilizers and organic manure contain abundantly cations essentially for plant growth such as K, Ca, Mg or Zn, or other heavy metals like Fe, Cu, or Cd (Raven and Loeppert, 1997; Huang et al., 2008; Cheraghi et al., 2012). The application of fertilizers may constitute anthropogenic cation sources to individual fields promoting the

formation of OM-mineral associations. On the other hand, crops are known to have different demands for specific cations such as Fe and Ca, which they accumulate in their biomass (Hell and Stephan, 2003; Hansen et al., 2006; White, 2015). The removal of biomass from the fields could lead to a loss of cations as basis for the formation of OM-mineral associations from the field, and the loss might be crop specific.

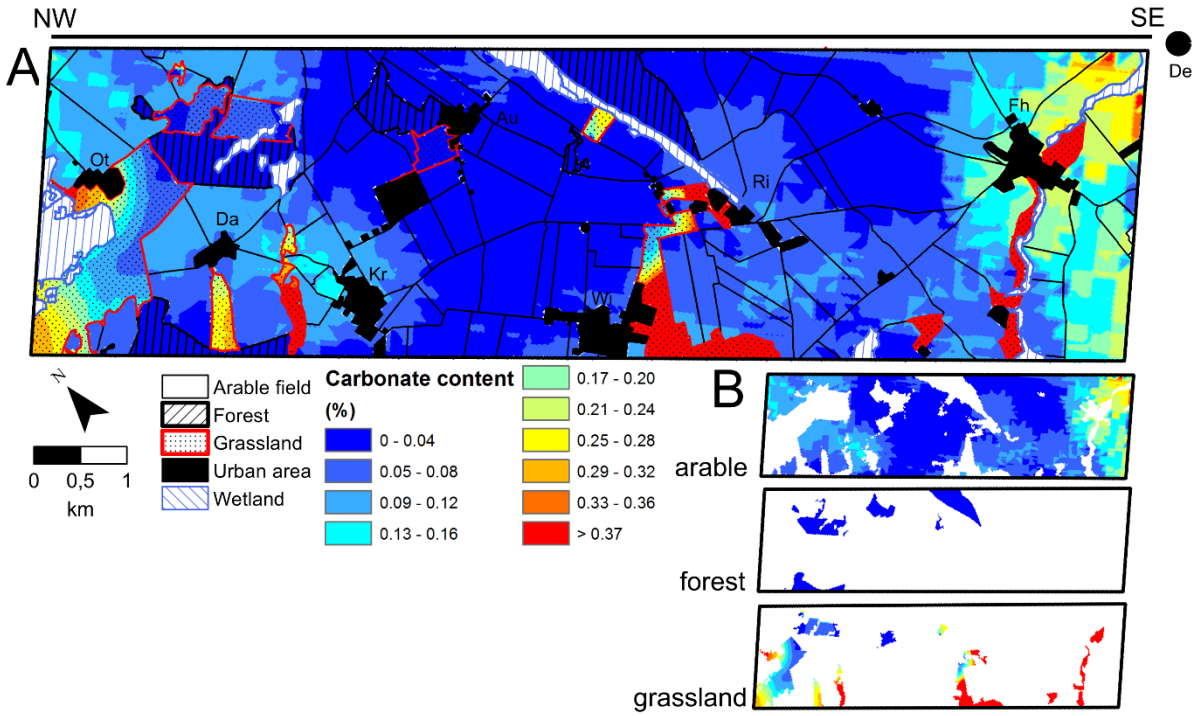

Fig. 6.1. Ordinary kriging (A) on inorganic carbon (CO_3-C, %) for top soils sampled from the three land-use types. The area interpolated to generate each land-use type map is shown in (B) and includes the same scale. Areas not interpolated include wetlands > 1 ha and urban areas.

6.3 Land-management and climatic impacts

All these mechanisms, though being highly relevant for the C and N dynamics in the kettle hole catchments, were not visible at the landscape scale using isoscapes, i.e. isoscapes did not account for the impact of topography and environmental conditions altered by kettle holes (chapter 2). This was partly due to the chosen grid size of the study site and a smaller grid size might allow for detecting these patterns. Instead, land-management activities together with the landscape scale precipitation gradient were the most important drivers of the C and N dynamics at the landscape scale.

The fact that C_3 crop species partly experienced water stress (c.f. Grossiord et al., 2014) and were sensitive in their WUE_i to precipitation in my study has further implications on the C dynamics in the landscape. A higher WUE_i that is achieved by stomatal closure and thus imprinted in the plant OM (Farquhar et al., 1982), could be indicative for reduced plant production (Blum, 2005; McDowell et al., 2008) and thus for lower OM inputs into the soil. Consequently, reduced OM content in the soil horizon occurs in patches of the landscape,

which might already be negatively affected by lower precipitation, may lead to a lower water holding capacity (Emerson, 1995; Manns and Berg, 2014), which in turn further increase the drought exposure risks for plants. Though a slight correlation of $r^2 = 0.27$ between the amount of precipitation and the $\delta^{13}C$ of SOM was found across the study site (~ 11 km), this gradient in $\delta^{13}C$ of SOM is not reflected by the SOC content from the same sampling locations (Fig. 6.2). Thus, an effect of water stress and WUE_i on SOM is not likely in the studied area. However, such mechanisms might be more evident in landscapes with stronger rainfall gradients. As such, given the variation in precipitation ranging from ~ 500 to ~ 850 mm across the whole moraine landscape of NE Germany (WebWerdis, Deutscher Wetterdienst, Offenbach am Main 2012), OM inputs of water stressed plants and thus SOC contents may vary here to a greater extent.

While corn altered the $\delta^{13}C$ of SOM only after a few rotations, molar C:N ratios and SOC contents were not different across fields with different times of corn rotation ($r^2 = 0.02$). Generally, SOC contents of arable top soils ranged between 0.7 and 2 % (Fig. 6.2) and similar values were also found for the CarboZALF study site (Aldana Jague et al., 2016; Miller et al., 2016). These findings indicate that the complex crop cultivation history in the Quillow catchment led to a rather homogeneous distribution of SOC in the landscape.

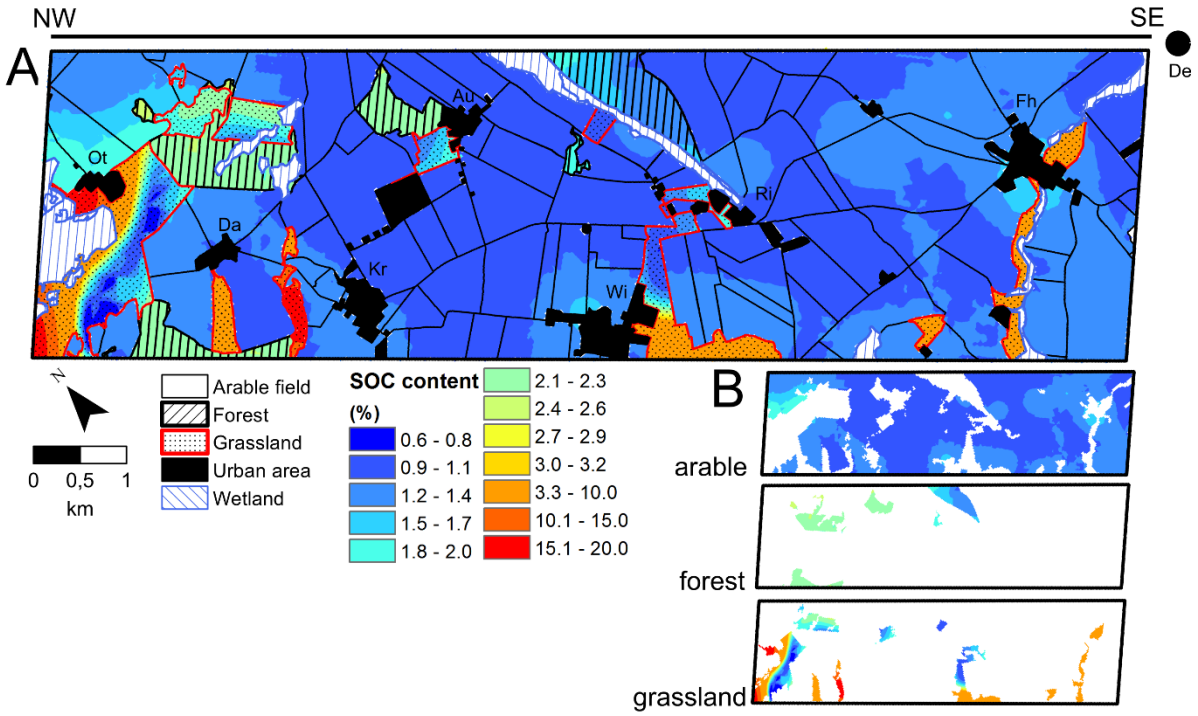

Fig. 6.2. Ordinary kriging (A) on soil organic carbon content (SOC, in %) for top soils sampled from the three land-use types. See chapter 2.3.6 for a more detailed explanation of the interpolation. Grasslands are highlighted with red borders and forests with black borders. The area interpolated to generate each land-use type map is shown in (B) and includes the same scale. Areas not interpolated include wetlands > 1 ha and urban areas.

With respect to N, higher N contents could be expected on fields with slurry application since liquid slurry known to increase the plant and soil N content (Choi et al., 2003; Choi et al., 2006). However, I did not find significantly higher N contents in SOM in fields which have received a decadal slurry input ($p = 0.67$, student's t-test) (Fig. 6.3). This finding is in agreement with the general observation that the application of N fertilizers both chemical and organic results in significant N losses from the soil via ammonia volatilization and nitrate leaching (Goulding et al., 2000; Choi et al., 2006).

We also need to consider that the soil C and N contents could vary with the soil type and texture, i.e. due to different water holding capacities and soil fertility via clay contents. Since the best resolution of the soil type map for the federal state of Brandenburg is only 300 m and the legend sometimes even comprises of multiple soil types for a specific area (LBGR, 2007), but soil types can change within several meters, I refrain from linking soil C and N contents to soil types.

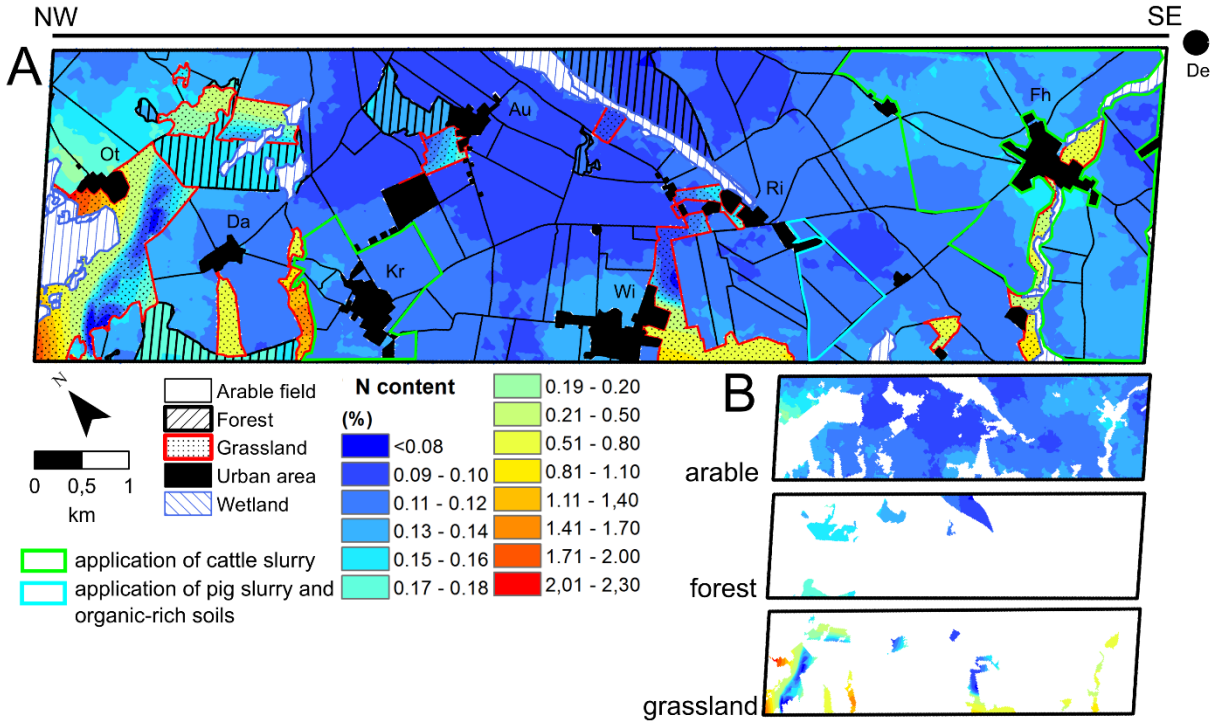

Fig. 6.3. Ordinary kriging (A) on nitrogen contents (N, %) for top soils sampled from the three land-use types. The area interpolated to generate each land-use type map is shown in (B) and includes the same scale. Areas not interpolated include wetlands > 1 ha and urban areas. Highlighted areas show the application of cattle slurry (green borders) and the application of pig slurry plus organic-rich soils (cyan borders).

6.4 Grassland and forests

Only SOM and OM fractions from arable soils were investigated over the transect and aggregate scale (chapter 4) making a transfer of the identified mechanisms on C and N dynamics in grasslands and forests difficult. Several studies highlighted the combined impacts

of erosion, microbial decomposition and plant input in grasslands leading to higher OC contents in depositional areas (Yoo et al., 2006; Berhe et al., 2012; Park et al., 2014; Fissore et al., 2017). Berhe et al. (2012) showed that OM stabilization via organically complexed Fe and poorly crystalline Fe phases was of high importance in depositional areas in a Californian grassland as they were supplied to these areas via erosion. Similarly, erosion could have led to the downslope transport of reactive Fe phases in grasslands of the moraine landscape of NE Germany assessed in my study. Furthermore, the high carbonate contents up of to 6.1 % in grasslands in the region assessed in my thesis (Fig. 6.1) points to the importance of Ca^{2+}-OM associations. The highest carbonate contents are predominantly found on calcaric Histosols, indicating the former formation of peat on glacial tills (Almendinger and Leete, 1998). Grasslands on Histosols also bear the highest SOC contents with up to 23.6 % highlighting their importance for C storage and dynamics in the landscape.

Furthermore, erosion can be important in forests distributing large amounts of OM (Meusburger et al., 2013; McCorkle et al., 2016). Forest soils have lower pH values than soils from grasslands and agricultural fields with even lower pH values in coniferous compared to deciduous forests (Johnson and Cole, 2005). Low pH values promote the formation of Fe-OM associations via poorly crystalline Fe and Al phases and ligand exchange in forest subsoils (Kleber et al., 2005) and topsoils (Kaiser et al., 2016). Furthermore, Kayler et al. (2011) suggested OM in forests to be in patches encrusting micrometer sized micro-aggregates of clay. Differences in the magnitude of contents of Fe-OM associations and micrometer-sized micro-aggregates between different forest patches could explain the lower SOC contents in the large forest located in the center of the study site right east to the elongated lake (Fig. 6.2). Alternatively, plant species composition and density might vary between forests in my study area and/or small scale abiotic environmental conditions such as in soil texture and moisture might be different. The observation that N contents of top soils are higher in the western forest patches (Fig. 6.3) might indicate more favorable conditions for plant growth and corresponds to the previous hypothesis from chapter 2 regarding smaller forest fragments were more impacted by land-management activities on the adjacent surrounding fields. The role of Ca^{2+}-OM associations might be of less importance f in forests given the low carbonate contents of < 0.1 % (Fig. 6.1).

Nevertheless, grasslands and forests should be included into the general perspective of C and N dynamics in agricultural moraine landscapes given their proportion of 10.4 and 5.9 %, respectively, in the study site. Forests even make up 24.4 % in the Uckermark region (Kleeberg et al., 2016a) and roughly cover 30 % of the landscape in Germany and whole Europe (FAO, 2015). Furthermore, larger stagnant wetlands of > 1 ha, which basically comprise of fens, lakes, and reed-dominated areas make up ~ 3.4 % of the area assessed, and were predominant in the western part of the study site from chapter 4. Especially fens are

of high importance for the C and N dynamics given their high storage potential of OM in peat. However, in this study the focus was on kettle holes as small inland water bodies in the landscape that can also store OM in their sediments.

6.5 The role of kettle holes in the landscape

I could clearly show the tight coupling of the aquatic kettle holes with their surrounding terrestrial catchments from the aggregate to the landscape scale. For the regional landscape scale without focusing on smaller scale topography (chapter 2), it was suggested that plants from the surrounding fields (i.e. crops) and grasses were the dominant OM input into surface sediments of arable and grassland kettle holes. Based on the findings from the regional kettle holes scale (chapter 3) and transect scale (chapter 4), that rather macrophytes and phytoplankton and periphytic algae were the dominant source for only the surface sediments, I have at least partially to reject the suggestion from chapter 2. New data from other studies within the project LandScales for the same sp-type kettle hole Kr (chapter 4), another sp-type kettle hole close to the village Rittgarten (Ri) approximately 3 km east of Kr (Flury et al., in revision; Kazanjian et al., submitted), as well as a subset of the kettle holes from the regional kettle hole scale (chapter 3) (Attermeyer et al., in press), provide further information on the OM sources into kettle holes. Autochthonous (defined as lignin-poor OM) OM from phytoplankton and periphytic algae were also suggested as dominant sources to surface sediments (top 2 cm) from 10 kettle holes that were for the most congruent to the kettle holes from the regional kettle hole scale of this study (Attermeyer et al., in press). Further autochthonous OM from submerged macrophytes (e.g. *Ceratophyllum submersum, Potamogeton perfoliatus*) and free-floating macrophytes (e.g. *Spirodela polyrhiza, Lemna spp*) was with > 90 % an important contribution to OM collected in sediment traps in the kettle holes of Ri and Kr (Flury et al., in revision). Though this autochthonous OM having a labile (easy available to microbes) character was found to be the most important OM source to the surface sediments of Ri and Kr, this OM was also subjected to extensive aerobic carbon degradation by benthic microbial activity resulting mostly in CO_2 production under low O_2 contents < 2 mg l^{-1} in the water column, which prevailed almost throughout the entire year (Flury et al., in revision; Kazanjian et al., submitted). Therefore, Flury et al. (in revision) concluded that most of the autochthonous OM was mineralized before burial and that preferentially more recalcitrant allochthonous OM was susceptible to burial. This conforms to my findings that the deeper sediments rather reflected allochthonous OM (more lignin-rich) with high C:N ratios (Fig. 3.2b) due to the encroachment of these emergent macrophytes. Allochthonous OM sources may have derived from emergent macrophytes (e.g. *Phragmites australis, Phalaris arundinacea, or Carex acutiformis*) and floating-leaved macrophytes rooted in the sediment (e.g. *Polygonium amphibium*) as occurring in the Ri and Kr kettle holes (Flury et al., in revision; Kazanjian et al., submitted). In fact,

Kazanjian et al. (submitted) found daily gross primary production (GPP) rates of 1.77 g C m^{-2} d^{-1} for RG and 1.83 g C m^{-2} d^{-1} for Kr, that were dominated by macrophytes in general with up to 90 % of GPP from May to November. More precisely, emergent macrophytes accounted for around 50 % of this GPP and periphyton prevailed throughout the rest of the year from December to April.

Nevertheless, the described importance of autochthonous OM sources via primary production to surface sediments requires the existence of stable water columns as it applies to sp-type kettle holes (Flury et al., in revision). The low C:N ratios < 12 found for surface sediments from t-type kettle holes indicates the importance of autochthonous OM also for these types (Fig. 3.2a). This might be due to longer wet conditions via enhanced precipitation in the years before the sampling in July/August 2013 expanding the period being water filled in t-type kettle holes. In fact, the average annual precipitation from 2010 to 2012 amounted to 592 mm being significantly higher than the average sums in the period from 1992 to 2009 amounting to 483 mm ($p < 0.01$; AgroScapeLab Quillow, Dedelow).

The suggested quick mineralization of labile OM from autochthonous sources characterizes kettle holes as important CO_2 sources in the landscape (Merbach et al., 2002; Reverey et al., 2016). However, not only OM from autochthonous OM sources can be mineralized, but also the OM in the sediments. This may in particular account for the t-type kettle holes with enhanced aerobic mineralization during desiccation of the sediment and temperature increase (Fierer and Schimel, 2002; Johnson et al., 2004; Boon, 2006). The progressing aeration and increasing mineralization in the sediment from the edge to the center during water level dropdown can also release significant amounts of CO_2 from sediments from sp-type kettle holes.

Furthermore, anoxic conditions are likely to occur in some kettle holes, especially the sp-type kettle holes with the permanent water columns throughout the year. As such, anoxic and suboxic conditions were identified for the Ri kettle hole from May to September during the bloom of the duckweed (*Spirodela polyrhiza*) (Kleeberg et al., 2016b) exhausting the O_2 in the water column (Scheffer et al., 2003). This may lead to production of CH_4 and N_2O in the water column. As such, high CH_4 production was found for the open water and the reed belt consisting of emergent macrophytes for both the Kr and Ri kettle hole from May to September 2013 measured on a monthly basis by a greenhouse gas analyzer (ABB – Los Gatos Research, San Jose, CA, USA) (Fig. 6.4) (C. Lisbôa, unpublished; see also Kazanjian et al., submitted). Given the already low O_2 contents in the water column and the high TOC contents of deeper sediments with the abundance of peat (Table A3), anoxic conditions are likely to occur in the sediments (A. Kleeberg, personal communication). These anoxic conditions prevent OM in sediments from mineralization (Isidorova et al., 2016). Furthermore, CH_4 can also be formed in the sediment columns (Sobek et al., 2012), especially in those of the sp-type kettle holes.

Longer waterlogging periods in the t-type kettle holes could also favor formation of CH_4 in these kettle hole types. This suggestion is in agreement with my experiences during the sediment sampling in July/August 2013 when I observed the release of bubbles from sediment cores and even from the water column from some t-type kettle holes, while I walked through the kettle holes. Consequently, kettle holes are on the one hand important GHG sources in the landscape (Merbach et al., 2002; Richter, 2014), but may also store large amounts of OM from emergent macrophytes in their deeper sediments via anaerobic stabilization. This hypothesis contributes to the general idea that aquatic inland water bodies simultaneously act as both OC sinks and CH_4 sources (Sobek et al., 2012) and we are under pressure to keep this OC in the sediments with respect to the global climate change.

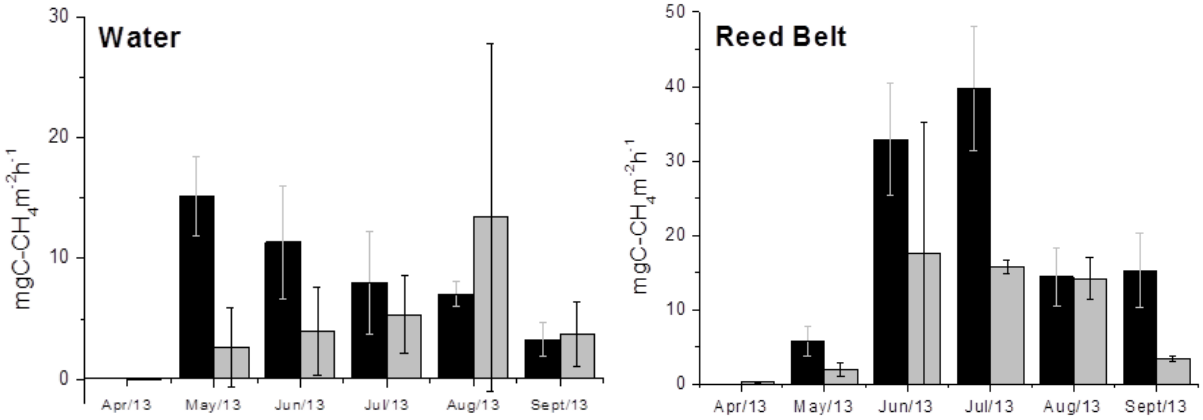

Fig. 6.4. Methane production in the semi-permanently water-filled Rittgarten (black bars) and Kraatz (grey bars) kettle holes for the open water (left) and the reed belt (right) from April to September 2013 (data from C. Lisbôa, unpublished).

In addition to anaerobic stabilization, the transect study (chapter 4) provided evidence for stabilization of OM via mineral association and the terrestrial origin of the OM in these associations. Since the physio-chemical fractionation was only performed for sediments from the Kr kettle hole and only for the sediment horizon 2 to 7 cm, the following discussion on the importance of OM-mineral associations in kettle hole sediments mostly related to that particular system. Even though the kettle hole assessed is largely representative for the whole landscape, generalizations need to be made with caution. The input of clay- and silt-sized particles via erosion into the Kr kettle hole makes soil transport also likely into other arable kettle holes (Frielinghaus and Vahrson, 1998; Kalettka and Rudat, 2006; Kleeberg et al., 2016a). However, we have to keep in mind that the Kr kettle hole had a relatively steep catchment compared to other kettle holes based on my field observations making the degree of soil input into kettle holes highly variable over the landscape. Nevertheless, the doubling in sedimentation rates for the Ri kettle hole and even a fivefold increase for Kr kettle hole after 1983 (Kleeberg et al., 2016a) due to the intensification of agricultural practices (Bayerl, 2006)

could indicate a progressing importance of soil erosion into kettle holes and thus increase the significance of OM-mineral associations in future times.

Given the proposed high contribution of OM from emergent macrophytes to the sediment (Flury et al., in revision) and the overall high internal GPP (Kazanjian et al., submitted), it is also possible that OM from emergent macrophytes partly contributed to the OM in mineral-associated OM fractions. For instance, OM from emergent macrophytes could be part of OM_{ER} via anaerobically stabilization as indicated by the three times higher OC contents compared to OM_{ER} from soils. Furthermore, autochthonous OM could attach to the existing Fe phases in the water column and sediment forming clusters as it was shown for a Luvisol by Vogel et al. (2014). On the other hand, anoxic conditions in the kettle hole may cause the microbially mediated reduction of Fe(III) in poorly crystalline and well-crystallized Fe phases into Fe(II) and liberate the associated terrestrial OM (Weber et al., 2006). Whether significant amounts of terrestrial born OM are still part of the OM-mineral associations in kettle holes need to be shown by techniques that aim for assessing the molecular structure of the OM such as solid-state ^{13}C nuclear magnetic resonance (NMR) spectroscopy (Deshmukh et al., 2001; Sanderman et al., 2015).

Given the different periods of aeration between sp-type and t-type kettle holes, the pathway and magnitude of OM-mineral association could also vary between kettle holes of different hydroperiod. As such, Lalonde et al. (2012) suggested OM to be stabilized via organically-complexed Fe forming chelates with high C:Fe ratios > 7 under anoxic conditions, which tended to be stable against anaerobic degradation, a binding mechanism also likely in the anoxic sp-type kettle holes sediments. Fe can also be mobilized from the sediment when it is present in its reduced form in the absence of O_2 (Campbell and Torgersen, 1980; Davison, 1993). As such, Fe concentrations could be lower in sp-type kettle hole sediments. Consequently, Fe concentrations could not only be higher in sediments from t-type kettle holes, but the oxidation of Fe(II) to Fe(III) is accompanied with an increase in poorly crystalline and well-crystallized Fe phases, which are able to bind OM (Davison, 1993; Rue and Bruland, 1995). Whether the mobilization of Fe from the sediment is a process at work in the kettle holes assessed in my thesis remains unclear given that Fe should be associated with OM (Lalonde et al., 2012). Furthermore, we have to keep in mind that Fe is not only able to bind OM, but also P (Søndergaard et al., 2003) and S (Kleeberg et al., 2013). Kleeberg et al. (2016b) found high evidence for P binding via Fe(OOH) associations and for S binding via FeS_x in the Kr kettle hole providing less Fe available for the formation of OM-Fe associations. Nevertheless, P and S binding via Fe is regarded only to account for small proportions of Fe since most of the Fe is associated via OM (Lalonde et al., 2012; Kleeberg et al., 2013).

I further suggested the stabilization of OM directly via Ca^{2+} or Ca^{2+} with clay sized Al-silicates interactions for the Kr kettle hole, which seems also likely for the other kettle holes.

With respect to Ca^{2+}, we also have to keep in mind that Ca^{2+} can form $CaCO_3$ and biogenic apatite ($Ca_5(PO_4)_3$-OH) at neutral pH values making Ca^{2+} inaccessible to stabilize OM, a phenomenon suggested for Ri (Kleeberg et al., 2016b).

Since I expected many kettle holes to be in contact with the groundwater table over the year, a transport of cations out of the kettle hole may represent an important loss of cations need for the formation of OM-mineral associations. Berthold et al. (2004) and Heagle et al. (2013) found lateral groundwater recharge to be important for the leaching of salts in Canadian prairie wetlands, which accumulated under the adjacent uplands, e.g. as gypsum. The loss of cations might be of particular importance for t-type kettle holes, which I assumed to be in a stronger contact with groundwater. In turn, groundwater discharge into kettle holes may supply cations during winter and spring refilling. Therefore, the individual connection to the groundwater body could considerably drive the amount of cations as basis for OM-mineral interaction. Similar to OM-mineral associations in soils, the magnitude of OM-mineral association in sediments can also largely depend on the soil types and the exposure of the glacial tills from the caRG and clay-rich Bt horizons from the eLV.

With respect to forest kettle holes, the contribution of beech litter was ubiquitous to surface sediments, but the low $\delta^{15}N$ did not persist in deeper sediments pointing to a fast turnover of the litter in the surface sediments. Tree litter is usually quickly processed in forested streams and lakes and supports heterotrophic respiration and consequently represents an important allochthonous C and N source into the water column (Rubbo et al., 2006; Kreutzweiser et al., 2008). Since I also found indications for anoxic conditions in forest kettle holes via the high TOC contents (Table A3) favoring anaerobic microbial decomposition, I hypothesize these kettle holes as possible GHG sources in the landscape. Given the low evaporation and the stable boundary layer within forests, I suspect many forest kettle holes to stay under anoxic conditions throughout the year. Thus and together with the tree litter input, forest kettle holes have high potentials for storing OM in their sediments. In contrast to arable and grassland kettle holes, forest kettle holes did not comprise of a typical vegetation belt consisting of emergent macrophytes like *Phragmites australis* or *Phalaris arundinacea*. However, I often found other emergent macrophytes such as *Sparganium erectum* in the center of these kettle holes, which represent an additional allochthonous OM source to the sediments. The role of periphytic algae and phytoplankton remains not fully clear, but given the low C:N ratios of surface sediments, makes an algae contribution likely to an unknown extent.

7. Conclusion and outlook

My PhD thesis has demonstrated that the mechanisms driving C and N dynamics in moraine agricultural landscapes vary greatly across the investigated scale: from the aggregate to landscape level, where stable isotopes are powerful tools to identify these mechanisms. I could show that heterogeneities exist for the OM stabilization mechanisms and contents across a typical geomorphic toposequence, and that those patterns were not visible at the regional landscape scale. However, isoscapes allowed for capturing climatic impacts, land-use differences and impacts of land-management activities on the C and N dynamics. As such, small-scale spatial heterogeneities on single fields and landscape diversities are essential to understand C and N dynamics at the regional landscape scale (Premke et al., 2016). Ultimately, capturing the dynamics across scales is indispensable for the development of better policies on protecting SOC stocks and ensuring the sustainable use of agricultural soils (O'Rourke et al., 2015).

My study could show that kettle holes can function as C and N sinks for emergent macrophyte-derived OM in the landscape independently from the hydroperiod. Since I also found strong indications for both aerobic and anaerobic microbial decomposition promoting GHG emissions, the question whether kettle holes as small inland water bodies act as net C and N sinks in the landscape remains open (Sobek et al., 2012; Chmiel et al., 2016). Though kettle holes were regarded as being tightly coupled with their surrounding catchments in terms of sinks for nutrients and soils (Frielinghaus and Vahrson, 1998; Lischeid and Kalettka, 2012), allochthonous OM from emergent macrophytes and autochthonous OM from floating and submerged macrophytes and algae seemed to surpass OM inputs via soil particles and plants from their catchments. Nevertheless, soil input via erosion is of high importance for the formation of OM-mineral associations as OM stabilization mechanism in addition to anaerobic stabilization and increasing burial rates. These associations can be of higher significance in means of the global climate change, i.e. when drought events favor aerobic microbial decomposition of labile, easy microbially available OM (Reverey et al., 2016). I conclude that kettle holes as small inland water bodies in moraine landscapes are crucial to be included when assessing C and N dynamics at the landscape scale (Cole et al., 2007; Downing et al., 2008) given on the one hand their high potential of OM storage in their sediments and their impact on the environmental conditions in their catchments, and on the other hand their function as potential GHG sources.

On a long term, the continuous exposure of glacial till will serve as inorganic C source into the landscape and will reduce soil fertility and therefore plant growth on steep slopes. However, the relocation of organic particles, and small mineral particles and aggregates directly associated with OM or serving as the basis for the formation of OM-mineral associations, will allow for more burial of OM in colluvic soils (Berhe et al., 2012; Hu et al.,

2016). The ongoing climate change can further induce drought and extreme rainfall events altering the C and N dynamics of the landscape e.g. via reduced plant productivity or accelerated soils erosion.

Future studies may focus on GHG emissions from soils in the catchment of kettle holes to test whether the environmental and erosional gradients reflected in by the OM fractions are expressed in GHG emissions. Furthermore, studies should encompass soils from the shoreline as they represent aquatic-terrestrial transitions zones due to fluctuating water levels and need to be regarded as hotspots for C and N turnover (Merbach et al., 2002; Hefting et al., 2013; Richter, 2014). Since I explored the pathways of OM stabilization in one sediment horizon of an agricultural kettle hole only, research is necessary on the OM-mineral associations of a larger set of sediments from kettle holes of different land-use, management intensity and hydroperiod to account for spatial heterogeneities. On a landscape perspective, it should be tested whether topographic pattern will be visible in stable isotope ratios of single fields. All these further attempts may help to even better understand C and N dynamics in moraine agricultural landscapes and the role of kettle holes as C and N sinks or sources in the landscape.

Acknowledgements

First of all, my biggest thanks go to Dr. Zachary Kayler for all the support during the last years! I definitively could not have written this thesis without you! Thank you for sharing your knowledge on isotope geochemistry with me, which inspired me to keep on working as an isotope geochemist, and for improving my scientific skills. I enjoyed working with you and I hope we can collaborate sometime again.

Further big thanks go to my supervisor Dr. Arthur Gessler from the WSL in Switzerland. I am thankful for all the support and your valuable comments on the manuscripts, which really helped to improve them. After talking to you, I always felt highly motivated in keeping on writing.

I also want to express my gratitude to my other two reviewers Prof. Dr. Jutta Zeitz from the Humboldt-Universität zu Berlin and PD Dr. Michael Zech from the Technische Universität Dresden. I really appreciate that you were reviewing this thesis.

I am very grateful to Dr. Katrin Premke from the IGB, Berlin, for all the helpful discussions and keeping me motivated all the time. Thank you for all the financial support for my stays abroad.

Further thanks go to the LandScales team for the opportunity of presenting my work during our meetings and the fruitful discussions, and especially to Carsten Hoffmann for his help on the soil science and to Andreas Kleeberg for his help on sediments.

Special thanks to Dr. Rota Wagai from the NIAES in Tsukuba, Japan. I am really happy for the opportunity of being a visiting scientist at your institute and I am looking forward for further collaboration.

I am also very thankful to Dr. Ulrike Hagemann for all the support and as contact person for all the small things a PhD student has to cope with, and Ines Mann for all the organizational support, both from the Institute of Landscape Biogeochemistry of ZALF.

I am thankful to Thomas Wagner, Ruben Yague, Susanne Remus who helped me with the preparation of my thousands of samples, and Susanne Remus and Dr. Sara Herrero Martín for the isotope measurements during my absence when I was in Japan.

Special thanks go to my handball team, the supergeile NARVA IV, especially to Philipp Meinert, Falko Gill und Bruno Steinmetz. The sport and all the fun with you were a welcome distraction.

Thanks to Isabell von Rein, my office mate and very good friend, for all the funny conversations and being a fellow-sufferer in terms of writing a PhD thesis.

I like to thank my flat mate and very good friend Thomas Lopp for the common time and the beers that we had together while watching football and hanging around in Berlin, which greatly helped to distract me from this thesis.

I also want to thank my parents and my brother for all the support during the last years.

Watashi no Ryoko :-) Finally, I want to thank you. Thank you for always being there for me and believing into me. You are my inspiration and my motivation. I cannot wait for next year anymore. Dai suki

References

Abtew W. and Melesse A. (2012) Lake Evaporation. In *Evaporation and Evapotranspiration* (eds. W. Abtew and A. Melesse). Springer, Amsterdam. pp. 109–132.

Aldana Jague E., Sommer M., Saby N. P. A., Cornelis J. T., Van Wesemael B. and Van Oost K. (2016) High resolution characterization of the soil organic carbon depth profile in a soil landscape affected by erosion. *Soil Tillage Res.* **156**, 185–193.

Alewell C., Schaub M. and Conen F. (2009) A method to detect soil carbon degradation during soil erosion. *Biogeosciences* **6**, 2541–2547.

Almendinger J. E. and Leete J. H. (1998) Peat characteristics and groundwater geochemistry of calcareous fens in the Minnesota River Basin , U.S.A. *Biogeochemistry* **43**, 17–41.

Amelung W. and Zech W. (1999) Minimisation of organic matter disruption during particle-size fractionation of grassland epipedons. *Geoderma* **92**, 73–85.

Amundson R., Austin A. T., Schuur E. A. G., Yoo K., Matzek V., Kendall C., Uebersax A., Brenner D. and Baisden W. T. (2003) Global patterns of the isotopic composition of soil and plant nitrogen. *Global Biogeochem. Cycles* **17**, 1031.

Andrews J. E., Greenaway A. M. and Dennis P. F. (1998) Combined carbon isotope and C/N ratios as indicators of source and fate of organic matter in a poorly flushed, tropical estuary: Hunts Bay, Kingston Harbour, Jamaica. *Estuar. Coast. Shelf Sci.* **46**, 743–756.

Arnarson T. S. and Keil R. G. (2007) Changes in organic matter-mineral interactions for marine sediments with varying oxygen exposure times. *Geochim. Cosmochim. Acta* **71**, 3545–3556.

Asano M. and Wagai R. (2014) Distinctive organic matter pools among particle-size fractions detected by solid-state 13C-NMR, δ13C and δ15N analyses only after strong dispersion in an allophanic Andisol. *Soil Sci. Plant Nutr.* **61**, 242–248.

Attermeyer K., Grossart H. P., Flury S. and Premke K. Bacterial processes and biogeochemical changes in the water body of kettle holes - mainly driven by autochthonous organic matter? *Aquat. Sci.*, in press.

Aufdenkampe A. K., Mayorga E., Raymond P. A., Melack J. M., Doney S. C., Alin S. R., Aalto R. E. and Yoo K. (2011) Riverine coupling of biogeochemical cycles between land, oceans, and atmosphere. *Front. Ecol. Environ.* **9**, 53–60.

Bachmann J., Guggenberger G., Baumgartl T., Ellerbrock R. H., Urbanek E., Goebel M.-O., Kaiser K., Horn R. and Fischer W. R. (2008) Physical carbon-sequestration mechanisms under special consideration of soil wettability. *J. Plant Nutr. Soil Sci.* **171**, 14–26.

Badrian M. (2015) Hydrobiogeochemische Untersuchungen an Söllen. Beuth University of Applied Sciences.

Bai E., Boutton T. W., Liu F., Ben Wu X. and Archer S. R. (2013) 15N isoscapes in a subtropical savanna parkland : spatial-temporal perspectives. *Ecosphere* **4**, (1):4.

Balesdent J. (1996) The significance of organic separates to carbon dynamics and its modelling in some cultivated soils. *Eur. J. Agron.* **47**, 485–493.

Balesdent J., Besnard E., Arrouays D. and Chenu C. (1998) The dynamics of carbon in particle-size fractions of soil in a forest-cultivation sequence. *Plant Soil* **201**, 49–57.

Barnes C. J. and Allison G. B. (1988) Tracing of water movement in the unsaturated zone using stable isotopes of hydrogen and oxygen. *J. Hydrol.* **100**, 143–176.

Bateman A. S., Kelly S. D. and Jickells T. D. (2005) Nitrogen isotope relationships between crops and fertilizer: implications for using nitrogen isotope analysis as an indicator of agricultural regime. *J. Agric. Food Chem.* **53**, 5760–5765.

Bauhus J., Paré D. and Côté L. (1998) Effects of tree species, stand age and soil type on soil microbial biomass and its activity in a southern boreal forest. *Soil Biol. Biochem.* **30**, 1077–1089.

Bayerl G. (2006) *Geschichte der Landnutzung in der Region Barnim-Uckermark*. ed. B.-B. A. der Wissenschaften, Materialien der Interdisziplinären Arbeitsgruppe Zukunftsorientierte Nutzung ländlicher Räume – Land Innovation Nr. 12., Berlin., Berlin.

Bellanger B., Huon S., Velasquez F., Vallès V., Girardin C. and Mariotti A. (2004) Monitoring soil organic carbon erosion with δ13C and δ15N on experimental field plots in the Venezuelan Andes. *Catena* **58**, 125–150.

Beniston J. W., Shipitalo M. J., Lal R., Dayton E. A., Hopkins D. W., Jones F., Joynes A. and Dungait J. A. J. (2015) Carbon and macronutrient losses during accelerated erosion under different tillage and residue management. *Eur. J. Soil Sci.* **66**, 218–225.

Berggren M., Ström L., Laudon H., Karlsson J., Jonsson A., Giesler R., Bergström A. K. and Jansson M. (2010) Lake secondary production fueled by rapid transfer of low molecular weight organic carbon from terrestrial sources to aquatic consumers. *Ecol. Lett.* **13**, 870–880.

Berhe A. A. (2012) Decomposition of organic substrates at eroding vs. depositional landform positions. *Plant Soil* **350**, 261–280.

Berhe A. A., Harden J. W., Torn M. S. and Harte J. (2008) Linking soil organic matter dynamics and erosion-induced terrestrial carbon sequestration at different landform positions. *J. Geophys. Res. Biogeosciences* **113**, G04039.
Berhe A. A., Harden J. W., Torn M. S., Kleber M., Burton S. D. and Harte J. (2012) Persistence of soil organic matter in eroding versus depositional landform positions. *J. Geophys. Res. Biogeosciences* **117**, G02019.
Berhe A. A., Harte J., Harden J. W. and Torn M. S. (2007) The significance of the erosion-induced terrestrial carbon sink. *Bioscience* **57**, 337–346.
Berthold S., Bentley L. R. and Hayashi M. (2004) Integrated hydrogeological and geophysical study of depression-focused groundwater recharge in the Canadian prairies. *Water Resour. Res.* **40**, W06505.
Billings S. and Gaydess E. (2008) Soil nitrogen and carbon dynamics in a fragmented landscape experiencing forest succession. *Landsc. Ecol.* **23**, 581–593.
Bird J. A., Kleber M. and Torn M. S. (2008) 13C and 15N stabilization dynamics in soil organic matter fractions during needle and fine root decomposition. *Org. Geochem.* **39**, 465–477.
Blanco-Canqui H. and Lal R. (2007) Soil structure and organic carbon relationships following 10 years of wheat straw management in no-till. *Soil Tillage Res.* **95**, 240–254.
Blum A. (2005) Drought resistance, water-use efficiency, and yield potential—are they compatible, dissonant, or mutually exclusive? *Aust. J. Agric. Res.* **56**, 1159–1168.
Boon P. I. (2006) Biogeochemistry and bacterial ecology of hydrologically dynamic wetlands. In *Ecology of Freshwater and Estuarine Wetlands* (eds. D. P. Batzer and R. R. Sharitz). University of California Press, Berkeley. pp. 115–176.
Bowen G. J. (2010) Isoscapes: Spatial Pattern in Isotopic Biogeochemistry. *Annu. Rev. Earth Planet. Sci.* **38**, 161–187.
Bremner J. M., Heintze S. G., Mann P. J. G. and Lees H. (1946) Metallo-organic complexes in Soil. *Nature* **158**, 790–791.
Bremner J. M. and Lees H. (1949) Studies on soil organic matter: Part II. The extraction of organic matter from soil by neutral reagents. *J. Agric. Sci.* **39**, 274–279.
Brooks J. R., Wigington P. J., Phillips D. L., Comeleo R. and Coulombe R. (2012) Willamette River Basin surface water isoscape (δ18O and δ2H): temporal changes of source water within the river. *Ecosphere* **3**, (5):39.
Brüggemann N., Gessler A., Kayler Z., Keel S. G., Badeck F., Barthel M., Boeckx P., Buchmann N., Brugnoli E., Esperschütz J., Gavrichkova O., Ghashghaie J., Gomez-Casanovas N., Keitel C., Knohl A., Kuptz D., Palacio S., Salmon Y., Uchida Y. and Bahn M. (2011) Carbon allocation and carbon isotope fluxes in the plant-soil-atmosphere continuum: a review. *Biogeosciences* **8**, 3457–3489.
Buffam I., Turner M. G., Desai A. R., Hanson P. C., Rusak J. A., Lottig N. R., Stanley E. H. and Carpenter S. R. (2011) Integrating aquatic and terrestrial components to construct a complete carbon budget for a north temperate lake district. *Glob. Chang. Biol.* **17**, 1193–1211.
Campbell P. and Torgersen T. (1980) Maintenance of iron meromixis by iron redeposition in a rapidly flushed monimolimnion. *Can. J. Fish. Aquat. Sci.* **37**, 1303–1313.
Casciotti K. L., Sigman D. M. and Ward B. B. (2003) Linking diversity and stable isotope fractionation in ammonia-oxidizing bacteria. *Geomicrobiol. J.* **20**, 335–353.
Cheng S.-L., Fang H.-J., Yu G.-R., Zhu T.-H. and Zheng J.-J. (2010) Foliar and soil 15N natural abundances provide field evidence on nitrogen dynamics in temperate and boreal forest ecosystems. *Plant Soil* **337**, 285–297.
Cheraghi M., Lorestani B. and Merrikhpour H. (2012) Investigation of the effects of phosphate fertilizer application on the heavy metal content in agricultural soils with different cultivation patterns. *Biol. Trace Elem. Res.* **145**, 87–92.
Chmiel H. E., Kokic J., Denfeld B. A., Einarsdóttir K., Wallin M. B., Koehler B., Isidorova A., Bastviken D., Ferland M.-È. and Sobek S. (2016) The role of sediments in the carbon budget of a small boreal lake. *Limnol. Oceanogr.* **61**, 1814–1825.
Choi W.-J., Ro H.-M. and Hobbie E. A. (2003) Patterns of natural 15N in soils and plants from chemically and organically fertilized uplands. *Soil Biol. Biochem.* **35**, 1493–1500.
Choi W. J., Arshad M. a., Chang S. X. and Kim T. H. (2006) Grain 15N of crops applied with organic and chemical fertilizers in a four-year rotation. *Plant Soil* **284**, 165–174.
Clark I. and Fritz P. (1997) *Environmental Isotopes in Hydrogeology*., CRC Press, Boca Raton, Florida.
Cohen A. S. (2003) *Paleolimnology: the history and evolution of lake systems*., Oxford University Press, New York.
Cole J. J., Carpenter S. R., Pace M. L., Van De Bogert M. C., Kitchell J. L. and Hodgson J. R. (2006)

Differential support of lake food webs by three types of terrestrial organic carbon. *Ecol. Lett.* **9**, 558–568.
Cole J. J., Prairie Y. T., Caraco N. F., Mcdowell W. H., Tranvik L. J., Striegl R. G., Duarte C. M., Kortelainen P., Downing J. A., Middelburg J. J. and Melack J. (2007) Plumbing the Global Carbon Cycle: Integrating Inland Waters into the Terrestrial Carbon Budget. *Ecosystems* **10**, 171–184.
Colombo C., Palumbo G., He J. Z., Pinton R. and Cesco S. (2014) Review on iron availability in soil: Interaction of Fe minerals, plants, and microbes. *J. Soils Sediments* **14**, 538–548.
Conrad O., Bechtel B., Bock M., Dietrich H., Fischer E., Gerlitz L., Wehberg J., Wichmann V. and Böhner J. (2015) System for Automated Geoscientific Analyses (SAGA) v. 2.1.4. *Geosci. Model Dev.* **8**, 1991–2007. Available at: http://www.geosci-model-dev.net/8/1991/2015/gmd-8-1991-2015.html.
Constantin J., Beaudoin N., Laurent F., Cohan J. P., Duyme F. and Mary B. (2011) Cumulative effects of catch crops on nitrogen uptake, leaching and net mineralization. *Plant Soil* **341**, 137–154.
Côté L., Brown S., Paré D., Fyles J. and Bauhus J. (2000) Dynamics of carbon and nitrogen mineralization in relation to stand type , stand age and soil texture in the boreal mixedwood. *Soil Biol. Biochem.* **32**, 1079–1090.
Craig H. (1961) Isotopic variations in meteoric waters. *Science (80-.).* **133**, 1702–1703.
Craig H. and Gordon L. I. (1965) Deuterium and oxygen 18 variations in the ocean and the marine atmosphere. In *Proceedings of a Conference on Stable Isotopes in Oceanographic Studies and Palaeotemperatures, Spoleto, Italy* (ed. E. Tongiorgi). Lischi and Figli, Pisa. pp. 9–130.
Craine J. M., Elmore A. J., Wang L., Augusto L., Baisden W. T., Brookshire E. N. J., Cramer M. D., Hasselquist N. J., Hobbie E. A., Kahmen A., Koba K., Kranabetter J. M., Mack M. C., Marin-Spiotta E., Mayor J. R., McLauchlan K. K., Michelsen A., Nardoto G. B., Oliveira R. S., Perakis S. S., Peri P. L., Quesada C. A., Richter A., Schipper L. A., Stevenson B. A., Turner B. L., Viani R. A. G., Wanek W. and Zeller B. (2015) Convergence of soil nitrogen isotopes across global climate gradients. *Sci. Rep.* **5**, 8280.
Dansgaard W. (1964) Stable isotopes in precipitation. *Tellus* **4**, 436–468.
Davidson A. M., Jennions M. and Nicotra A. B. (2012) Do invasive species show higher phenotypic plasticity than native species and, if so, is it adaptive? A meta-analysis. *Ecol. Lett.* **14**, 419–431.
Davison W. (1993) Iron and manganese in lakes. *Earth-Science Rev.* **34**, 119–163.
DeFries R. S., Foley J. A. and Asner G. P. (2004) Land-use choices: balancing human needs and ecosystem function. *Front. Ecol. Environ.* **2**, 249–257.
Deshmukh A. P., Chefetz B. and Hatcher P. G. (2001) Characterization of organic matter in pristine and contaminated coastal marine sediments using solid-state C-13 NMR, pyrolytic and thermochemolytic methods: A case study in the San Diego harbor area. *Chemosphere* **45**, 1007–1022.
Deumlich D., Schmidt R. and Sommer M. (2010) A multiscale soil-landform relationship in the glacial-drift area based on digital terrain analysis and soil attributes. *J. Plant Nutr. Soil Sci.* **173**, 843–851.
Dijkstra P., LaViolette C. M., Coyle J. S., Doucett R. R., Schwartz E., Hart S. C. and Hungate B. A. (2008) 15N enrichment as an integrator of the effects of C and N on microbial metabolism and ecosystem function. *Ecol. Lett.* **11**, 389–397.
DIN 19684-6 (1997) Methods of soil investigations for agricultural engineering - Chemical laboratory tests - Part 6: Determination of iron soluble in oxalate solution. In Beuth Verlag, Berlin.
DIN ISO 10390 (1997) Soil quality - Determination of pH (ISO 10390:2005). In Beuth Verlag, Berlin.
DIN ISO 10694 (1995) Soil quality - Determination of organic and total carbon after dry combustion (elementary analysis). In Beuth Verlag, Berlin.
DIN ISO 11260 (1994) Soil quality - Determination of effective cation exchange capacity and base saturation level using barium chloride solution (ISO 11260:2011). In Beuth Verlag, Berlin.
DIN ISO 11277 (2002) Soil quality - Determination of particle size distribution in mineral soil material - Method by sieving and sedimentation (ISO 11277:2009). In Beuth Verlag, Berlin.
Doetterl S., Berhe A. A., Nadeu E., Wang Z., Sommer M. and Fiener P. (2016) Erosion, deposition and soil carbon: A review of process-level controls, experimental tools and models to address C cycling in dynamic landscapes. *Earth-Science Rev.* **154**, 102–122.
Doetterl S., Cornelis J. T., Six J., Bodé S., Opfergelt S., Boeckx P. and Van Oost K. (2015) Soil redistribution and weathering controlling the fate of geochemical and physical carbon stabilization mechanisms in soils of an eroding landscape. *Biogeosciences* **12**, 1357–1371.
Doetterl S., Six J., Van Wesemael B. and Van Oost K. (2012) Carbon cycling in eroding landscapes: Geomorphic controls on soil organic C pool composition and C stabilization. *Glob. Chang. Biol.* **18**, 2218–2232.

Dogramaci S., Firmani G., Hedley P., Skrzypek G. and Grierson P. F. (2015) Evaluating recharge to an ephemeral dryland stream using a hydraulic model and water, chloride and isotope mass balance. *J. Hydrol.* **521**, 520–532.
Downing J. A., Cole J. J., Middelburg J. J., Striegl R. G., Duarte C. M., Kortelainen P., Prairie Y. T. and Laube K. A. (2008) Sediment organic carbon burial in agriculturally eutrophic impoundments over the last century. *Global Biogeochem. Cycles* **22**, GB1018.
Dungait J. A. J., Ghee C., Rowan J. S., McKenzie B. M., Hawes C., Dixon E. R., Paterson E. and Hopkins D. W. (2013) Microbial responses to the erosional redistribution of soil organic carbon in arable fields. *Soil Biol. Biochem.* **60**, 195–201.
Ehleringer J. R., Bowen G. J., Chesson L. A., West A. G., Podlesak D. W. and Cerling T. E. (2008) Hydrogen and oxygen isotope ratios in human hair are related to geography. *Proc. Natl. Acad. Sci.* **105**, 2788–2793.
Ellerbrock R. H., Gerke H. H. and Deumlich D. (2016) Soil organic matter composition along a slope in an erosion-affected arable landscape in North East Germany. *Soil Tillage Res.* **156**, 209–218.
Emerson W. W. (1995) Water-retention, organic-C and soil texture. *Aust. J. Soil Res.* **33**, 241–251.
Esmeijer-Liu A. J., Kürschner W. M., Lotter A. F., Verhoeven J. T. A. and Goslar T. (2012) Stable carbon and nitrogen isotopes in a peat profile are influenced by early stage diagenesis and changes in atmospheric CO2 and N Deposition. *Water. Air. Soil Pollut.* **223**, 2007–2022.
Euliss N. H., LaBaugh J. W., Fredrickson L. H., Mushet D. M., Laubhan M. K., Swanson G. A., Winter T. C., Rosenberry D. O. and Nelson R. D. (2004) The wetland continuum: a conceptual framework for interpreting biological studies. *Wetlands* **24**, 448–458.
Evans R. D. (2001) Physiological mechanisms influencing plant nitrogen isotope composition. *Trends Plant Sci.* **6**, 121–126.
Fang H., Yu G., Cheng S., Zhu T., Zheng J., Mo J., Yan J. and Luo Y. (2010) Nitrogen-15 signals of leaf-litter-soil continuum as a possible indicator of ecosystem nitrogen saturation by forest succession and N loads. *Biogeochemistry* **102**, 251–263.
FAO (2015) Global Forest Resources Assessment 2015. In *FAO Forestry Paper No. 1* UN Food and Agriculture Organization, Rome.
FAO (2014) World reference base for soil resources 2014. In *World Soil Resources Reports 106* UN Food and Agriculture Organization, Rome.
Farquhar G. D., Ehleringer J. R. and Hubick K. (1989) Carbon isotope discrimination and photosynthesis. *Annu. Rev. Plant Physiol. Plant Mol. Biol.* **40**, 503–537.
Farquhar G. D. and Richards R. A. (1984) Isotopic composition of plant carbon correlates with water-use efficiency of wheat genotypes. *Aust. J. Plant Physiol.* **11**, 539–552.
Farquhar G., O'Leary M. and Berry J. (1982) On the relationship between carbon isotope discrimination and the intercellular carbon dioxide concentration in leaves. *Aust. J. Plant Physiol.* **9**, 121–137.
Farrar J., Hawes M., Jones D. and Lindow S. (2003) How roots control the flux of carbon to the rhizosphere. *Ecology* **84**, 827–837.
Ferone J. M. and Devito K. J. (2004) Shallow groundwater-surface water interactions in pond-peatland complexes along a Boreal Plains topographic gradient. *J. Hydrol.* **292**, 75–95.
Fierer N. and Schimel J. P. (2002) Effects of drying-rewetting frequency on soil carbon and nitrogen transformations. *Soil Biol. Biochem.* **34**, 777–787.
Fissore C., Dalzell B. J., Berhe A. A., Voegtle M., Evans M. and Wu A. (2017) Influence of topography on soil organic carbon dynamics in a Southern California grassland. *Catena* **149**, 140–149.
Flury S., Attermeyer K., Kazanjian G., Zlatanovic S., Grossart H.-P., Hilt S., Casper P. and Premke K. Benthic microbial mineralization and organic carbon uptake in kettle holes: lignin-poor organic carbon as a major driver. *Ecosystems*, in revision.
Foley J. A., Defries R., Asner G. P., Barford C., Bonan G., Carpenter S. R., Chapin F. S., Coe M. T., Daily G. C., Gibbs H. K., Helkowski J. H., Holloway T., Howard E. A., Kucharik C. J., Monfreda C., Patz J. A., Prentice I. C., Ramankutty N. and Snyder P. K. (2005) Global consequences of land use. *Science (80-.).* **309**, 570–574.
Foulquier A., Volat B., Neyra M., Bornette G. and Montuelle B. (2013) Long-term impact of hydrological regime on structure and functions of microbial communities in riverine wetland sediments. *Microb. Ecol.* **85**, 211–226.
Fox J. F. and Papanicolaou A. N. (2007) The use of carbon and nitrogen isotopes to study watershed erosion processes. *J. Am. Water Resour. Assoc.* **43**, 1047–1064.
Frank D. A. and Evans R. D. (1997) Effects of Native Grazers on Grassland N Cycling in Yellowstone National Park. *Ecology* **78**, 2238–2248.
Frielinghaus M. and Vahrson W.-G. (1998) Soil translocation by water erosion from agricultural cropland into wet depressions (morainic kettle holes). *Soil Tillage Res.* **46**, 23–30.

Fromin N., Pinay G., Montuelle B., Landais D., Ourcival C. M., Joffre R. and Lensi R. (2010) Impact of seasonal sediment desiccation and rewetting on microbial processes involved in greenhouse gas emissions. *Ecohydrology* **3**, 339–348.
Fry B. (2006) *Stable Isotope Ecology*., Springer, New York.
Garnier E. and Navas M.-L. (2011) A trait-based approach to comparative functional plant ecology: concepts, methods and applications for agroecology. A review. *Agron. Sustain. Dev.* **32**, 365–399.
Gat J. R. (1996) Oxygen and hydrogen isotopes in the hydrologic cycle. *Annu. Rev. Earth Planet. Sci.* **24**, 225–262.
Gaudig G., Couwenberg J. and Joosten H. (2006) Peat accumulation in kettle holes: bottom up or top down ? *Mires Peat* **1**, Article 06, http://www.mires-and-net/, ISSN 1.
Gerke H. H. and Hierold W. (2012) Vertical bulk density distribution in C-horizons from marley till as indicator for erosion history in a hummocky post-glacial soil landscape. *Soil Tillage Res.* **125**, 116–122.
Gerke H. H., Koszinski S., Kalettka T. and Sommer M. (2010) Structures and hydrologic function of soil landscapes with kettle holes using an integrated hydropedological approach. *J. Hydrol.* **393**, 123–132.
Gerke H. H., Rieckh H. and Sommer M. (2016) Interactions between crop, water, and dissolved organic and inorganic carbon in a hummocky landscape with erosion-affected pedogenesis. *Soil Tillage Res.* **156**, 230–244.
Gibson J. J., Birks S. J. and Edwards T. W. D. (2008) Global prediction of δA and δ2H- δ18O evaporation slopes for lakes and soil water accounting for seasonality. *Global Biogeochem. Cycles* **22**, GB2031.
Gibson J. J. and Edwards T. W. D. (2002) Regional water balance trends and evaporation-transpiration partitioning from a stable isotope survey of lakes in northern Canada. *Global Biogeochem. Cycles* **16**, 1026.
Gibson J. J., Edwards T. W. D., Birks S. J., St Amour N. A., Buhay W. M., McEachern P., Wolfe B. B. and Peters D. L. (2005) Progress in isotope tracer hydrology in Canada. *Hydrol. Process.* **19**, 303–327.
Golchin A., Oades J. M., Skjemstad J. O. and Clarke P. (1994) Soil structure and carbon cycling. *Aust. J. Soil Res.* **32**, 1043–1068.
Gołdyn B., Chudzińska M., Barałkiewicz D. and Celewicz-Gołdyn S. (2015) Heavy metal contents in the sediments of astatic ponds: Influence of geomorphology, hydroperiod, water chemistry and vegetation. *Ecotoxicol. Environ. Saf.* **118**, 103–111.
Gonfiantini R. (1986) Environmental isotopes in lake studies. In *Handbook of Environmental Isotope Geochemistry* (eds. F. Peter and J. C. Fontes). Elsevier, New York. pp. 113–168.
Goulding K. W. T., Poulton P. R., Webster C. P. and Howe M. T. (2000) Nitrate leaching from the Broadbalk Wheat Experiment, Rothamsted, UK, as influenced by fertilizer and manure inputs and the weather. *Soil Use Manag.* **16**, 244–250.
Gregorich E. G., Beare M. H., McKim U. F. and Skjemstad J. O. (2006) Chemical and biological characteristics of physically uncomplexed organic matter. *Soil Sci. Soc. Am. J.* **70**, 975–985.
Gregorich E. G., Beare M. H., Stoklas U. and St-Georges P. (2003) Biodegradability of soluble organic matter in maize-cropped soils. *Geoderma* **113**, 237–252.
Grossiord C., Granier A., Ratcliffe S., Bouriaud O., Bruelheide H., Checko E., Forrester D. I., Muhie Dawud S., Finér L., Pollastrini M., Scherer-Lorenzen M., Valladares F., Bonal D. and Gessler A. (2014) Tree diversity does not always improve resistance of forest ecosystems to drought. *Proc. Natl. Acad. Sci.* **111**, 14812–14815.
Hansen N. C., Hopkins B. G., Ellsworth J. W. and Jolley V. D. (2006) Iron nutrition in field crops. In *Iron nutrition in plants and rhizospheric microorganisms* (eds. L. L. Barton and J. Abadía). Springer, Dordrecht, Netherlands. pp. 23–59.
Hanson P. C., Pace M. L., Carpenter S. R., Cole J. J. and Stanley E. H. (2015) Integrating landscape carbon cycling: research needs for resolving organic carbon budgets of lakes. *Ecosystems* **18**, 363–375.
Harden J. W., Sharpe J. M., Parton W. J., Ojima D. S., Fries T. L., Huntington T. G. and Dabney S. M. (1999) Dynamic replacement and loss of soil carbon on eroding cropland. *Global Biogeochem. Cycles* **13**, 885–901.
Häring V., Fischer H., Cadisch G. and Stahr K. (2013) Implication of erosion on the assessment of decomposition and humification of soil organic carbon after land use change in tropical agricultural systems. *Soil Biol. Biochem.* **65**, 158–167.
Harris D., Horwáth W. R. and van Kessel C. (2001) Acid fumigation of soils to remove carbonates prior to total organic carbon or carbon-13 isotopic analysis. *Soil Sci. Soc. Am. J.* **65**, 1853–1856.

Hastings M. G., Jarvis J. C. and Steig E. J. (2009) Anthropogenic impacts on nitrogen isotopes of ice-core nitrate. *Science (80-.).* **324**, 1288.
Hatfield J. L., Boote K. J., Kimball B. A., Ziska L. H., Izaurralde R. C., Ort D., Thomson A. M. and Wolfe D. (2011) Climate impacts on agriculture: implications for crop production. *Agron. J.* **103**, 351–370.
Hayashi M., Kamp G. Van Der and Rudolph D. L. (1998) Water and solute transport between a prairie wetland and adjacent upland, 1. Water balance. *J. Hydrol.* **207**, 42–55.
Heagle D., Hayashi M. and Kamp G. Van Der (2013) Surface-subsurface salinity distribution and exchange in a closed-basin prairie wetland. *J. Hydrol.* **478**, 1–14.
Heal O. W., Anderson J. M. and Swift M. J. (1997) Plant litter quality and decomposition: an historical overview. In *Driven by Nature - Plant Litter Quality and Decomposition* (eds. G. Cadisch and K. E. Giller). CAB International, Wallingford, UK. pp. 3–32.
Heaton T. H. E. (1986) Isotopic studies of nitrogen pollution in the hydrosphere and atmosphere: a review. *Chem. Geol.* **59**, 87–102.
Hedges J. I. and Keil R. G. (1995) Sedimentary organic matter preservation: an assessment and speculative sysnthesis. *Mar. Chem.* **49**, 137–139.
Hedges J. I. and Oades J. M. (1997) Comparative organic geochemisties of soils and marine sediments. *Org. Geochem.* **27**, 319–361.
Hefting M. M., van den Heuvel R. N. and Verhoeven J. T. A. (2013) Wetlands in agricultural landscapes for nitrogen attenuation and biodiversity enhancement: Opportunities and limitations. *Ecol. Eng.* **56**, 5–13.
Hell R. and Stephan U. W. (2003) Iron uptake, trafficking and homeostasis in plants. *Planta* **216**, 541–551.
Hellmann C., Werner C. and Oldeland J. (2016) A spatially explicit dual-isotope approach to map regions of plant-plant interaction after exotic plant invasion. *PLoS One* **11**, e0159403.
Herczeg A. L., Smith A. K. and Dighton J. C. (2001) A 120 year record of changes in nitrogen and carbon cycling in Lake Alexandrina, South Australia: C:N, δ15N and δ13C in sediments. *Appl. Geochemistry* **16**, 73–84.
Hilton R. G., Galy A., Hovius N., Kao S. J., Horng M. J. and Chen H. (2012) Climatic and geomorphic controls on the erosion of terrestrial biomass from subtropical mountain forest. *Global Biogeochem. Cycles* **26**, GB3014.
Hobbie E. A. and Högberg P. (2012) Nitrogen isotopes link mycorrhizal fungi and plants to nitrogen dynamics. *New Phytol.* **196**, 367–382.
Holgerson M. A. and Raymond P. A. (2016) Large contribution to inland water CO2 and CH4 emissions from very small ponds. *Nat. Geosci.* **9**, 222–226.
Holtgrieve G. W., Schindler D. E., Hobbs W. O., Leavitt P. R., Ward E. J., Bunting L., Chen G., Finney B. P., Gregory-Eaves I., Holmgren S., Lisa M. J., Lisi P. J., Nydick K., Rogers L. A., Saros J. E., Selbie D. T., Shapley M. D., B W. P. and Wolfe A. P. (2011) A coherent signature of anthropogenic nitrogen deposition to remote watersheds of the Northern Hemisphere. *Science (80-.).* **334**, 1545–1548.
Horita J., Rozanski K. and Cohen S. (2008) Isotope effects in the evaporation of water: a status report of the Craig-Gordon model. *Isotopes Environ. Health Stud.* **44**, 23–49.
Houghton R. A. (2007) Balancing the global carbon budget. *Annu. Rev. Earth Planet. Sci.* **35**, 313–347.
Houghton R. A. and Goodale C. (2004) Effects of land-use change on the carbon balance of terrestrial ecosystems. In *Ecosystems and land use change* (eds. R. DeFries, G. P. Asner, and R. A. Houghton). Washington, DC. pp. 85–98.
Houlton B. Z. and Bai E. (2009) Imprint of denitrifying bacteria on the global terrestrial biosphere. *Proc. Natl. Acad. Sci.* **106**, 21713–21716.
Houlton B. Z., Sigman D. M., Schuur E. A. G. and Hedin L. O. (2007) A climate-driven switch in plant nitrogen acquisition within tropical forest communities. *Proc. Natl. Acad. Sci.* **104**, 8902–8906.
Hu Y., Berhe A. A., Fogel M. L., Heckrath G. J. and Kuhn N. J. (2016) Transport-distance specific SOC distribution: Does it skew erosion induced C fluxes? *Biogeochemistry* **128**, 339–351.
Huang G., Han L., Yang Z. and Wang X. (2008) Evaluation of the nutrient metal content in Chinese animal manure compost using near infrared spectroscopy (NIRS). *Bioresour. Technol.* **99**, 8164–8169.
Hudson B. D. (1994) Soil organic matter and available water capacity. *J. Soil Water Conserv.* **49**, 189–194.
Hulthe G., Hulth S. and Hall P. O. J. (1998) Effect of oxygen on degradation rate of refractory and labile organic matter in continental margin sediments. *Geochim. Cosmochim. Acta* **62**, 1319–1328.

IPCC I. P. on C. C. (2013) *Climate Change 2013: The Physical Basis*. eds. T. F. Stocker, D. Qin, G.-K. Plattner, M. M. B. Tignor, S. K. Allen, J. Boschung, A. Nauels, Y. Xia, V. Bex, and P. M. Midgley, Cambridge University Press, New York.
Ireland A. W., Booth R. K., Hotchkiss S. C. and Schmitz J. E. (2012) Drought as a Trigger for Rapid State Shifts in Kettle Ecosystems: Implications for Ecosystem Responses to Climate Change. *Wetlands* **32**, 989–1000.
Isidorova A., Bravo A. G., Riise G., Bouchet S., Björn E. and Sobek S. (2016) The effect of lake browning and respiration mode on the burial and fate of carbon and mercury in the sediment of two boreal lakes. *J. Geophys. Res. G Biogeosciences* **121**, 233–245.
Ito A. (2007) Simulated impacts of climate and land-cover change on soil erosion and implication for the carbon cycle, 1901 to 2100. *Geophys. Res. Lett.* **34**, L09403.
Jansson M., Hickler T., Jonsson A. and Karlsson J. (2008) Links between terrestrial primary production and bacterial production and respiration in lakes in a climate gradient in subarctic Sweden. *Ecosystems* **11**, 367–376.
Johnson D. W. and Cole D. W. (2005) Nutrient cycles in conifer forests. In *Ecostems of the World: 6 - Coniferous forests* (ed. F. Anderson). Elsevier, Amsterdam. pp. 427–450.
Johnson W. C., Boettcher S. E., Poiani K. A. and Guntenspergen G. (2004) Influence of weather extremes on the water levels of glaciated prairie wetlands. *Wetlands* **24**, 385–398.
Kahmen A., Wanek W. and Buchmann N. (2008) Foliar delta(15)N values characterize soil N cycling and reflect nitrate or ammonium preference of plants along a temperate grassland gradient. *Oecologia* **156**, 861–870.
Kaiser K. and Kalbitz K. (2012) Cycling downwards – dissolved organic matter in soils. *Soil Biol. Biochem.* **52**, 29–32.
Kaiser K., Mikutta R. and Guggenberger G. (2007) Increased stability of organic matter sorbed to ferrihydrite and goethite on aging. *Soil Sci. Soc. Am. J.* **71**, 711–719.
Kaiser M., Ellerbrock R. H. and Sommer M. (2009) Separation of coarse organic particles from bulk surface soil samples by electrostatic attraction. *Soil Sci. Soc. Am. J.* **73**, 2118–2130.
Kaiser M., Ellerbrock R. H., Wulf M., Dultz S., Hierath C. and Sommer M. (2012) The influence of mineral characteristics on organic matter content, composition, and stability of topsoils under long-term arable and forest land use. *J. Geophys. Res. Biogeosciences* **117**, G02018.
Kaiser M., Wirth S., Ellerbrock R. H. and Sommer M. (2010) Microbial respiration activities related to sequentially separated, particulate and water-soluble organic matter fractions from arable and forest topsoils. *Soil Biol. Biochem.* **42**, 418–428.
Kaiser M., Zederer D. P., Ellerbrock R. H., Sommer M. and Ludwig B. (2016) Effects of mineral characteristics on content, composition, and stability of organic matter fractions separated from seven forest topsoils of different pedogenesis. *Geoderma* **263**, 1–7.
Kalbitz K., Schmerwitz J., Schwesig D. and Matzner E. (2003) Biodegradation of soil-derived dissolved organic matter as related to its properties. *Geoderma* **113**, 273–291.
Kalettka T. and Rudat C. (2006) Hydrogeomorphic types of glacially created kettle holes in North-East Germany. *Limnologica* **36**, 54–64.
Kalettka T., Rudat C. and Quast J. (2001) “Potholes” in Northeast German agro-landscapes: functions, land use impacts, and protection strategies. In *Ecosystem Approaches to Landscape Management in Central Europe* (eds. J. D. Tenhunen, R. Lenz, and R. Hantschel). Springer, Berlin. pp. 291–298.
van der Kamp G. and Hayashi M. (2009) Groundwater-wetland ecosystem interaction in the semiarid glaciated plains of North America. *Hydrogeol. J.* **17**, 203–214.
Kang Y., Khan S. and Ma X. (2009) Climate change impacts on crop yield, crop water productivity and food security - A review. *Prog. Nat. Sci.* **19**, 1665–1674.
Kayler Z. E., Kaiser M., Gessler A., Ellerbrock R. H. and Sommer M. (2011) Application of δ13C and δ15N isotopic signatures of organic matter fractions sequentially separated from adjacent arable and forest soils to identify carbon stabilization mechanisms. *Biogeosciences* **8**, 2895–2906.
Kazahaya K. and Yasuhara M. (1994) A hydrogen isotopic study of spring waters in Mt. Yatsugatake, Japan, application to groundwater recharge and flow processes. *J. Japanese Asscociaion Hydrol. Sci.* **24**, 107–119.
Kazanjian G., Flury S., Attermeyer K., Kalettka T., Kleeberg A., Premke K., Köhler J. and Hilt S. Primary production in nutrient-rich kettle holes with differing plant communities and consequences for nutrient and carbon cycling. *Hydrobiologia*, submitted.
Keil R. G., Tsamakis E., Fuh C. B., Giddings J. C. and Hedges J. I. (1994) Mineralogical and textural controls on the organic composition of coastal marine sediments: Hydrodynamic separation using SPLITT-fractionation. *Geochim. Cosmochim. Acta* **58**, 879–893.
Keiluweit M., Bougoure J. J., Nico P. S., Pett-Ridge J., Weber P. K. and Kleber M. (2015) Mineral

protection of soil carbon counteracted by root exudates. *Nat. Clim. Chang.* **5**, 588–595.
Kendall C. and Caldwell E. A. (1998) Fundamentals of isotope geochemistry. In *Isotope tracers in catchment hydrology* (eds. C. Kendall and J. J. McDonnell). Elsevier, Amsterdam. pp. 51–68.
Kendall C. and Coplen T. B. (2001) Distribution of oxygen-18 and deuterium in river waters across the United States. *Hydrol. Process.* **15**, 1363–1393.
Kerley S. J. and Jarvis S. C. (1996) Preliminary studies of the impact of excreted N on cycling and uptake of N in pasture systems using natural abundance stable isotopic discrimination. *Plant Soil* **178**, 287–294.
Kirkels F. M. S. A., Cammeraat L. H. and Kuhn N. J. (2014) The fate of soil organic carbon upon erosion, transport and deposition in agricultural landscapes - A review of different concepts. *Geomorphology* **226**, 94–105.
Kleber M., Eusterhues K., Keiluweit M., Mikutta C., Mikutta R. and Nico P. S. (2015) Mineral-Organic Associations: Formation, Properties, and Relevance in Soil Environments. *Adv. Agron.* **130**, 1–140.
Kleber M., Mikutta R., Torn M. S. and Jahn R. (2005) Poorly crystalline mineral phases protect organic matter in acid subsoil horizons. *Eur. J. Soil Sci.* **56**, 717–725.
Kleeberg A., Herzog C. and Hupfer M. (2013) Redox sensitivity of iron in phosphorus binding does not impede lake restoration. *Water Res.* **47**, 1491–1502.
Kleeberg A., Neyen M. and Kalettka T. (2016) Element-specific downward fluxes impact the metabolism and vegetation of kettle holes. *Hydrobiologia* **766**, 261–274.
Kleeberg A., Neyen M., Schkade U.-K., Kalettka T. and Lischeid G. (2016) Sediment cores from kettle holes in NE Germany reveal recent impacts of agriculture. *Environ. Sci. Pollut. Res.* **23**, 7409–7424.
Kögel-Knabner I., Guggenberger G., Kleber M., Kandeler E., Kalbitz K., Scheu S., Eusterhues K. and Leinweber P. (2008) Organo-mineral associations in temperate soils: Integrating biology, mineralogy, and organic matter chemistry. *J. Plant Nutr. Soil Sci.* **171**, 61–82.
Kramer M. G., Sollins P., Sletten R. S. and Swart P. K. (2003) N isotope fractionation and measures of organic matter alteration during decomposition. *Ecology* **84**, 2021–2025.
Kreitler C. W. (1979) Nitrogen-isotope ratio studies of soils and groundwater nitrate from alluvial fan aquifers in Texas. *J. Hydrol.* **42**, 147–170.
Kreutzweiser D. P., Good K. P., Capell S. S. and Holmes S. B. (2008) Leaf-litter decomposition and macroinvertebrate communities in boreal forest streams linked to upland logging disturbance. *J. North Am. Benthol. Soc.* **27**, 1–15.
Kuznetsova A., Brockhoff P. B. and Christensen R. H. B. (2016) lmerTest: tests in linear mixed effects models. Available at: https://cran.r-project.org/web/packages/lmerTest/index.html.
Lal R. (2008) Sequestration of atmospheric CO2 in global carbon pools. *Energy Environ. Sci.* **1**, 86–100.
Lal R. (2003) Soil erosion and the global carbon budget. *Environ. Int.* **29**, 437–450.
Lalonde K., Mucci A., Ouellet A. and Gélinas Y. (2012) Preservation of organic matter in sediments promoted by iron. *Nature* **483**, 198–200.
LBGR (2007) *Bodengeologische Übersichtskarte im Maßstab 1:300 000 (BÜK 300)*., Cottbus. Available at: http://www.lbgr.brandenburg.de/sixcms/detail.php/622802.
Lehmann J. and Kleber M. (2015) The contentious nature of soil organic matter. *Nature* **528**, 60–68.
Lehmann M. F., Bernasconi S. M., Barbieri A. and McKenzie J. A. (2002) Preservation of organic matter and alteration of its carbon and nitrogen isotope composition during simulated and in situ early sedimentary diagenesis. *Geochim. Cosmochim. Acta* **66**, 3573–3584.
Lichtfouse E., Dou S., Houot S. and Barriuso E. (1995) Isotope evidence for soil organic carbon pools with distinct turnover rates - II. Humic substances. *Org. Geochem.* **23**, 845–847.
Lischeid G. and Kalettka T. (2012) Grasping the heterogeneity of kettle hole water quality in Northeast Germany. *Hydrobiologia* **689**, 63–77.
Lischeid G., Kalettka T., Merz C. and Steidl J. (2016) Monitoring the phase space of ecosystems: Concept and examples from the Quillow catchment, Uckermark. *Ecol. Indic.* **65**, 55–65.
Liu F., Zhang G.-L., Sun Y.-J., Zhao Y.-G. and Li D.-C. (2013) Mapping the three-dimensional distribution of soil organic matter across a subtropical hilly landscape. *Soil Sci. Soc. Am. J.* **77**, 1241–1253.
Lloyd C. E. M., Michaelides K., Chadwick D. R., Dungait J. A. J. and Evershed R. P. (2016) Runoff- and erosion-driven transport of cattle slurry: Linking molecular tracers to hydrological processes. *Biogeosciences* **13**, 551–566.
Lopes M. S. and Araus J. L. (2006) Nitrogen source and water regime effects on durum wheat photosynthesis and stable carbon and nitrogen isotope composition. *Physiol. Plant.* **126**, 435–445.

von Lützow M. V., Kögel-Knabner I., Ekschmitt K., Matzner E., Guggenberger G., Marschner B. and Flessa H. (2006) Stabilization of organic matter in temperate soils: Mechanisms and their relevance under different soil conditions - A review. *Eur. J. Soil Sci.* **57**, 426–445.
von Lützow M., Kögel-Knabner I., Ekschmitt K., Flessa H., Guggenberger G., Matzner E. and Marschner B. (2007) SOM fractionation methods: Relevance to functional pools and to stabilization mechanisms. *Soil Biol. Biochem.* **39**, 2183–2207.
Maclean R. A., English M. C. and Schiff S. L. (1995) Hydrological and hydrochemical response of a small Canadian Shield catchment to late winter rain-on-snow events. *Hydrol. Process.* **9**, 845–863.
Manns H. R. and Berg A. A. (2014) Importance of soil organic carbon on surface soil water content variability among agricultural fields. *J. Hydrol.* **516**, 297–303.
Marín-Spiotta E., Gruley K. E., Crawford J., Atkinson E. E., Miesel J. R., Greene S., Cardona-Correa C. and Spencer R. G. M. (2014) Paradigm shifts in soil organic matter research affect interpretations of aquatic carbon cycling: Transcending disciplinary and ecosystem boundaries. *Biogeochemistry* **117**, 279–297.
Mariotti A., Germon J. C., Hubert P., Kaiser P., Letolle R., Tardieux A. and Tardieux P. (1981) Experimental determination of nitrogen kinetic isotope fractionation: Some principles; illustration for the denitrification and nitrification processes. *Plant Soil* **62**, 413–430.
Masiello C. A., Chadwick O. A., Southon J., Torn M. S. and Harden J. W. (2004) Weathering controls on mechanisms of carbon storage in grassland soils. *Global Biogeochem. Cycles* **18**, GB4023.
Mayer L. M. (1994) Surface area control of organic carbon accumulation in continental shelf sediments. *Geochim. Cosmochim. Acta* **58**, 1271–1284.
McCorkle E. P., Berhe A. A., Hunsaker C. T., Johnson D. W., McFarlane K. J., Fogel M. L. and Hart S. C. (2016) Tracing the source of soil organic matter eroded from temperate forest catchments using carbon and nitrogen isotopes. *Chem. Geol.* **445**, 172–184.
McDowell N., Pockman W. T., Allen C. D., Breshears D. D., Cobb N., Kolb T., Plaut J., Sperry J., West A., Williams D. G. and Yepez E. A. (2008) Mechanisms of plant survival and mortality during drought: Why do some plants survive while others succumb to drought? *New Phytol.* **178**, 719–739.
Menzel P., Gaye B., Wiesner M. G., Prasad S., Stebich M., Das B. K., Anoop A., Riedel N. and Basavaiah N. (2013) Influence of bottom water anoxia on nitrogen isotopic ratios and amino acid contributions of recent sediments from small eutrophic Lonar Lake, central India. *Limnol. Oceanogr.* **58**, 1061–1074.
Merbach W., Kalettka T., Rudat K. and Augustin J. (2002) Trace gas emissions from riparian areas of small eutrophic inland waters in Northeast-Germany. In *Wetlands in Central Europe* (eds. G. Broil, W. Merbach, and E.-M. Pfeiffer). Springer, Heidelberg. pp. 235–244.
Meusburger K., Mabit L., Park J.-H., Sandor T. and Alewell C. (2013) Combined use of stable isotopes and fallout radionuclides as soil erosion indicators in a forested mountain site, South Korea. *Biogeosciences* **10**, 5627–5638.
Meyers P. A. (1994) Preservation of elemental and isotopic source identification of sedimentary organic matter. *Chem. Geol.* **114**, 289–302.
Michalski G., Kolanowski M. and Riha K. M. (2015) Oxygen and nitrogen isotopic composition of nitrate in commercial fertilizers, nitric acid, and reagent salts. *Isotopes Environ. Health Stud.* **51**, 382–391.
Mikha M. M., Rice C. W. and Milliken G. A. (2005) Carbon and nitrogen mineralization as affected by drying and wetting cycles. *Soil Biol. Biochem.* **37**, 339–347.
Mikutta R., Kleber M., Torn M. S. and Jahn R. (2006) Stabilization of soil organic matter: Association with minerals or chemical recalcitrance? *Biogeochemistry* **77**, 25–56.
Mikutta R., Mikutta C., Kalbitz K., Scheel T., Kaiser K. and Jahn R. (2007) Biodegradation of forest floor organic matter bound to minerals via different binding mechanisms. *Geochim. Cosmochim. Acta* **71**, 2569–2590.
Milcu A., Roscher C., Gessler A., Bachmann D., Gockele A., Guderle M., Landais D., Piel C., Escape C., Devidal S., Ravel O., Buchmann N., Gleixner G., Hildebrandt A. and Roy J. (2014) Functional diversity of leaf nitrogen concentrations drives grassland carbon fluxes. *Ecol. Lett.* **17**, 435–444.
Miller A. E., Schimel J. P., Meixner T., Sickman J. O. and Melack J. M. (2005) Episodic rewetting enhances carbon and nitrogen release from chaparral soils. *Soil Biol. Biochem.* **37**, 2195–2204.
Miller B. A., Koszinski S., Hierold W., Rogasik H., Schröder B., Van Oost K., Wehrhan M. and Sommer M. (2016) Towards mapping soil carbon landscapes: Issues of sampling scale and transferability. *Soil Tillage Res.* **156**, 194–208.
Moni C., Derrien D., Hatton P.-J., Zeller B. and Kleber M. (2012) Density fractions versus size separates: does physical fractionation isolate functional soil compartments? *Biogeosciences* **9**,

5181–5197.
Mouvenchery Y. K., Kučerík J., Diehl D. and Schaumann G. E. (2012) Cation-mediated cross-linking in natural organic matter: A review. *Rev. Environ. Sci. Biotechnol.* **11**, 41–54.
Müller H. H. (1998) Die brandenburgische Landwirtschaft von 1800 bis 1914/18 im Überblick. In *Geschichte der Landwirtschaft in Brandenburg* (eds. V. Klemm, G. Darkow, and B. H. R). Mezögazda, Budapest. pp. 9–75.
Nadeu E., Gobin A., Fiener P., van Wesemael B. and van Oost K. (2015) Modelling the impact of agricultural management on soil carbon stocks at the regional scale: The role of lateral fluxes. *Glob. Chang. Biol.* **21**, 3181–3192.
Neyen M. (2014) Depositional characteristics of glacial kettle holes at Kraatz and Rittgarten, NE Brandenburg, Germany. University of Potsdam.
Nitzsche K. N., Kalettka T., Premke K., Lischeid G., Gessler A. and Kayler Z. E. (2017) Land-use and hydroperiod affect kettle hole sediment carbon and nitrogen biogeochemistry. *Sci. Total Environ.* **574**, 46–56.
Nitzsche K. N., Verch G., Premke K., Gessler A. and Kayler Z. E. (2016) Visualizing land-use and management complexity within biogeochemical cycles of an agricultural landscape. *Ecosphere* **7**, e01282.
O'Rourke S. M., Angers D. A., Holden N. M. and Mcbratney A. B. (2015) Soil organic carbon across scales. *Glob. Chang. Biol.* **21**, 3561–3574.
Olesen J. E. and Bindi M. (2002) Consequences of climate change for European agricultural productivity, land use and policy. *Eur. J. Agron.* **16**, 239–262.
van Oost K., Quine T. A., Govers G., De Gryze S., Six J., Harden J. W., Ritchie J. C., McCarty G. W., Heckrath G., Kosmas C., Giraldez J. V, Marques da Silva J. R. and Merckx R. (2007) The impact of agricultural soil erosion on the global carbon cycle. *Science (80-.).* **318**, 626–629.
Palik B., Batzer D. D., Buech R., Nichols D., Cease K., Egeland L. and Streblow D. E. (2001) Seasonal pond characteristics across a chronosequence of adjacent forest ages in Northern Minnesota, USA. *Wetlands* **21**, 532–542.
Park J. H., Meusburger K., Jang I., Kang H. and Alewell C. (2014) Erosion-induced changes in soil biogeochemical and microbiological properties in Swiss Alpine grasslands. *Soil Biol. Biochem.* **69**, 382–392.
Parnell A., Inger R., Bearhop S. and Jackson A. L. (2008) SIAR: stable isotope analysis in R.
Pätzig M., Kalettka T., Glemnitz M. and Berger G. (2012) What governs macrophyte species richness in kettle hole types? A case study from Northeast Germany. *Limnologica* **42**, 340–354.
Paul E. A. and Clark F. E. (1996) *Soil Microbiology and Biochemistry*., Academic Press, San Diego.
Paustian K., Six J., Elliott E. T. and Hunt H. W. (2000) Management options for reducing CO2 emissions from agricultural soils. *Biogeochemistry* **48**, 147–163.
Pennock D. J., van Kessel C., Farrell R. E. and Sutherland R. A. (1992) Landscape-scale variations in denitrification. *Soil Sci. Soc. Am. J.* **56**, 770–776.
Poeplau C., Aronsson H., Myrbeck Å. and Kätterer T. (2015) Effect of perennial ryegrass cover crop on soil organic carbon stocks in southern Sweden. *Geoderma Reg.* **4**, 126–133.
Poeplau C., Don A., Vesterdal L., Leifeld J., Van Wesemael B., Schumacher J. and Gensior A. (2011) Temporal dynamics of soil organic carbon after land-use change in the temperate zone - carbon response functions as a model approach. *Glob. Chang. Biol.* **17**, 2415–2427.
Premke K., Attermeyer K., Augustin J., Cabezas A., Casper P., Deumlich D., Gelbrecht J., Gerke H., Gessler A., Grossart H. P., Hilt S., Hupfer M., Kalettka T., Kayler Z. E., Lischeid G., Sommer M. and Zak D. (2016) The importance of landscape complexity for carbon fluxes on the landscape level: Small-scale heterogeneity matters. *WIREs Water*, DOI: 10.1002/wat2.1147.
Rascher K. G., Hellmann C., Máguas C. and Werner C. (2012) Community scale 15N isoscapes: tracing the spatial impact of an exotic N2-fixing invader. *Ecol. Lett.* **15**, 484–91.
Rasse D. P., Rumpel C. and Dignac M. F. (2005) Is soil carbon mostly root carbon? Mechanisms for a specific stabilisation. *Plant Soil* **269**, 341–356.
Raven K. P. and Loeppert R. H. (1997) Trace element composition of fertilizers and soil amendments. *Am. Soc. Agron.* **26**, 551–557.
Reverey F., Grossart H. P., Premke K. and Lischeid G. (2016) Carbon and nutrient cycling in kettle holes depending on hydrological dynamics: a review. *Hydrobiologia* **775**, 1–20.
Richter L. (2014) Einfluss von Substrat und Feuchteregime auf die Treibhausgasflüsse im Uferbereich eines Solls. Johannes Gutenberg-Universität Mainz.
Rieckh H., Gerke H. H., Siemens J. and Sommer M. (2014) Water and Dissolved Carbon Fluxes in an Eroding Soil Landscape Depending on Terrain Position. *Vadose Zo. J.* **13**, 1–39.
Rieckh H., Gerke H. H. and Sommer M. (2012) Hydraulic properties of characteristic horizons depending on relief position and structure in a hummocky glacial soil landscape. *Soil Tillage Res.*

125, 123–131.
Robinson D. (2001) δ 15 N as an integrator of the nitrogen. *Trends Ecol. Evol.* **16**, 153–162.
Roschewitz I., Thies C. and Tscharntke T. (2005) Are landscape complexity and farm specialisation related to land-use intensity of annual crop fields? *Agric. Ecosyst. Environ.* **105**, 87–99.
Rubbo M. J., Cole J. J. and Kiesecker J. M. (2006) Terrestrial subsidies of organic carbon support net ecosystem production in temporary forest ponds: Evidence from an ecosystem experiment. *Ecosystems* **9**, 1170–1176.
Rue E. L. and Bruland K. W. (1995) Complexation of iron(III) by natural organic ligands in the Central North Pacific as determined by a new competitive ligand equilibration/adsorptive cathodic stripping voltammetric method. *Mar. Chem.* **50**, 117–138.
Saffih-Hdadi K. and Mary B. (2008) Modeling consequences of straw residues export on soil organic carbon. *Soil Biol. Biochem.* **40**, 594–607.
Sanderman J., Krull E., Kuhn T., Hancock G., McGowan J., Maddern T., Fallon S. and Steven A. (2015) Deciphering sedimentary organic matter sources: Insights from radiocarbon measurements and NMR spectroscopy. *Limnol. Oceanogr.* **60**, 739–753.
Saurer M., Siegenthaler U. and Schweingruber F. (1995) The climate-carbon isotope relationship in tree rings and the significance of site conditions. *Tellus* **47**, 320–330.
Saurer M. and Siegwolf R. T. W. (2007) Human Impacts on Tree-Ring Growth Reconstructed from Stable Isotopes. In *Stable Isotopes as Indicators of Ecological Change* (eds. T. E. Dawson and R. T. W. Siegwolf). Elsevier, Amsterdam, Netherlands. pp. 49–62.
Schaub M. and Alewell C. (2009) Stable carbon isotopes as an indicator for soil degradation in an alpine environment (Urseren Valley, Switzerland). *Rapid Commun. Mass Spectrom.* **23**, 1499–1507.
Scheffer M., Szabo S., Gragnani A., Van Nes E. H., Rinaldi S., Kautsky N., Norberg J., Roijackers R. M. M. and Franken R. J. M. (2003) Floating plant dominance as a stable state. *Proc. Natl. Acad. Sci.* **100**, 4040–4045.
Schlichting E., Blume H.-P. and Stahr K. (1995) *Bodenkundliches Praktikum*., Blackwell, Berlin.
Schmidt M. W. I., Torn M. S., Abiven S., Dittmar T., Guggenberger G., Janssens I. A., Kleber M., Kögel-Knabner I., Lehmann J., Manning D. A. C., Nannipieri P., Rasse D. P., Weiner S. and Trumbore S. E. (2011) Persistence of soil organic matter as an ecosystem property. *Nature* **478**, 49–56.
Schrumpf M. and Kaiser K. (2015) Large differences in estimates of soil organic carbon turnover in density fractions by using single and repeated radiocarbon inventories. *Geoderma* **239**–**240**, 168–178.
Schrumpf M., Kaiser K., Guggenberger G., Persson T., Kögel-Knabner I. and Schulze E. D. (2013) Storage and stability of organic carbon in soils as related to depth, occlusion within aggregates, and attachment to minerals. *Biogeosciences* **10**, 1675–1691.
Seibt U., Rajabi A., Griffiths H. and Berry J. A. (2008) Carbon isotopes and water use efficiency: sense and sensitivity. *Oecologia* **155**, 441–454.
Senbayram M., Dixon L., Goulding K. W. T. and Bol R. (2008) Long-term influence of manure and mineral nitrogen applications on plant and soil 15N and 13C values from the Broadbalk Wheat Experimenty. *Rapid Commun. mass Spectrom.* **22**, 1735–1740.
Shaw D. A., Vanderkamp G., Conly F. M., Pietroniro A. and Martz L. (2012) The fill-spill hydrology of prairie wetland complexes during drought and deluge. *Hydrol. Process.* **26**, 3147–3156.
Sierra C. A., Trumbore S. E., Davidson E. A., Vicca S. and Janssen I. (2015) Sensitivity of decomposition rates of soil organic matter with respect to simultaneous changes in temperature and moisture. *J. Adv. Model. Earth Syst.* **7**, 335–356.
Six J., Bossuyt H., Degryze S. and Denef K. (2004) A history of research on the link between (micro)aggregates, soil biota, and soil organic matter dynamics. *Soil Tillage Res.* **79**, 7–31.
Six J., Elliott E. . and Paustian K. (2000) Soil macroaggregate turnover and microaggregate formation: a mechanism for C sequestration under no-tillage agriculture. *Soil Biol. Biochem.* **32**, 2099–2103.
Skrzypek G., Mydłowski A., Dogramaci S., Hedley P., Gibson J. J. and Grierson P. F. (2015) Estimation of evaporative loss based on the stable isotope composition of water using "Hydrocalculator." *J. Hydrol.* **523**, 781–789.
Smith P. D., Martino D., Cai Z., Gwary D., Janzen H., Kumar P., Mccarl B., Ogle S., O'Mara F., Rice C., Scholes B. and Sirotenko O. (2007) Mitigation. Contribution of Working Group III to the Fourth Assessment Report of the Intergovernmental Panel on Climate Change. In *Climate Change 2007* (eds. B. Metz, O. R. Davidson, P. R. Bosch, R. Dave, and L. A. Meyer). Cambridge University Press, Cambridge, United Kingdom and New York, NY, USA.
Smith P., Martino D., Cai Z., Gwary D., Janzen H., Kumar P., Mccarl B., Ogle S., Mara F. O., Rice C., Scholes B., Sirotenko O., Howden M., Mcallister T., Pan G., Romanenkov V. and Schneider U.

(2008) Greenhouse gas mitigation in agriculture. *Philos. Trans. R. Soc. B* **363**, 789–813.
Sobek S., Delsontro T., Wongfun N. and Wehrli B. (2012) Extreme organic carbon burial fuels intense methane bubbling in a temperate reservoir. *Geophys. Res. Lett.* **39**, L01401.
Sobek S., Durisch-Kaiser E., Zurbrügg R., Wongfun N., Wessels M., Pasche N. and Wehrli B. (2009) Organic carbon burial efficiency in lake sediments controlled by oxygen exposure time and sediment source. *Limnol. Oceanogr.* **54**, 2243–2254.
Sollins P., Kramer M. G., Swanston C., Lajtha K., Filley T., Aufdenkampe A. K., Wagai R. and Bowden R. D. (2009) Sequential density fractionation across soils of contrasting mineralogy: Evidence for both microbial- and mineral-controlled soil organic matter stabilization. *Biogeochemistry* **96**, 209–231.
Sommer M., Augustin J. and Kleber M. (2016) Feedbacks of soil erosion on SOC patterns and carbon dynamics in agricultural landscapes-The CarboZALF experiment. *Soil Tillage Res.* **156**, 182–184.
Sommer M., Fiedler S., Glatzel S. and Kleber M. (2004) First estimates of regional (Allgäu, Germany) and global CH4 fluxes from wet colluvial margins of closed depressions in glacial drift areas. *Agric. Ecosyst. Environ.* **103**, 251–257.
Sommer M., Gerke H. H. and Deumlich D. (2008) Modelling soil landscape genesis — A “time split” approach for hummocky agricultural landscapes. *Geoderma* **145**, 480–493.
Søndergaard M., Jensen J. P. and Jeppesen E. (2003) Role of sediment and internal loading of phosphorus in shallow lakes. *Hydrobiologia* **506**–**509**, 135–145.
Song Z., Müller K. and Wang H. (2014) Biogeochemical silicon cycle and carbon sequestration in agricultural ecosystems. *Earth-Science Rev.* **139**, 268–278.
Spears B. M., Carvalho L., Perkins R., Kirika A. and Paterson D. M. (2007) Sediment phosphorus cycling in a large shallow lake: Spatio-temporal variation in phosphorus pools and release. *Hydrobiologia* **584**, 37–48.
Stallard R. F. (1998) Terrestrial sedimentation and the carbon cycle: Coupling weathering and erosion to carbon burial. *Global Biogeochem. Cycles* **12**, 231–257.
Stevenson F. J. (1994) *Humus chemistry: genesis, composition, reactions*., John Wiley & Sons, New York.
Still C. and Powell R. (2010) Continental-scale distributions of vegetation stable carbon isotope ratios. In *Isoscapes: Understanding movement, pattern, and process on the Earth through isotope mapping* (eds. J. B. West, G. J. Bowen, T. E. Dawson, and K. Tu). Springer, New York. pp. 179–194.
Sun W., Zhao Y., Huang B., Shi X., Landon Darilek J., Yang J., Wang Z. and Zhang B. (2012) Effect of sampling density on regional soil organic carbon estimation for cultivated soils. *J. Plant Nutr. Soil Sci.* **175**, 671–680.
Sutherland R. A., van Kessel C., Farrell R. E. and Pennock D. J. (1993) Landscape-scale variations in plant and soil nitrogen-15 natural abundance. *Soil Sci. Soc. Am. J.* **57**, 169–178.
Swanston C. W., Torn M. S., Hanson P. J., Southon J. R., Garten C. T., Hanlon E. M. and Ganio L. (2005) Initial characterization of processes of soil carbon stabilization using forest stand-level radiocarbon enrichment. *Geoderma* **128**, 52–62.
Tahir S. and Marschner P. (2016) Clay amendment to sandy soil - effect of clay concentration and ped size on nutrient dynamics after residue addition. *J. Soils Sediments* **16**, 2072–2080.
Takebayashi Y., Koba K., Sasaki Y., Fang Y. and Yoh M. (2010) The natural abundance of 15N in plant and soil-available N indicates a shift of main plant N resources to NO3(-) from NH4(+) along the N leaching gradient. *Rapid Commun. mass Spectrom.* **24**, 1001–1008.
Taylor S., Feng X., Kirchner J. W., Osterhuber R., Klaue B. and Renshaw C. E. (2001) Isotopic evolution of a seasonal snowpack and its melt. *Water Resour. Res.* **37**, 759–769.
Teranes J. L. and Bernasconi S. M. (2000) The record of nitrate utilization and productivity limitation provided by δ15N values in lake organic matter - a study of sediment trap and core sediments from Baldeggersee, Switzerland. *Limnol. Oceanogr.* **45**, 801–813.
Thevenon F., Adatte T., Spangenberg J. E. and Anselmetti F. S. (2012) Elemental (C/N ratios) and isotopic (δ15Norg, δ13Corg) compositions of sedimentary organic matter from a high-altitude mountain lake (Meidsee, 2661 m a.s.l., Switzerland): implications for Lateglacial and Holocene Alpine landscape evolution. *The Holocene* **22**, 1135–1142.
Thomas B., Lischeid G., Steidl J. and Dannowski R. (2012) Regional catchment classification with respect to low flow risk in a Pleistocene landscape. *J. Hydrol.* **475**, 392–402.
Tilman D., Cassman K. G., Matson P. A., Naylor R. and Polasky S. (2002) Agricultural sustainability and intensive production practices. *Nature* **418**, 671–677.
Tiner R. W. (2003) Geographically isolated wetlands of the United States. *Wetlands* **23**, 494–516.
Torn M. S., Lapenis A. G., Timofeev A., Fischer M. L., Babikov B. V. and Harden J. W. (2002) Organic

carbon and carbon isotopes in modern and 100-year-old-soil archives of the Russian steppe. *Glob. Chang. Biol.* **8**, 941–953.
Tranvik L. J., Downing J. a., Cotner J. B., Loiselle S. a., Striegl R. G., Ballatore T. J., Dillon P., Finlay K., Fortino K. and Knoll L. B. (2009) Lakes and reservoirs as regulators of carbon cycling and climate. *Limnol. Oceanogr.* **54**, 2298–2314.
Trumbore S. (2009) Radiocarbon and Soil Carbon Dynamics. *Annu. Rev. Earth Planet. Sci.* **37**, 47–66.
Tubiello F. N., Amthor J. S., Boote K. J., Donatelli M., Easterling W., Fischer G., Gifford R. M., Howden M., Reilly J. and Rosenzweig C. (2007) Crop response to elevated CO2 and world food supply - A comment on “Food for Thought. . .” by Long et al., Science 312:1918–1921, 2006. *Eur. J. Agron.* **26**, 215–223.
Ussiri D. and Lal R. (2013) *Soil emission of nitrous oxide and its mitigation*., Springer, Dordrecht, Netherlands.
Varshney R. K., Bansal K. C., Aggarwal P. K., Datta S. K. and Craufurd P. Q. (2011) Agricultural biotechnology for crop improvement in a variable climate: hope or hype? *Trends Plant Sci.* **16**, 363–371.
Vepraskas M. J. and Craft C. B. (2016) *Wetland Soils: Genesis, Hydrology, Landscapes, and Classification*. 2nd ed., CRC Press, Boca Raton, Florida.
Verburg P. H., Neumann K. and Nol L. (2011) Challenges in using land use and land cover data for global change studies. *Glob. Chang. Biol.* **17**, 974–989.
Verhoeven J. T. A., Arheimer B., Yin C. and Hefting M. M. (2006) Regional and global concerns over wetlands and water quality. *Trends Ecol. Evol.* **21**, 96–103.
Verpoorter C., Kutser T., Seekell D. A. and Tranvik L. J. (2014) A global inventory of lakes based on high-resolution satellite imagery. *Geophys. Res. Lett.* **41**, 6396–6402.
Vogel C., Mueller C. W., Höschen C., Buegger F., Heister K., Schulz S., Schloter M. and Kögel-Knabner I. (2014) Submicron structures provide preferential spots for carbon and nitrogen sequestration in soils. *Nat. Commun.* **5**, 2947.
Wagai R., Mayer L. M., Kitayama K. and Shirato Y. (2013) Association of organic matter with iron and aluminum across a range of soils determined via selective dissolution techniques coupled with dissolved nitrogen analysis. *Biogeochemistry* **112**, 95–109.
Wang Q., Wang S. and Huang Y. (2008) Comparisons of litterfall, litter decomposition and nutrient return in a monoculture Cunninghamia lanceolata and a mixed stand in southern China. *For. Ecol. Manage.* **255**, 1210–1218.
Wattel-Koekkoek E. J. W., Buurman P., Van Der Plicht J., Wattel E. and Van Breemen N. (2003) Mean residence time of soil organic matter associated with kaolinite and smectite. *Eur. J. Soil Sci.* **54**, 269–278.
Weathers K. C., Cadenasso M. L. and Pickett S. T. A. (2001) Forest Edges as Nutrient and Pollutant Concentrators: Potential Synergisms between Fragmentation, Forest Canopies, and the Atmosphere. *Conserv. Biol.* **15**, 1506–1514.
Webb J., Pain B., Bittman S. and Morgan J. (2010) The impacts of manure application methods on emissions of ammonia, nitrous oxide and on crop response-A review. *Agric. Ecosyst. Environ.* **137**, 39–46.
Weber K. A., Achenbach L. A. and Coates J. D. (2006) Microorganisms pumping iron: anaerobic microbial iron oxidation and reduction. *Nat. Rev.* **4**, 752–764.
Weise L., Ulrich A., Moreano K., Gessler A., Kayler Z., Steger K., Zeller B., Rudolph K., Knezevic-Jaric J. and Premke K. (2016) Water level changes affect carbon turnover and microbial community composition in lake sediments. *FEMS Microbiol. Ecol.* **92**, 1–14.
Werner C., Schnyder H., Cuntz M., Keitel C., Zeeman M. J., Dawson T. E., Badeck F.-W., Brugnoli E., Ghashghaie J., Grams T. E. E., Kayler Z. E., Lakatos M., Lee X., Máguas C., Ogée J., Rascher K. G., Siegwolf R. T. W., Unger S., Welker J., Wingate L. and Gessler A. (2012) Progress and challenges in using stable isotopes to trace plant carbon and water relations across scales. *Biogeosciences* **9**, 3083–3111.
West J. B., Bowen G. J., Dawson T. E. and Tu K. (2010) *Isoscapes: Understanding movement, pattern, and process on the Earth through isotope mapping*., Springer, New York.
West J. B., Sobek A. and Ehleringer J. R. (2008) A simplified GIS approach to modeling global leaf water isoscapes. *PLoS One* **3**, e2447.
West P. C., Gibbs H. K., Monfreda C., Wagner J., Barford C. C., Carpenter S. R. and Foley J. A. (2010) Trading carbon for food: global comparison of carbon stocks vs. crop yields on agricultural land. *Proc. Natl. Acad. Sci.* **107**, 19645–19648.
White P. J. (2015) Calcium. In *Handbook of Plant Nutrition* (eds. A. V Barker and D. J. Pilbeam). CRC Press, Boca Raton, Florida. pp. 165–198.
White W. M. (2015) *Isotope Geochemistry*., John Wiley & Sons, Oxford, UK.

Wirth S. (1999) Soil microbial properties across an encatchment in the moraine, agricultural landscape of northeast Germany. *Geomicrobiol. J.* **16**, 207–219.
Wolf U., Fuß R., Höppner F. and Flessa H. (2014) Contribution of N2O and NH3 to total greenhouse gas emission from fertilization: Results from a sandy soil fertilized with nitrate and biogas digestate with and without nitrification inhibitor. *Nutr. Cycl. Agroecosystems* **100**, 121–134.
Wolfe B. B., Karst-Riddoch T. L., Hall R. I., Edwards T. W. D., English M. C., Palmini R., McGowan S., Leavitt P. R. and Vary S. R. (2007) Classification of hydrological regimes of northern floodplain basins (Peace–Athabasca Delta, Canada) from analysis of stable isotopes (d18O, d2H) and water chemistry. *Hydrogeol. J.* **21**, 151–168.
Woo M.-K. and Rowsell R. D. (1993) Hydrology of a prairie slough. *J. Hydrol.* **146**, 175–207.
Xiang S. R., Doyle A., Holden P. a. and Schimel J. P. (2008) Drying and rewetting effects on C and N mineralization and microbial activity in surface and subsurface California grassland soils. *Soil Biol. Biochem.* **40**, 2281–2289.
Yoneyama T. (1996) Characterization of natural 15N abundance of soils. In *Mass spectrometry of soils* (eds. T. Boutton and S. Yamasaki). Marcel Dekker, Inc., New York. pp. 205–245.
Yoneyama T., Kouno K. and Yazaki J. (1990) Variation of natural 15N abundance of crops and soils in Japan with special reference to the effect of soil conditions and fertilizer application. *Plant Nutr. Soil Sci.* **36**, 667–675.
Yoo K., Amundson R., Heimsath A. M. and Dietrich W. E. (2006) Spatial patterns of soil organic carbon on hillslopes: Integrating geomorphic processes and the biological C cycle. *Geoderma* **130**, 47–65.
Yuan F., Sheng Y., Yao T., Fan C., Li J., Zhao H. and Lei Y. (2011) Evaporative enrichment of oxygen-18 and deuterium in lake waters on the Tibetan Plateau. *J. Paleolimnol.* **46**, 291–307.
Zech M., Bimüller C., Hemp A., Samimi C., Broesike C., Hörold C. and Zech W. (2011) Human and climate impact on (15)N natural abundance of plants and soils in high-mountain ecosystems: a short review and two examples from the Eastern Pamirs and Mt. Kilimanjaro. *Isotopes Environ. Health Stud.* **47**, 286–296.
Zhao S. and Liu S. (2014) Scale criticality in estimating ecosystem carbon dynamics. *Glob. Chang. Biol.* **20**, 2240–2251.
Zhou G., Guan L., Wei X., Tang X., Liu S., Liu J., Zhang D. and Yan J. (2008) Factors influencing leaf litter decomposition: An intersite decomposition experiment across China. *Plant Soil* **311**, 61–72.
Ziter C., Bennett E. and Gonzales A. (2014) Temperate forest fragments maintain aboveground carbon stocks out to the forest edge despite changes in community composition. *Oecologia* **176**, 893–902.

List of co-authors

Ellerbrock, Ruth: Leibniz Centre for Agricultural Landscape Research (ZALF), Institute of Soil Landscape Research, Eberswalder Str. 84, 15374 Muencheberg, rellerbrock@zalf.de

Gessler, Arthur: Swiss Federal Institute for Forest, Snow and Landscape Research (WSL), Zuercherstrasse 111, 8903 Birmensdorf, Switzerland, arthur.gessler@wsl.ch

Hoffmann, Carsten: Leibniz Centre for Agricultural Landscape Research (ZALF), Agricultural Landscape Data Centre, Eberswalder Str. 84, 15374 Muencheberg, hoffmann@zalf.de

Kaiser, Michael: University of Kassel, Department of Environmental Chemistry, Nordbahnhofstr. 1a, 37213 Witzenhausen, Germany, michael.kaiser@uni-kassel.de

Kalettka, Thomas: Leibniz Centre for Agricultural Landscape Research (ZALF), Institute of Landscape Hydrology, Eberswalder Str. 84, 15374 Muencheberg, Germany, tkalettka@zalf.de

Kayler, Zachary Eric: USDA Forest Service, Northern Research Station, Lawrence Livermore National Laboratory, Livermore, California 94550 USA, zkayler@fs.fed.us

Kleeberg, Andreas: State Laboratory Berlin-Brandenburg, Department Geology, Soil, Waste, Stahnsdorfer Damm 77, 14532 Kleinmachnow, Germany, Andreas.Kleeberg@Landeslabor-bbb.de

Lischeid, Gunnar: Leibniz Centre for Agricultural Landscape Research (ZALF), Institute of Landscape Hydrology, Eberswalder Str. 84, 15374 Muencheberg, Germany, lischeid@zalf.de

Premke, Katrin: Leibniz-Institute of Freshwater Ecology and Inland Fisheries, Chemical Analytic and Biogeochemistry, Mueggelseedamm 310, 12587 Berlin, Germany, premke@igb-berlin.de

Verch, Gernot: Leibniz Centre for Agricultural Landscape Research (ZALF), Agricultural Landscape Data Centre, Research Station Dedelow, Steinfurther Str. 14, 17291 Prenzlau, Germany, verch@zalf.de

Selbstständigkeitserklärung

Hiermit erkläre ich, dass ich die vorliegende Doktorarbeit selbstständig und ausschließlich unter Verwendung der angegebenen Quellen sowie ohne unzulässige Hilfe Dritter angefertigt habe. Diese Doktorarbeit wurde bisher weder im Inland noch im Ausland in gleicher oder ähnlicher Form oder auszugsweise einer Prüfungsbehörde vorgelegt.

Berlin, den 5.12.2016

Kai Nitzsche

Appendix

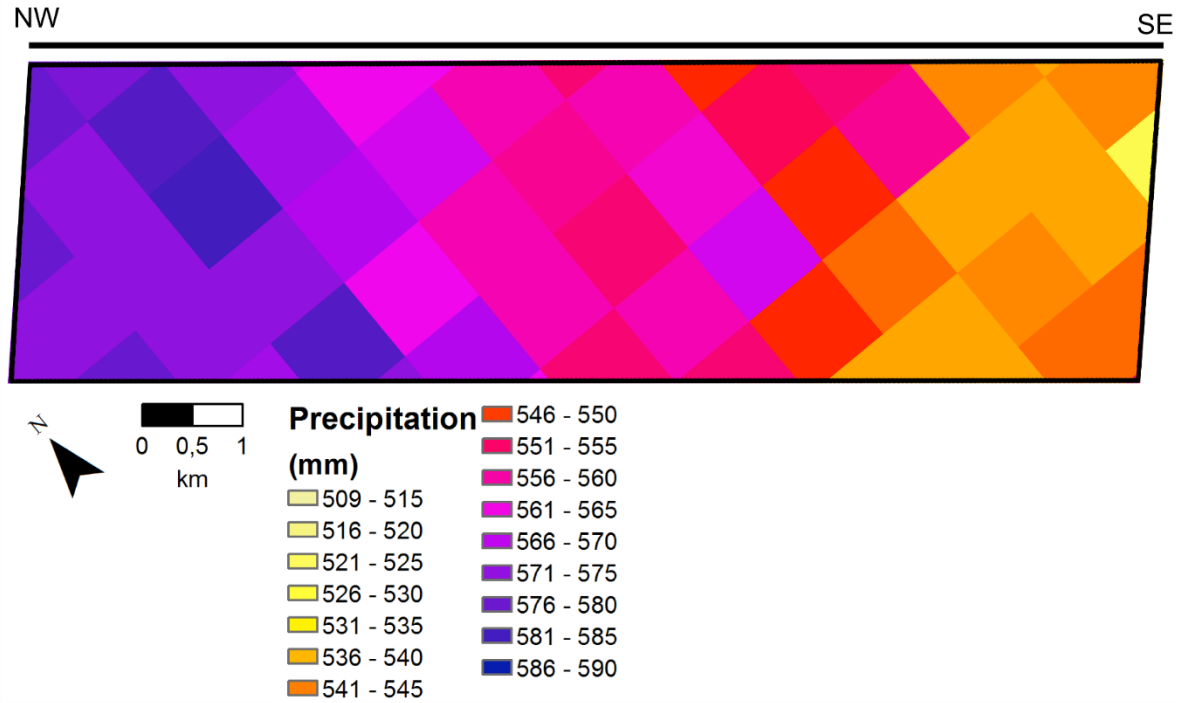

Fig. A1. Annual mean precipitation (mm) based on data from 1981 to 2010 indicates a precipitation gradient of around 45 mm from NW to SE (WebWerdis, Deutscher Wetterdienst, Offenbach am Main 2012). A multi-stage modeling procedure was used to derive the gradient and no weather station was located within the sampling area.

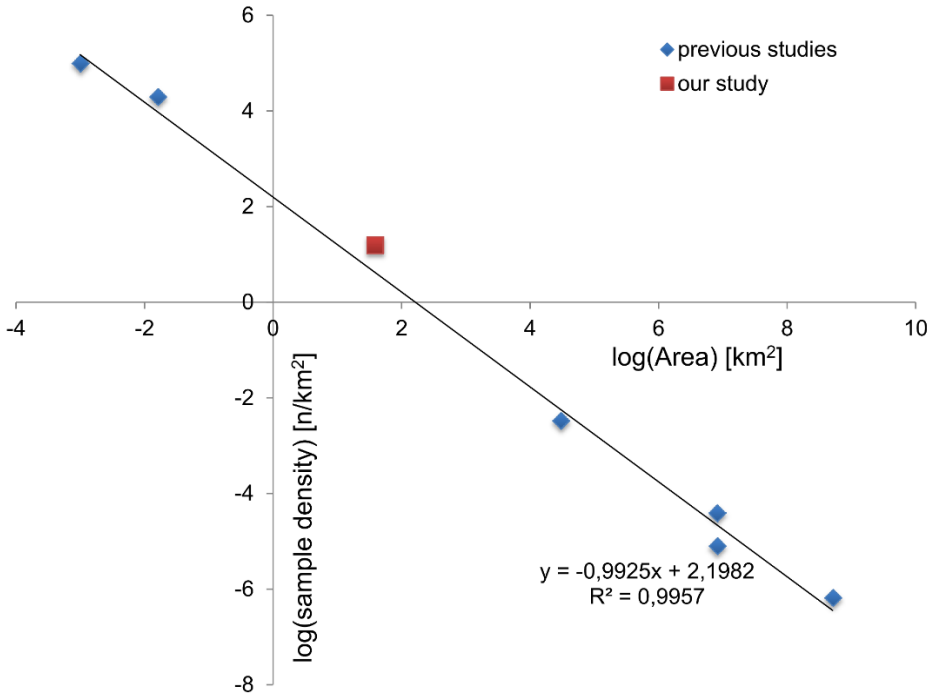

Fig. A2. Comparison of sampling densities vs total sampling area for selected studies (Kendall and Coplen, 2001; West et al., 2008; Ehleringer et al., 2008; Brooks et al., 2012; Rascher et al., 2012; Bai et al., 2013) with this study. Sampling density is defined as the logarithm of the number of samples n per 1 km2 (log(n/1 km²)) vs. logarithm of total sampling area in km² (log(area)).

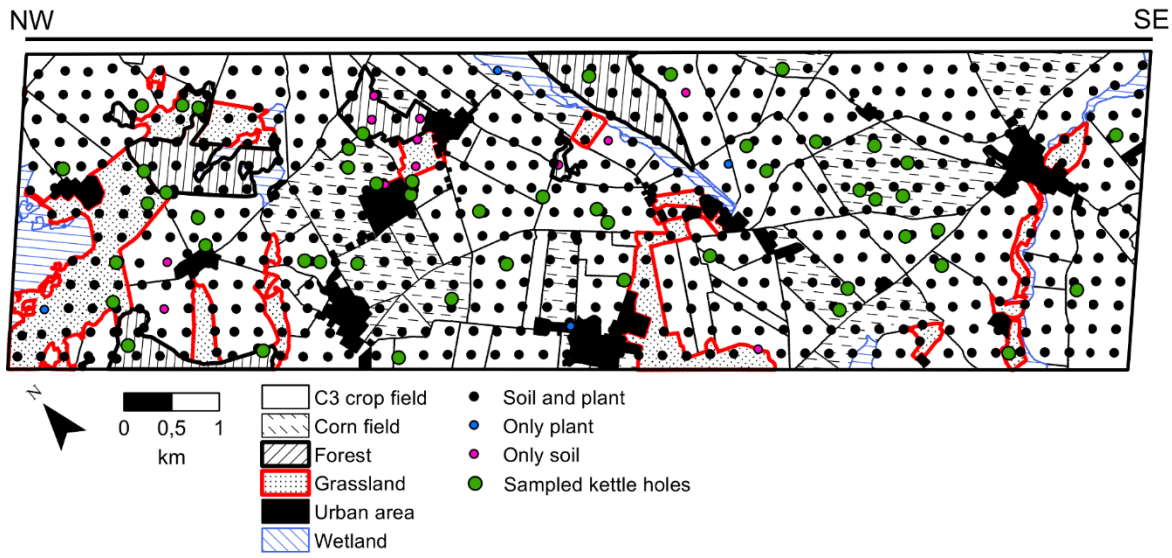

Fig. A3. Positions of sampled plants, soils and kettle holes within the arable, grassland and forest land-use type. Wetlands are defined as > 1 ha and thus are not considered to be kettle holes.

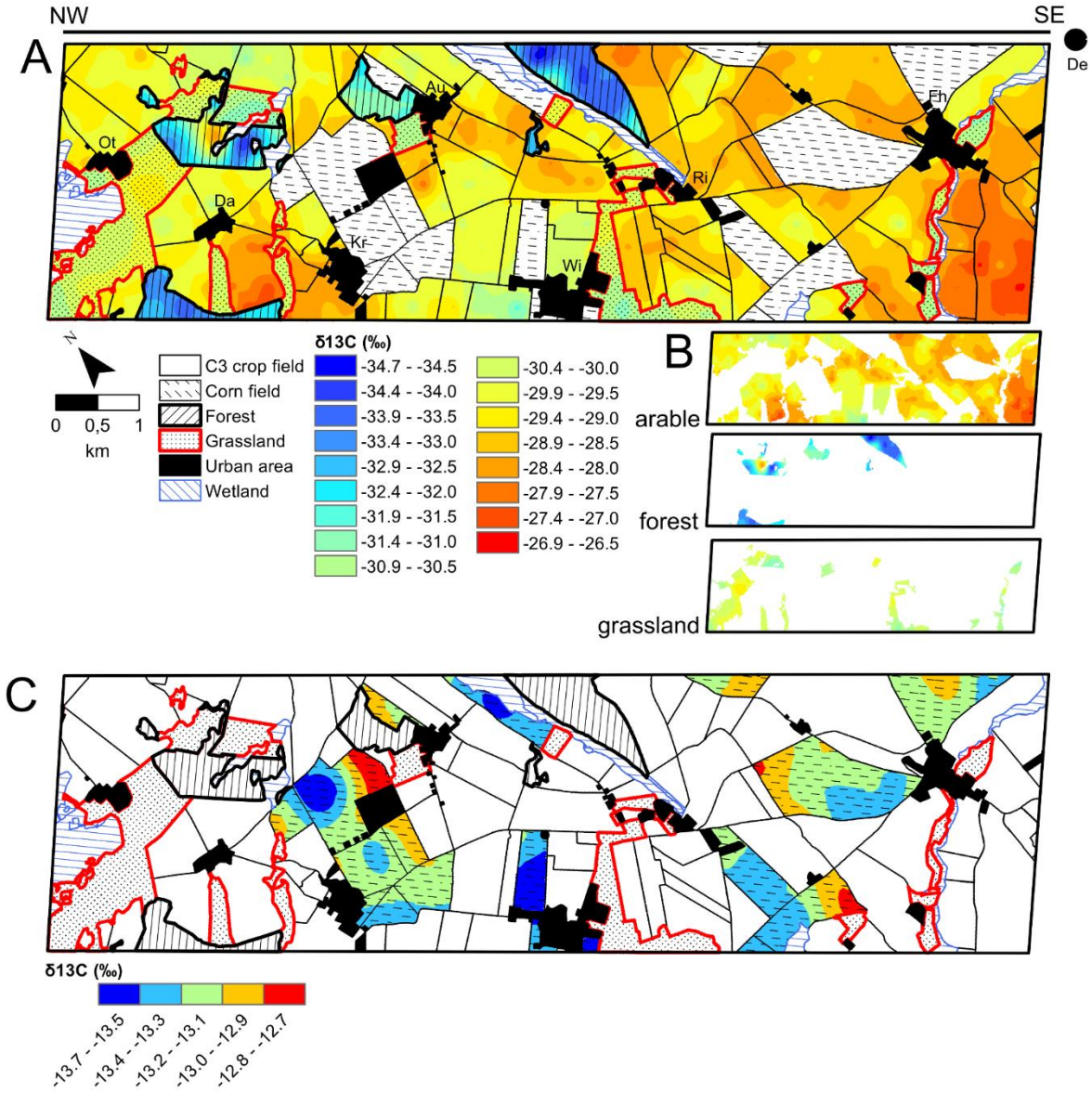

Fig. A4. Isoscapes (A) of $\delta^{13}C$ (‰) for C_3 plants sampled from the three land-use types using ordinary kriging. Interpolation was performed first for each land-use type independent of other types. The three isoscapes were then compiled into one overall isoscape using a common scale. Grasslands are highlighted with red borders and forests with black borders The area interpolated to generate each land-use type isoscape is shown in B using the same scale. Areas not interpolated include wetlands >1 ha and urban areas. The isoscape of corn (C_4 plant) has its own scale due to isotopic differences between C_3 and C_4 plants (C).

$\delta^{13}C$ pattern of C_3 plants are equivalent to WUE_i pattern. C_3 crops show a depletion in ^{13}C from SE to NW. This is in contrast to beech and dandelion, which show the contrasting pattern and are more enriched in the NW and in the center. Corn (a C_4 species) shows no clear trend.

Table A1. Tukey's HSD test on $\delta^{13}C$, $\delta^{15}N$, $\Delta\delta^{15}N$ of plants and soils and on $\delta^{13}C$ and $\delta^{15}N$ of kettle hole sediments for each land-use type giving differences (in ‰) ± SE and p values.

Land-use and isotope	Difference (‰)	p value
$\delta^{13}C_{soil}$		
arable-forest	-0.5 ± 0.1	< 0.01
arable-grassland	-1.0 ± 0.1	< 0.01
forest-grassland	-0.5 ± 0.2	< 0.01
$\delta^{13}C_{plant}$		
C_3 crops-beech	-3.4 ± 0.2	< 0.01
C_3 crops-dandelion	-1.3 ± 0.2	< 0.01
beech-dandelion	+2.2 ± 0.2	< 0.01
$\delta^{15}N_{soil}$		
arable-forest	-5.3 ± 0.2	< 0.01
arable-grassland	-1.4 ± 0.2	< 0.01
forest-grassland	+3.9 ± 0.3	< 0.01
$\delta^{15}N_{plant}$		
crops-beech	-8.0 ± 0.4	< 0.01
crops-dandelion	-1.4 ± 0.4	< 0.01
beech-dandelion	+6.6 ± 0.5	< 0.01
$\Delta\delta^{15}N$		
crops-beech	-2.8 ± 0.5	< 0.01
crops-dandelion	0.0 ± 0.4	0.99
beech-dandelion	+2.8 ± 0.6	< 0.01
$\delta^{13}C_{sediments}$		
arable-forest	-0.1 ± 0.2	0.98
arable-grassland	+0.2 ± 0.5	0.89
forest-grassland	+0.1 ± 0.7	0.98
$\delta^{15}N_{sediments}$		
arable-forest	+4.0 ± 1.0	< 0.01
arable-grassland	-0.8 ± 0.8	0.58
forest-grassland	+3.2 ± 1.2	0.02

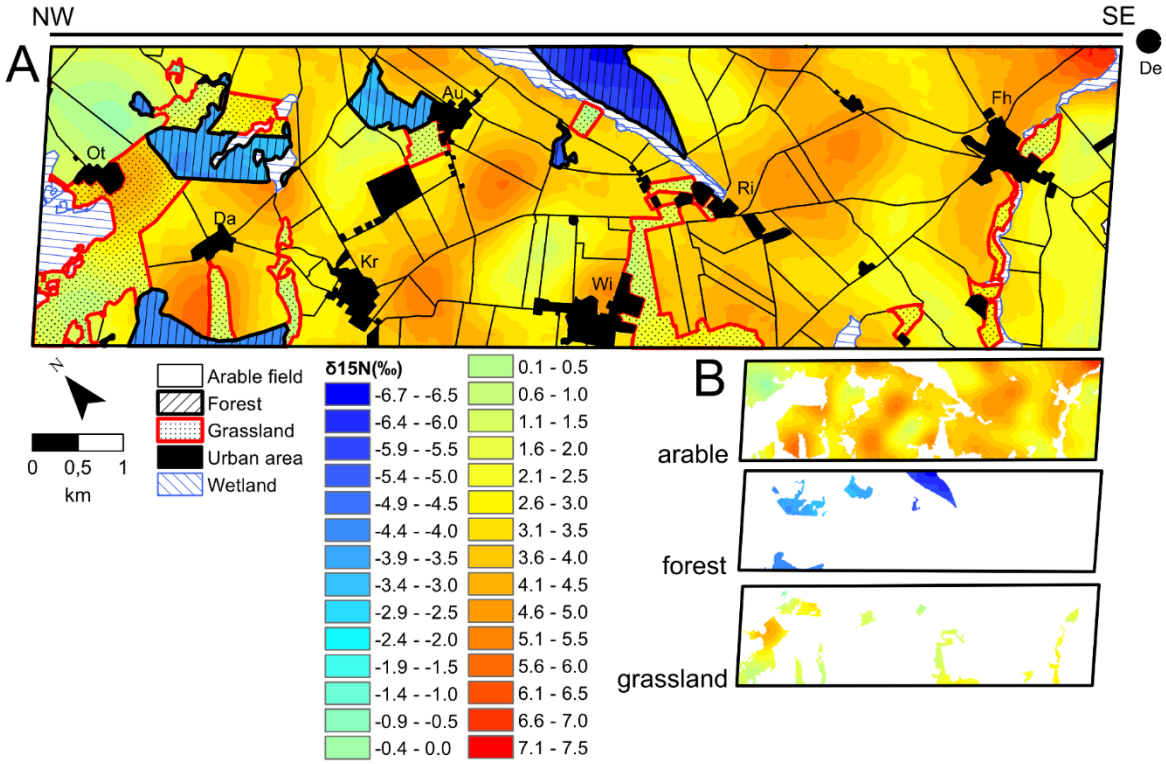

Fig. A5. Isoscapes (A) of $\delta^{15}N$ (‰) for plants sampled from the three land-use types using ordinary kriging. Interpolation was performed first for each land-use type independent of other types. The three isoscapes were then compiled into one overall isoscape using a common scale. Grasslands are highlighted with red borders and forests with black borders. The area interpolated to generate each land-use type isoscape is shown in B using the same scale. Areas not interpolated include wetlands > 1 ha and urban areas. This isoscape is in a general agreement with the $\Delta\delta^{15}N$ indicating that the ^{15}N plant isotopic composition is more dominant than the soil one. Crops are most enriched ranging from -0.2 to +7.3 ‰, but show no clear pattern. However in the SE part, this pattern has changed a little bit (more red colours). Dandelion with +0.7 to +4.5 ‰ is less enriched compared to crops. Beech is depleted in ^{15}N with -6.7 to -3.1 ‰.

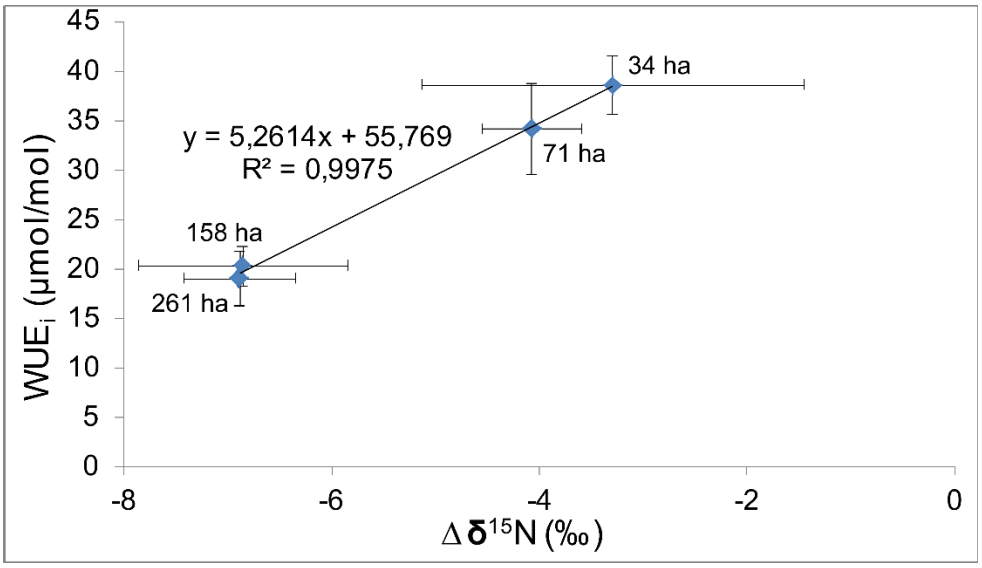

Fig. A6. Intrinsic water use efficiency (WUE_i, µmol/mol) vs. $\Delta\delta^{15}N$ (‰) ± SE for our four forests stands. We see differences between smaller forests, which have a closer N cycle ($\Delta\delta^{15}N$ closer to 0) and are more water-use efficient compared to larger ones. There is a linear relationship ($r^2 = 0.99$) between WUE_i and $\Delta\delta^{15}N$ with a slope of 5.3.

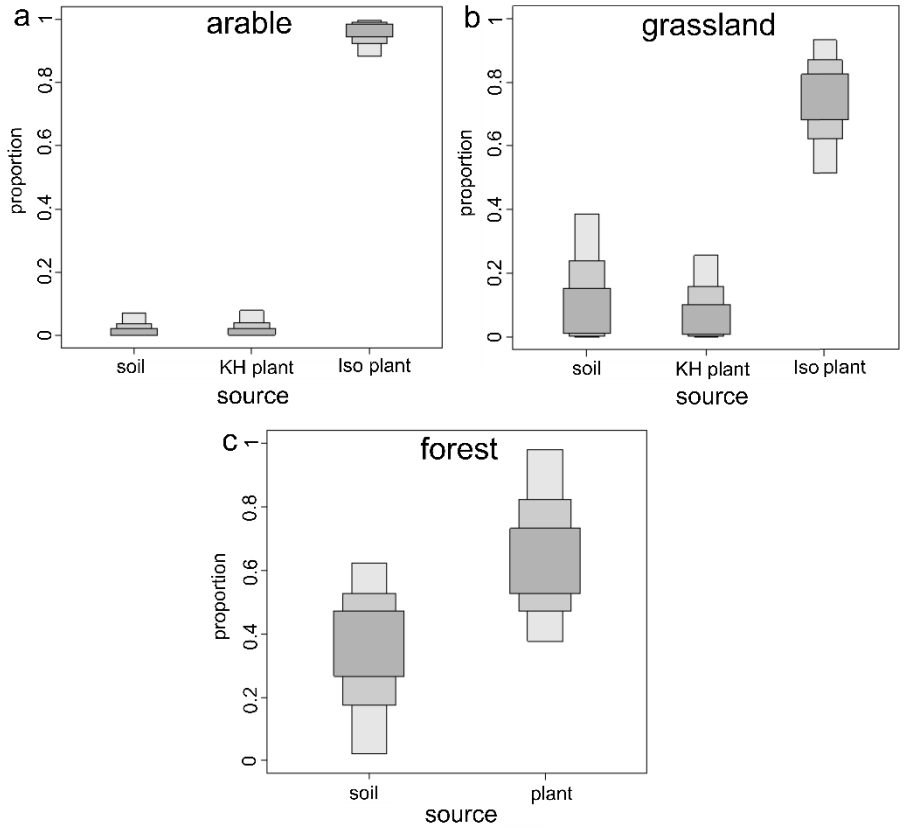

Fig. A7a-c. Mixing model results. Range of $\delta^{13}C$ and $\delta^{15}N$ sediment partition (95, 75, 25 % credibility intervals). For 'soil' we took for each kettle hole the mean values of at the most four closest soil samples provided that the land use did not change and the positions remained in the same fields for kettle holes located in arable fields. Kettle holes located in arable fields (a) with KH plant = *Phalaris arundinacea*; Iso plant = mean value of sampled C_3 crops (see Table 2.2). Kettle holes located in grasslands (b) with KH plant = *Phalaris arundinacea*; Iso plant = mean value of sampled dandelion. Kettle holes located in forests (c) with Plant = closest beech.

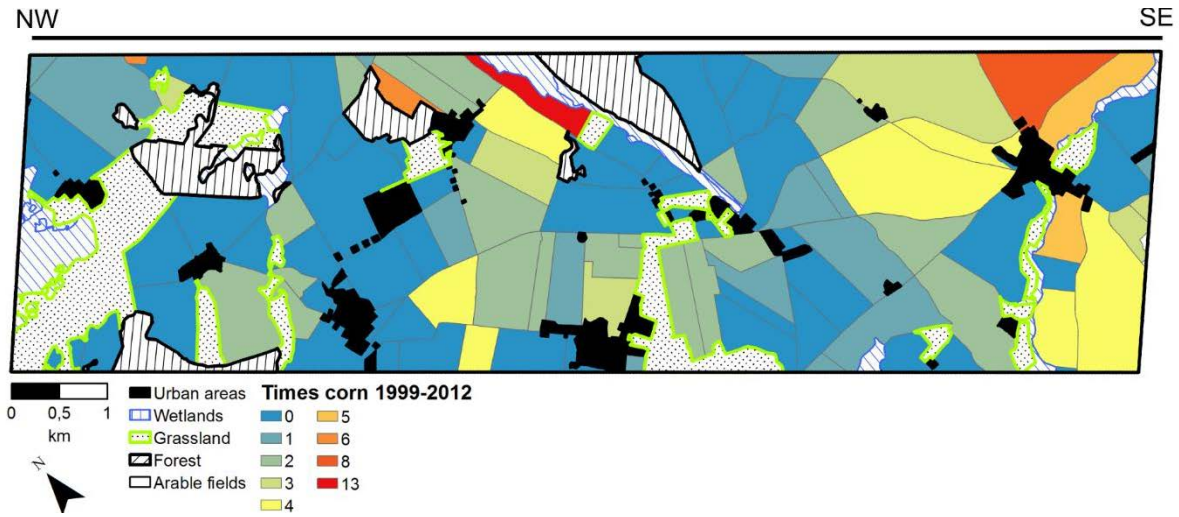

Figure A8. Cultivation of corn from 1999 to 2012 on the fields in the sampling area (Research Station, Dedelow and Department of Landscape Information Systems (yrs. 2006 to 2012): InVeKoS, Ministry for Infrastructure and Land Planning, Brandenburg (yrs. 1999 to 2005)).

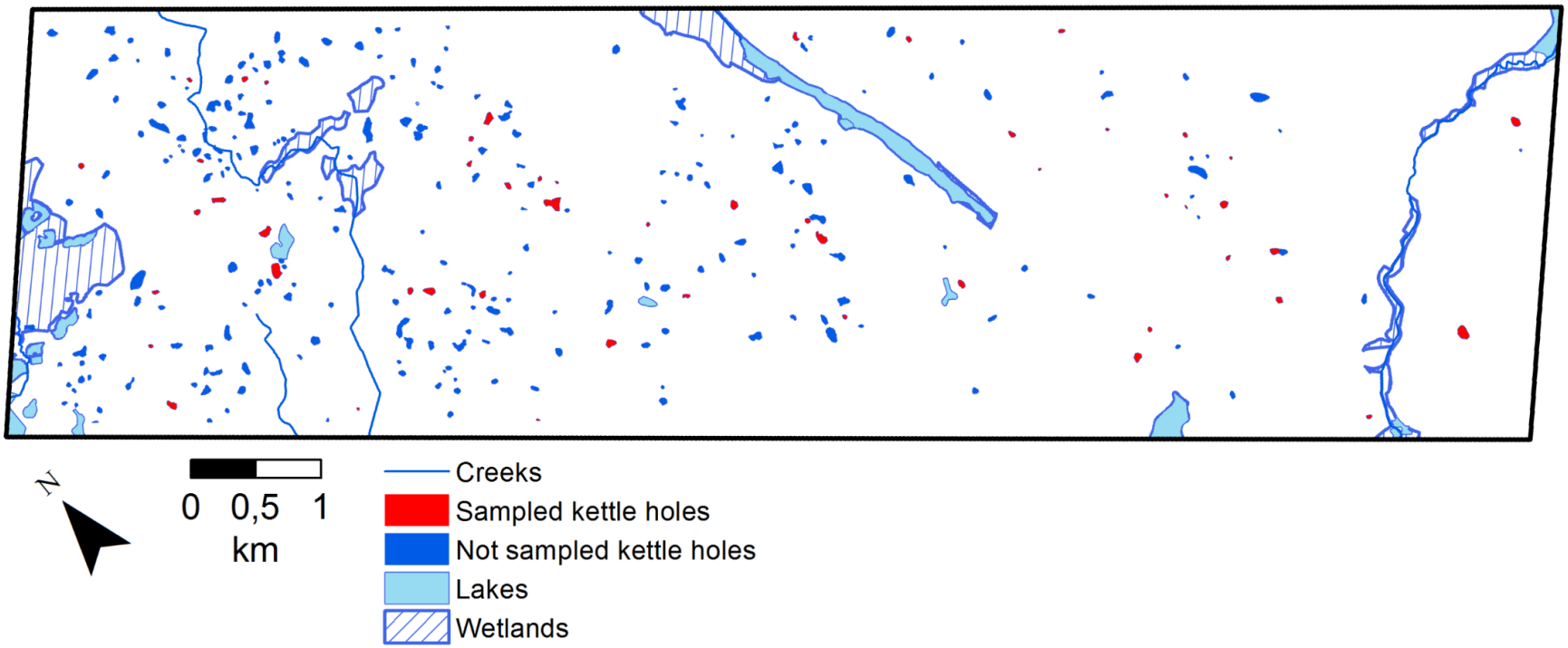

Fig. A9. Distribution of water bodies in the study site. Wetlands comprise of moors and reed-dominated areas.

Table A2. Abiotic parameters and locations of sampled kettle holes.

Kettle hole	Latitude (°)	Longitude (°)	Land-use	Hydro-period	Succession type with dominant vegetation[a]	Ele-vation (m)	Size (m^2)	Size class[c]	Water level[b] (cm)
53-Fr2	53.372515	13.747504	arable	t-type	edge type	63.9	826	2	40
288-Ri6	53.388154	13.701519	arable	t-type	full reed/egde type	74.6	2695	3	dry
218-Kr2	53.396389	13.667672	arable	t-type	full reed with phalaris/egde type with shore woods	87.5	3226	4	5
209-Kh2	53.359047	13.778478	arable	t-type	full reed type	49.0	3510	4	5
189-Fi2	53.363528	13.730249	arable	t-type	edge type	76.8	798	2	130
37-Kh4	53.359713	13.744100	arable	t-type	edge type with shore woods	56.9	1649	3	20
302-Au5	53.390808	13.692271	arable	t-type	edge type with shore woods	76.3	572	2	dry
52-Fr1	53.370087	13.741377	arable	t-type	edge type with reed	67.7	503	2	40
67-Fr5	53.376944	13.731723	arable	t-type	edge type with phalaris/full reed type with phalaris	74.8	247	1	40
165-Ot6	53.418347	13.644933	arable	t-type	edge type with shore woods/full reed type	96.6	1265	3	10
958-Ot4	53.418365	13.660845	arable	t-type	wood type	93.3	357	2	10
333-Kr3	53.384769	13.668011	arable	t-type	edge type/full reed type	96.7	138	1	40
206-Kh1	53.349963	13.758361	arable	t-type	wood type with alnus	63.3	5985	4	15
49-Kh6	53.363989	13.742498	arable	t-type	edge type with phalaris	61.1	851	2	40
70-Fr3	53.383563	13.743650	arable	t-type	edge type with typha	61.9	2875	3	140
88-Wi2	53.385305	13.690492	arable	t-type	edge type with reed	82.2	1029	3	20
61-Fi4	53.374021	13.716415	arable	t-type	edge type with shore woods	69.5	2103	3	110
184-Fi3	53.368473	13.742419	arable	t-type	edge type with shore woods	66.1	210	1	160
190-Fi1	53.362444	13.727117	arable	t-type	edge type with phragmites	73.4	2662	3	50
86-Kr4	53.385971	13.680265	arable	t-type	edge type with phragmites	85.0	3066	3	140
68-Fr6	53.379980	13.731692	arable	t-type	edge type with phalaris/full reed type with phalaris	72.5	1450	3	30
142-Fr1	53.369319	13.749940	arable	t-type	edge type with phalaris/full reed type with phalaris	68.7	295	1	120
66-Fr4	53.376201	13.740741	arable	t-type	edge type with phalaris	63.3	394	2	120
47-Kh5	53.362526	13.747106	arable	t-type	edge type with reed	60.3	2613	3	100
1501-Au4	53.401763	13.680374	arable	sp-type	edge type	83.4	965	2	100
182-Kr1	53.397399	13.665813	arable	sp-type	edge type with reed	88.3	1476	3	80
134-Au6	53.398862	13.682292	arable	sp-type	edge type with phalaris	83.4	1457	3	120
72-Ri4	53.389675	13.729308	arable	sp-type	edge type with phalaris	70.6	1111	3	150
79-Wi1	53.377259	13.703471	arable	sp-type	edge type with reed	71.9	744	2	50
51-Fh1	53.367143	13.746117	arable	sp-type	edge type	65.8	2307	3	140
202-Da1	53.406822	13.656865	arable	sp-type	edge type with phragmites	87.5	4004	4	150
341-Kr6	53.394073	13.672119	arable	sp-type	edge type with reed	92.6	1796	3	70
143-Au3	53.403085	13.682317	arable	sp-type	edge type typha	83.3	892	2	50
222-Au1	53.396077	13.685440	arable	sp-type	edge type with phalaris	80.9	7376	4	135
197-Ri1	53.384092	13.706982	arable	sp-type	edge type with phragmites	74.6	1045	3	60
258-Ri5	53.382468	13.707032	arable	sp-type	edge type with phalaris	73.7	4297	4	160
885-Da4	53.404338	13.655133	arable	sp-type	edge type with phragmites	87.2	6174	4	80
820-Kr5	53.393180	13.651909	forest	t-type	edge type with herbs	82.2	238	1	20
244-Ot1	53.410540	13.655406	forest	t-type	edge type	89.9	3044	4	10
245-Ot2	53.413436	13.654756	forest	t-type	edge type with herbs	96.0	826	2	50
906-Da3	53.401462	13.635737	forest	sp-type	edge type with shore woods	98.6	2823	3	100
1516-Au2	53.403381	13.685542	forest	sp-type	edge type with shore woods	81.4	3516	4	80
97-Ri3	53.394366	13.719035	forest	sp-type	edge with glyceria fluitans	71.3	1437	3	40
212-Kh3	53.349327	13.743812	grassland	t-type	full reed type with typha	54.6	844	2	dry
1518-Au7	53.396833	13.686754	grassland	t-type	full reed type	80.4	295	1	dry
1517-Au8	53.396954	13.686906	grassland	t-type	full reed type	80.2	712	2	dry
943-Ot5	53.414912	13.667688	grassland	t-type	full reed type with typha	92.6	645	2	dry
176-Da5	53.410817	13.652017	grassland	t-type	edge type with shore woods/full reed type	90.4	1399	3	30
203-Da2	53.408290	13.642395	grassland	t-type	edge type with typha	95.2	996	2	100
942-Ot3	53.416030	13.665971	grassland	sp-type	edge type with sedges and reed	92.2	1301	3	150
907-Da6	53.405524	13.638137	grassland	sp-type	edge type with sedges	95.9	577	2	90

[a]the succession type and dominant vegetation after the slash were observed during dry conditions

[b]water level during first sampling in July/August 2013

[c]after Pätzig et al. (2012)

Table A3: Depth horizon, total organic carbon (TOC) and total nitrogen (TN) concentrations of deeper sediments (in wt%).

Kettle hole	Latitude (°)	Longitude (°)	Land-use	Hydroperiod	Depth (cm)	TOC (wt%)	TN (wt%)
53-Fr2	53.372515	13.747504	arable	t-type	5-10	6.14	0.59
					15-20	2.86	0.25
288-Ri6	53.388154	13.701519	arable	t-type	30-35	2.04	0.16
218-Kr2	53.396389	13.667672	arable	t-type	15-20	17.78	1.16
					40-50	13.64	0.77
209-Kh2	53.359047	13.778478	arable	t-type	15-20	1.33	0.16
189-Fi2	53.363528	13.730249	arable	t-type	5-10	2.66	0.33
					15-20	2.11	0.26
37-Kh4	53.359713	13.744100	arable	t-type	15-20	4.97	0.50
					30-35	5.12	0.47
302-Au5	53.390808	13.692271	arable	t-type	10-15	1.80	0.19
					17-20	15.27	1.01
52-Fr1	53.370087	13.741377	arable	t-type	NA	3.83	0.41
67-Fr5	53.376944	13.731723	arable	t-type	2-5	3.47	0.40
					5-10	2.46	0.31
165-Ot6	53.418347	13.644933	arable	t-type	15-20	1.90	0.22
958-Ot4	53.418365	13.660845	arable	t-type	20-25	19.17	1.28
					30-35	2.35	0.2
333-Kr3	53.384769	13.668011	arable	t-type	5-10	9.74	0.97
					20-25	0.68	0.08
206-Kh1	53.349963	13.758361	arable	t-type	18-25	43.46	1.82
49-Kh6	53.363989	13.742498	arable	t-type	15-20	11.30	1.11
70-Fr3	53.383563	13.743650	arable	t-type	5-10	7.34	0.81
					15-20	4.09	0.41
88-Wi2	53.385305	13.690492	arable	t-type	5-10	9.32	0.87
					15-20	1.65	0.19
61-Fi4	53.374021	13.716415	arable	t-type	5-10	1.29	0.16
					15-20	1.90	0.19
184-Fi3	53.368473	13.742419	arable	t-type	5-10	2.60	0.29
190-Fi1	53.362444	13.727117	arable	t-type	5-10	6.77	0.63
					15-20	15.69	1.17
86-Kr4	53.385971	13.680265	arable	t-type	10-15	11.93	1.06
					25-30	25.08	1.71
68-Fr6	53.379980	13.731692	arable	t-type	5-10	3.96	0.45
					20-25	2.11	0.22
142-Fr1	53.369319	13.749940	arable	t-type	5-10	4.28	0.49
					15-20	3.43	0.39
66-Fr4	53.376201	13.740741	arable	t-type	2-5	3.52	0.44
					5-10	7.13	0.75
47-Kh5	53.362526	13.747106	arable	t-type	15-20	2.37	0.33
1501-Au4	53.401763	13.680374	arable	sp-type	NA	3.85	0.32
182-Kr1	53.397399	13.665813	arable	sp-type	2-7	3.30	0.38
					20-25	6.55	0.61
134-Au6	53.398862	13.682292	arable	sp-type	10-15	9.84	0.82
					20-22	17.63	0.85
72-Ri4	53.389675	13.729308	arable	sp-type	10-15	6.69	0.67
					20-25	10.39	0.88
79-Wi1	53.377259	13.703471	arable	sp-type	10-15	7.46	0.69
51-Fh1	53.367143	13.746117	arable	sp-type	5-10	3.48	0.30
					15-20	1.99	0.19
202-Da1	53.406822	13.656865	arable	sp-type	15-20	17.00	0.94
341-Kr6	53.394073	13.672119	arable	sp-type	8-12	8.26	0.69
					15-20	41.38	1.54

Continuation of Table A3.

Kettle hole	Latitude (°)	Longitude (°)	Land-use	Hydroperiod	Depth (cm)	TOC (wt%)	TN (wt%)
143-Au3	53.403085	13.682317	arable	sp-type	5-10	11.17	0.87
					15-20	10.01	0.76
222-Au1	53.396077	13.685440	arable	sp-type	15-20	18.62	1.28
197-Ri1	53.384092	13.706982	arable	sp-type	10-15	8.21	0.72
258-Ri5	53.382468	13.707032	arable	sp-type	20-25	7.81	0.49
					30-35	4.31	0.39
885-Da4	53.404338	13.655133	arable	sp-type	15-20	22.68	1.29
820-Kr5	53.393180	13.651909	forest	t-type	10-15	9.11	0.78
244-Ot1	53.410540	13.655406	forest	t-type	15-20	12.64	0.98
					25-30	8.94	0.72
245-Ot2	53.413436	13.654756	forest	t-type	15-20	9.54	0.68
					25-30	7,94	0.48
906-Da3	53.401462	13.635737	forest	sp-type	10-15	3.58	0.30
1516-Au2	53.403381	13.685542	forest	sp-type	10-15	21.73	1.52
					15-20	7.59	0.56
97-Ri3	53.394366	13.719035	forest	sp-type	10-15	7.08	0.74
					20-25	4.01	0.32
212-Kh3	53.349327	13.743812	grassland	t-type	15-20	17.78	1.16
1518-Au7	53.396833	13.686754	grassland	t-type	15-20	1.82	0.20
					55-60	2.12	0.20
1517-Au8	53.396954	13.686906	grassland	t-type	45-50	4.26	0.41
					70-75	3.07	0.27
943-Ot5	53.414912	13.667688	grassland	t-type	15-20	7.20	0.64
					70-75	24.25	1.08
176-Da5	53.410817	13.652017	grassland	t-type	10-15	11.71	15,50
					15-20	4.99	0.52
203-Da2	53.408290	13.642395	grassland	t-type	15-20	4.56	0.38
942-Ot3	53.416030	13.665971	grassland	sp-type	7-12	2.09	0.22
907-Da6	53.405524	13.638137	grassland	sp-type	5-10	4.37	0.48
					15-20	3.77	1.33

Table A4. Overview of taken water samples (x) for $\delta^{18}O$ and δD analysis from sampling periods for each individual kettle hole.

Kettle hole	Land-use	Hydroperiod	July/August 2013	July 2014	December 2104	April 2015	July 2015
53-Fr2	arable	t-type	x[a]	-	-	x	-
288-Ri6	arable	t-type	-[b]	-	-	-	-
218-Kr2	arable	t-type	x	-	-	x	-
209-Kh2	arable	t-type	x	-	-	-	-
189-Fi2	arable	t-type	x	-	-	-	-
37-Kh4	arable	t-type	x	-	-	-	-
302-Au5	arable	t-type	-	-	-	x	-
52-Fr1	arable	t-type	x	-	-	x	-
67-Fr5	arable	t-type	x	-	-	x	-
165-Ot6	arable	t-type	x	-	-	x	-
958-Ot4	arable	t-type	x	-	-	x	-
333-Kr3	arable	t-type	x	-	-	x	-
206-Kh1	arable	t-type	x	-	x	x	-
49-Kh6	arable	t-type	x	-	-	x	-
70-Fr3	arable	t-type	x	x	-	x	-
88-Wi2	arable	t-type	x	-	-	x	-
61-Fi4	arable	t-type	x	x	-	x	-
184-Fi3	arable	t-type	x	x	-	x	-
190-Fi1	arable	t-type	x	x	-	x	-
86-Kr4	arable	t-type	x	x	-	x	-
68-Fr6	arable	t-type	x	-	-	-	-
142-Fr1	arable	t-type	x	-	-	x	-
66-Fr4	arable	t-type	x	-	-	x	-
47-Kh5	arable	t-type	x	-	-	x	-
1501-Au4	arable	sp-type	x	x	x	x	x
182-Kr1	arable	sp-type	x	x	x	x	x
134-Au6	arable	sp-type	x	-	x	x	x
72-Ri4	arable	sp-type	x	x	x	x	x
79-Wi1	arable	sp-type	x	x	x	x	x
51-Fh1	arable	sp-type	x	x	x	x	x
202-Da1	arable	sp-type	x	x	x	x	x
341-Kr6	arable	sp-type	x	x	x	x	x
143-Au3	arable	sp-type	x	x	x	x	x
222-Au1	arable	sp-type	x	x	x	x	x
197-Ri1	arable	sp-type	x	x	x	x	x
258-Ri5	arable	sp-type	x	x	x	x	x
885-Da4	arable	sp-type	x	x	x	x	x
820-Kr5	forest	t-type	x	-	-	-	-
244-Ot1	forest	t-type	x	x	-	x	x
245-Ot2	forest	t-type	x	-	-	x	x
906-Da3	forest	sp-type	x	x	x	x	x
1516-Au2	forest	sp-type	x	x	x	x	x
97-Ri3	forest	sp-type	x	x	x	x	x
212-Kh3	grassland	t-type	-	-	-	-	-
1518-Au7	grassland	t-type	-	-	-	x	-
1517-Au8	grassland	t-type	-	-	-	x	-
943-Ot5	grassland	t-type	-	-	-	x	-
176-Da5	grassland	t-type	x	-	-	x	-
203-Da2	grassland	t-type	x	-	-	x	-
942-Ot3	grassland	sp-type	x	x	x	x	x
907-Da6	grassland	sp-type	x	x	x	x	x

[a]sample taken (x); kettle hole dry during the time of sampling (-)

Table A5. Parameters used for the estimation of evaporative loss *f* based on the *Hydrocalculator* software provided by Skrzypek et al. (2015). Temperature, rel. Humidity and δ_{rain} are mean values from April to July. The inital $\delta D_{initial}$ and $\delta^{18}O_{initial}$ of kette hole water are obtained from the intersection between the LEL and LMWL.

Year	Temperature (°C)	rel. Humidity	$\delta D_{initial}$ (‰)	$\delta^{18}O_{initial}$ (‰)	δD_{rain} (‰)	$\delta^{18}O_{rain}$ (‰)	Slope of LEL
July/August 2013	14.0	0.73	-46.5	-6.9	-48.1	-6.8	3.73
July 2014	13.6	0.75	-43.9	-6.6	-41.3	-6.1	3.67
July 2015	12.0	0.71	-48.2	-7.1	-49.3	-6.8	3.88
April-July 2015	13.9	0.70	-[a]	-[a]	-49.1	-6.8	4.34

[a]equals isotopic composition of kettle hole water sampled in April 2015

Table A6. Surface sediment mean $\delta^{13}C$, $\delta^{15}N$ (in ‰) and molar C:N ratio ± standard errors (SE).

Land-use	Hydroperiod	$\delta^{13}C$ (‰)	$\delta^{15}N$ (‰)	C:N
Arable	all (n = 37)	-28.7 ± 0.2	3.7 ± 0.3	9.4 ± 0.2
	t-type (n = 24)	-28.7 ± 0.3	4.4 ± 0.3	9.7 ± 0.2
	sp-type (n = 13)	-28.8 ± 0.3	2.3 ± 0.5	8.7 ± 0.5
Grassland	all (n = 8)	-28.3 ± 0.3	2.9 ± 0.6	9.8 ± 0.6
	t-type (n = 6)	-28.1 ± 0.3	3.6 ± 0.6	9.5 ± 0.6
	sp-type (n = 2)	-28.9 ± 0.5	0.8 ± 0.7	10.8 ± 1.2
Forest	all (n = 6)	-28.5 ± 0.3	-0.3 ± 1.7	9.2 ± 1.0
	t-type (n = 3)	-28.3 ± 0.3	1.2 ± 3.2	10.8 ± 0.9
	sp-type (n = 3)	-28.8 ± 0.6	-1.9 ± 1.3	7.7 ± 1.4

Table A7. Deeper sediment (2 - 75 cm) mean $\delta^{13}C$ and $\delta^{15}N$ (in ‰) and molar C:N ratio ± standard error (SE).

Hydroperiod	$\delta^{13}C$ (‰)	$\delta^{15}N$ (‰)	C:N
sp-type (n = 27)	-28.4 ± 0.1	3.1 ± 0.2	15.2 ± 0.9
t-type (n = 56)	-28.2 ± 0.1	4.8 ± 0.3	13.1 ± 0.5

Table A8. Mean $\delta^{18}O$ and δD (in ‰) ± SE of kettle hole water from the growing season (July/August 2013, 2014 and 2015) and dormant season (December 2014 and April 2015).

Land-use	Hydroperiod	July/August 2013			July 2014			December 2014		
		n	$\delta^{18}O$ (‰)	δD (‰)	n	$\delta^{18}O$ (‰)	δD (‰)	n	$\delta^{18}O$ (‰)	δD (‰)
Arable	all (n = 37)	35	-3.1 ± 0.3	-32.6 ± 1.3	17	0.5 ± 0.4	-17.6 ± 1.5	14	-4.3 ± 0.4	-38.4 ± 2.1
	t-type (n = 24)	22	-3.4 ± 0.4	-34.2 ± 1.6	5	1.7 ± 0.8	-12.6 ± 2.6	1	-8.0	-57.4
	sp-type (n = 13)	13	-2.6 ± 0.5	-29.7 ± 2.2	12	0.0 ± 0.5	-19.6 ± 1.5	13	-4.1 ± 0.3	-36.9 ± 1.6
Grassland	all (n = 8)	4	-3.8 ± 0.7	-35.6 ± 2.6	2	-0.6 ± 0.7	-25.1 ± 3.8	2	-3.1 ± 1.7	-34.0 ± 7.8
	t-type (n = 6)	2	-4.7 ± 0.4	-37.6 ± 0.1	n.a.	n.a.	n.a.	n.a.	n.a.	n.a.
	sp-type (n = 2)	2	-2.8 ± 0.8	-33.6 ± 5.8	2	-0.6 ± 0.7	-25.1 ± 3.8	2	-3.1 ± 1.7	-34.0 ± 7.8
Forest	all (n = 6)	6	-5.6 ± 0.3	-39.1 ± 1.4	4	-3.9 ± 0.3	-33.6 ± 0.5	3	-6.3 ± 0.4	-47.0 ± 2.9
	t-type (n = 3)	3	-5.1 ± 0.4	-68.8 ± 1.5	1	-3.1	-32.3	n.a.	n.a.	n.a.
	sp-type (n = 3)	3	-6.1 ± 0.2	-41.4 ± 1.5	3	-4.2 ± 0.1	-34.0 ± 0.2	3	-6.3 ± 0.4	-47.0 ± 2.9

Land-use	Hydroperiod	April 2015			July 2015		
		n	$\delta^{18}O$ (‰)	δD (‰)	n	$\delta^{18}O$ (‰)	δD (‰)
Arable	all (n = 37)	30	-5.5 ± 0.2	-44.4 ± 0.8	13	-0.1 ± 0.3	-20.7 ± 1.2
	t-type (n = 24)	17	-5.5 ± 0.2	-45.5 ± 1.0	n.a.	n.a.	n.a.
	sp-type (n = 13)	13	-5.4 ± 0.3	-42.9 ± 1.3	13	-0.1 ± 0.3	-20.7 ± 1.2
Grassland	all (n = 8)	7	-6.0 ± 0.4	-47.9 ± 2.0	2	-1.1 ± 0.7	-27.8 ± 3.4
	t-type (n = 6)	5	-6.3 ± 0.3	-49.1 ± 1.6	n.a.	n.a.	n.a.
	sp-type (n = 2)	2	-5.4 ± 1.5	-45.0 ± 6.6	2	-1.1 ± 0.7	-27.8 ± 3.4
Forest	all (n = 6)	5	-6.7 ± 0.3	-50.4 ± 2.0	5	-3.6 ± 0.3	-34.2 ± 1.2
	t-type (n = 3)	2	-6.2 ± 0.5	-47.7 ± 1.7	2	-3.3 ± 0.4	-34.2 ± 1.8
	sp-type (n = 3)	3	-7.0 ± 0.3	-52.2 ± 2.9	3	-3.9 ± 0.4	-35.1 ± 1.7